

University of Nevada, Reno

**The Geomorphology, Eolian Activity, and Petrology of the  
Winnemucca Dune Complex, Humboldt County, Nevada, USA**

A thesis submitted in partial fulfillment of the  
requirements for the degree of Master of Science in  
Geology

by

Nathaniel E. Pepe

Dr. Nick Lancaster/Thesis Advisor

May, 2014

UMI Number: 1559479

All rights reserved

INFORMATION TO ALL USERS

The quality of this reproduction is dependent upon the quality of the copy submitted.

In the unlikely event that the author did not send a complete manuscript and there are missing pages, these will be noted. Also, if material had to be removed, a note will indicate the deletion.



UMI 1559479

Published by ProQuest LLC (2014). Copyright in the Dissertation held by the Author.

Microform Edition © ProQuest LLC.

All rights reserved. This work is protected against unauthorized copying under Title 17, United States Code



ProQuest LLC.  
789 East Eisenhower Parkway  
P.O. Box 1346  
Ann Arbor, MI 48106 - 1346

© by Nathaniel Elias Pepe 2014

All Rights Reserved



## THE GRADUATE SCHOOL

We recommend that the thesis  
prepared under our supervision by

**NATHANIEL ELIAS PEPE**

entitled

**The Geomorphology, Eolian Activity, and Petrology of the  
Winnemucca Dune Complex, Humboldt County, Nevada,  
USA**

be accepted in partial fulfillment of the  
requirements for the degree of

**MASTER OF SCIENCE**

Nicholas Lancaster, Ph. D., Advisor

James V. Taranik, Ph. D., Committee Member

Steven G. Wesnousky, Ph. D., Committee Member

Peter E. Wigand, Ph. D., Graduate School Representative

Marsha H. Read, Ph. D., Dean, Graduate School

May, 2014

## ABSTRACT

The objective of this research was to determine the size, shape, activity of dunes, petrological characteristics, and provenance of sand in the Winnemucca Dune Complex (WDC). Methods and procedures included the extraction of weather records from meteorological stations, generating surficial landform maps, measuring dune advancement from historical aerial imagery, and field sampling of sand for laboratory inspection of grain size and mineralogical composition. Grain size parameters and textural classification of dune sand were quantitatively determined using a Laser Granulometer and GRADISTAT v.8 (Blott & Pye 2001). The mineralogical composition and physical classification of dune sand was semi-quantitatively and qualitatively analyzed using fine powder X-ray Diffractometry and stained standard thin sections. Results were plotted on ternary diagrams with Quartz-Feldspar-Lithic (Folk 1974) and Quartz-Alkali feldspar-Plagioclase (Streckeisen 1976, 1978) overlays.

Measurements from surficial landform maps estimate wind-blown deposits are distributed on 472.2 km<sup>2</sup> of terrain. Active dunes are universally dominated by unique configurations of intermediate shaped barchan and parabolic dunes. For the purpose of this study these features were termed as barchanbolic. WDC is primarily covered by 6 crescentic complexes, 1 large sand sheet, and discontinuous sets of compound barchanbolic-parabolic dune fields. The crescentic complexes are composed of closely spaced barchanoidal and transverse ridges with occasional star dunes. Between the complexes are repetitive sequences of compound and individual barchanbolic-parabolic dunes that laterally radiate towards the bounding perimeter of WDC. Sand sheets, ramps,

climbing, descending, cliff-top, and lee dunes are also present along mountain crests and hillsides. Sand sheets ( $56.3 \text{ km}^2$ ) and active dunes ( $162 \text{ km}^2$ ) extend across  $218.3 \text{ km}^2$  which constitutes 46.2% of the wind-blown deposits in WDC. Since the year 1980 sand dunes have been advancing at maximum rates from 1.6 to  $6.9 \text{ myr}^{-1}$  on an azimuth of 35- $130^\circ$ . Rose diagrams and historical wind records verify the sand dunes reach peak advancement rates during the warm season months of April to the middle of July. During this time of year the strongest winds prevail from west-southwest when the daily maximum wind speed is near  $7 \text{ ms}^{-1}$ . Measurements of sand dune advancement rates from the years 1980-2012 show eolian activity has spatiotemporally fluctuated within the complex.

WDC sand was observed to have distinguishing textural attributes. Sediments from active dunes were mesokurtic, symmetrical, and trended towards moderately well sorted medium sand. Sediments from stable dunes were mesokurtic and trended towards moderately sorted fine sand but varied in skew from symmetrical to fine. Micro-stereoscopic inspection of bulk samples, thin sections, and the QFL ternary diagram revealed that sand traveling down the sediment transport corridor will physically weather from a White to Grey & Very Pale Brown Litharenite into a Very Dark Grey to Light Yellowish Brown & Pale Brown Feldspathic litharenite sand. The QAP ternary analysis and X-ray Diffractometry demonstrated that during the processes of dune stabilization and mineralogical maturation of sand the relative weight percent of total Quartz will increase ( $20 \rightarrow 68\%$ ) and the percent relative abundance of lithic material will decrease ( $100 \rightarrow 45\%$ ). Feldspar minerals were plentiful and ranged from 32 to 80 relative weight

percent. The mineralogical maturity of sand when interpreted by the ratio of Quartz to Feldspar grades the maturation as low to fractionally intermediate. The QAP ternary diagram demonstrates there are distinct mineralogical differences within the sand and that mixing of sediments from various supply sources have contributed to its composition. Similar to findings from the Mojave Desert (Zimbelman & Williams 2002) the abundance of Feldspar and lack of Quartz enrichment in WDC dune sand may imply the mineralogical maturity is directly inherited from the parent material. The lack of Quartz enrichment also indicates WDC is geologically young and most likely has not endured extended periods of inactivity. Prominent angular to subangular grains in WDC sediments suggest dune sand has not been transported over extremely long distances. Potential sediment supply sources for dune sand may include the Jungo terrane, Comforter Basin Formation, McDermitt-Santa Rose volcanic field, and sedimentary deposits from Lake Lahontan.

## **ACKNOWLEDGEMENTS**

I would like to give tribute to Dr. James V. Taranik who is posthumously serving on my committee. Without his support and expertise this thesis may have not been possible. My advisor Nick Lancaster has been an invaluable resource and afforded me the opportunity to research the Winnemucca Dune Complex. Additional guidance from Robert Negrini (California State University, Bakersfield), Peter Wigand (University of Nevada, Reno), and Steve Wesnousky (University of Nevada, Reno) has also helped ensure the success of this project. It has been a great honor and privilege to have worked with everyone involved.

Funding for this study was made possible by a Geological Society of America Graduate Research Grant, the Jonathon O. Davis Nevada Scholarship in Quaternary Sciences & Geomorphology, and Hourly Technical employment in the Division of Earth and Ecosystems Science at the Desert Research Institute, Reno, Nevada.

I would also like to thank my family and the following individuals who have been integral to my professional development and progression in the geosciences; Donna Macknet (Black Rock Institute, Reno), Don Foss (retired College of Marin, Ca.), Paula Noble (University of Nevada, Reno), and Dean Stanphill (GC Environmental, Reno).

## TABLE OF CONTENTS

Chapter	Page
ABSTRACT	I
ACKNOWLEDGEMENTS	IV
TABLE OF CONTENTS	V
LIST OF FIGURES	IX
LIST OF TABLES	XII
LIST OF IMAGES	XIII
LIST OF PLATES	XIV
CHAPTER 1: INTRODUCTION	1
1.1 Objective	1
1.2 Methodology	2
1.3 Regional location	3
1.4 Project site description	8
1.5 Previous research	11
CHAPTER 2: ENVIRONMENTAL SETTING	14
2.1 Introduction	14
2.2 Climate	14
2.3 Wind	15
2.4 Temperature	18
2.5 Precipitation	21
2.6 Wildfires	21
2.7 Vegetation	22

## TABLE OF CONTENTS

Chapter	Page
2.8 Wildlife _____	28
<b>CHAPTER 3: LOCAL GEOLOGY _____</b>	<b>31</b>
3.1 Introduction _____	31
3.2 Mesozoic bedrock _____	31
3.3 Cretaceous intrusions _____	33
3.4 Tertiary volcanic deposits _____	33
<i>Nevada Ignimbrite flare-up</i> _____	33
<i>McDermitt-Santa Rosa volcanic field and the Yellowstone hotspot</i> _____	36
<i>Northern Nevada Rift</i> _____	37
3.5 Pliocene to Holocene sedimentary deposits _____	39
3.6 Late Holocene to present _____	44
<b>CHAPTER 4: GEOMORPHOLOGY AND EOLIAN ACTIVITY _____</b>	<b>46</b>
4.1 Introduction _____	46
4.2 Mapping method _____	46
4.3 Types of sand dunes, morphometry, and spatial coverage _____	50
4.4 Description of mapped units _____	65
4.4.1 Desert Valley to the Slumbering Hills (Map 1) _____	65
<i>Mormon Dan Butte</i> _____	71
<i>Western flank of the Slumbering Hills</i> _____	72
4.4.2 Crest of the Slumbering Hills to Silver State Valley (Map 2) _____	76
<i>Center of Silver State Valley to the crest of the Bloody Run Hills</i> _____	82

## TABLE OF CONTENTS

Chapter	Page
4.4.3 Crest of the Bloody Run Hills to Paradise Valley (Map 2) _____	86
<i>Highway 95 to the center of Paradise Valley</i> _____	90
4.5 Direction and rate of sand dune advancement in Desert Valley_____	93
4.6 Direction and rate of sand dune advancement in Silver State Valley _____	97
4.7 Direction and rate of sand dune advancement in Paradise Valley _____	100
<b>CHAPTER 5: PETROLOGY</b> _____	<b>104</b>
5.1 Introduction _____	104
5.2 Sampling and pretreatments _____	104
5.3 Determination of grain size parameters _____	106
<i>Mean grain size and Sorting</i> _____	107
<i>Skew and Kurtosis</i> _____	109
<i>Grain size and dune morphometry</i> _____	114
5.4 Sand color _____	115
5.5 Compositional analysis of dune sand _____	117
<i>Quartz</i> _____	118
<i>Feldspars</i> _____	119
<i>Other minerals</i> _____	120
5.6 QFL ternary analysis and classification of sand _____	123
5.7 QAP ternary analysis and provenance of sand _____	125
5.8 Relevant petrographic observations _____	128
5.9 Discussion _____	129

## TABLE OF CONTENTS

Chapter	Page
CHAPTER 6: DISCUSSION _____	133
6.1 Spatial extent of sand and major dune forms _____	133
6.2 Activity and shape of sand dunes _____	135
6.3 Textural, physical, and mineralogical characteristics of dune sand _____	140
6.4 Provenance of sand _____	142
6.6 Suggestions for further research _____	146
CITED REFERENCES_____	149
APPENDIX A: DIRECTION AND RATE OF SAND DUNE ADVANCEMENT _____	157
APPENDIX B: SAMPLE LOGS _____	165
APPENDIX C: SAMPLE LOCATION MAPS _____	171
PLATES	

## LIST OF FIGURES

Figure	Page
1.1: Regional location of the Winnemucca Dune Complex	4
1.2: Project location map of the Winnemucca Dune Complex	5
1.3: Aerial view from the west side of the Winnemucca Dune Complex	6
1.4: Aerial view of the east side of the Winnemucca Dune Complex	7
2.1: Wind records from the Winnemucca WSO airport (1948-2013)	16
2.2: Wind rose diagrams of the Great Basin	17
2.3: Drift potential of sand at Winnemucca WSO airport	17
2.4: Seasonal average temperature and precipitation at Winnemucca WSO airport	20
3.1: Location of the Luning-Fencemaker fold-and-thrust belt	32
3.2: Location of the Nevada Ignimbrite flare-up	35
3.3: Detailed geologic cross section of the North Hill deposit	36
3.4: Location of the McDermitt caldera and Yellowstone hotspot	37
3.5: Location of the Northern Nevada Rift Central and Western sections	38
3.6: Theoretical areal extent of shorelines and pertinent sills for middle-late Pleistocene Lake Lahontan in northern Nevada	42
3.7: Lahontan lake-level curve	43
4.1: Dimensions used to measure sand dune morphometry	48
4.2: Barchanolic sand dune in Paradise Valley	55
4.3: Parabolic sand dune approaching Highway 95 in Paradise Valley	56
4.4: Merging barchan sand dunes in Silver State Valley	56

## LIST OF FIGURES

Figure	Page
4.5: Compound and individual barchanbolic-parabolic sand dunes in the center of Paradise Valley	57
4.6: Transverse and barchanoidal ridges in the Silver State Eastern Complex	58
4.7: Northeast aerial view of Silver State Valley	59
4.8: Northeast-easterly aerial view of the western flank of the Slumbering Hills	60
4.9: Barchanoidal ridges in an isolated crescentic complex in Desert Valley	61
4.10: Stabilized to semi-active braided linear dunes transforming to stable and active parabolic dunes in Desert Valley	62
4.11: Topographic profile of Desert Valley	69
4.12: Southwest corner of Map 1 (Plate 3.1) in Desert Valley	70
4.13: Topographic profile of the western flank of the Slumbering Hills	71
4.14: Mormon Dan Butte from Map 1 (Plate 3.1) in Desert Valley	72
4.15: Northwest corner of Map 1 (Plate 3.1) showing the western flank of the Slumbering Hills	75
4.16: Topographic profile of the Slumbering Hills to the Bloody Run Hills	80
4.17: Western section of Map 2 (Plate 3.2) showing the eastern flank of the Slumbering Hills to the center of Silver State Valley	81
4.18: Central section of Map 2 (Plate 3.2) showing the center of Silver State Valley to the Bloody Run Hills	85
4.19: Topographic profile of the eastern flank of the Bloody Run Hills to the center of Paradise Valley	88

## LIST OF FIGURES

Figure	Page
4.20: Eastern section of Map 2 (Plate 3.2) showing the crest of the Bloody Run Hills to the center of Paradise Valley _____	89
4.21: Rose diagram showing direction of sand dune advancement in Desert Valley to the Slumbering Hills _____	96
4.22: Rate of sand dune advancement in Desert Valley to the Slumbering Hills _____	96
4.23: Rose diagram showing direction of sand dune advancement in Silver State Valley _____	99
4.24: Rate of sand dune advancement in Silver State Valley _____	99
4.25: Rose diagram showing direction of sand dune advancement in Paradise Valley	103
4.26: Rate of sand dune advancement in Paradise Valley _____	103
5.1: Particle size distribution of active and stable sand dunes _____	110
5.2: Change in mean grain size of dune sand from west side to east side of WDC _____	111
5.3: Bivariate analysis of grain size and sand dune type _____	112
5.4: Bivariate analysis of skew, sorting, and morphometry _____	113
5.5: Quartz-Feldspar-Lithic ternary diagram _____	124
5.6: Quartz-Alkali feldspar-Plagioclase ternary diagram _____	127
6.1: Rose diagram showing direction of sand dune advancement for the entire Winnemucca Dune Complex _____	136
6.2: Length to width ratios, spacing, activity, and shape of sand dunes _____	139
6.3: Theoretical model of middle-late Pleistocene to early Holocene Lake Lahontan shorelines in southern Desert Valley_____	145

## LIST OF TABLES

Table	Page
1: Meteorological station data and results from dry adiabatic lapse rate calculations	19
2: Plant list for the Winnemucca Dune Complex	24
3: Morphometry of sample sites in the Winnemucca Dune Complex	49
4: Spatial coverage of various wind-blown deposits	54
5: Morphometry of various wind-blown deposits	54
6: Direction and rate of sand dune advancement in Desert Valley to the Slumbering Hills	93
7: Direction and rate of sand dune advancement in Silver State Valley	97
8: Direction and rate of sand dune advancement in Paradise Valley	100
9: Grain size and morphometry of various dune forms	114
10: Summary of sand color in the Winnemucca Dune Complex	116
11: Summary of X-ray Diffractometry and inspection of thin sections	121

## LIST OF IMAGES

Image	Page
#1-4: Plant communitites in the Winnemucca Dune Complex	10
#5: Sand dunes advancing across Highway 95 in Paradise Valley	13
#6-7: Twisted Cleomella and West Humboldt wind loving buckwheat	25
#8-10: Sand veiny dock, Desert sand verbena, and Dune primrose	25
#11-12: Desert globemallow and Sharpleaf penstemon	26
#13-14: Indian ricegrass and Great Basin Red harvester ant mound	27
#15-16: Barchan sand dune and barchanoidal ridge	63
#17-18: Wind-rippled crescentic dune and asymmetric star dune	64
#19: Dune islands in Desert Valley	69
#20: Center of Silver State Valley	80
#21: Coarse platy grains of Muscovite-Sericite in dune sand	122
#22: Train travelling east over Pronto Pass on the Transcontinental railroad	146

## LIST OF PLATES

Plate

3.1: Map 1: Surficial landform map of Desert Valley to the Slumbering Hills

3.2: Map 2: Surficial landform map of Silver State Valley and Paradise Valley

## CHAPTER 1: INTRODUCTION

### 1.1 Objective

The objective of this thesis was to explore and analyze the geomorphology, petrology, and eolian activity of the Winnemucca Dune Complex (WDC). Observations from the field and aerial imagery were used in conjunction with laboratory results from a Laser Granulometer and X-ray Diffractometer to address the following 6 questions;

- 1) What is the size and spatial extent of WDC?
- 2) What types of sand dunes occur in the complex?
- 3) What is the direction and rate of dune advancement?
- 4) What are the physical and textural characteristics of sand from WDC?
- 5) Do any relationships exist between the texture of sand and the shape of dunes?
- 6) Can potential bedrock sources be determined from the petrology of WDC sand?

There is a twofold justification for this study. The first reason is because the geomorphology of WDC has not been adequately studied. Previous works have only focused on bits and pieces of the complex and neglected to accurately describe the areal coverage of wind-blown deposits, activity of dunes, and provenance of sand. The second reason for this study is additional research of WDC is required to help address the impacts of drifting sand on local infrastructure. Wind-blown sand in WDC has caused significant property damage and fatal traffic accidents. The geomorphology, eolian activity, and petrology of WDC must be properly documented to ensure that future land management plans can effectively prevent the loss of life and successfully conserve the natural resources of the area.

## 1.2 Methodology

This research employed a variety of methods and procedures that included the extraction of data from available weather records, generating surficial landform maps, and field sampling of dune sand for laboratory inspection of grain size and mineralogical composition. Spreadsheets, bivariate plots, rose and ternary diagrams were used to evaluate measurements, observations, qualitative comparisons, and quantitative analyses.

Long-term weather patterns and flooding were studied and assessed using historical records from meteorological monitoring stations and research by others. Data from meteorological monitoring stations was provided by the Western Regional Climate Center at the Desert Research Institute.

Surficial landform maps were created with ArcGIS v.9.31 & v.10 using satellite imagery, historical aerial photographs, and field observations. The type, size, and spatial extent of wind-blown deposits were measured to provide a general geomorphic description of the landscape. The morphometry, direction, and rate of advancement were also compared to determine whether any relationships exist between the shape and activity of sand dunes.

In the laboratory sand samples were prepared for micro-stereoscopic inspection and testing on a Laser Granulometer. Sand color was qualitatively determined using Munsell Soil Color charts. Grain size parameters and the textural classification of dune sand were quantitatively calculated using GRADISTAT v.8 (Blott & Pye 2001) and equations accordant with Folk & Ward (1957). The mineralogical composition was analyzed using fine powder X-ray Diffractometry and standard thin sections with staining procedures after Dickson (1965) & Houghton (1980). Results were plotted on ternary diagrams using

TriPlot v.4.1.2. Quartz-Feldspar-Lithic (Folk 1974) and Quartz-Alkali feldspar-Plagioclase (Streckeisen 1976, 1978) overlays were placed on the diagrams to physically classify sand and identify possible bedrock sources for dune sediments.

### **1.3 Regional location**

The Winnemucca Dune Complex is located in the north-central portion of the Great Basin (Figure 1.1) approximately 12 kilometers north of Winnemucca in Humboldt County, Nevada. WDC is the largest dune complex in Nevada. It extends ~60 kilometers (Figure 1.2) in an easterly direction across 3 basins (Desert Valley, Silver State Valley, and Paradise Valley) and 2 mountain ranges (Slumbering Hills and the Bloody Run Hills section of the Santa Rosa Range; Figure 1.3) before terminating on the east side of the ephemeral riverine system of the Little Humboldt River and Gumboot Lake (Figure 1.4). The complex slightly exceeds 500 km<sup>2</sup> in size with active sand dunes occupying 162 km<sup>2</sup> of terrain.

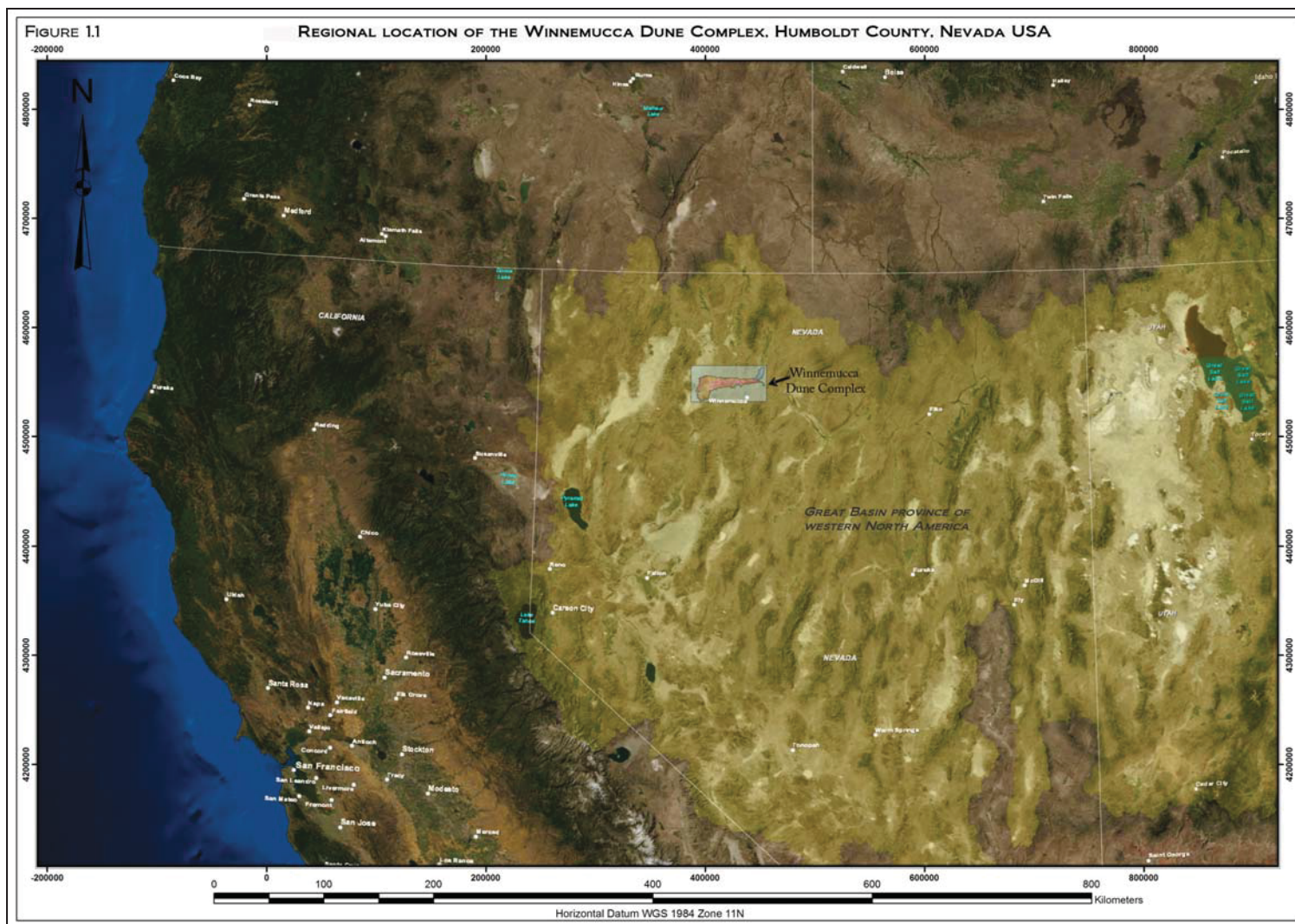


**Figure 1.1:** Regional location of the Winnemucca Dune Complex.

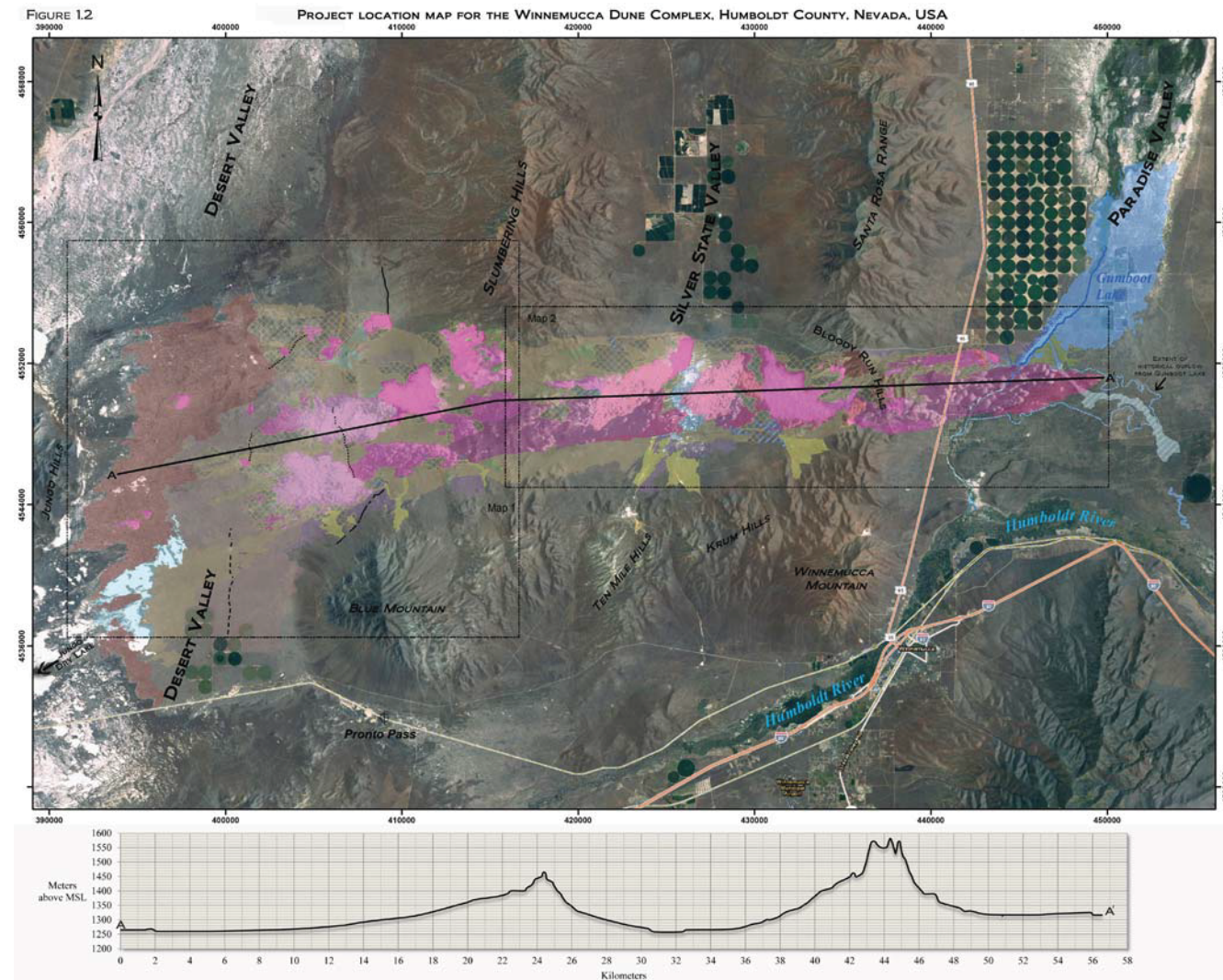
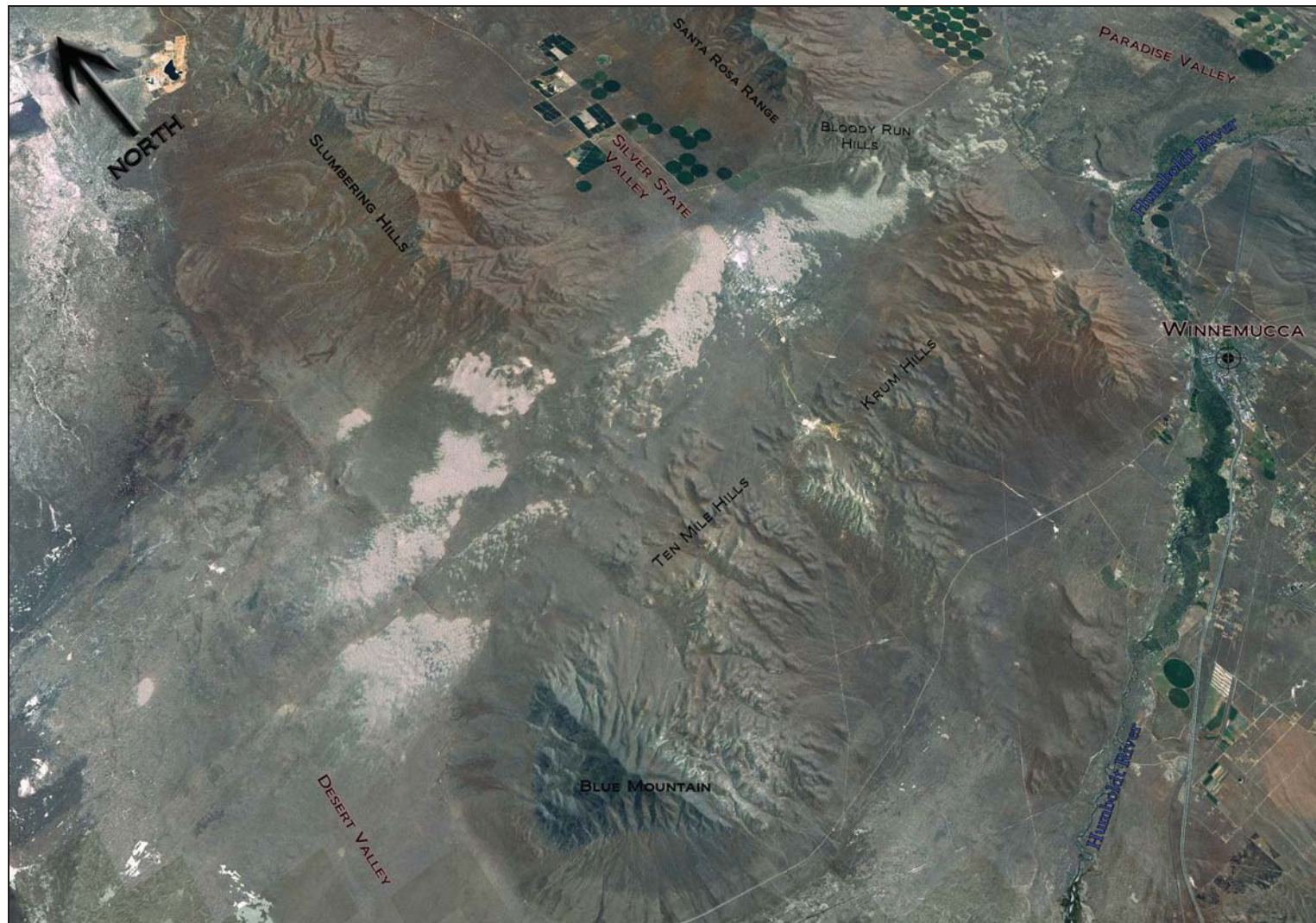


Figure 1.2: Project location map for the Winnemucca Dune Complex.



**Figure 1.3:** Aerial view from the west side of the Winnemucca Dune Complex.



**Figure 1.4:** Aerial view of the east side of the Winnemucca Dune Complex.

## 1.4 Project site description

Mountain hillslopes have low to moderate gradients and subdued bedrock outcrops that are almost completely mantled with sand. Topography in all three basins is relatively flat and low lying (Figure 1.2). WDC varies in altitude from 1255 meters above Mean Sea Level (MSL) in Silver State Valley to 1703 meters above MSL at Sombrero Peak in the Slumbering Hills, and 1664 meters above MSL in the Bloody Run Hills. Wind-rippled crescentic dunes with transverse and barchanoidal ridges dominate each section of the complex. Compound barchanbolic-parabolic and occasional star dunes laterally radiate behind ridges into individual dunes. Sand sheets, ramps, linear, parabolic, climbing, falling, and shadow dunes form on mountain passes, between major fields, and along the periphery of WDC. In many areas vegetation consisting of grasslands, desert shrub (Image #1-3), sagebrush steppe (Image #4), and psammophytes (sand loving plants) stabilize the sand dunes permitting some parabolic tails and linear dune lengths to exceed 2 kilometers. Maximum dune heights observed during this study approached 28 meters, however average dune height throughout most of the complex falls between 5-18 meters. Measurements from aerial photographs, satellite images, and topographic maps of Humboldt County from the years of 1980 and 2013 reveals the rate of dune advancement has varied 0 to 6.9 meters per year ( $\text{myr}^{-1}$ ) on an azimuth of 35-130°.

The environmental setting and climate of WDC classifies as cold semi-arid steppe with an annual monthly mean temperature of  $\sim 9.2^{\circ}\text{C}$ . Strong diurnal fluctuations in temperature, continuous rapid cooling from late summer to early winter (Martin 2012), multi-directional winds prevailing from the west (Jewell & Nicoll 2011), and distinct

warm-cold seasons are characteristic weather patterns in this locality of the Great Basin. During the warm season months of April to September monthly average temperatures are around  $16.1^0$  C. Cold season months of October to March have a monthly average temperature of  $2.6^0$  C. Light snow from frontal storms in the winter ( $\sim 61.5 \text{ cm yr}^{-1}$ ) is the predominant form of precipitation although scattered rain ( $\sim 20.8 \text{ cm yr}^{-1}$ ) can also occur throughout the year. Geospatial data and an environmental assessment by the Bureau of Land Management Winnemucca District Office (BLM 2012, 2013) indicate that at least 12 large wildfires have occurred directly in or near the vicinity of WDC since 1985.

WDC is a well-known source of drifting sand that has been impacting local economies and infrastructure since their initial settlement in the late 1800s. Intense dust storms and sandstorms causing “white-outs” (sometimes locally referred to as “brown-outs”) have been responsible for traffic accident fatalities, snapping power line poles, burial of residential homes, and damming of the Little Humboldt River which results with large magnitude floods on Gumboot Lake. These hazards are further exacerbated by numerous anthropogenic disturbances which mottle the landscape, degrade dunes, liberate fugitive dust, and provide fuel for wildfires. The most notable of these disturbances include; the Blue Mountain Geothermal Power Plant, Newmont’s Sandman project site, multiple livestock grazing allotments, and the Bureau of Land Management ATV Park in Paradise Valley.



**Image #1-4:** Plant Communities in the Winnemucca Dune Complex.

## 1.5 Previous research

One of the first recounts of WDC in scientific literature is by Israel Cook Russell (1885) in his USGS Monograph, “Geological History of Lake Lahontan, a Quaternary Lake of Northwestern Nevada”. Russell portrays WDC as a “belt” of eastward drifting sand and estimates the belt is 64.4 kilometers long, 13-16 kilometers wide, and 22.86 meters in thickness. In section 3 of the monograph, he evaluates “exceptional” sedimentary deposits of Lake Lahontan and describes the dunes of WDC; “The sand here is of a light creamy-yellow color, and forms beautifully curved ridges and waves that are covered with fret-work of wind-ripples, and frequently marked in the most curious manner by the foot-prints of animals, thus forming strange hieroglyphics that are sometimes difficult to translate.”

At the end of the section 3, Russell speculates on the provenance of sand; “It is impossible to trace the sands forming these various dunes to their sources, but we may be sure that they have traveled far and were not derived from the waste of the rocks in their present neighborhood...It is possible, as has been suggested by previous writers, that these various areas all belong to a single series, and are formed of the beach sands of the Pacific which have been blown inland by the prevailing westerly winds. It seems more probable, however, that they owe their origin to the sub aerial disintegration of the granites of the Sierra Nevada.”

A more recent general description of WDC is provided by Smith (1982) in his discussion about sand dunes in North American deserts. He describes stabilized and active “u-shaped” dunes, small barchans, and transverse dunes as the primary forms with heights reaching ~20 meters. Smith determined that sand dunes in Desert Valley are advancing on an azimuth of 70-75° and spatially distribute over ~50 square kilometers. Dune advancement in WDC is also mentioned by Keller (1985). He notes that drifting sand in Paradise Valley encroaches onto the apron of Highway 95 (Image #5) which requires maintenance crews from the Nevada Department of Transportation to remove 4,500 to

12,000 cubic meters of material each year. In these same areas, Keller reports sand dunes are advancing at the rate of  $\sim 12 \text{ myr}^{-1}$ . WDC was also studied by Trexler & Melhorn (1986). They investigated the area to determine if “booming sand” existed within the complex. Dune sediments in Paradise Valley were estimated by Trexler & Melhorn to be composed of well sorted very fine sand with a mean grain size of  $170 \mu\text{m}$  ( $2.6\phi$ ). They proclaimed that “booming sounds” could not be “elicited” in any portions of WDC.

Well known research pertaining to WDC was presented by Jonathan Ogden Davis (1982; 1983; 1987<sup>1</sup>; 1990). He proposed prior to late Pleistocene times the Humboldt River (Figure 1.2) spilled through Pronto Pass into Desert Valley and drained north-northwest as a tributary to the Quinn River. Davis argued that if the Humboldt River flowed into Desert Valley a delta would have been deposited somewhere in the basin just past the spill point. He also speculated the delta deposits from the Humboldt River were exposed and degraded following the Holocene recession of Lake Lahontan. Davis believed the delta sediments subsequently became the source of sand responsible that was for the formation of dunes in WDC. Eissmann (1990) further explored this theory in the field and with LANDSAT TM imagery but unfortunately did not document any visual or physical evidence to substantiate previous claims by Davis.

Overall, the geomorphology of WDC is poorly understood. Geographic isolation, sparse population, and historically deficient resource management plans are the principle reasons why WDC lacks previous research. It is inevitable the synergistic effects of climate change, shorter wildfire return intervals, enforcement of the Endangered Species Act, and fatal traffic accidents on Highway 95 will mandate future studies.



**Image #5:** Sand dunes advancing eastward across Highway 95 at the ATV Park in Paradise Valley.  
View to the southwest with Winnemucca Mountain in the background above the dunes.

## CHAPTER 2: ENVIRONMENTAL SETTING

### 2.1 Introduction

This chapter will discuss the climate, weather patterns, flora, and fauna which comprise the environmental setting of the Winnemucca Dune Complex.

### 2.2 Climate

The environmental setting and climate of WDC classifies as cold semi-arid steppe with an annual monthly mean temperature of  $\sim 9.2^{\circ}$  C. Precipitation consists mostly of light snow  $\sim 61.5 \text{ cm yr}^{-1}$  and lesser amounts of scattered rainfall  $\sim 20.8 \text{ cm yr}^{-1}$ . Strong diurnal fluctuations in wind, temperature, continuous rapid cooling from late summer to early winter, and distinct warm-cold seasons are typical weather patterns in this region of the Great Basin. Climate locally supports vegetative communities consisting of grasslands, desert scrub, sagebrush steppe, and psammophytes (sand loving plants). Invasive grasses have colonized the entire complex except the surfaces of active sand dunes and the playas in Desert Valley and Silver State Valley. The unique combination of topography, soils, plant communities, and climate sustain a plethora of indigenous flora and fauna which includes at least 19 sensitive at-risk species.

Orographic effects from the distant Sierra Nevada Mountains broadly influence the direction of storm tracts, amount of available precipitation, temperature, and the rate of sand dune advancement. Local orographic effects are also generated by the Jackson Mountains and Santa Rosa Range. In the winter this setting will sometimes produce a thermal inversion in the northern portion of Paradise Valley that causes cold air to sink and circulate south towards Winnemucca. Long-term atmospheric circulation in the area

is periodically driven and modulated by changes in weather patterns affiliated with the El Niño Southern Oscillation, Pacific Decadal Oscillation, and the Pacific North American teleconnection pattern.

### 2.3 Wind

The strength and directionality of wind is highly variable. Typical “down-valley” winds that originate from the northeast will shift in the afternoon to “up-valley” winds that prevail from the southwest (Martin 2012). Hourly wind records (years 1948-2013) from the Winnemucca WSO airport compiled by WeatherSpark (Vector Magic) indicate that daily wind speeds vary from 0 to  $8 \text{ ms}^{-1}$  (meters per second) and rarely exceed  $11 \text{ ms}^{-1}$ . Seasonally the model (Figure 2.1) shows the strongest winds prevail from the west to southwest during the warm season months of April to the middle of July when the average daily maximum wind speed is near  $7 \text{ ms}^{-1}$  and the daily mean wind speed is very close to  $4 \text{ ms}^{-1}$ . The model also shows that during the cold season months of mid-October to early February calmer winds prevail from the south with an average daily maximum wind speed slightly below  $6 \text{ ms}^{-1}$  and a daily mean wind speed slightly above  $3 \text{ ms}^{-1}$ .

Storm-tracks and winds capable of entraining sand commonly result from cold frontal systems that originate on the leeward side of the Sierra Nevada Mountains (Jewell & Nicoll 2011). These synoptic systems are normally associated with late-winter to early-summer extratropical cyclones that cause strong winds to be driven from the west and southwest. Jewell & Nicoll (2011) have calculated the drift potential (DP) and resultant drift potential (RDP) for sand at the Winnemucca WSO airport from the years 1950-2000 for winds velocities  $\geq 6 \text{ ms}^{-1}$  over 16 compass directions. Their computations have

determined a DP total from all compass directions at ~143 vector units, RDP/DP ratio of ~0.5, and a resultant drift direction of ~78-79° (Figure 2.2). The relatively low values of DP, RDP/DP, and multiple modes on the wind rose diagram in Figure 2.2 classify the winds after Fryberger & Dean (1979) as low energy with complex to obtuse bimodal directionality. Jewell & Nicoll (2011) also document that drift potential at the Winnemucca WSO airport has been relatively decreasing in strength since the year 1954 (Figure 2.3).

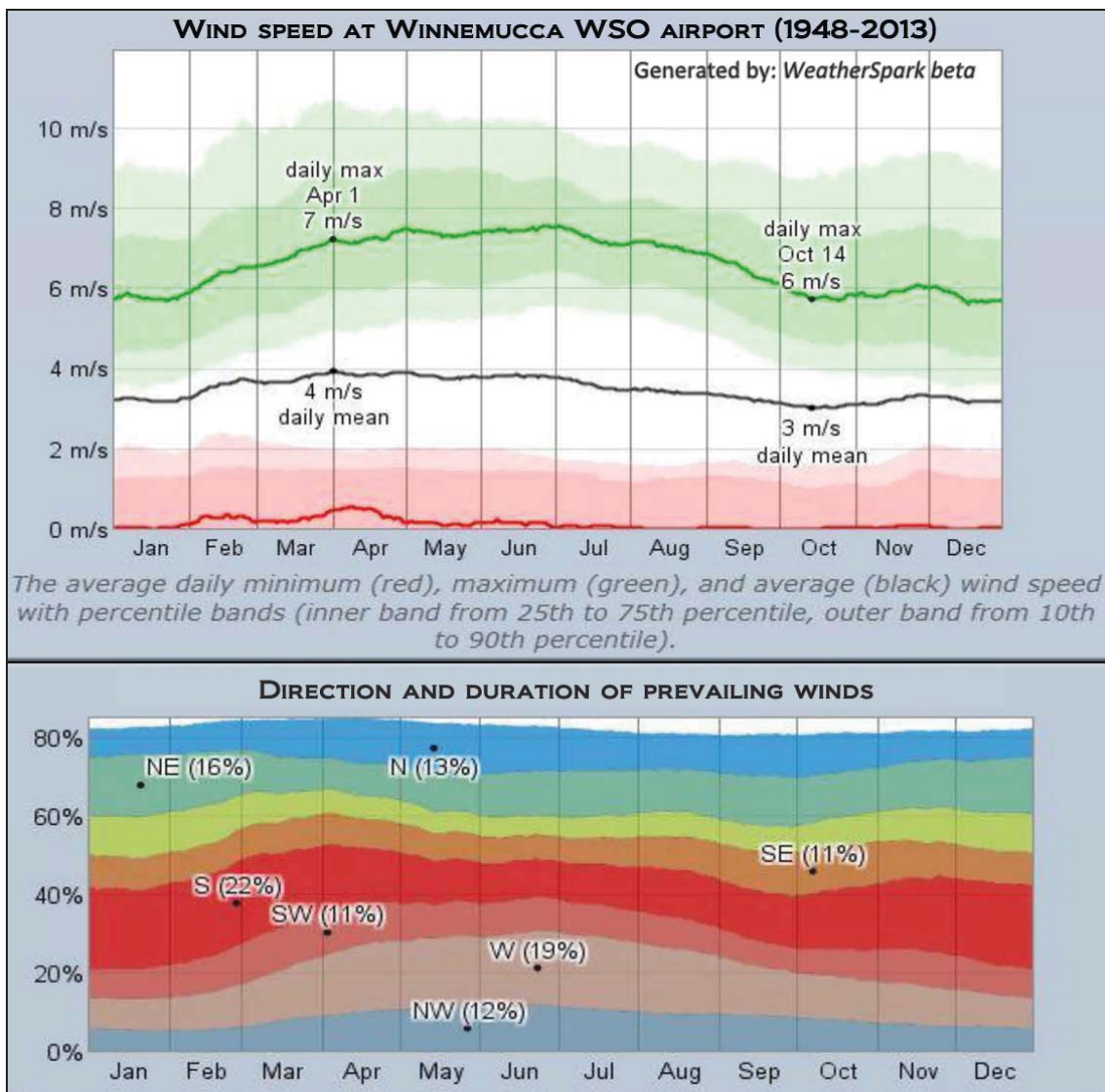
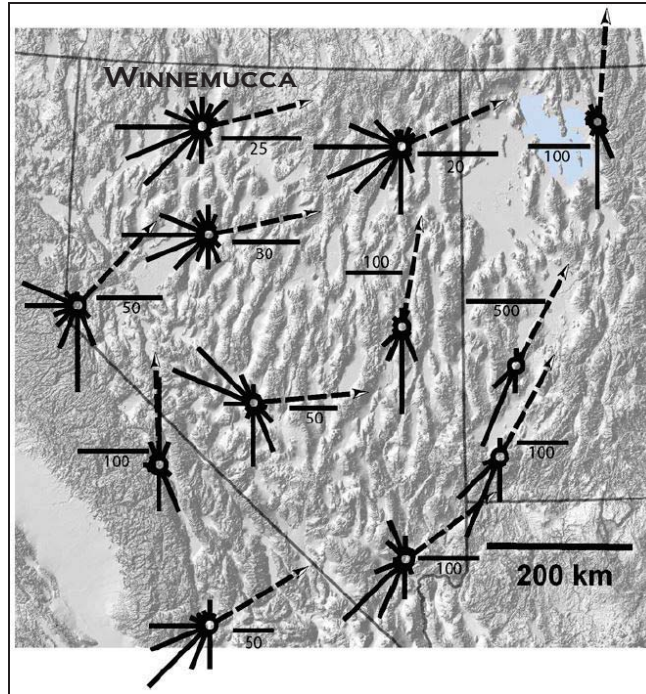
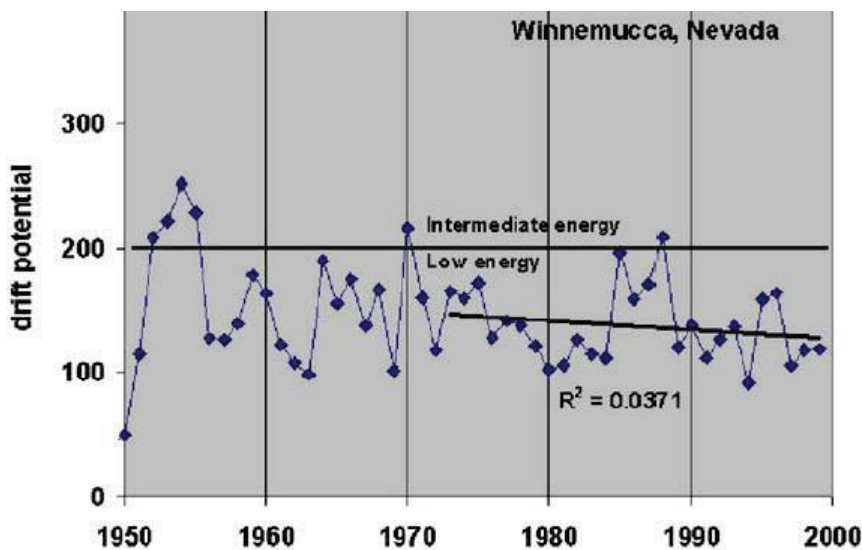


Figure 2.1: WeatherSpark model of wind records from Winnemucca WSO airport (1948-2013).



**Figure 2.2:** Wind rose diagrams of the Great Basin. Reprinted from *Geomorphology*, v.129, Jewell, P.W., Nicoll, K., Wind regimes and aeolian transport in the Great Basin, USA, Figure 2, p.3, © 2011, with permission from Elsevier. The diagrams were generated from meteorological observations recorded between the years 1950 to 2000. Dashed lines represent the resultant drift direction (RDD). Scale bars next to diagrams show the magnitude of resultant drift potential (RDP) in vector units.



**Figure 2.3:** Drift potential of sand at the Winnemucca WSO airport. Reprinted from *Geomorphology*, v. 129, Jewell, P.W., Nicoll, K., Wind regimes and aeolian transport in the Great Basin, USA, Figure 6, p. 7, © 2011, with permission from Elsevier. Drift potential (DP) calculated from meteorological observations between the years 1950 to 2000 at the Winnemucca WSO airport using the summation of 16 compass directions for wind velocities  $\geq$  6 meters per second ( $ms^{-1}$ ). The average drift potential for the period of measurement is  $\sim 143$  vector units.

## 2.4 Temperature

Temperature in Winnemucca is highly regulated by the presence of upper-level low pressure systems that settle and persist in the region during the spring months (Martin 2012). Compared to other locations in the Great Basin this setting will produce unusually lower mean temperatures during the transition between cold to warm seasons. In autumn these upper-level lows are regularly absent which allows for a rapid and continuous drop in daily mean temperature until shortly after the winter solstice. Following the solstice daily mean temperatures begin to gradually rise until late July (Martin 2012). Significant diurnal fluctuations in temperature are another distinguishing characteristic for the area. Day to night temperatures may change as much as  $16.7^{\circ}\text{C}$  in the winter and  $22.2^{\circ}\text{C}$  in the summer (Martin 2012).

Monthly temperature records from the Winnemucca WSO airport (Figure 2.4) were analyzed to determine the seasonal average temperature for the cold season months of October to March and warm season months of April to September. Dry adiabatic lapse rate calculations were also used to predict the annual average temperature, monthly maximum, monthly minimum, and daily extreme surface temperature at different altitudes inside of WDC. Additional records (Table 1) from meteorological monitoring stations at Paradise Valley Ranch and Jungo-Meyer Ranch were collected to assist lapse rate calculations. Each of the stations is distributed around the margin of WDC between the altitudes of 1281 meters above MSL (Jungo-Meyer Ranch) and 1426 meters above MSL (Paradise Valley Ranch). The sand dunes are vertically distributed between the altitudes of 1255 meters to 1703 meters above MSL.

Assuming a standard dry adiabatic lapse rate of  $9.8^0\text{C}$  per 1000 meters, the potential temperature at the lowest elevation in WDC was predicted using;

$$\text{Low elevation Temp.} = (\text{Jungo-Meyer Ranch } T^0) + [(1281-1255\text{m}) \times (0.0098^0\text{Cm}^{-1})].$$

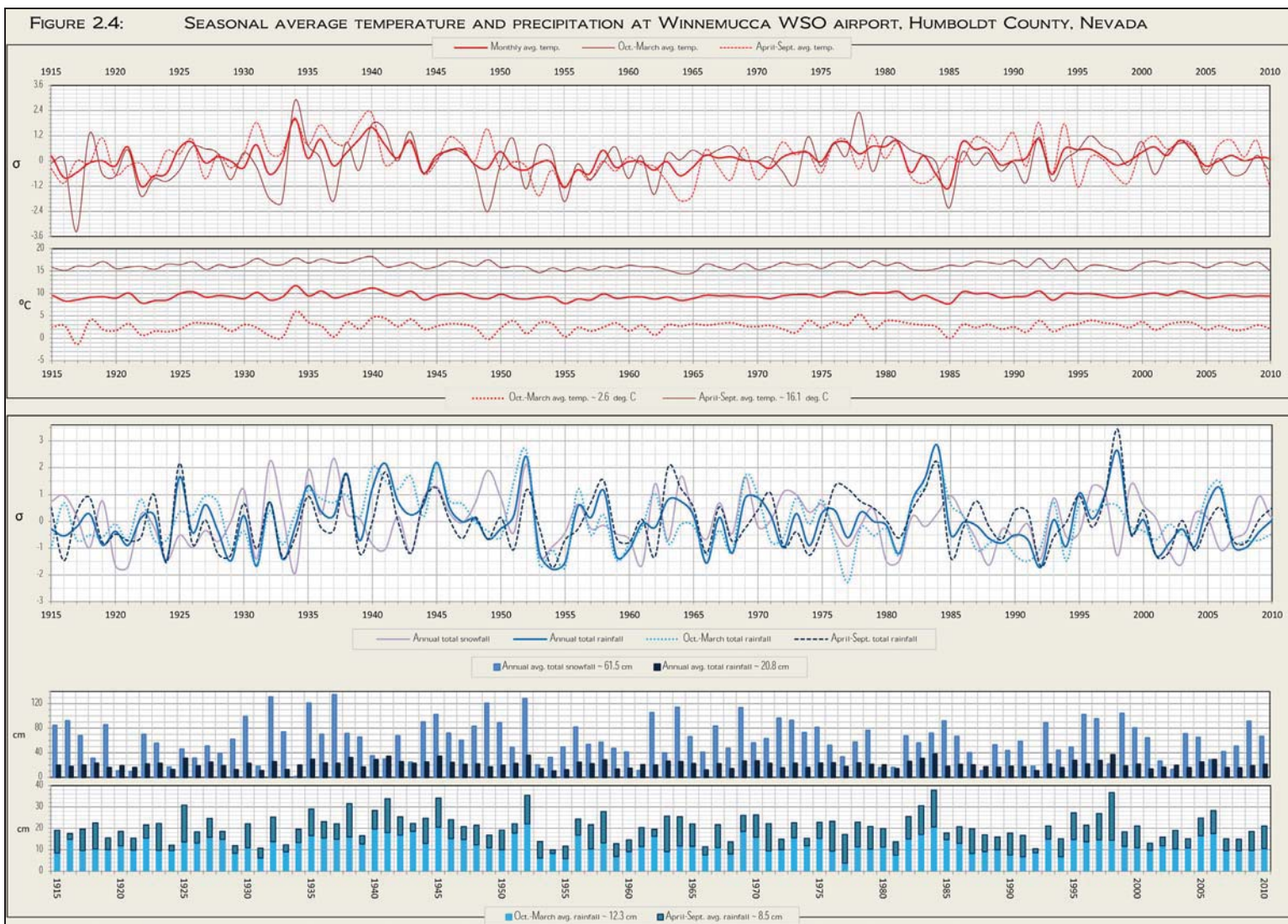
The potential temperature at the highest elevation in WDC was predicted using;

$$\text{High elevation Temp.} = (\text{Paradise Valley Ranch } T^0) - [(1703-1426\text{m}) \times (0.0098^0\text{Cm}^{-1})].$$

**Table 1:** Meteorological station data and results from dry adiabatic lapse rate calculations

	MEAN TEMPERATURE Station location	Years of observation	Elevation (m)	Annual Mean ( $^0\text{C}$ )	Monthly Max. ( $^0\text{C}$ )	Monthly Min ( $^0\text{C}$ )	Extreme Max. ( $^0\text{C}$ )	Extreme Min. ( $^0\text{C}$ )
1	Winnemucca WSO Airport	1877 - 2012	1310	9.4	18.3	0.6	38.7	-22.7
2	Paradise Valley Ranch	1894 - 2010	1426	8.8	17.9	-0.6	38.1	-22.9
3	Dry lapse rate @ + 277m		1703	6.1	15.2	-3.3	35.4	-25.6
4	Jungo-Meyer Ranch	1968 - 1986	1281	10.7	19.0	2.8	39.5	-17.5
5	Dry lapse rate @ -26m		1255	11.0	19.3	3.1	39.8	-17.2
			Avg.	9.2	17.9	0.5	38.3	-21.2
			Range(+, -)	1.8, -3.1	1.4, -2.7	2.6, -2.8	1.5, -2.9	4, -4.4

Calculations in Table 1 estimate within WDC the annual average temperature is  $9.2^0\text{C}$  with monthly average maximum and minimum temperatures of  $17.9^0$  to  $0.5^0\text{C}$ . The monthly average temperature during the cold season is  $2.6^0\text{C}$  (Figure 2.4) with monthly extreme minimum temperatures between  $-25.6^0$  to  $-17.2^0\text{C}$  (Table 1). The warm season monthly average temperature rises to  $16.1^0\text{C}$  (Figure 2.4) with monthly extreme maximum temperatures ranging from  $35.4^0$  to  $39.8^0\text{C}$  (Table 1).



## 2.5 Precipitation

Monthly rainfall records (Figure 2.4) from the years 1915-2010 at the Winnemucca WSO airport reveal an annual average rainfall of 20.8 centimeters. About 59% of total annual rainfall occurs between the cold months of October to March (12.3 cm). During the warm season months of April to September average total rainfall amounts are noticeably lower (8.5 cm).

The annual average snowfall (Figure 2.4) was determined using monthly snowfall records between the years 1915-2010 from the Winnemucca WSO airport and Golconda meteorological monitoring stations. Every year since 1915 snowfall varying from  $1.3 \text{ cm yr}^{-1}$  to  $134.6 \text{ cm yr}^{-1}$  has been recorded by at least one of the meteorological monitoring stations. Figure 2.4 estimates  $61.5 \text{ cm yr}^{-1}$  as the annual average snowfall during the period of 1915 to 2010.

## 2.6 Wildfires

Wildfires are profuse and common. The entire complex is located in Humboldt County which has the highest incidence rate of wildfires in the state of Nevada (Resource Concepts Inc. 2005). The Bureau of Land Management Nevada State Office reports that between the years 1980-2011 there were 1514 fire ignitions in Humboldt County which burned a total of 2,391,245 acres (BLM 2012; BLM 2013). Environmental assessments (BLM 2010) and geospatial data indicate at least 12 wildfires have occurred directly in or near the vicinity of WDC since 1985. Documented fires were in the years; 1985, 1986, 1987, 1996, 1999, 2000, 2001, 2003, 2006, 2011, 2012, and 2013. Fire return intervals for desert scrub (100-125 years) and sagebrush steppe-grasslands (50-85 years) habitats

have dramatically dropped since 1996. This has been attributed to the spread of invasive grasses and noxious weeds that have displaced indigenous plants resulting with a shortening of fire return intervals into the 5-8 year range (BLM 2013).

## 2.7 Vegetation

The general floral assemblage of WDC can be divided into 4 overlapping communities; grasslands, desert shrub, sagebrush steppe, and sand loving plants (psammophytes). Table 2 lists the species that were observed in the field during the course of this study.

Cheatgrass (*Bromus tectorum*) and Red brome (*Bromus rubens*) are the most abundant plants. They have successfully colonized most of the complex except the surface of active dunes and the playas in Desert Valley and Silver State Valley. Other invasive plants and noxious weeds known to occur in the area include; Salt cedar (*Tamarix ramosissima*), Perennial pepperweed (*Lepidium latifolium L.*), Leafy spurge (*Euphorbia esula L.*), Russian thistle (*Salsola tragus*), and Tumble mustard (*Sisymbrium altissimum*).

Grassland and desert shrub mix and broadly distribute across the entire complex. Desert shrub increases in density near water sources and is the predominant floristic community at low elevations in each valley. Grassland flora includes; Cheatgrass, Red brome, Tumble mustard, Russian thistle, Perennial pepperweed, Desert dandelion (*Taraxacum officinale*), Squirrel tail (*Sitanion hystrrix*), Sandberg bluegrass (*Poa sacunda*), Twisted cleomella (*Cleomella plocasperma*, Image #6) Fuzzy borage (*Cryptantha sp?*), and Money buckwheat (*Eriogonum nummulare*). Desert shrubs observed in the field consisted of; Black greasewood (*Sarcobatus vermiculatus*), Four-wing saltbush (*Atriplex canescens*), Shadscale (*Atriplex confertifolia*), Salt cedar, Bud sagebrush (*Picrothamnus*

*desertorum*), Lahontan and/or Alkali sagebrush (*Arbuscula longiloba* and/or *longicaulis*), and Gray horsebrush (*Tetradymia canescens*).

Vegetation belonging to the sagebrush steppe community is concentrated on the slopes and crests of the mountain ranges. Primary sagebrush steppe taxa include; Great Basin big sage (*Artemisia tridentata*), Gray ephedra (*Ephedra nevadensis*), Rubber rabbitbrush (*Chrysothamnus nauseosa*), and Green rabbitbrush (*Chrysothamnus viscidiflorus*). Understory plants are comprised of; Mule ears (*Wyethia mollis* and/or *amplexicaulis*), Rusty lupin (*Lupinus pusillus*), Cordelia beardtongue (*Penstemon floribundus*), Wild buckwheat (*Eriogonum sp?*), Crested wheatgrass (*Agropyron desertorum*), Great Basin wildrye (*Elymus cinerus*), Mariposa big pod lily (*Calochortus eurycarpus*), Pussy paws (*Cistanthe monandra*), and Indian paintbrush (*Castilleja sp?*).

Psammophytes (sand loving plants) are tabular and insular to sand dunes, intradune areas, and loose unconsolidated deposits of sand. Vegetation from this community is comprised of native forbs and herbaceous plants. The major psammophytic taxa include; West Humboldt wind loving buckwheat (*Eriogonum anemophilum*, Image #7), Sand veiny dock or Sand winged dock (*Rumex venosus*, Image #8), Desert sand verbena (*Abronia villosa*, Image #9), Transmontane sand verbena (*Abronia turbinata*), Lahontan indigo bush (*Psorothamnus kingii*), Nevada orcytes (*Orcytes nevadensis*), Dune primrose (*Oenothera deltoids*, Image #10), Desert globemallow (*Sphaeralcea ambigua*, Image #11), Cleome Fewleaf spiderflower (*Cleome sparsifolia*), Nevada dune beardtongue (*Penstemon arenarius*), Sharpleaf penstemmon (*Penstemon accuminatus*, Image #12), and Indian ricegrass (*Oryzopsis hymenoides*, Image #13).

The Nevada BLM and Nevada Natural Heritage Program (NNHP) have specially designated the following flora as sensitive at-risk species; Cordelia beardtongue, Nevada dune beardtongue, West Humboldt wind loving buckwheat, Money buckwheat, Lahontan indigo bush, and Nevada orcytes.

**Table 2:** Plant list for the Winnemucca Dune Complex

Community	Common name	Family	Genus species
All	Cheatgrass	Poaceae	<i>Bromus tectorum</i>
All	Red brome	Poaceae	<i>Bromus rubens</i>
All	Pussy paws	Portulacaceae	<i>Cistanthe monandra</i>
All	West Humboldt wind loving buckwheat	Polygonaceae	<i>Eriogonum anemophilum</i>
SS	Great Basin big sage	Asteraceae	<i>Artemisia tridentata</i>
SS	Gray ephedra	Ephemeraceae	<i>Ephedra nevadensis</i>
SS	Mariposa big pod lily	Liliaceae	<i>Calochortus eurycarpus</i>
SS-Dunes	Rusty lupin	Fabaceae	<i>Lupinus pusillus</i>
SS-Dunes	Desert moss	Pottiaceae	?
SS-Dunes	Cordelia beardtongue	Plantaginaceae	<i>Penstemon floribundus</i>
DS-SS	Squirrel tail	Poaceae	<i>Sitanion hystric</i>
DS-SS	Great Basin wildrye	Poaceae	<i>Elymus cinerus</i>
DS-SS	Crested wheatgrass	Poaceae	<i>Agropyron desertorum</i>
DS-SS	Sandberg bluegrass	Poaceae	<i>Poa sacunda</i>
DS-SS	Desert dandelion	Asteraceae	<i>Taraxacum officinale</i>
DS-SS	Mule ears	Asteraceae	<i>Wyethia (mollis and/or amplexicaulis)</i>
DS-SS	Rubber rabbitbrush	Asteraceae	<i>Chrysothamnus nauseosus</i>
DS-SS	Green rabbitbrush	Asteraceae	<i>Chrysothamnus viscidiflorus</i>
DS-SS	Bud sagebrush	Asteraceae	<i>Picrothamnus desertorum</i>
DS-SS	Lahontan and/or Alkali sagebrush	Asteraceae	<i>Arbuscula (longiloba and/or longicaulis)</i>
DS-SS	Desert marigold	Asteraceae	<i>Baileya multiradiata</i>
DS-SS	other Wild buckwheat	Polygonaceae	<i>Eriogonum sp?</i>
DS-SS	Money buckwheat	Polygonaceae	<i>Eriogonum nummulare</i>
DS-SS	Narrowleaf	Polygonaceae	<i>Rumex stenophyllus</i>
DS-SS	Fuzzy borage	Boraginaceae	<i>Cryptantha sp?</i>
DS-SS	Tumble mustard	Brassicaceae	<i>Sisymbrium altissimum</i>
DS-SS	Perennial pepperweed	Brassicaceae	<i>Lepidium latifolium L.</i>
DS-SS	Indian paintbrush	Orobanchaceae	<i>Castilleja sp?</i>
DS-SS	Leafy spurge	Euphorbiaceae	<i>Euphorbia esula L.</i>
DS-SS	Russian thistle	Chenopodiaceae	<i>Salsola tragus</i>
DS	Black greasewood	Chenopodiaceae	<i>Sarcobatus vermiculatus</i>
DS	Shadscale	Chenopodiaceae	<i>Atriplex confertifolia</i>
DS	Gray horsebrush	Asteraceae	<i>Tetradymia canescens</i>
DS	Four-wing saltbush	Amaranthaceae	<i>Atriplex canescens</i>
DS	Salt cedar	Tamaricaceae	<i>Tamarix ramosissima</i>
DS-Dunes	Twisted cleomella, Alkali stinkweed	Cleomaceae	<i>Cleomella plocasperma</i>
DS-Dunes	Cleome Fewleaf spiderflower	Cleomaceae	<i>Cleome sparsifolia</i>
DS-Dunes	Nevada dune beardtongue	Plantaginaceae	<i>Penstemon arenarius</i>
DS-Dunes	Sharpleaf penstemon	Plantaginaceae	<i>Penstemon accuminatus</i>
DS-Dunes	Indian ricegrass	Poaceae	<i>Oryzopsis hymenoides</i>
DS-Dunes	Desert globemallow	Malvaceae	<i>Sphaeralcea ambigua</i>
DS-Dunes	Transmontane sand verbena	Nyctaginaceae	<i>Abronia turbinata</i>
Dunes	Desert sand verbena	Nyctaginaceae	<i>Abronia villosa</i>
Dunes	Sand veiny dock, Sand winged dock	Polygonaceae	<i>Rumex venosus</i>
Dunes	Dune primrose	Onagraceae	<i>Oenothera deltoides</i>
Dunes	Lahontan indigo bush	Fabaceae	<i>Psorothamnus kingii</i>
Dunes	Nevada orcytes	Solanaceae	<i>Oryctes nevadensis</i>
Lil. Humboldt	Coyote willow, Sandbar willow?	Salicaceae	<i>Salix exigua</i>
ALL = PRESENT IN ALL AREAS			
DS = DESERT SHRUB & GRASSLANDS			
SS = SAGEBRUSH STEPPE			
DUNES = PSAMMOPHYTE "SAND LOVING PLANTS"			
DUNES, INTRADUNES & LOOSE UNCONSOLIDATED DEPOSITS OF SAND			

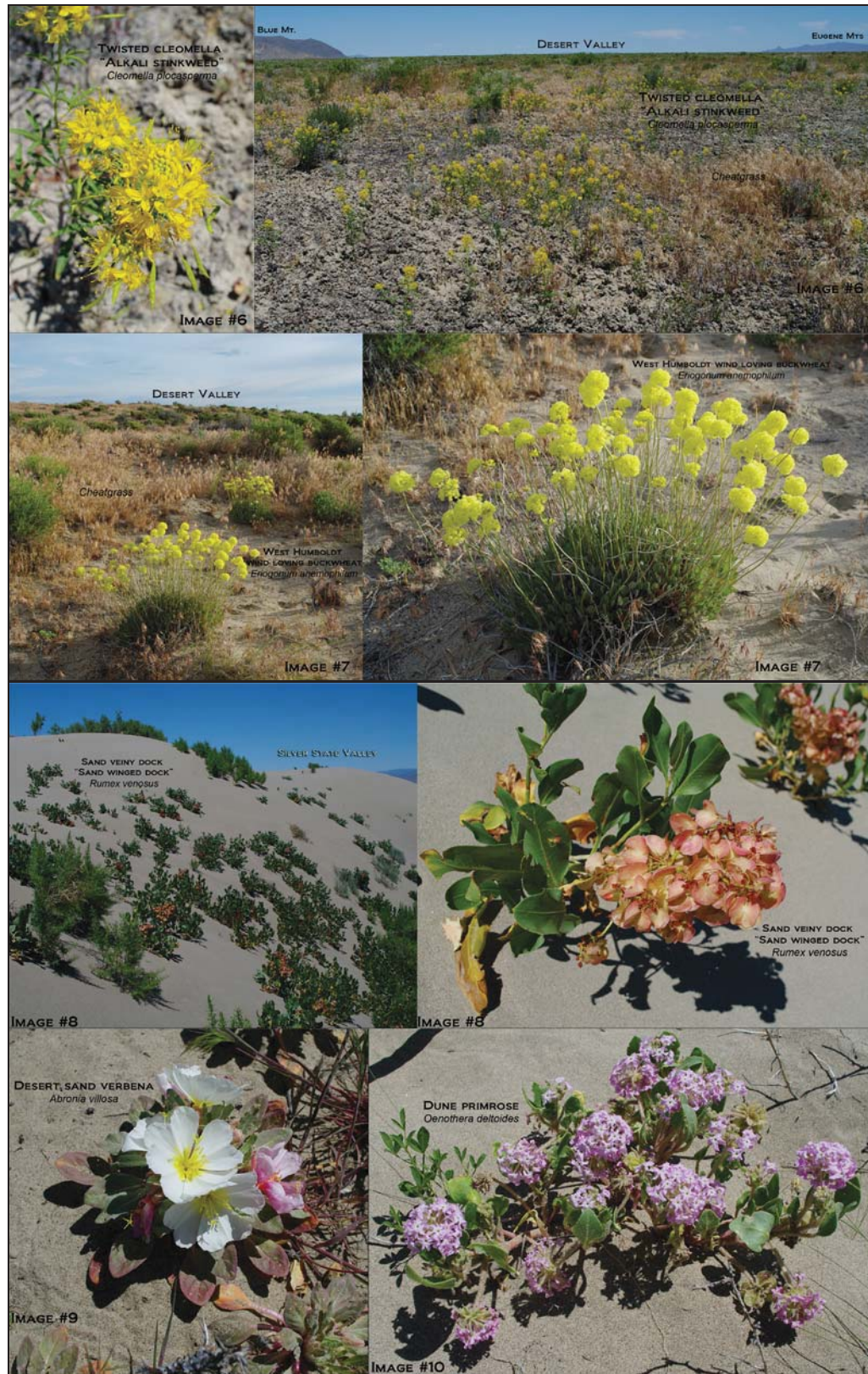


**Image #6-10:** Twisted Cleomella, West Humboldt wind loving buckwheat, Sand veiny dock, Desert sand verbena, and Dune primrose.

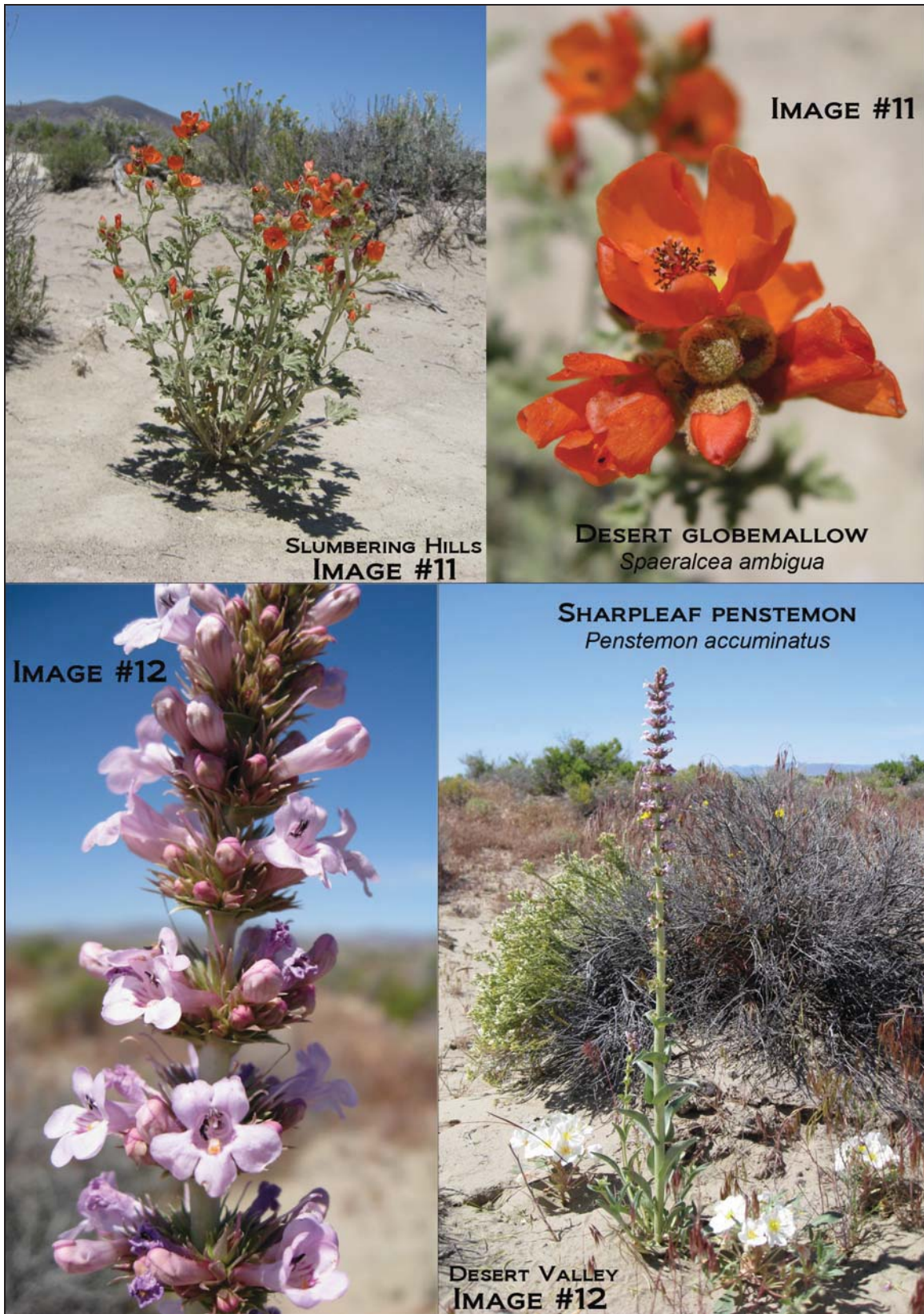


Image #11-12: Desert globemallow and Sharpleaf penstemon.

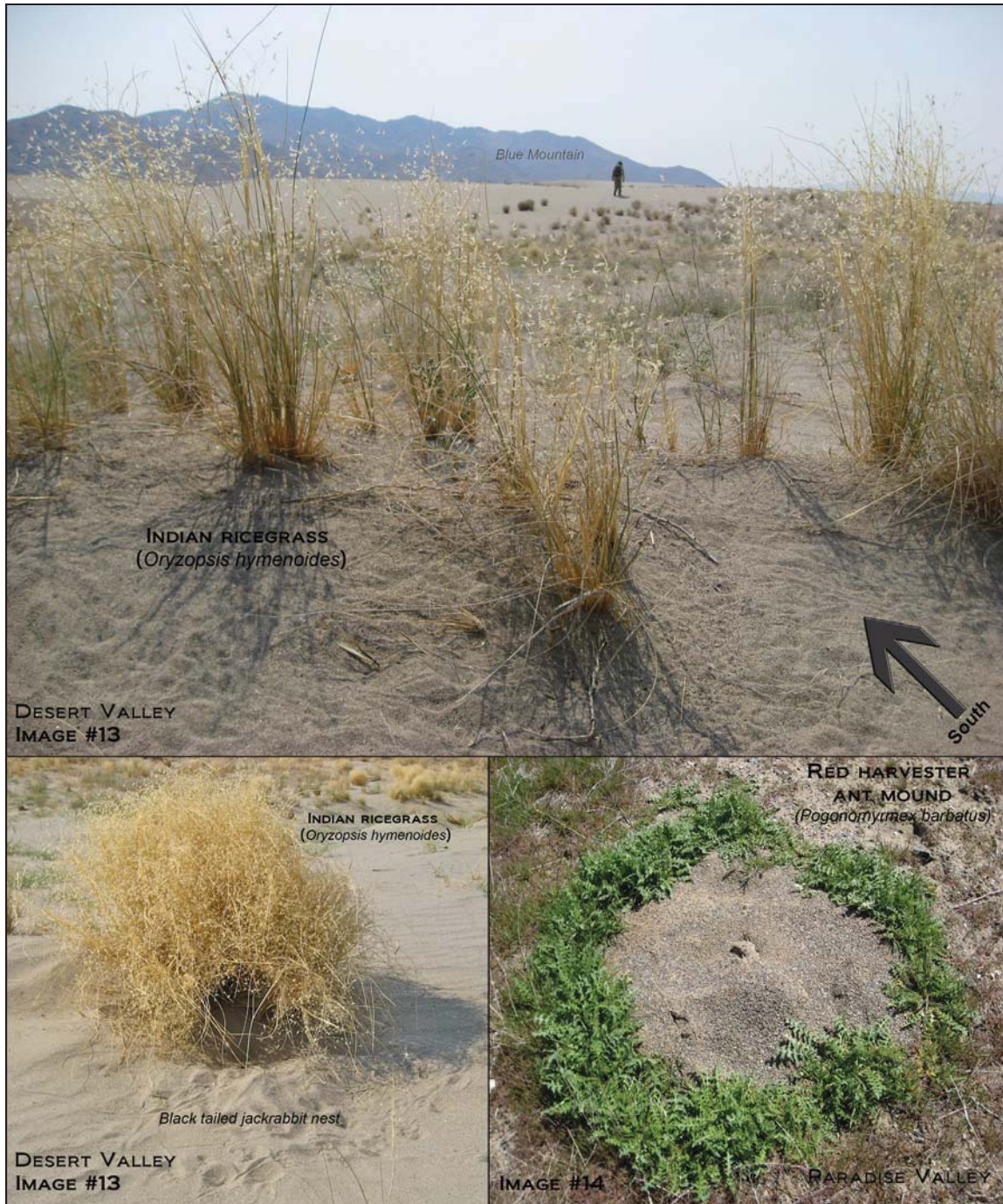


Image #13-14: Indian ricegrass and Great Basin Red harvester ant mound.

## 2.8 Wildlife

The most successful organism (excluding humans) in WDC is clearly the Great Basin Red harvester ant (*Pogonomyrmex barbatus*). Every available landscape surface not covered by active sand dunes or irrigated for agricultural purposes has been colonized by Red harvester ants. Ant nests occasionally include a stripped area with a fertilized crop circle (Image #14) surrounding an entrance mound (sometimes covered in vegetative litter) composed of sand and pebbles. The mounds are ~1.5 meters in width and have elaborate tunnel systems that can stretch over 10 square meters.

Other insect populations documented in WDC (Hardy & Andrews 1987; Epps et al 1998; Federal Register 2007; BLM 2013<sup>1</sup>) include; Bleached sandhill skipper (*Polites sabuleti sinemaculata*), Rice's blue butterfly (*Euphilotes pallescens ricei*), Honey Lake blue butterfly (*Euphilotes pallescens calneva*), Darkling sand dune obligate beetle (*Eusattus muricatus*), and the Humboldt serican scarab (*Serica humboldti*).

Desert horned (*Phrynosoma platyrhinos*) and Long-nosed leopard lizards (*Gambelia wislizenii*) routinely burrow into the sides of stabilized dunes close to insect nests. The Great Basin collared lizard (*Crotaphytus bicinctores*), and Great Basin fence lizard (*Sceloporus occidentalis*) are also present in shrubbery adjacent to playas and drainage channels. Digested and partially magnetized phalanx bones of Great Basin fence lizards can occasionally be found in active and stable sand dunes.

Large game Pronghorn (*Antilocapra americana*) and Mule deer (*Odocoileus hemionus*) inhabit the region year-round feeding off desert shrub, grasses, and adjacent farmlands. Prior to extensive BLM roundups in the late 2000s wild horses freely roamed many areas

in the region. Encounters are infrequent but wild horses can still be spotted near farmland in Desert Valley. Bobcats (*Lynx rufus*) are present although it is uncertain whether or not they build dens inside the complex. Borrowing mammals and reptiles that inhabit WDC normally reside on the sides of parabolic dune tails, tops of vegetated linear dunes, and sporadically among stabilized sand dunes.

Other faunal species confirmed to populate WDC (BLM 2007; BLM 2010; BLM 2013) include; Kit fox (*Vulpes macrotis*), Pygmy rabbit (*Brachylagus idahoensis*), Black tailed jackrabbit (*Lepus californicus*), American badger (*Taxidea taxus*), Coyote (*Canis latrans*), Bushy-tailed woodrat (*Neotoma cinerea*), Desert kangaroo mouse (*Dipodomys deserti*), Desert Valley dark kangaroo mouse (*Microdipodops megacephalus albiventer*), Deer mouse (*Peromyscus maniculatus*), Great Basin rattlesnake (*Crotalus oreganus*), and the Great Basin gopher snake (*Pituophis catenifer deserticola*).

The only avifauna recognized (BLM 2010; BLM 2013) to dwell inside the complex is the Western burrowing owl (*Athene cunicularia hypugaea*). Upland game birds comprised of Greater sage-grouse (*Centrocercus urophasianus*), Chukar partridge (*Alectoris graeca*), and Mourning dove (*Zenaida macroura*) are frequently observed along the perimeter of WDC in the sagebrush steppe of the Slumbering Hills, Krum Hills, Ten Mile Hills, and Bloody Run Hills. During the daytime Golden eagles, Prairie falcons, and Turkey vultures circle the dunes in search of dead or distressed prey. Piles of midden from crows, ravens, and vultures accumulate at the crest of tall dunes in many portions of the complex.

The Nevada BLM and NNHP have specially designated the following fauna as sensitive at-risk species; Greater sage grouse, Pygmy rabbit, Western burrowing owl, Kit fox, Desert Valley dark kangaroo mouse, Desert kangaroo mouse, Desert horned lizard, Long-nosed leopard lizard, Great Basin collared lizard, Humboldt serican scarab, Bleached sandhill skipper, Rice's blue butterfly, and the Honey Lake blue butterfly.

The United States Fish & Wildlife Service (USFWS) has also listed; Bleached sandhill skipper, Pygmy rabbit, Western burrowing owl, Desert Valley dark kangaroo mouse, and Desert kangaroo mouse as species of concern. Recently the USFWS announced that the Greater sage grouse has become a threatened species candidate and anticipates it will be formally added to the list in the near future.

## CHAPTER 3: LOCAL GEOLOGY

### **3.1 Introduction**

The local geology of Desert Valley, Silver State Valley, and Paradise Valley that is relevant to WDC will be chronologically discussed in this chapter.

### **3.2 Mesozoic bedrock**

Mesozoic basement rocks underlie portions of the valleys and constitute the core of the mountains in the region. They are a thick 6 km allochthonous package of late Triassic (early-middle Norian stage) to early Jurassic metasedimentary bedrock (Wyld 2000). In the areas directly surrounding WDC the basement rocks have been lithostratigraphically designated to the following formations; Raspberry, Grass Valley, Singas, O'Neill, and the Auld Lang Syne Group (Compton 1960; Willden 1964; Burke & Silberling 1973; Elison & Speed 1989; Wyld 2002; Gustin et al 2007). The rocks are compositionally derived of fine grained siliciclastic, volcaniclastic, and carbonate-rich material that accumulated in a deep marine basin and shallow continental shelf (Wyld 2000). Following deposition the sediments were uplifted in a back-arc setting, metamorphosed into a hornfels-greenschist facies (Colgan et al 2004; Gustin et al 2007), and tightly folded ~153-100 Ma (Wyld et al 2001) by the Luning-Fencemaker fold-and-thrust belt (Figure 3.1). These particular events produced a diverse assemblage of phyllite, slate, shale, quartzite, sandstone, siltstone, and mudstone. Previous researchers have referred to the formations as members of the Jungo terrane (Silberling et al 1987) or Fencemaker allochthon (Oldow 1984).

The Singas Formation is exposed in the northeast corner of WDC and underlies the sand dunes in the Bloody Run Hills (Compton 1960; Lupe & Silberling 1985). In the western

medial section and south-southwestern boundary of the complex scattered outcrops of the Raspberry and O'Neill Formations are present in the Slumbering Hills, Ten Mile Hills and on the northern slopes of Blue Mountain (Anderson 2013). Quartzite from the O'Neill Formation is reported by Lauha et al (2010) to form distinct ridges on the southern side of the Slumbering Hills just to the north-northwest of the sand dunes. The Grass Valley Formation is found on the western slopes of Blue Mountain (Fairbank & Ross 1999) but is less abundant in the vicinity of WDC. In general, outcrops from the Jungo terrane are mostly subdued and in many areas they are mantled with sand, dust, fluvio-lacustrine deposits, and alluvium.

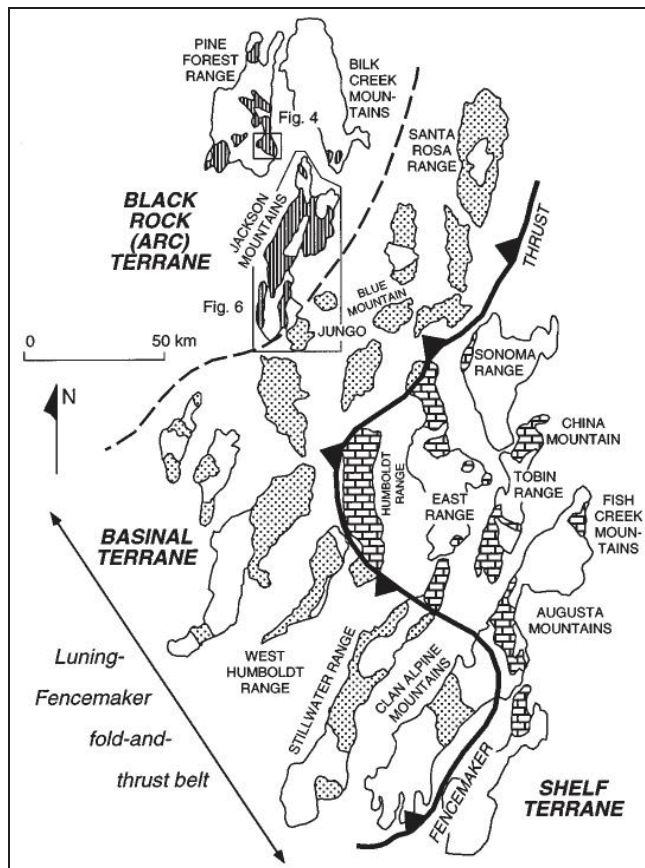


**Figure 3.1:** Location of Luning-Fencemaker fold-and-thrust belt. Reprinted with permission from: Wyld, S., 2000, Triassic evolution of the arc and backarc of northwest Nevada, and evidence for extensional tectonism: *Geological Society of America Special Paper 347*, Fig. 1, 23 p.

### **3.3 Cretaceous intrusions**

Throughout the hills and ranges the Jungo terrane is intruded by discontinuous Cretaceous plutons, stocks, and dikes of granodiorite that are accompanied by a thin section of tonalite (~102 Ma; Wyld et al 2001). Colgan et al (2006) have estimated an age of the granodiorite in the Santa Rosa Range and Slumbering Hills between 116-98 Ma. The most apparent intrusions of granodiorite form short steep cliffs along the eastern flank of the Jungo Hills in Desert Valley and the central section of the Slumbering Hills. Anderson (2013) has mapped additional outcrops of granodiorite on Blue Mountain and in the Ten Mile Hills. Exposures of tonalite are limited to the western flanks of the Santa Rosa Range to the north of the sand dunes in Silver State Valley and Quinn River Valley (Compton 1960; Rogers 1999; Wyld et al 2001).

### **3.4 Tertiary volcanic deposits**

Younger bedrock associated with the Nevada Ignimbrite flare-up, Yellowstone hotspot, McDermitt-Santa Rosa volcanic field, and the Northern Nevada Rift overlies and intrudes the Jungo terrane and Cretaceous plutons in many portions of the precinct. Surface exposures occur in tracts of the Jungo Hills, Slumbering Hills, Ten Mile Hills, Krum Hills, and Bloody Run Hills. They form small jagged buttes that are partially mantled by sand, fluvio-lacustrine gravel bars, beach deposits, and encrustations of tufa at elevations below 1340 meters above MSL.

#### ***Nevada Ignimbrite flare-up***

The oldest units from the volcanic suite are primarily composed of ash-flow tuffs, pumice lapilli, and canyon filling basalt flows that erupted during the Nevada Ignimbrite flare-up

between 46-19.5 Ma (Henry & John 2013). Figure 3.2 shows the approximate location of the affiliated calderas and direction of correlated flows which extensively covered the topography on the eastern segment of the complex. Several of the ignimbrites crop out within the sand dunes on the Slumbering Hills and others protrude in the Ten Mile Hills and Krum Hills.

On the western flanks of the saddle between the Slumbering Hills and Ten Mile Hills at the Sandman project North Hill site are a variety of volcanic flows, rhyolite-dacite tuffs, pyroclastic, and epiclastic deposits that resulted from the flare-up. The deposits have been thoroughly mapped by Anderson (2013) and are documented to include; basaltic trachy-andesite ( $22.53 \pm 0.04$  Ma), Nine Hill ash-flow tuff (~25.4 Ma), and mixtures of undifferentiated, lapilli lithic, vitric, fiamme, and pumice rich tuffs. Oligocene-Miocene siltstone, sandstone, sharpstone, and conglomerate interbed with the volcanic rocks. The owners (Newmont Mining Corp.) of the Sandman project have informally used their own nomenclature to describe the sequence as the Comforter Basin Formation (Lauha et al 2010). Parts of the formation are shown to outcrop in or directly underlay the sand dunes at the North Hill site (Figure 3.3). The most notable are exposures of conglomerate along the saddle between the Slumbering Hills and Ten Mile Hills. Outcrops and buried sections are composed of thin foreset, topset, and chaotic beds of silty sand with pebbles that support subrounded to rounded gravels. All of the sediments from the conglomerate exhibit mineralogical provenance from basement rocks in the Jungo terrane and units in the Comforter Basin Formation (Anderson 2013). Near the south side of the Crescent-Sombrero Complex (Map 1; Plate 3.1) on the Slumbering Hills the Comforter Basin

Formation is estimated to reach 198-244 meters in thickness (Figure 3.3; Anderson 2013).

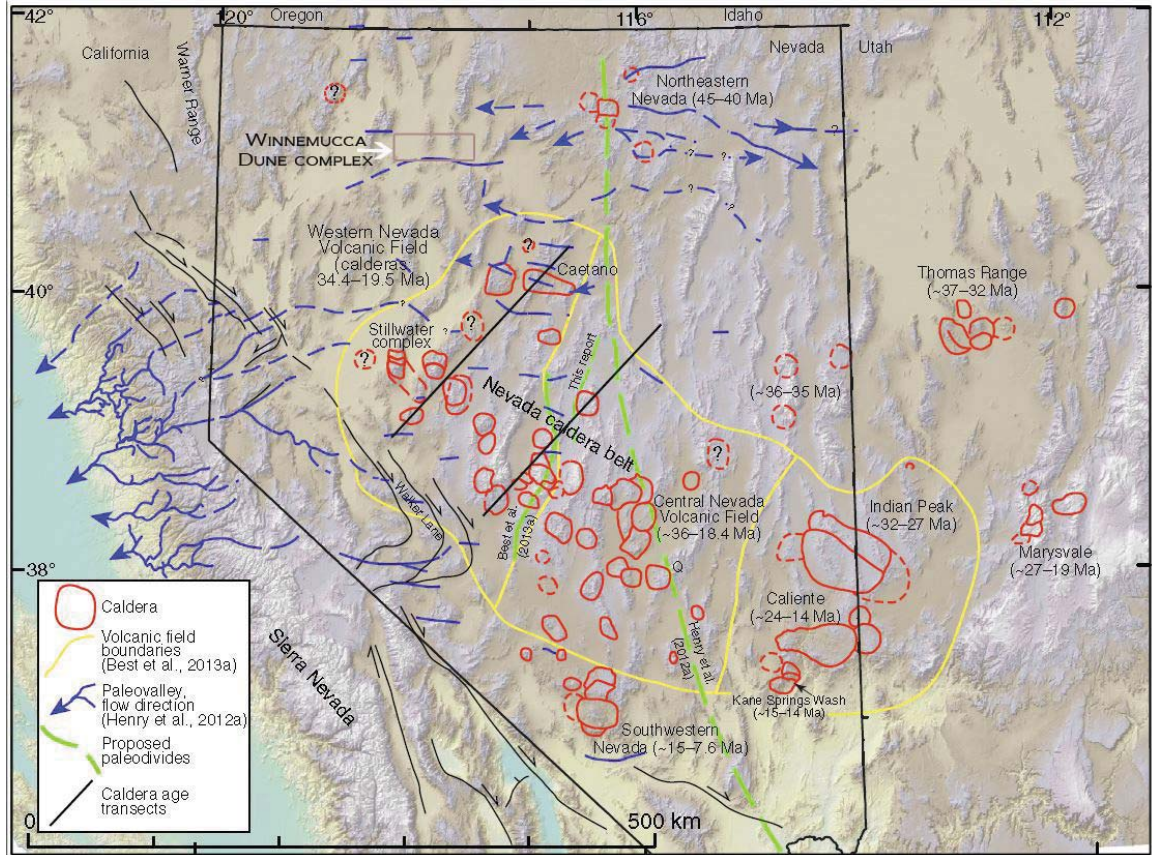


**Figure 3.2:** Location of the Nevada Ignimbrite flare-up. Reprinted with permission from: Henry, C.D., John, D.A., 2013, Magmatism, ash-flow tuffs, and calderas of the ignimbrite flareup in the western Nevada volcanic field, Great Basin, USA: *Geosphere*, v. 9, no. 4, p. 951-1000, Figure 1. Location of WDC added to figure.

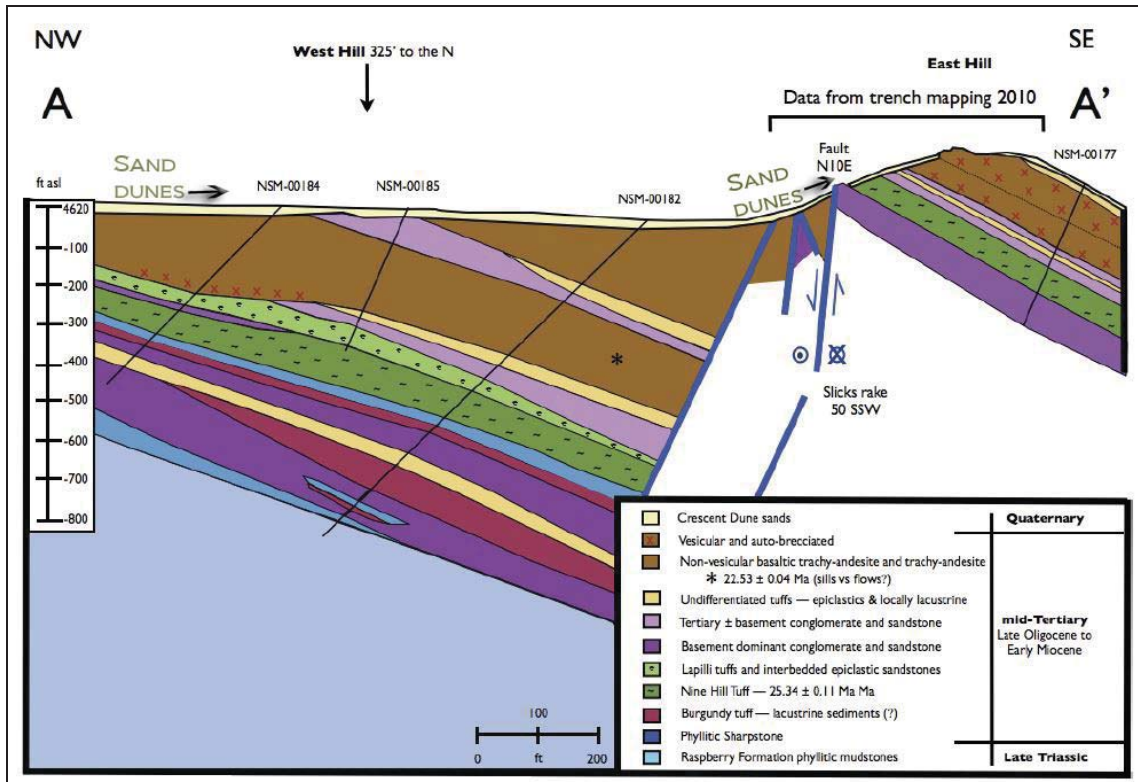


**Figure 3.3:** Detailed geologic cross section of the North Hill deposit at the Sandman project site. Reprinted from open source document: Anderson, R.M., Jr., 2013, Stratigraphy of the Sandman low sulfidation Au deposits, Winnemucca, Nevada [M.S. Thesis]: University of Nevada, Reno, Figure 25, 175 p. Direction of sand dune advancement added to figure.

### ***McDermitt-Santa Rosa volcanic field and the Yellowstone hotspot***

The second oldest volcanic rocks in the demesne of WDC are inconspicuous but widespread to the north in Kings River Valley, Quinn River Valley, and the Slumbering Hills. These rocks are related to the formation of the McDermitt-Santa Rosa volcanic field (Figure 3.4) and migration of the Yellowstone hotspot (Colgan et al 2004). The McDermitt-Santa Rosa volcanic field created a series of calderas which erupted and collapsed  $\sim 17.3$ – $13.6$  Ma (Nash et al 1995; Conrad et al 1993). Each of the eruptions discharged numerous types of pyroclastics and lava flows which include; air-fall ash, vitreous glass, pumice lapilli, ash-flow tuffs (welded and un-welded), lithic ash-flows, trimodal lava flows, sills, dikes, and domes composed of rhyolite, dacite, and basalt.

Secondary sedimentary deposits of seismically-induced debris flows (Giroux et al 2008) were also triggered during the eruptions.

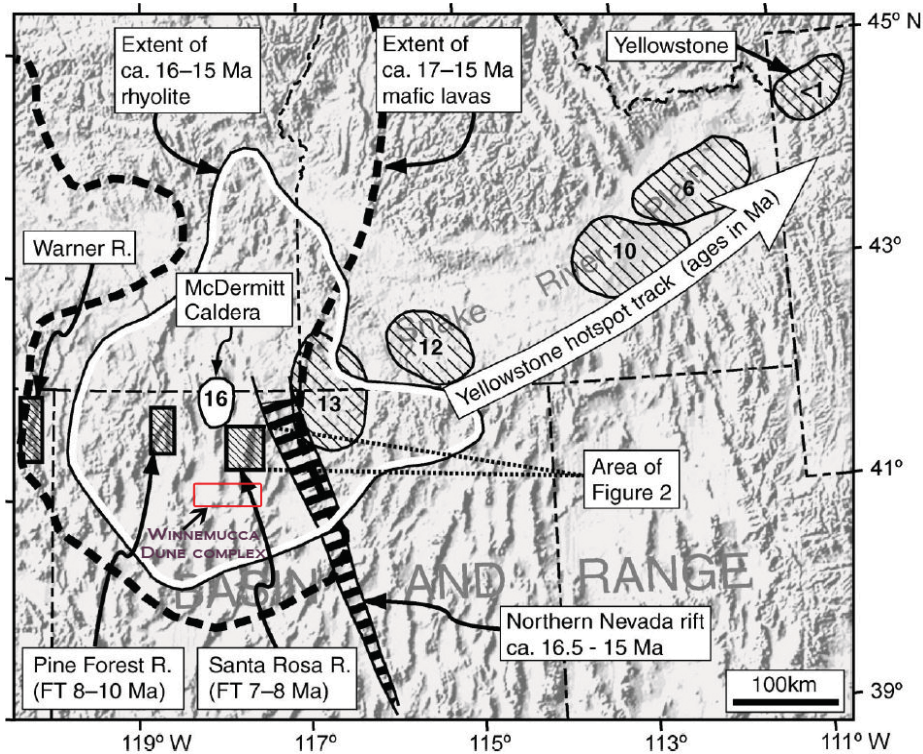


**Figure 3.4:** Location of the McDermitt caldera and Yellowstone hotspot. Reprinted with permission from: Colgan, J.O., Dumitru, T.A., Miller, E.L., 2004, Diachroneity of Basin and Range extension and Yellowstone hotspot volcanism in northwestern Nevada: *Geology*, v. 32, no. 2, Figure 1, p. 121-124. Location of WDC added to figure.

### Northern Nevada Rift

Shortly after the inception of the McDermitt-Santa Rosa volcanic field ~16.5-15 Ma (John et al 2000) a system of tectonic rifts coevally developed with the passage of the Yellowstone hotspot (Figure 3.4). The system is referred to as the Northern Nevada Rift (NNR). Hypabyssal diorite-gabbro (Wyld 2002) and volcanic dikes of andesite-basalt (John et al 2000) were emplaced through the rifts. During its initiation at least 2 parallel lineaments named the NNR Central and NNR Western (Ponce et al 2010) formed through WDC (Figure 3.5). The rifts released mafic dikes and swarms that intruded older rocks

in Desert Valley, Slumbering Hills, Krum Hills, Ten Mile Hills, and Silver State Valley. Geothermal fluids accumulated along the structures of NNR and have persisted to the present time. In the Miocene epoch the dispersion of these fluids along NNR lineaments and intersections of north & east-northeast trending faults (Anderson 2013) permitted hydrothermal alteration and secondary mineralization within host rocks. High sulfidation enrichment of magmatic stockworks and low-sulfidation epithermal alteration of deposits from the McDermitt-Santa Rosa volcanic field and Comforter Basin Formation created omnifarious grades of Ag-Au ore. Segments of the deposits are currently being extracted at the Sleeper Mine and prospected for at the Sandman project site in the Slumbering Hills and Ten Mile Hills (Gustin et al 2007; Giroux et al 2008; Anderson 2013).

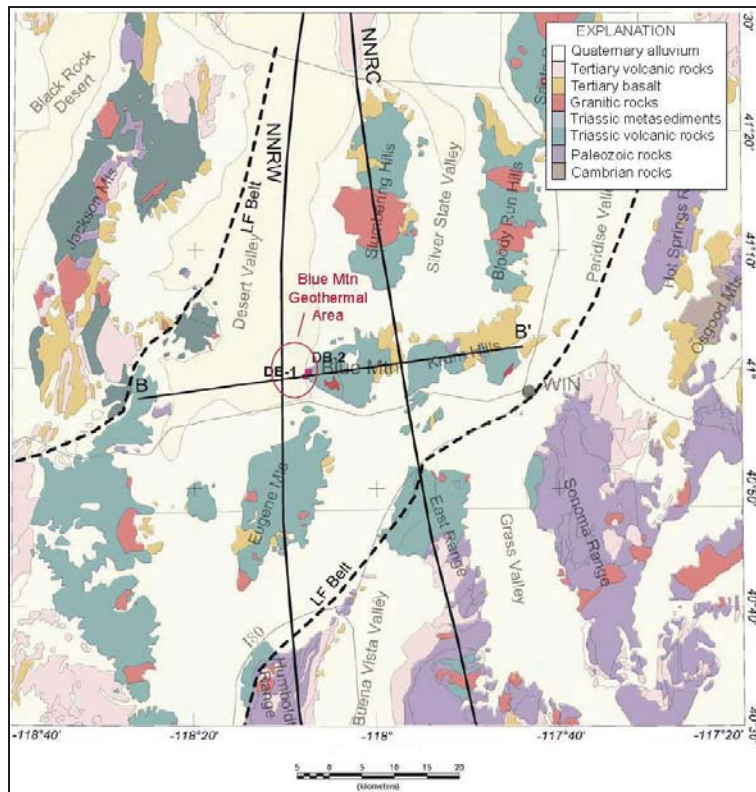


**Figure 3.5:** Location of the Northern Nevada Rift Central & Western sections. Reprinted with permission from: Ponce, D.A., Glen, J.M., Watt, J.T., Casteel, J., 2010, Geophysical Setting of the Blue Mountain Geothermal Area, North-Central Nevada and its Relationship to a Crustal-Scale Fracture Associated with the Inception of the Yellowstone Hotspot: *Geothermal Resources Council Transactions*, v. 34, Figure 1, p. 881-885.

### 3.5 Pliocene to Holocene sedimentary deposits

Excluding the sand dunes, late Neogene and Quaternary sedimentary deposits are abundant and non-conformably overlay a majority of the landscape surrounding WDC. These surficial features include deposits of alluvium, colluvium, lacustrine shorelines and strandlines related to the Eetza and Sehoo alloformations of Lake Lahontan.

Alluvial fans can be grouped into old and young deposits. The oldest alluvial fans are moderately incised, partially varnished, and located just below the mountain ridges. In each of the mountain ranges at an elevation of 1318-1334 meters above MSL the oldest alluvium tapers into middle to late Pleistocene highstand shorelines of Lake Lahontan. Conrad et al (1993) sampled a 2.1 Ma tephra from the oldest alluvium above the Sleeper Mine in the Slumbering Hills. The dated tephra suggests the oldest alluvium is at least late Pliocene in age. Young alluvial fans are located below the oldest alluvium along the lower slopes of the mountain ranges. The young alluvial fans are flat, planar, and have moderate to well-defined silt skirts. A majority of the young alluvial fans drain through the middle to upper Sehoo period shorelines from Lake Lahontan. The cross-cutting relationship implies the youngest alluvium must have started forming after the late Pleistocene to early Holocene epochs.

Lacustrine deposits from Lake Lahontan surround most of WDC and rim the mid-slopes on the mountains. The highest shorelines and wave-cut terraces bisect the aprons of the oldest alluvium and engrave bedrock on the ranges. Stratigraphic evidence from Lake Lahontan in northern Nevada signifies the lake had four trans-regressive cycles (lacustrals) that are split and described by Morrison (1991) from lower most unit

upwards; unnamed unit (age undetermined), the Rye Patch (610-635 ka), Eetza (350-130 ka), and Sehoo (35-8 ka) alloformations. In the vicinity of WDC geomorphic features that resulted from oscillations in lake-level consist of: offshore-near shore laminar beds of sandy silt, flat to inclined foreshore beds of silty sand with pebbles, gravel & sand beaches, back-beach embankments, shallow embayments, lagoons, barrier bars, v-bars, alluvial deltas, spits, tombolos, and wave-cut terraces. Precipitation of calcium carbonate from the mixing of lake water also produced deposits of lithoid and dendritic tufa.

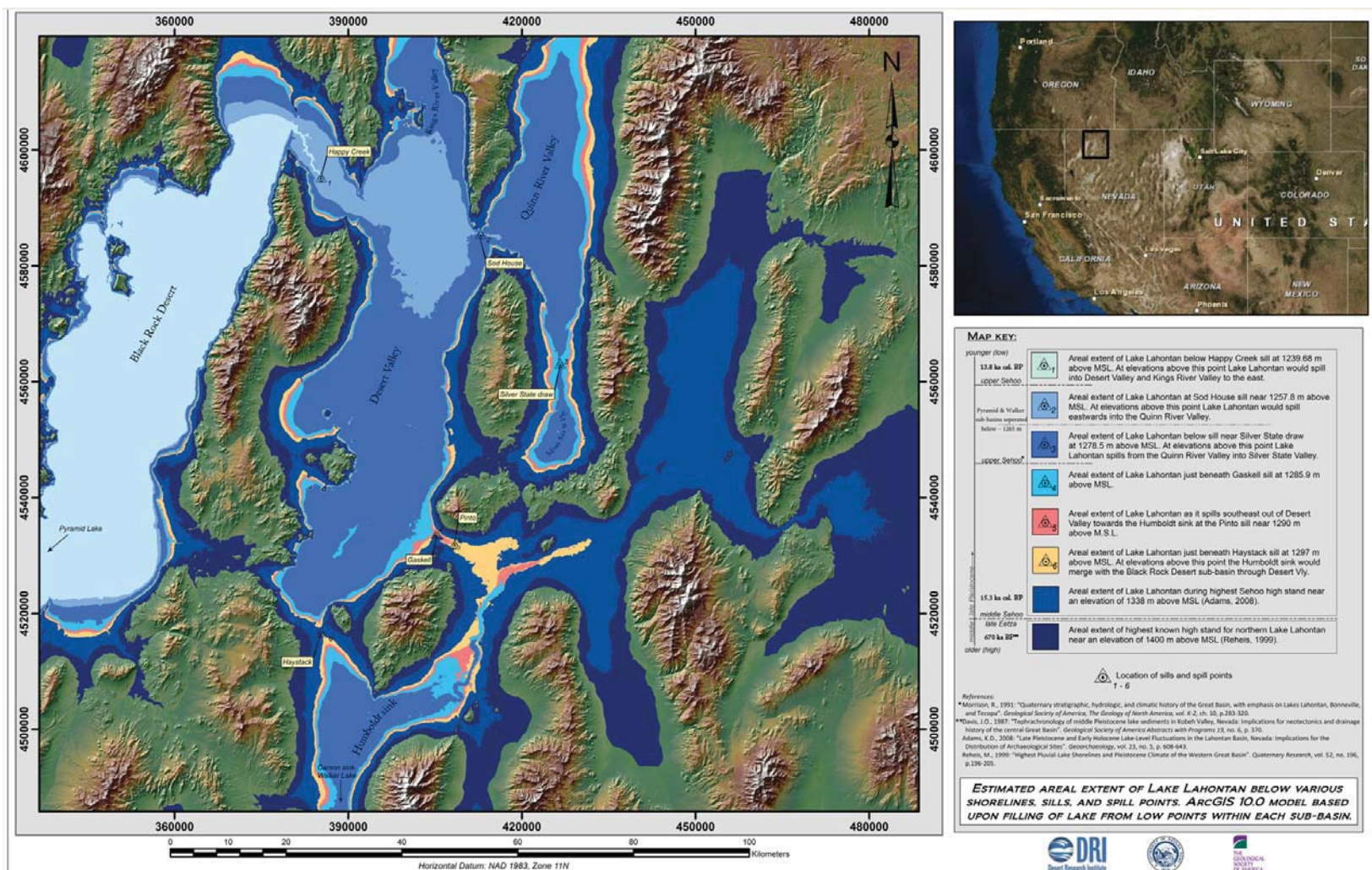
The highest shorelines of Lake Lahontan correlate to either the Rye Patch or Eetza alloformations that are documented (Davis 1987) and mapped (Reheis 1999) up to a maximum elevation of 1400 meters above MSL. The Rye Patch and Eetza footprint is obscure in WDC. However a disjunct sequence of 3 to 4 wave-cut bedrock terraces near subbasin outlet-inlets and topographic gaps in the Jungo Hills, Eugene Mountains, Blue Mountain, Ten Mile Hills, Krum Hills, and the Santa Rosa Range may be representative of these lacustral periods.

Stratigraphy from the Sehoo alloformation marks a sustained highstand near the middle of the lacustral during the late Pleistocene (Morrison 1991; Benson, Kashgarian & Rubin 1995) at  $\sim 15.22 \pm 0.12$  ka cal. BP (Adams & Wesnousky 1998) between the elevations of 1338-1340 meters above MSL (Adams et al 2008). A minimum age of  $\sim 15.15$  ka for the highstand was estimated using varnish microlamination layering by Liu & Broecker (2013). After the Sehoo highstand Lake Lahontan rapidly lowered to below 1238 meters above MSL by  $\sim 13.8$  ka cal. BP (Thompson, Benson & Hattori 1986). Deposits from the retreat of Lake Lahontan are extensive and copiously form a succession of 10 to 11 low

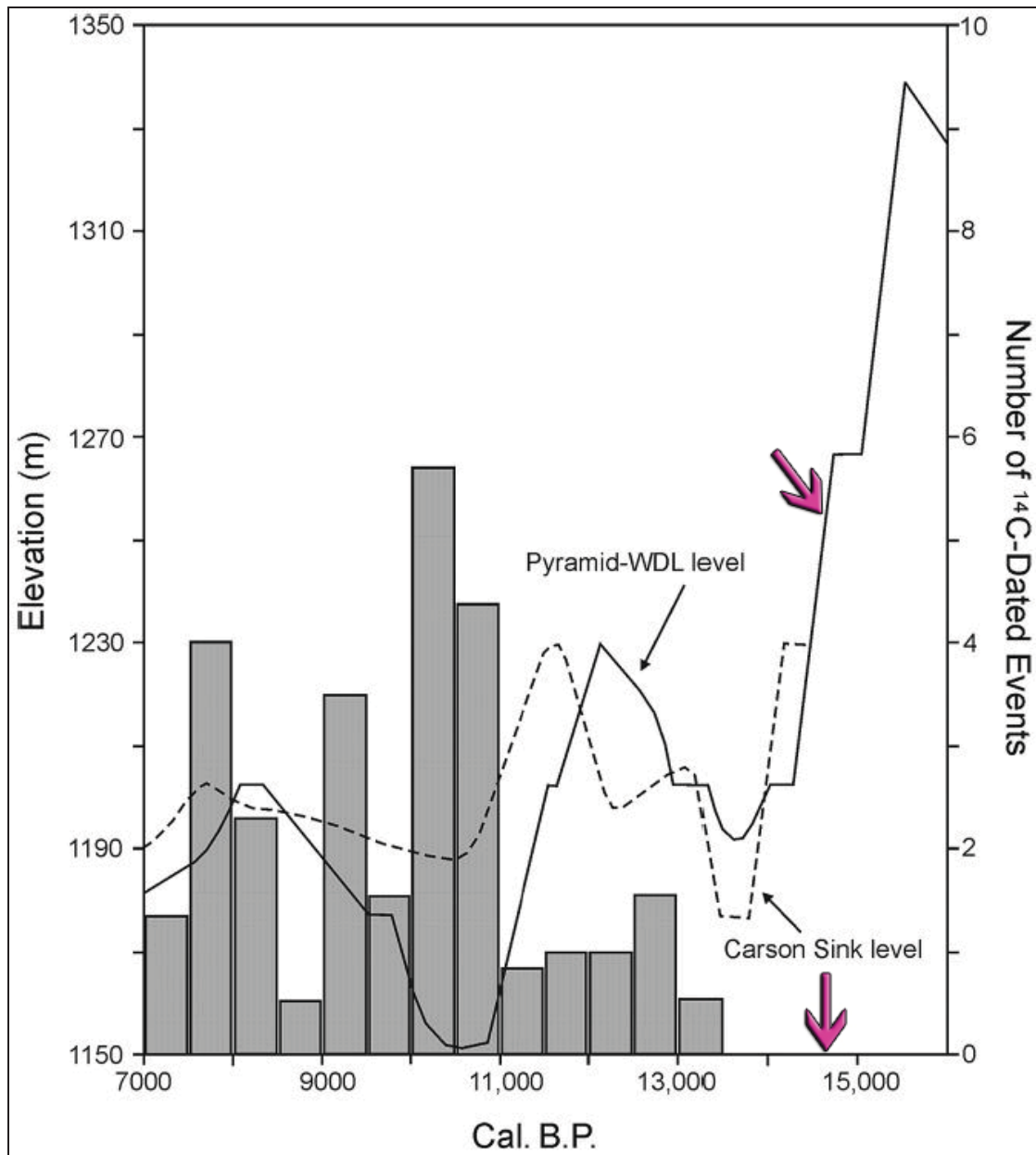
lying linear to arcuate shaped beaches. The deposits off-lap and down-lap below the highest discernable strandline on the Slumbering Hills (Dufurrena & Rigby 1988), western flanks of the southern Santa Rosa Range, and northern flanks of the Krum Hills.

Figure 3.6 shows a hypothetical visualization for the spatial extent of Lake Lahontan and the location of relevant sills during the Eetza and Sehoo stages. It is clear from the figure that wind-blown sand could not transport across each of the valleys until the beginning of the upper Sehoo when lake-level dropped to the elevation of the sill at Sod House (1257.8 meters above MSL). Dune formation may have existed prior to this time amidst the mountain passes on the Slumbering Hills and Bloody Run Hills. Nonetheless an extensive dune field would have not been possible until Lake Lahontan and water trapped in Desert Valley and Silver State Valley permanently receded below 1255-1278 meters above MSL. At 1255 meters above MSL no water would remain in any of the valleys and the eolian transport of sand would only be hindered by climate, vegetation, and topographic obstacles.

The model on Figure 3.6 demonstrates it is highly plausible that WDC began to spread into a large complex sometime between 15.3 to 13.8 ka cal. BP. Assuming the recession of Lake Lahontan occurred at a constant rate this time interval can be tightly constrained using the lake-level curves (Adams et al 2008) from Pyramid Lake-Winnemucca Dry Lake and Carson Sink subbasins (Figure 3.7) to an extrapolated age of ~14.7 to 14.5 ka cal. BP.



**Figure 3.6:** Theoretical areal extent of shorelines and pertinent sills for middle-late Pleistocene Lake Lahontan in northern Nevada.



**Figure 3.7:** Lahontan lake-level curve. Reprinted with permission from: Adams, K.D., Goebel, T., Graf, K., Smith, G.M., Camp, A.J., Briggs, R.W., Rhode, D., 2008, Late Pleistocene & Early Holocene Lake-Level Fluctuations in the Lahontan Basin, Nevada: Implications for the Distribution of Archaeological Sites: *Geoarchaeology*, v. 23, no. 5, Figure 7, p. 635, © 2008 Wiley Periodicals, Inc. Lake-level curve for the Pyramid Lake-Winnemucca Dry Lake and Carson Sink western subbasins of Lake Lahontan. Upper pink arrow indicates the approximate lake-level elevation when the eastern subbasins in the proximity of the WDC would have become completely cut-off from Lake Lahontan. Lower pink arrow indicates a maximum age of dune formation in WDC.

### **3.6 Late Holocene to present**

Following the recession of Lake Lahontan and proceeding the formation of WDC periodic floods in Desert Valley, Silver State Valley, and Paradise Valley have regulated sediment availability, distribution of sand, and activity of dunes. Throughout most of the very late Holocene flood waters have accumulated at the lowest altitudes in each basin and resulted with the formation of ephemeral lakes (units Qp1 & Qfp). These lakes have limited sand supply and accommodation space that is necessary for the advancement of dunes. There is very strong geomorphic evidence shown on Maps 1-2 (Plates 3.1 & 3.2) that when alluvial channels flood in Desert Valley and Silver State Valley they deluge the sand dunes near the valley floor, overflow their banks, and radially spread (unit Qfl2) producing extensive sheetwash deposits and ponds that degrade or completely eliminate vast parcels of dunes. The entire eastern margin of WDC is also spatiotemporally controlled by the timing and magnitude of floods. However floods in this area are regionally connected and caused by events on the Little Humboldt River and Gumboot Lake (Qp2, Qp3 on Map 2; Plate 3.2).

Gumboot Lake is a north-south trending ephemeral riverine-playa system that briefly forms a shallow lake during above average wet seasons in the central portion of Paradise Valley. The lake is fed by the Little Humboldt River which collects runoff from the Santa Rosa Range and the Owyhee Plateau draining an area of 6494 km<sup>2</sup> (Prudic & Herman 1996) with a total channel length of ~86 km (BLM 2013). During years with average or below average precipitation the Little Humboldt River will run dry as it approaches the northern edge of Gumboot Lake. When discharge does reach Gumboot Lake it normally

becomes obstructed on the south-side of the lake where advancing sand dunes bury the channel of the Little Humboldt River. Previous researchers have documented that over the last 130 years Gumboot Lake has formed 35 times (Leoltz et al 1949; U.S. Soil Conservation Service 1962; Cohen 1964; Harrill & Moore 1970; U.S. Army 1975; Prudic & Herman 1996; Nevada Division of Water Planning 2000). Records also show that at least 16 times discharge out of Gumboot Lake was able to breach the sand dunes and allow the Little Humboldt River to extend south towards the confluence on the main stem of the Humboldt River. A majority of these floods have resulted with scouring, leveling, and the complete removal of sand dunes.

In the early 1950s dredging operations were sponsored by local farmers to build an earthen canal through Gumboot Lake and remove sand from the downstream channel of the Little Humboldt River. Several decades later in 1975 the Chimney Reservoir in the Little Humboldt Valley was constructed upstream from Gumboot Lake for recreational purposes and to help mitigate floods in Paradise Valley. Dredging and the installation of Chimney Reservoir effectively contained floods and to date have prevented large scale damage to infrastructure and adjacent farmlands. Gumboot Lake continues to form but rarely exceeds the size of 8 km<sup>2</sup>.

## CHAPTER 4: GEOMORPHOLOGY AND EOLIAN ACTIVITY

### 4.1 Introduction

This chapter will discuss the geomorphology and eolian activity for all areas in WDC that were explored in the field and observed on aerial or satellite imagery. Section 4.2 will disclose the methodology used to generate surficial landform Maps 1-2 (Plates 3.1 & 3.2), measure sand dune morphometry, and determine the rate of sand dune advancement. Section 4.3 examines the type, shape, and spatial coverage of relevant wind-blown deposits. When it is applicable the appropriate unit nomenclature from surficial landform Maps 1-2 is included in parenthesis. Section 4.4 provides an in-depth description and supplemental information for Maps 1-2. At the end of the chapter in sections 4.5 to 4.7 the direction and rate of sand dune advancement is discussed and evaluated.

### 4.2 Mapping method

Surficial landform Maps 1-2 were compiled using ArcGIS (v.9.3 & v.10) and the Environmental Systems Research Institute (ESRI) world imagery\_931 layer. The ESRI imagery layer was a seamless color mosaic generated with the best available imagery from the years 2012-2013. Sources used to generate the mosaic include; DigitalGlobe & Aerials Express (0.3 and 0.6 meter resolution), GeoEye (1 meter resolution), and I-cubed (1 meter resolution) satellite images. Landscape features were graphically mapped on imagery between an absolute map scale of 1:300 and 1:900. The spatial coverage of wind-blown deposits was determined using converted shapefile polygons. Distance between dunes (spacing), length, and width for each sampled dune site were measured on the ESRI imagery layer using the line tool in ArcGIS. Figure 4.1 illustrates the

dimensions that were measured to describe the shape of dunes. Measurements at specific sample locations are listed in Table 3. Dune shapes were classified by length to width ratios using the scheme developed by Pye (1993). The specific L/W values and classes for this system are; Lunate < 0.4 < Hemicyclic < 1 < Lobate < 3 < Elongate. Specific dune types such as star, linear, and ridges were excluded from the system, but when it was possible class names were applied to complex crescentic dunes and ridges.

Dune heights were calculated [ $h = (\text{length of lee slip face}) \times \sin(\text{apparent dip}^{\circ})$ ] in the field by measuring the length and apparent dip of the lee slip face at the brink of each sample site. Inclination and length measurements were made using a Brunton compass and 100 meter measuring tape. Adjacent sand dunes and other arbitrary locations were also measured to ensure that values were representative of the complex.

The rate of sand dune advancement was estimated using ESRI imagery and seamless color orthoquadrangles of Humboldt County produced by the National Agriculture Imagery Program from the years 1994, 1999-2000, and 2006. United States Geological Survey (USGS) 24k Provisional Edition topographic maps published between the years 1981 to 1985 were also used to measure rates of sand dune advancement. USGS quads were compiled from field investigations performed in 1977. However dune field planimetry on the final map series was revised using aerial photographs collected in the year 1980. Provisional Edition 24K topographic quads include; Golconda Butte 41117-A5-TM-025, Weso 41117-A6-TM-024, Winnemucca Mountain 41117-A7-TM-024, Barrett Springs 41117-A8-TM-024, Bloody Run Peak 41117-B7-TM-024, Silver State Draw 41117-B8-TM-024, Mormon Dan Butte 41118-A1-TM-024, Lay Waterhole 41118-

A2-TM-024, Sombrero Peak 41118-B1-TM-024, and Presnel Well 41118-B2-TM-024.

Sand dune advancement was measured by drawing lines along the lee slip face of study dunes for each year of measurement. Maximum and minimum distances between lee slip faces from respective years of imagery were recorded at each site. The direction of dune advancement was resolved from ESRI imagery in the azimuth system and plotted on rose diagrams (Figures 4.21, 4.23, & 4.25). Results from the measurements are detailed in Appendix A.

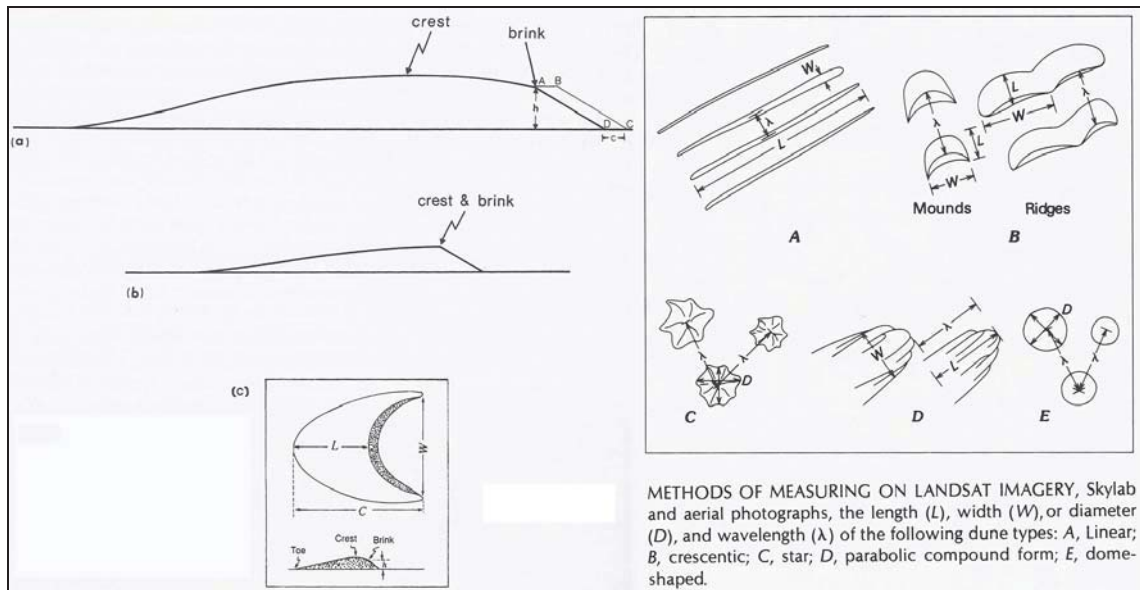


**Figure 4.1:** Dimensions used to measure sand dune morphometry. (Left) Reprinted with kind permission from Springer Science and Business Media from: Springer-Verlag Berlin Heidelberg, Aeolian Sand and Sand Dunes, 2009, Ch. 6, Pye, K., Tsoar, H., Figure 6.18a-c, © 2009. (Right) Open source document reprinted from: Breed, C.S., Grow, T., 1979, Morphology and Distribution of Dunes in Sand Seas Observed by Remote Sensing: *in* McKee, E.D., ed., A Study of Global Sand Seas: United States Geological Survey Professional Paper 1052, Ch. J., p. 258.

**Table 3:** Morphometry of sample sites in the Winnemucca Dune Complex

	Sample #	Study site	Dune type	Mean ( $\phi$ )	Sort. ( $\phi$ )	Skeww. ( $\phi$ )	Kurt. ( $\phi$ )	Spacing (m)	Length (m)	Width (m)	L/W	Height (m)	Class.
1	WDC-102-DV-25	NE of Power Plant	Barchan	2.111	0.644	0.057	0.970	133	70	127	0.551	9.2	Hemicyclic
2	WDC-092-PV-37	South of Feed lot	Barchan	2.502	0.528	0.035	0.980	125	70	107	0.654	6.8	Hemicyclic
3	WDC-040-SS-05	Central dune field	Barchan	1.953	0.636	0.051	0.940	258	112	260	0.431	12.2	Hemicyclic
4	WDC-041-SS-06	Central dune field	Barchan	2.140	0.580	0.026	0.941	212	100	170	0.588	12.2	Hemicyclic
5	WDC-088-PV-33	South of Feed lot	Compound Barchan	2.249	0.549	0.056	1.005	162	49	95	0.516	3.7	Hemicyclic
6	WDC-091-PV-36	South of Feed lot	Compound Barchan-B.bolic	2.151	0.662	0.038	0.978	2030	230	205	1.1	8.4	Lobate
7	WDC-039-SS-04	Central dune field	Compound Barchan	1.998	0.577	0.036	0.945	227	132	291	0.454	24.4	Hemicyclic
8	WDC-104-DV-27	NE of Power Plant	Compound Barchan	1.831	0.607	0.031	0.933	196	98	110	0.891	9.9	Hemicyclic
9	WDC-105-DV-28	NE of Power Plant	Compound Barchan	1.573	0.521	0.005	0.944	146	80	95	0.842	14.5	Hemicyclic
10	WDC-036-SS-01	Eastern Complex	Barchanoidal ridge	1.991	0.702	0.046	0.934	100	96	191	0.503	9.2	Hemicyclic
11	WDC-037-SS-02	Eastern Complex	Barchanoidal ridge	1.995	0.629	0.043	0.932	143	84	96	0.875	9.2	Hemicyclic
12	WDC-038-SS-03	Eastern Complex	Barchanoidal ridge	1.989	0.557	0.026	0.939	130	75	180	0.417	18.3	Hemicyclic
13	WDC-093-SS-23	Eastern Complex	Barchanoidal ridge	1.701	0.631	0.043	0.936	112	90	190	0.474	16.7	Hemicyclic
14	WDC-094-SS-24	Eastern Complex	Barchanoidal ridge	1.711	0.564	0.030	0.944	88	82	410	0.200	14.5	Lunate
15	WDC-095-SS-25	Eastern Complex	Barchanoidal ridge	1.617	0.501	0.007	0.954	112	62	235	0.264	24.4	Lunate
16	WDC-096-SS-26	Eastern Complex	Barchanoidal ridge	1.839	0.589	0.024	0.942	91	66	112	0.589	18.3	Hemicyclic
17	WDC-078-SS-19	Western dune field	Barchanoidal ridge	2.362	0.565	0.007	0.938	101	75	106	0.708	11.5	Hemicyclic
18	WDC-005-PV-05	ATV Park	Barchanobolic	2.106	0.593	0.025	0.967	175	718	339	2.1	6.7	Lobate
19	WDC-090-PV-35	South of Feed lot	Barchanobolic	2.383	0.554	0.052	0.994	865	966	184	5.3	13.7	Elongate
20	WDC-073-PV-28	North ATV-Sand Pass rd.	Barchanobolic	1.902	0.580	0.000	0.943	471	455	261	1.7	15.3	Lobate
21	WDC-074-PV-29	North ATV-Sand Pass rd.	Barchanobolic	1.988	0.592	0.031	0.955	872	940	478	2.0	12.2	Lobate
22	WDC-076-PV-31	North ATV-Sand Pass rd.	Barchanobolic	2.087	0.632	0.037	0.939	1255	1546	403	3.8	9.2	Elongate
23	WDC-001-PV-01	ATV Park	Complex Crescentric	2.323	0.613	0.023	0.970	174	197	350	0.563	4.6	Hemicyclic
24	WDC-002-PV-02	ATV Park	Complex Crescentric	1.987	0.743	0.029	0.972	212	197	350	0.563	7.6	Hemicyclic
25	WDC-003-PV-03	ATV Park	Complex Crescentric	2.088	0.593	0.029	0.969	241	197	350	0.563	9.4	Hemicyclic
26	WDC-004-PV-04	ATV Park	Complex Crescentric	2.160	0.585	0.024	0.964	disturbed	112	145	0.772	5.5	Hemicyclic
27	WDC-006-PV-06	ATV Park	Complex Crescentric	2.165	0.570	0.026	0.953	disturbed	disturbed	disturbed	n/a	5.4	disturbed
28	WDC-007-PV-07	ATV Park	Complex Crescentric	2.056	0.573	0.036	0.959	disturbed	disturbed	disturbed	n/a	7.2	disturbed
29	WDC-008-PV-08	ATV Park	Complex Crescentric	1.932	0.583	0.046	0.963	250	144	260	0.554	8.8	Hemicyclic
30	WDC-089-PV-34	South of Feed lot	Complex Crescentric	2.660	0.567	0.041	1.000	77	68	85	0.800	10.7	Hemicyclic
31	WDC-079-SS-20	Western dune field	Complex Crescentric	2.188	0.651	0.009	0.928	225	48	103	0.466	8.4	Hemicyclic
32	WDC-103-DV-26	NE of Power Plant	Complex Crescentric	2.035	0.670	0.042	0.935	235	115	210	0.548	16.0	Hemicyclic
33	WDC-067-SS-14	Western Complex	Star	2.694	0.577	-0.014	0.947	100	d = 44	d = 44	1.0	8.4	Star
34	WDC-068-SS-15	Western Complex	Star	2.392	0.563	0.002	0.936	118	d = 85	d = 85	1.0	14.5	Star
35	WDC-070-SS-17	Western Complex	Star	2.498	0.575	-0.004	0.943	114	d = 40	d = 40	1.0	6.9	Star
36	WDC-080-SS-21	Western dune field	Star	2.317	0.561	0.012	0.935	157	d = 100	d = 100	1.0	11.5	Star
37	WDC-061-SS-09	NE of Barretts Springs	Parabolic	1.843	0.498	0.013	0.947	834	754	206	3.7	6.1	Elongate
38	WDC-060-SS-08	NE of Barretts Springs	Parabolic	2.021	0.546	0.015	0.935	831	754	206	3.7	9.2	Elongate
39	WDC-010-PV-10	East side of i95	Parabolic	2.373	0.491	0.004	0.943	2395	2158	210	10.2	3.7	Elongate
40	WDC-012-PV-12	East side i95	Parabolic	2.457	0.509	0.007	0.944	1998	2088	105	20.0	3.7	Elongate
41	WDC-065-SS-13	East slope Slumbering Hills	Compound Parabolic	2.158	0.672	0.054	0.993	2650	3210	268	12.0	2.8	Elongate
42	WDC-009-PV-09	East side i95	Compound Parabolic	2.436	0.512	0.040	1.000	2395	2158	210	10.2	3.0	Elongate
43	WDC-011-PV-11	East side i95	Compound Parabolic	2.197	0.545	0.045	0.985	1824	1918	160	12.0	5.3	Elongate
44	WDC-017-PV-17	North ATV-Sand Pass rd.	semi-active Parabolic	2.355	0.559	0.024	0.966	210	400	44	9.0	4.6	Elongate
45	WDC-075-PV-30	North ATV-Sand Pass rd.	semi-active Parabolic	1.991	0.680	0.039	0.961	732	745	78	9.6	3.2	Elongate
46	WDC-077-PV-32	North ATV-Sand Pass rd.	semi-active Parabolic	2.402	0.515	0.018	0.967	1370	2030	228	8.9	2.4	Elongate
47	WDC-051-DV-08	West of DeLong Farms	semi-active Parabolic	2.368	0.611	0.025	0.957	763	803	155	5.2	1.1	Elongate
48	WDC-062-SS-10	East slope Slumbering Hills	semi-active Parabolic	2.038	0.628	0.056	0.976	972	2007	175	11.5	2.4	Elongate
49	WDC-064-SS-12	East slope Slumbering Hills	semi-active Parabolic	2.233	0.625	0.063	0.981	1350	1372	190	7.2	5.4	Elongate
50	WDC-059-SS-07	NE of Barretts Springs	semi-active Transverse	2.486	0.571	0.008	0.943	48	293	11	26.6	3.7	Transverse
51	WDC-029-QRV-03	W-side Riverside rd.	semi-active Transverse	1.995	0.855	0.085	0.954	45	134	38	3.5	4.3	Transverse
52	WDC-030-QRV-04	W-side Riverside rd.	semi-active Transverse	2.020	0.607	0.075	1.001	36	204	37	5.5	3.1	Transverse
53	WDC-032-BRD-01	W-side of Jackson Range	semi-active Transverse	2.064	0.622	0.045	0.980	27	151	22	6.7	3.4	Transverse
54	WDC-106-DV-29	NE of Power Plant	Vegetated Linear	2.349	0.841	0.073	1.039	268	6300	48	131.0	3.1	Linear
55	WDC-047-DV-04	South-East of Juniper Hills	Vegetated Braided Linear	2.463	0.543	0.018	0.955	138	1227	42	29.2	1.5	Braided Linear
56	WDC-048-DV-05	South-East of Juniper Hills	Vegetated Braided Linear	2.656	0.576	0.022	0.947	255	1724	40	43.1	2.4	Braided Linear
57	WDC-066-RP-03	Southwest of Racetrack	Vegetated Braided Linear	2.254	1.060	-0.126	0.989	115	1610	47	34.3	3.7	Braided Linear
58	WDC-013-PV-13	North ATV-Sand Pass rd.	stable Compound Parabolic	2.514	0.758	-0.024	1.020	2395	2158	210	10.2	3.5	Elongate
59	WDC-014-PV-14	North ATV-Sand Pass rd.	stable Compound Parabolic	2.526	0.650	0.024	0.989	2395	2158	210	10.2	3.5	Elongate
60	WDC-015-PV-15	North ATV-Sand Pass rd.	stable Compound Parabolic	2.450	0.633	0.015	0.972	2395	2158	210	10.2	3.5	Elongate
61	WDC-016-PV-16	North ATV-Sand Pass rd.	stable Compound Parabolic	2.555	0.689	0.035	0.982	2395	2158	210	10.2	3.5	Elongate
62	WDC-054-DV-11	West of DeLong Farms	stable Compound Parabolic	2.161	0.704	0.096	1.001	1982	2474	370	6.7	3	Elongate
63	WDC-019-PV-19	North ATV-Sand Pass rd.	stable Parabolic	2.453	0.670	0.051	0.958	1116	1074	55	19.5	4.9	Elongate
64	WDC-020-PV-20	West of Osgood Mts	stable Parabolic	2.269	0.784	0.044	0.990	n/a	422	98	4.3	4.3	Elongate
65	WDC-050-DV-07	West of DeLong Farms	stable Parabolic	2.260	0.714	0.048	0.963	763	803	155	5.2	1.1	Elongate
66	WDC-063-SS-11	East slope Slumbering Hills	stable Parabolic	2.277	0.716	0.079	0.987	1285	1332	85	15.7	1.8	Elongate
67	WDC-072-PV-27	East slope Bloody Run Hills	stable Parabolic	2.918	0.601	0.068	1.005	201	1575	105	15.0	1.2	Elongate
68	WDC-022-PV-22	West of Osgood Mts	stable Parabolic	2.245	0.881	0.118	1.037	148	451	168	2.7	3.7	Lobate
69	WDC-044-RP-01	South of Ten Mile Hills	stable Transverse	2.284	0.721	0.083	1.035	44	360	38	9.5	3.0	Transverse

**Table 3** continued: Morphometry of sample sites in the Winnemucca Dune Complex

	Sample #	Study site	Dune type	Mean ( $\phi$ )	Sort. ( $\phi$ )	Skew. ( $\phi$ )	Kurt. ( $\phi$ )	Spacing (m)	Length (m)	Width (m)	L/W	Height (m)	Class.
70	WDC-045-RP-02	South of Ten Mile Hills	stable Transverse	2.194	0.663	0.067	0.986	40	366	30	12.2	4.0	Transverse
71	WDC-031-GRV-05	SW above Gallagher Flat	stable Transverse	2.506	0.609	0.046	0.977	26	128	25	5.1	3.7	Transverse
72	WDC-084-DV-18	South of Delong Farms	stable Transverse	2.307	0.695	0.053	0.966	48	406	34	12.0	6.1	Transverse
73	WDC-099-DV-22	Gabica Butte	stable Transverse	2.370	0.696	0.074	0.978	50	356	24	14.8	3.1	Transverse
74	WDC-101-DV-24	Gabica Butte	stable Transverse	2.333	0.636	0.052	0.969	40	353	26	13.6	2.1	Transverse
75	WDC-035-BRD-04	W-side of Jackson Range	stable Transverse	2.142	0.716	0.041	0.969	78	173	34	5.1	3.4	Transverse
76	WDC-034-BRD-03	W-side of Jackson Range	stable Transverse	2.300	1.308	-0.043	0.971	46	107	36	3.0	4.3	Transverse
77	WDC-024-PV-24	SW of Osgood Mts	Undifferentiated	2.047	0.737	0.127	1.047	n/a	n/a	n/a	n/a	1.5	Undiff.
78	WDC-026-PV-26	SW of Osgood Mts	Undifferentiated	1.857	0.903	0.222	1.283	n/a	n/a	n/a	n/a	2.1	Undiff.
79	WDC-086-BRD-05	Northwest of Hycroft mine	Undifferentiated	2.107	1.145	0.074	0.907	n/a	n/a	n/a	n/a	2.1	Undiff.
80	WDC-071-SS-18	Western dune field	Undifferentiated	2.693	0.563	0.021	0.949	n/a	n/a	n/a	n/a	2.7	Undiff.
81	WDC-042-DV-01	East of Jungo Hills	Active Lunette	2.444	1.903	0.277	1.704	n/a	n/a	n/a	n/a	1.6	Palustrine
82	WDC-043-DV-02	East of Jungo Hills	Active Lunette	2.234	1.133	0.035	1.408	n/a	n/a	n/a	n/a	1.3	Palustrine
83	WDC-052-DV-09	West of DeLong Farms	Active Lunette	2.566	0.800	0.007	0.996	n/a	n/a	n/a	n/a	4.0	Palustrine
84	WDC-033-BRD-02	West side of Jackson Mts	Active Lunette	2.304	0.656	0.073	1.031	n/a	n/a	n/a	n/a	4.3	Palustrine
85	WDC-083-DV-17	South of Delong Farms	Active Lunette	2.062	0.729	0.083	1.003	n/a	n/a	n/a	n/a	3.4	Palustrine
86	WDC-053-DV-10	West of DeLong Farms	relict Lunette	3.714	2.464	0.611	2.009	n/a	n/a	n/a	n/a	n/a	Palustrine
87	WDC-056-DV-13	West of DeLong Farms	relict Lunette	3.731	2.127	0.475	1.065	n/a	n/a	n/a	n/a	n/a	Palustrine
88	WDC-057-DV-14	West of DeLong Farms	relict Lunette	2.790	1.280	0.354	1.949	n/a	n/a	n/a	n/a	n/a	Palustrine
89	WDC-058-DV-15	West of DeLong Farms	relict Lunette	3.032	1.716	0.446	2.054	n/a	n/a	n/a	n/a	n/a	Palustrine
90	WDC-046-DV-03	Southeast of Jungo Hills	Lakebed	2.594	0.650	0.088	1.034	n/a	n/a	n/a	n/a	n/a	Palustrine
91	WDC-049-DV-06	Southeast of Jungo Hills	Lakebed	2.569	0.583	0.008	0.948	n/a	n/a	n/a	n/a	n/a	Palustrine
92	WDC-081-SS-16	South of Delong Farms	Lakebed	4.340	2.330	0.355	0.863	n/a	n/a	n/a	n/a	n/a	Palustrine
93	WDC-085-DV-19	South of Delong Farms	Sandy Beach	3.030	1.121	0.313	1.492	n/a	n/a	n/a	n/a	n/a	Palustrine
94	WDC-097-DV-20	Southwest of Delong Farms	Sandy Beach	2.323	0.706	0.113	1.020	n/a	n/a	n/a	n/a	n/a	Palustrine
95	WDC-098-DV-21	Southwest of Delong Farms	Sandy Beach	2.379	0.687	0.114	1.052	n/a	n/a	n/a	n/a	n/a	Palustrine

#### 4.3 Types of sand dunes, morphometry, and spatial coverage

Active, stabilized, and degraded sand dunes expand over nearly 500 km<sup>2</sup> and blanket 472.2 km<sup>2</sup> of terrain in Desert Valley, Silver State Valley, and Paradise Valley. The spatial coverage and morphometry of various wind-blown deposits is listed on Tables 4 & 5.

Numerous types of individual, compound, and complex sand dunes occupy each of the valleys and ranges. However the majority of active dunes are universally dominated by various configurations of barchan and parabolic dunes. Morphodynamically there are three different ways that barchan-parabolic dunes are configured. 1) Upwind and centrally to each major dune field they transition into compound shapes that merge and contribute to the formation of crescentic complexes. 2) Towards the perimeter of major dune fields they diverge into compound or individual dunes. 3) Near or beyond the leeward side of each major dune field they overlap and transform into intermediate shapes that are difficult to classify (Qda5b).

For the purpose of this study the term “Barchanbolic” was used to describe sand dunes that had intermediate barchan-parabolic form (Figures 4.2 & 4.5). Barchanbolic dunes have a lee slip face with the shape of a barchan but also have moderately long parabolic tails (Figure 4.3). In some areas barchanbolic dunes are periodically composed of three tails; two lateral parabolic-like tails and one medial tail that places orthogonal to the crest of the dune at its midsection. Vegetation of various types stabilizes the tails on barchanbolic-parabolic dunes and impedes the flow of sand. These affects have produced some especially long tails that can exceed 3.2 kilometers in length.

Barchanbolic and parabolic dunes differed in height and shape but had similar intradune distances. The brink height of barchanbolic dunes was between 6 to 17 meters and intradune spacing was  $\leq$  2030 meters. Length to width ratios of barchanbolic dunes classified their shape as lobate and elongate. Parabolic brink heights were relatively meager at 1.2 to 8 meters. Intradune spacing between parabolic dunes ranged from 85 to 2650 meters. The shape of parabolic dunes was definitively elongate. Exploration in the field and evaluation of aerial imagery did not reveal a noticeable relationship among vegetative density, shape, spacing, or tail length of barchanbolic and parabolic dunes.

Barchan dunes (Figure 4.4; Image #15) predominately lacked vegetation and had brink heights of 3.7 to 25 meters with intradune lengths of  $\leq$  260 meters. The shape of barchans was primarily hemicyclic with rare lobate shapes that were only found on compound forms. Barchan dunes were located within or near the boundaries of crescentic complexes from unit Qda1.

Large crescentic complexes (Qda1) are developed in areas where barchan, barchanbolic, and parabolic dunes merge and coalesce. There are a total of six major crescentic complexes; the Paradise Complex (Figure 4.5), Silver State East, Silver State West (Figures 4.6 & 4.7), Desert Valley North, Slumbering Hills, and Crescent-Sombrero (Figure 4.8). Major and isolated complexes cover 26.9 km<sup>2</sup>. The crescentic complexes resemble sand seas and are comprised of star dunes, transverse ridges, (Figure 4.6) and barchanoidal ridges (Figures 4.6 & 4.9; Image #16) with hemicyclic and lunate shapes.

Major complexes are distinguished by the presence of well-defined wind-ripples (Image #17) and stoss-ward granular rippling along peripheral and upwind margins of dune fields. Spacing between ridges varied from 65 to 252 meters. The tallest dunes encountered were located on ridges where heights extended between 4.5 to 28 meters. Crescentic ridge heights reached a maximum of 28 meters along the bottom of Silver State Valley. Maximum ridge heights in Desert Valley were slightly below 23 meters and gradually increased in magnitude towards the center of each complex. Within the Paradise Valley Complex maximum ridge heights were only 4.5 to 6 meters. In Desert Valley and Silver State Valley asymmetric star dunes (Image #18) range from 6 to 16 meters in height with diameters of 40 to 100 meters. They are not widespread but can be occasionally found between ridges towards the western side of each complex. Behind the ridges, compound barchan-barchanbolic-parabolic dunes (Qda2, Qda2b, & Qda3) laterally radiate towards the northern and southern boundaries of WDC. As the compound dunes approach the boundaries they decrease in height, space further apart, and separate into individual dunes (Qda4).

Isolated barchanbolic, parabolic, and undifferentiated dunes mixed with sheeting sand (Qda5 & Qda6) are also present and mantle ~84.9 km<sup>2</sup>. Climbing dunes with transverse ridges (Qda7), descending dunes (Qda8), and sand ramps with cliff-top shadow (echo) dunes (Qda9 on Map 2; Plate 3.2) are prevalent on mountain passes and cover 5.6 km<sup>2</sup>. Collectively the active dune groups in WDC spread over a spatial extent of 162 km<sup>2</sup>.

Separate from the active dunes but an important component in WDC is an extensive sand sheet (Qss on Map 1; Plate 3.1) that stretches across a large part of Desert Valley. Barchanbolic and parabolic dunes are present along the northern, southern, and eastern perimeter, although within the 56.3 km<sup>2</sup> of sheet area dune formation is absent. Sand, silt, and dust from the sheet is transported in a northeast-easterly direction across the lowest elevations (1258-1278 meters above MSL) of Desert Valley towards the western flanks of Blue Mountain and the Slumbering Hills.

The remaining wind-blown deposits are comprised of stabilized, semi-active, and degraded sand dunes that longitudinally border the active dunes and encompass the western side of WDC. Large sections of stabilized linear dunes that transform into parabolic dunes (Qds1) shroud a total of 110.8 km<sup>2</sup> in WDC. They trend almost due east, have very low heights (1 to 3 meters), and are mottled by grasses and shrubs. Semi-active to stabilized transverse (Figure 4.7) and linear dunes (Qds2) are less abundant and distribute on at least 12.3 km<sup>2</sup>. They have relatively low heights (1.2 to 5.5 meters), close spacing (25 to 90 meters), and form with an orientation towards the northeast or southeast. Vegetated braided linear dunes (Qd/Qb on Map 1; Figure 4.10) incised by playettes are plentiful and stretch over 81 km<sup>2</sup>. They also have low heights (1.2 to 4

meters), are spaced from 25 to 270 meters apart, align west to east, and have exceptionally long lengths that exceed 6 kilometers in portions of Desert Valley. En masse stabilized and semi-active dunes veneer a total of 204.1 km<sup>2</sup>.

Degraded sand dunes (Qdd) cover 49.7 km<sup>2</sup> and have parabolic or undifferentiated shapes. They are situated near stable dunes on hillslopes, and valley bottoms. The morphology and location of these features denote they are regulated by a combination of forces that involve; growth of vegetation, flooding of drainage channels, ponding water, wildfires, livestock, and anthropogenic disturbances. Many of the degraded dunes are concentrated on southwesterly facing slopes below the crest of each range. Runoff from snowmelt and rainfall are most likely responsible for the formation for these features.

**Table 4:** Spatial coverage of various wind-blown deposits in the Winnemucca Dune Complex

Feature type	Map unit	Area (km <sup>2</sup> )	
Crescentic Complexes (Transverse-Barchanoidal Ridges & Stars)	Qda1	26.9	active total
Compound Barchan-Barchanbolic-Parabolic & Ridges	Qda2-2a	44.6	
Compound & Individual Barchanbolic-Parabolic, Undiff. & Sheets	Qda3-6	84.9	
Climbing, Descending, Ramping & Cliff-top	Qda7-9	5.6	
Continuous large Sand Sheets	Qss	56.3	
Stabilized Linear transforming to Parabolic	Qds1	110.8	semi active stable total
Semi Active-Stabilized Linear & Transverse	Qds2	12.3	
Vegetated Braided Linear incised by Playettes	Qd/Qb	81.0	
Degraded dunes	Qdd	49.7	
	All units	472.2	

**Table 5:** Morphometry of various wind-blown deposits in the Winnemucca Dune Complex

Dune type	Height (m)	Spacing (m)	Length (m)	Width (m)	Shape
Barchan	3.7 - 25	0 - 260	30 - 230	30 - 480	Hemicyclic with rare Lobate
Barchanbolic	6 - 17	0 - 2030	35 - 1850	30 - 490	Lobate & Elongate
Parabolic	1.2 - 8	85 - 2650	420 - 3210	20 - 380	Elongate
Ridges (Transverse & Barchanoidal)	4.5 - 28	65 - 252	20 - 200	60 - 600	Hemicyclic & Lunate
Crescentic Star-like	6 - 16	15 - 160	d = 40-100	d = 40-100	Asymmetric Star
Semi-active & Stabilized Linear	1 - 5.5	25 - 270	150 - 6300	8 - 50	Linear & Vegetated Braided
Semi-active & Stabilized Transverse	1.2 - 5.5	25 - 90	25 - 460	10 - 40	Transverse



**Figure 4.2:** Barchanolic sand dune in Paradise Valley. View is towards the north.



Figure 4.3: Parabolic sand dune approaching Highway 95 in Paradise Valley. View is towards the north.



Figure 4.4: Merging barchan sand dunes in Silver State Valley. View is towards the north

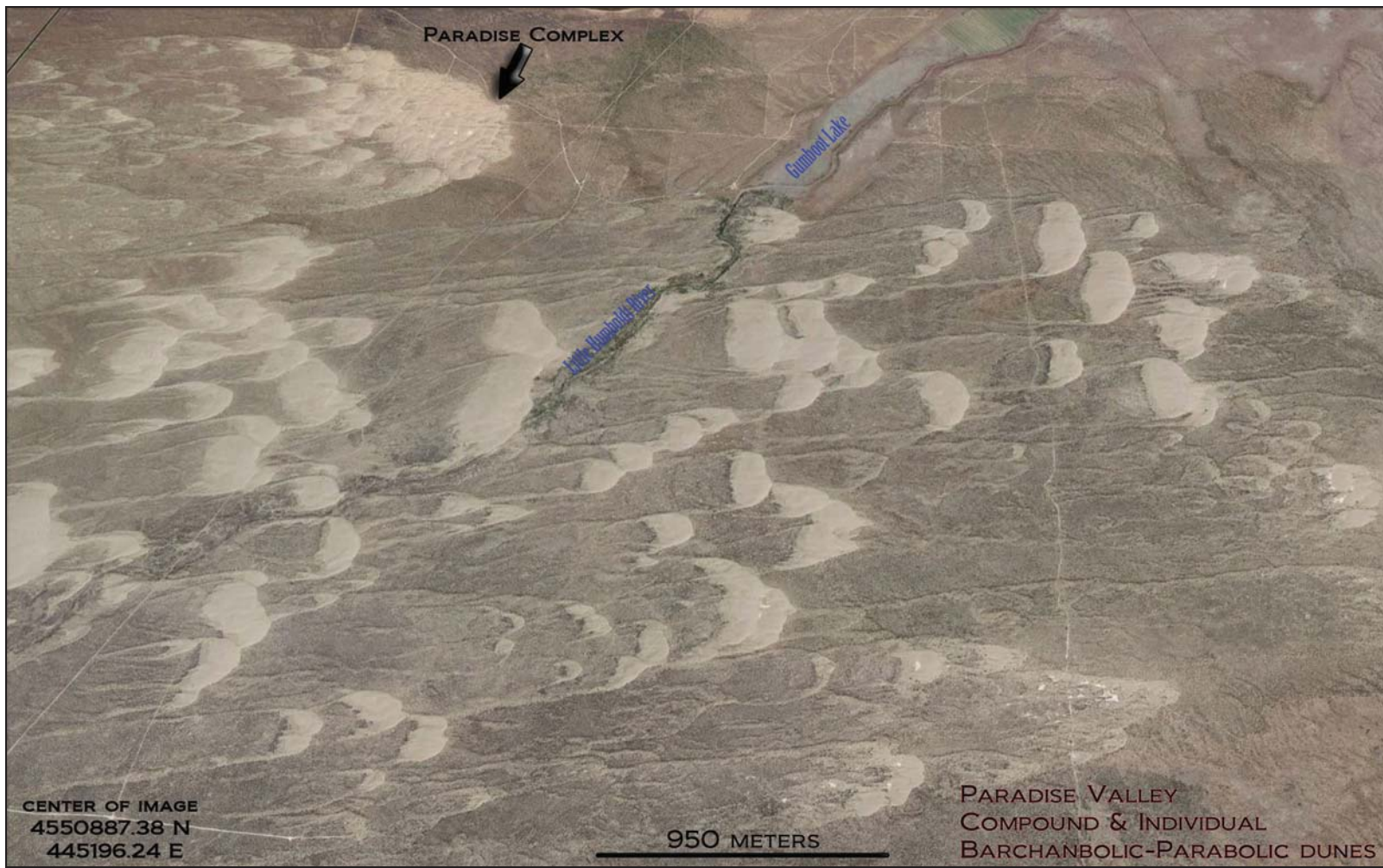


Figure 4.5: Compound and individual barchanobolic-parabolic sand dunes in the center of Paradise Valley. View is towards the north.

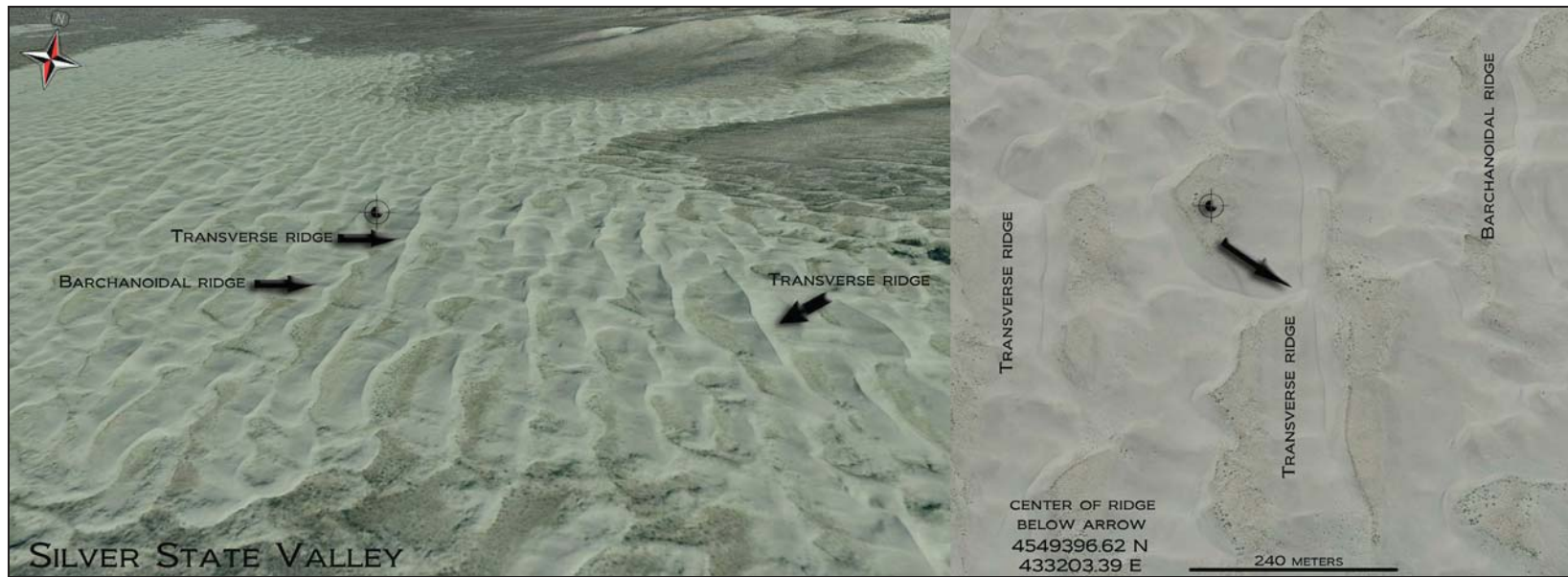


Figure 4.6: Transverse and barchanoidal ridges in the Silver State Eastern Complex. View on the right image is to the north.



Figure 4.7: Northeast aerial view of Silver State Valley.

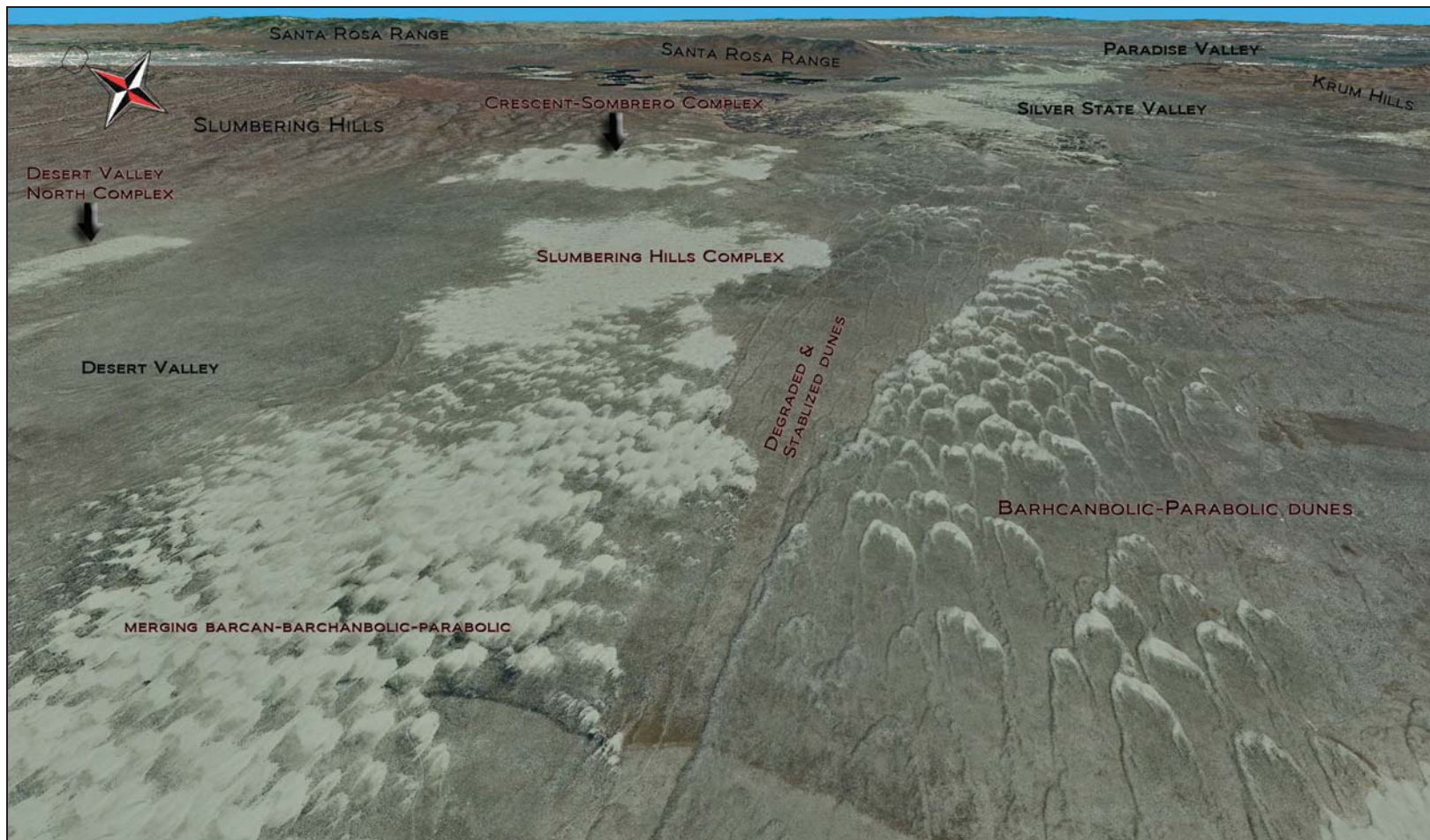
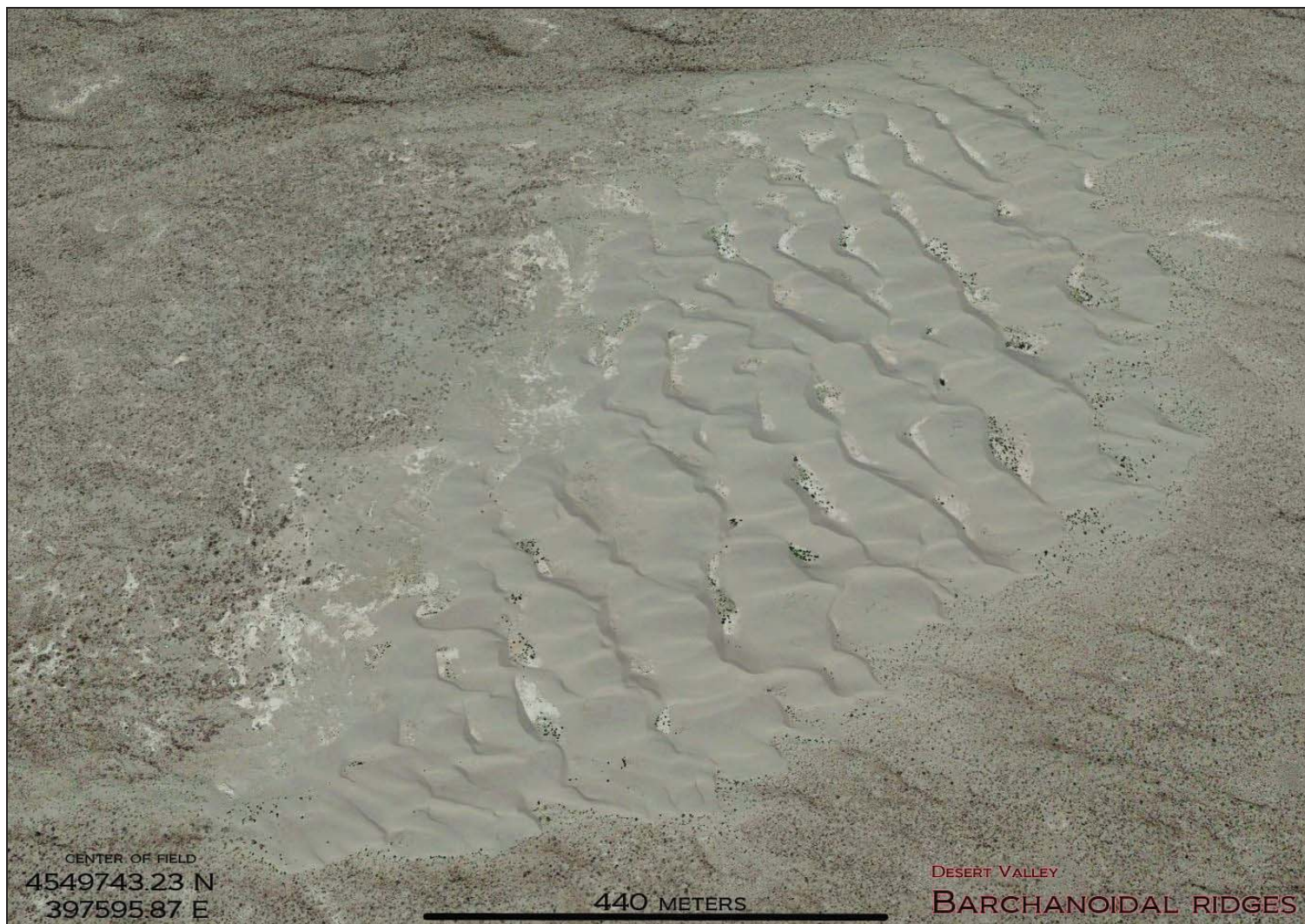


Figure 4.8: Northeast-easterly aerial view of the western flank of the Slumbering Hills.



**Figure 4.9:** Barchanoidal ridges in an isolated crescentic complex in Desert Valley. View is towards the north.



**Figure 4.10:** Stabilized to semi-active braided linear dunes transforming to stable and active parabolic dunes in Desert Valley.



**Image #15-16:** Barchan sand dune in Desert Valley (Top). Barchanoidal ridge in Silver State Valley with the Slumbering Hills in the background (Bottom). View in both images is towards the northwest.



**Image #17-18:** Wind-rippled crescentic dunes in Silver State Valley with the Krum Hills in the background (Top). Asymmetric star dune in Silver State Valley with the Slumbering Hills on the horizon (Bottom). View in both images is towards the southwest.

#### 4.4 Description of mapped units

##### 4.4:1 Desert Valley to the Slumbering Hills (Map 1)

Sand dune formation begins atop lacustrine deposits in the west-central portion of Desert Valley between the altitudes of 1258 to 1274 meters above MSL. At the western boundary of the complex sand dunes form on the same sedimentary deposit although the type, shape, and formative process are different in the northern and southern sections of the valley. Figure 4.11 shows a topographic profile for the area discussed in this section.

Located in the north are stabilized to semi-active dunes (subunit Qd) and three small crescentic complexes (Qda1) that overlay and originate from lacustrine deposits of Lake Lahontan (subunit Qb). The subunits Qb and Qd are indicated as unit Qb/Qd on Map 1 (Plate 3.1; also shown on Figure 4.12).

The underlying lacustrine deposits (Qb) are interpreted by location, elevation, and stratigraphic position after Morrison (1991) to belong to the middle member of the Sehoo alloformation (late Pleistocene). Qb consists of interbedded offshore, nearshore, and foreshore beach sediments. Offshore deposits are comprised of horizontal lakebeds with partially cemented silty sand and thin laminations of silt. Nearshore and foreshore deposits are comprised of horizontal to slightly inclined beds of pebbly sand and poorly to moderately sorted fine to medium sand. Resting on the top layer of the beach deposits are varnished tufa heads (diameter  $\leq$  8cm) with basal stems (length  $\leq$  3cm, width  $\leq$  3cm) of coarse sand. The occurrence of tufa heads is concentrated near the Jungo Hills in the northwest. To the east and south-southeast portions of Qb the tufa heads are sparse and rarely encountered.

The overlaying sand dunes from subunit Qd are composed of stabilized to semi-active deposits of braided linear and transverse dunes that transform across the center of the valley into semi-active elongate parabolic dunes (Qds1). Localized runoff from the sand dunes and adjacent Jungo Hills incises Qd and forms numerous isolated playettes.

Three small crescentic complexes (Qda1) form on top of Qd/Qb with individual parabolic and undifferentiated dunes along their perimeter. The crescentic complexes are comprised of lunate to hemicyclic shaped ridges that advance 0 to 6.1 myr<sup>-1</sup> on an azimuth of 75-90°. Surrounding Qda1 the linear and transverse sand dunes from Qd descend several meters in elevation towards the center of the valley and slowly deflate into sheeting sand (Qss). In areas where the dunes are not deflated they are partially to completely degraded (Qdd) by wildfires, ponding water, livestock, and biopeddurbation.

In the southern half of Desert Valley unit Qd/Qb is extensively eroded by runoff from Jungo Flat. When significant precipitation accumulates on Jungo Flat a shallow lake briefly forms and spills to the northeast into Qd/Qb. The overflow drains northeast of DeLong Farms through a series of braided channels that feed an ephemeral delta and matrix of paludal deposits (Qfp). The ephemeral delta (Qfp) has developed an elaborate network of playas, playettes, dune islands (Image #19), lagoons, beaches, and lunettes which prograde towards the center of Desert Valley and discharge into unit Qss.

Sediments scoured from Qd/Qb are transported to east side of Qfp and contribute to the formation of lunette dunes which encompass the entire eastern margin of Qfp. On the lee-side of the lunettes there are stabilized elongate parabolic dunes (Qds1) that stretch across the valley to the northwestern flanks of Blue Mountain.

The sand sheet (Qss) covers a majority of central Desert Valley (Figure 4.12) and extends almost all the way through WDC. It crosses the low point of the valley at 1258-1265 meters above MSL and extends northeast towards the Slumbering Hills and Blue Mountain. Unit Qss is bisected by a north-south and southwest-northeast trending soft sediment deformation lineament (dashed line on Figure 4.12) that is parallel to mapped sections of the Western Northern Nevada Rift (Ponce et al 2010; Figure 3.5). It also forms acute to orthogonal angles with range-front normal faults on the Slumbering Hills and Blue Mountain. The lineament is not inferred to be an infilled drainage because the feature cross-cuts the gradient of the basin. In several locations runoff is internally captured and entrenches the lineament making short discontinuous channels that terminate against sand dunes in units Qda1, Qda6, and Qds1.

On the east side of the valley the sand sheet (Qss) tapers into stabilized and degraded dunes from units Qds1, Qds2, and Qdd. Near the contacts of Qss, Qds1, and Qdd there are four small crescentic complexes (Qda1) composed of lunate to hemicyclic shaped ridges with scattered individual and compound forms of lobate barchanobolic, elongate parabolic, and undifferentiated dunes (Qda4 & Qda6). The crescentic complexes are advancing 0 to  $4.1 \text{ myr}^{-1}$  on an azimuth of  $70\text{-}102^\circ$ .

At the contact of Qss and Qds2 to the northwest of Blue Mountain Power Plant (Map 1 and Figure 4.12) are stabilized linear dunes which transform eastward into transverse dunes (Qds2). In this location, three young alluvial fans (Qa) draining from the Barbara Worth Spring and Blue Mountain Canyon have formed beneath a well-defined normal fault (shown on Map 1 and Figure 4.15). The distal lobes of the alluvial fans intersect the

complex and cross-cut, overlay, or degrade sand dunes belonging to units Qds2 and Qda2. Several sections of Qds2 deflect drainages from Qa and form small playettes between linear dunes. Sheetwash from the eastern fan creates a floodplain (Qfl2) that deluges the sand dunes and generates a ravinement surface which degrades segments of Qds1 and Qda3 (Figure 4.15).

To the north-northwest of the contact between Qss and Qds2 the density of individual and compound dunes (Qda4 & Qda6) begins to increase. In unit Qda4 elongate parabolic dunes are joined with lobate to elongate barchanbolic dunes that advance from 0 to 2.5  $\text{myr}^{-1}$  on an azimuth of 60-88 $^{\circ}$ . Just before the western slopes of the Slumbering Hills the parabolic-barchanbolic dunes (Qda4 & Qd6) start to merge and coalesce into large fields (Qda2). The large dune fields of Qda2 form on the east side of Desert Valley and traverse onto the Slumbering Hills at the rate 0.4 to 5.8  $\text{myr}^{-1}$  on an azimuth of 65-105 $^{\circ}$ .

Qda2 is split into two parallel fields separated by stabilized linear and elongate parabolic dunes from unit Qds1. Inside unit Qda2 are compound barchan, barchanbolic, and parabolic dunes with lunate, hemicyclic, and lobate shapes. The dunes merge into small crescentic complexes in the center of the unit and are distinguished by the presence of lunate to hemicyclic shaped barchanoidal ridges.

Figure 4.11 illustrates the elevational distribution of units Qd/Qb, Qds1, Qdd, Qss, Qfp, and Qda2. The rate of sand dune advancement for each unit discussed in this section and the following subsections is summarized on Table 6 (Section 4.5).

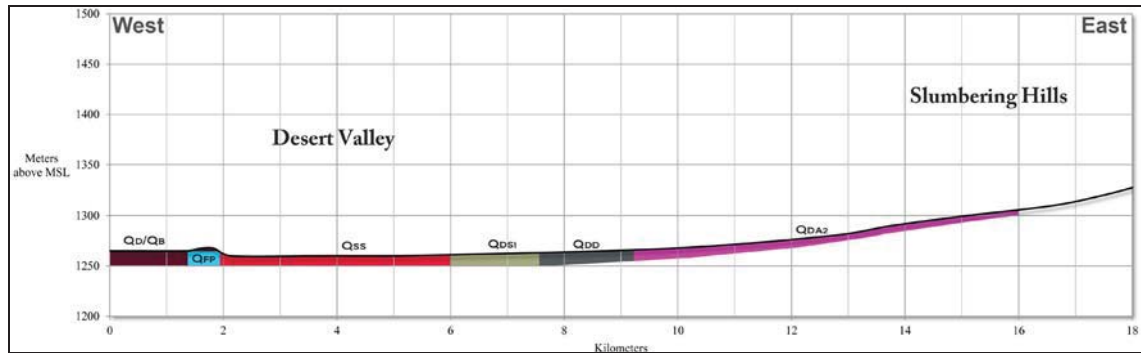


**Figure 4.11:** Topographic profile of Desert Valley combining features from north and south sections of Map 1. Unit thickness is not to scale. Qda2 is shown at proper map scale and includes net length of parallel fields.



**Image #19:** Dune islands from unit Qfp in Desert Valley.

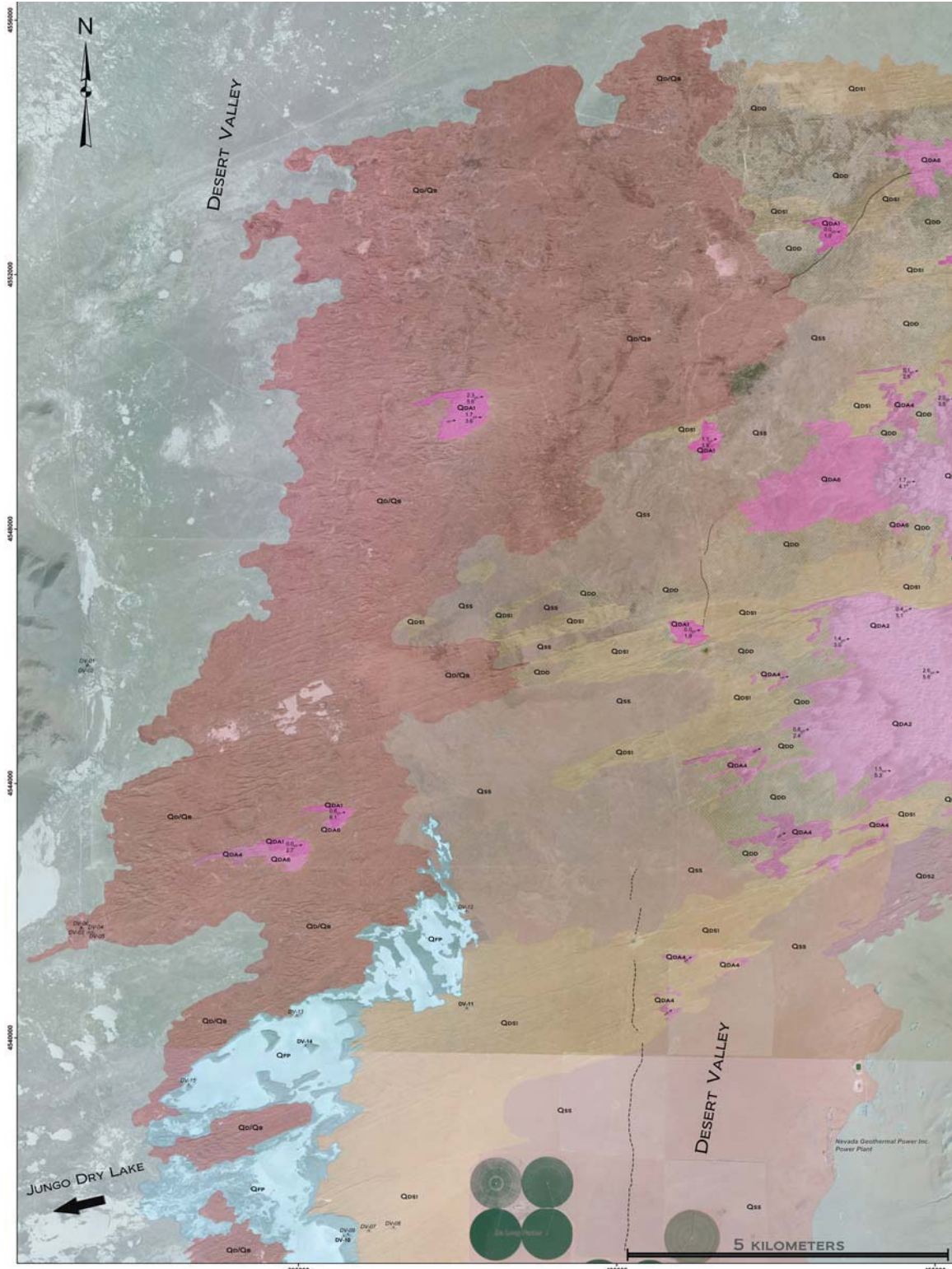


**Figure 4.12:** Southwest corner of Map 1 (Plate 3.1) in Desert Valley.

### Mormon Dan Butte

Mormon Dan Butte is located near the northern boundary of Map 1 (Plate 3.1) on the east side of Desert Valley upon the western flanks of the Slumbering Hills (Figures 4.13 & 4.14). The Butte outcrops on the valley floor and rises from 1290 to 1395 meters above MSL. Mormon Dan Butte is composed of metasedimentary bedrock from the Jungo terrane. The base of the Butte is covered by Lahontan strandlines and a variety of lacustrine deposits (Qb) that include; gravel bars, sandy beaches, embankments, and a tombolo. Mormon Dan Butte is indicated as Qb/TRr on Map 1 and Figure 4.14.

A majority of the landscape to the east of Mormon Dan Butte consists of stable and degraded dunes (Qds1 & Qdd). Although to the immediate northeast are active sand dunes from the Desert Valley North Complex (DVN; Figure 4.14). DVN is comprised of lunate to hemicyclic shaped barchanoidal ridges that advance 1.9 to 3.9  $\text{myr}^{-1}$  on an azimuth of 83-102°. On the south side of DVN are individual elongate parabolic and undifferentiated dunes which radially spread to the southeast (Qda6). Directly along the northeast leading edge of DVN is a prominent normal fault (Figure 4.14). The southern portion of DVN overlays and buries the fault. Directly to the south of the buried fault are stabilized parabolic dunes (Qds1), degraded dunes (Qdd), and a small sand sheet (Qss).

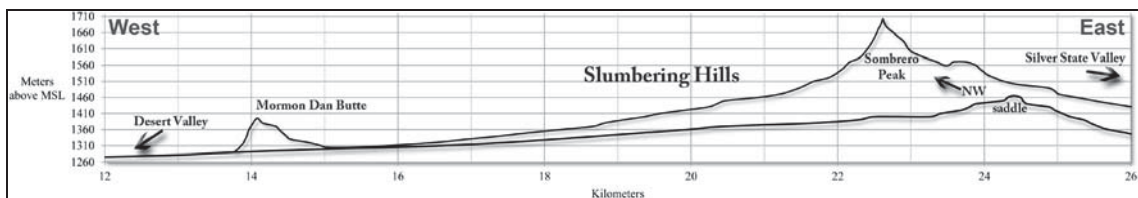


**Figure 4.13:** Topographic profile of the western flank of the Slumbering Hills showing the location of Mormon Dan Butte and Sombrero Peak. Lower profile line over the saddle is from Figure 1.2. The x-axis shows the total distance from the west side of Desert Valley.

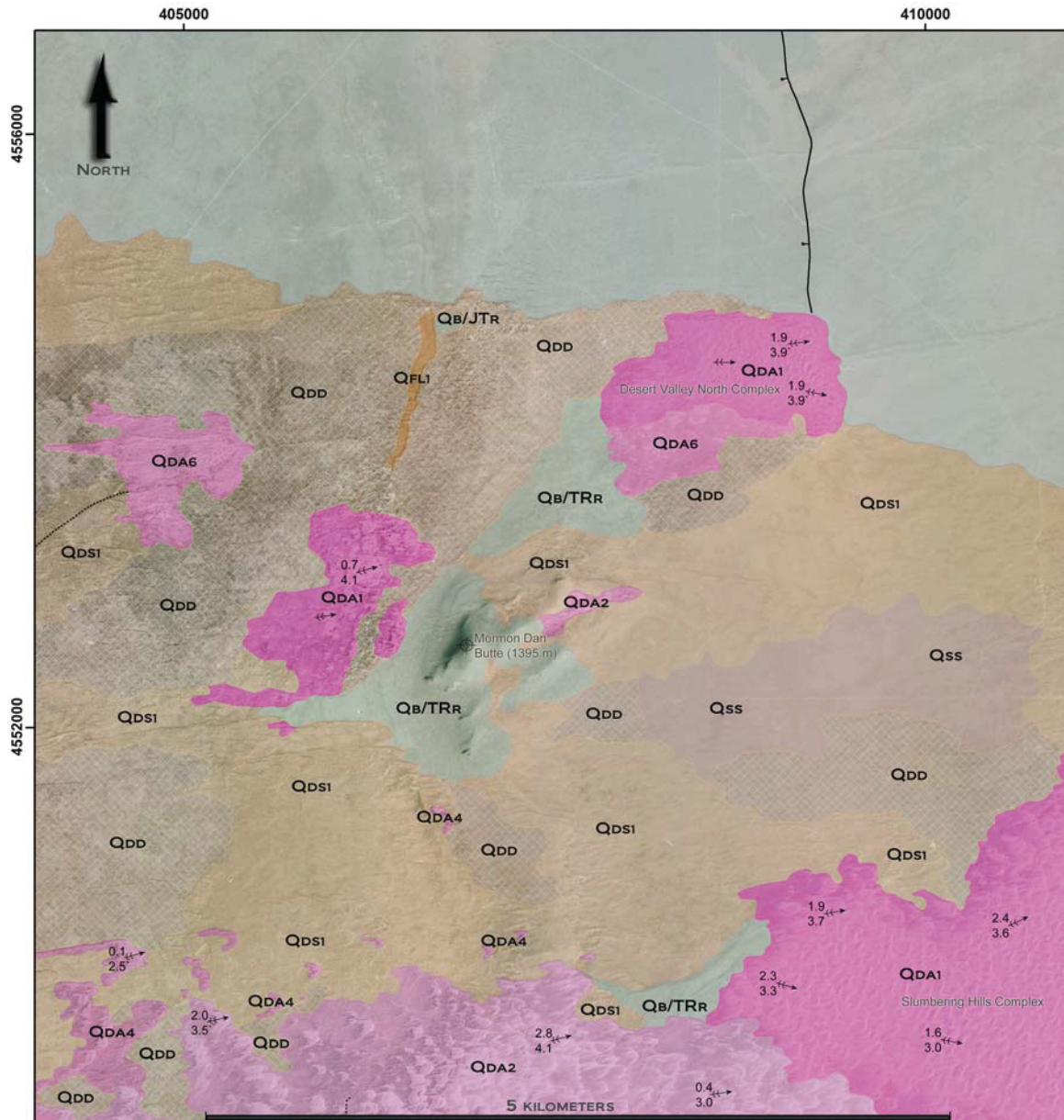


**Figure 4.14:** Mormon Dan Butte from Map 1 (Plate 3.1) in Desert Valley.

### *Western flank of the Slumbering Hills*

At the base of the Slumbering Hills two parallel dune fields composed of ridges, barchan, barchanbolic, and parabolic sand dunes from unit Qda2 (previously discussed in Section 4.4.1) extend out of Desert Valley. They progress approximately half-way up the western flanks of the hills and transition into the Slumbering Hills Complex (SHC) and a widely

spaced compound dune field (Qda3). The active dunes from SHC (Figure 4.15) and Qda3 are separated by a field of stabilized linear-parabolic dunes (Qds1).

Along the southern boundary of the map area Qda3 consists of widely spaced lobate to elongate shaped compound and individual barchanbolic-parabolic dunes. Qda3 forms two large dune fields that are offset towards the northeast by units Qds1 and Qda4. Near the eastern edge of Qda3 the sand dunes start to merge and stack into lunate to hemicyclic shaped crescentic ridges. On the western flanks and crest of the Slumbering Hills the fields are advancing at a rate of 0 to 3.3 myr<sup>-1</sup> on the azimuth 70-85°. Portions of Qda3 are stabilized by vegetation and degraded (Qdd) from wildfires, mining disturbances (Sandman project North Hill site), ponding water, livestock, and bioperturbation. The south-southeastern side of the southern field is incised by three floodplains (Qfl2) and two alluvial fans draining from an older unnamed fluvial channel (Qfl2), Blue Mountain Canyon, and off the northern slopes of Blue Mountain (shown on Map 1 and Figure 4.15).

To the north-northwest of Qda3 is the Slumbering Hills Complex (SHC) from unit Qda1. SHC is composed of wind-rippled lunate to hemicyclic shaped barchanoidal ridges, transverse ridges, and asymmetric star dunes. The periphery of the unit is comprised of compound barchan, barchanbolic, and parabolic dunes with hemicyclic, lobate, and elongate shapes. Ridges and compound dunes are advancing at a rate of 0.5 to 3.8 myr<sup>-1</sup> on the azimuth 65-105°. The east side of SHC is bordered by sheeting sand, parabolic and undifferentiated dunes from unit Qda5. Stabilized (Qds1) and degraded dunes (Qdd) contact the north-northeastern side of SHC and sporadically occur within Qda5. The

abundance of sheeting sand in Qda5 could indicate the stabilized (Qds1) and degraded dunes (Qdd) may have recently been reactivated from the loss of vegetation. It is also possible that airflow instabilities have resulted with scouring of SHC from supercritical winds or storm-blasts prevailing out of the west-southwest.

The east side of Qda5 is surrounded by stabilized (Qds1) and degraded dunes (Qdd) that contact the western boundary of the Crescent Sombrero Complex (CSC) beneath Sombrero Peak (1703 meters above MSL; Figure 4.13) and the Crescent Dunes summit (1522 meters above MSL). CSC (Qda1) is primarily comprised of lunate to hemicyclic shaped barchanoidal ridges and lesser amounts of transverse ridges and asymmetric star dunes. Along the upwind perimeter of the unit are compound barchan and barchanobolic dunes with hemicyclic to lobate shapes. Ridges and compound dunes are advancing 0.7 to 6.9  $\text{myr}^{-1}$  on an azimuth of 60-110°.

Along the southeast corner of CSC near the crest of the Slumbering Hills the ridges begin to merge, ramp, and form crescentic climbing dunes (Qda7). The climbing dunes are advancing 0 to 5.4  $\text{myr}^{-1}$  on an azimuth of 70-82°. At the crest of the hills unit Qda7 transforms into crescentic descending dunes (Qda8) and travels downslope into Silver State Valley. The descending dunes are advancing 0.5 to 5.4  $\text{myr}^{-1}$  at an azimuth of 60°. Below the crest of the Slumbering Hills the mountainside quickly decreases in slope which causes the leading edge of Qda8 to stack and increase in height. Immediately after stacking the descending dunes terminate on top of stabilized linear and parabolic dunes from unit Qds1. Units Qda1 (CSC), Qda7, Qda8, and Qds1 are shown on Figure 4.15.

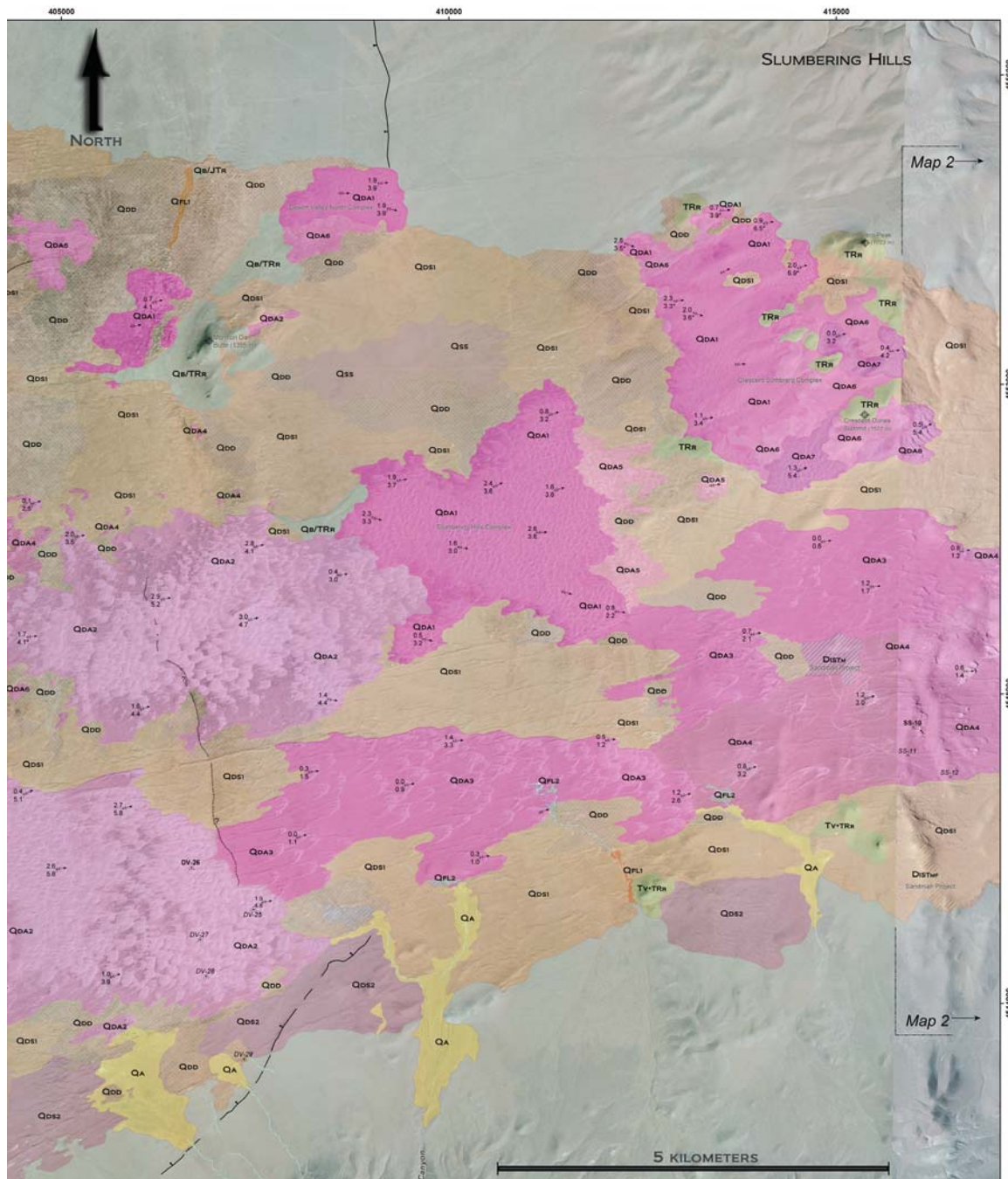


**Figure 4.15:** Northeast corner of Map 1 (Plate 3.1) showing the western flank of the Slumbering Hills.

#### **4.4.2 Crest of the Slumbering Hills to Silver State Valley (Map 2)**

The only sand dunes which completely traverse the crest of the Slumbering Hills and descend eastward into Silver State Valley are from unit Qda4. Dunes from Qda4 cross the crest to the southeast of Sombrero Peak at the saddle of the hills (Figures 4.13 & 4.16). Unit Qda4 consists of lobate to elongate shaped individual and compound barchanobolic-parabolic dunes that advance 0 to  $4.2 \text{ myr}^{-1}$  on an azimuth of  $60\text{-}102^\circ$ .

Map 2 (Plate 3.2) shows the broad placement of Qda4 from the crest of the Slumbering Hills to the lower elevations of Silver State Valley. On the lower eastern slopes of the Slumbering Hills intradune lengths begin to decrease as Qda4 merges with the dune fields from Qda2. In the south Qda4 skirts the south-southeastern perimeter of Qda2. After skirting Qda2 intradune lengths increase as Qda4 approaches the center of Silver State Valley and dissipates in unit Qda5b. The entire southern perimeter of Qda4 is bounded by stabilized linear and parabolic dunes from unit Qds1. Many sections of Qda4 are stabilized by vegetation or degraded by wildfires, mining disturbances, ponding water, livestock, ATVs, roadways, and bioperturbation.

Unit Qda5b begins forming along the eastern edge of Qda4 near the bottom of Silver State Valley. Qda5b is comprised of lobate to elongate shaped compound and individual barchanobolic-parabolic dunes that are advancing  $0.2$  to  $2.7 \text{ myr}^{-1}$  on an azimuth of  $73\text{-}76^\circ$ . Many portions of Qda5b are stabilized by vegetation and covered with fugitive dust and sheeting sand. The fugitive dust is most likely sourced from mining disturbances at the Sandman project site located upwind on the Slumbering Hills and Ten Mile Hills. Sheet sand on the unit suggests that sections of stabilized dunes within Qda5b may

have recently been reactivated from the loss of vegetation due to wildfire, livestock, and recreational activities. It is also possible that local airflow instabilities have delivered supercritical winds from the west-southwest which have scoured sand from upwind dunes in Qda4, Qda2, and Qds1.

On the eastern mid-slopes of the Slumbering Hills to the north of Qda4 is a long tabular field of crescentic descending dunes (Qda8) forming downwind and below stabilized linear-parabolic dunes from Qds1. Units Qda4 and Qda8 are separated by a fairly large floodplain (Qfl2) that is fed by runoff in the Slumbering Hills. The descending dunes from Qda8 are advancing 0.7 to 4.3  $\text{myr}^{-1}$  on an azimuth of 84-88°. Dunes from Qda8 on Map 2 (Plate 3.2) are similar to the descending dunes along the crest of the Slumbering Hills on Map 1 (Plate 3.1) however the field is much larger and well-developed. Along the midsection and leading edge of Qda8 the descending dunes stack as hillside gradients decrease and flatten out. The east side of Qda8 contacts and merges with unit Qda2.

In the central portion of Map 2 (Plate 3.2) unit Qda2 forms a large dune field composed of compound barchan, barchanobolic, and parabolic dunes with lunate, hemicyclic, and lobate shapes. Qda2 is advancing 0 to 5.5  $\text{myr}^{-1}$  on an azimuth of 81-115°. The eastern edge of Qda2 overlaps onto slower moving dunes from units Qda4, Qda5b, and stabilized dunes from Qds1. Along the north-northeastern contact of Qda2 are two small sections of sheeting sand, parabolic and undifferentiated dunes from unit Qda5. The far northeastern-eastern corner of Qda2 integrates with the Silver State Western Complex (SSWC) from unit Qda1.

SSWC (Qda1) is comprised of wind-rippled lunate to hemicyclic shaped barchanoidal ridges and compound barchan dunes. It also consists of asymmetric star and lobate barchanbolic dunes. SSWC is advancing 1 to 5.5 myr<sup>-1</sup> on an azimuth of 88-115° towards the center of Silver State Valley. The eastern side of SSWC contacts units Qdd, Qds1, Qp1, and Qfp. Between the years 1994-2006 wildfires, ponding water, and livestock significantly degraded the northeast corner of SSWC. Since 1996 dune activity in the degraded areas has dramatically increased.

Along the far northern edge of SSWC is an older very thin stabilized dune field boundary (Qds). Unit Qds has the shape of a parabolic tail and is composed of stabilized wind-blown deposits which once constituted the northern perimeter of active sand dunes. The western stoss-side of Qds begins above a large field of degraded dunes that overlay a sequence of late Pleistocene to early Holocene Sehoo beaches from Lake Lahontan (indicated as Qdd/Qb on Figure 4.17). Unit Qds discontinuously stretches 6.2 kilometers from 1388 meters above MSL down the eastern flanks of the Slumbering Hills to the bottom of Silver State Valley. The western margin of Qds may represent a paleo-location for the origin of sand dune advancement in SSWC.

The major dune fields in Silver State Valley are separated by a network of playas, playettes (Qp1), and paludal deposits (Qfp) along the low elevations of the basin at 1255-1267 meters above MSL (Image #20). Runoff from drainages in the northern and southern sections of Silver State Valley in the Slumbering Hills, Krum Hills, and Bloody Run Hills feed the network. When heavy rainfall or snowmelt accumulates in the center of Silver State Valley dune activity is impeded by ponding and flowing water. The

accumulation of water contributes to plant growth, limits sediment supply, and constricts the accommodation space that is necessary for the advancement of dunes.

Discharge entering the network from the south originates on a large alluvial fan (Qa) that drains off the Krum Hills. The distal lobes of the fan degrade, overlay, or cross-cut stabilized (Qds1 & Qds2) and active dunes (Qda5b) before forming several floodplains (Qfl2) that directly spill into Qfp. In the northern part of the valley there are multiple ephemeral drainages flowing southwest off the Bloody Run Hills. When excess runoff from the drainages reaches the valley floor it overflows into a primary drainage channel along the northeast leading edge of SSWC. The channel flows south against the leeward side of SSWC and spills into units Qp1 and Qfp. Additional runoff is also delivered to the primary channel from the Silver State draw on the eastern flanks of the Slumbering Hills. The primary drainage channel is indicated on Map 2 just to the east of sample location SS-18 above the north-northeast perimeter of SSWC (Figure 4.17).

Figure 4.16 uses the profile line from Figure 1.2 to illustrate the elevational distribution of units Qda2, Qda4, Qda5b, Qfp, and the saddle on the Slumbering Hills. The rate of sand dune advancement for each unit discussed in this section and the following subsection is summarized on Table 7 (Section 4.6).



**Image 20:** The center of Silver State Valley with the Bloody Run Hills in the background. View is towards the east. Author (N. Pepe) is sitting on a sand dune located at the leeward side of the Silver State Western Complex (SSWC). The small playa (Qp1) in the center of the image separates SSWC from unit Qda2 in the center of the valley. Below the Bloody Run Hills along the horizon is the Silver State Eastern Complex (SSEC).

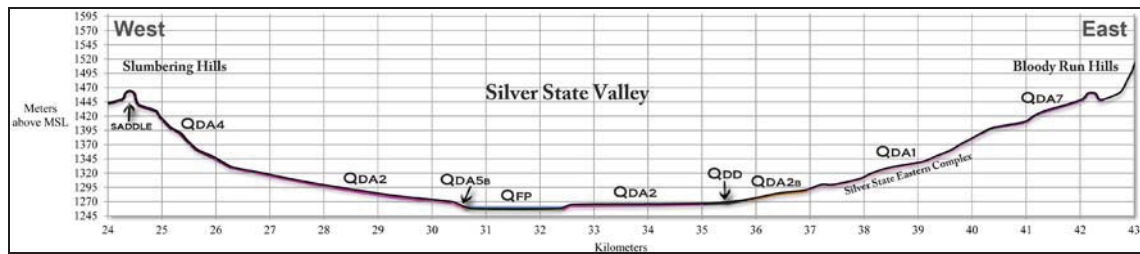


**Figure 4.16:** Topographic profile of the Slumbering Hills to the Bloody Run Hills. Unit thickness is not to scale. The x-axis displays the total distance from the west side of Desert Valley.

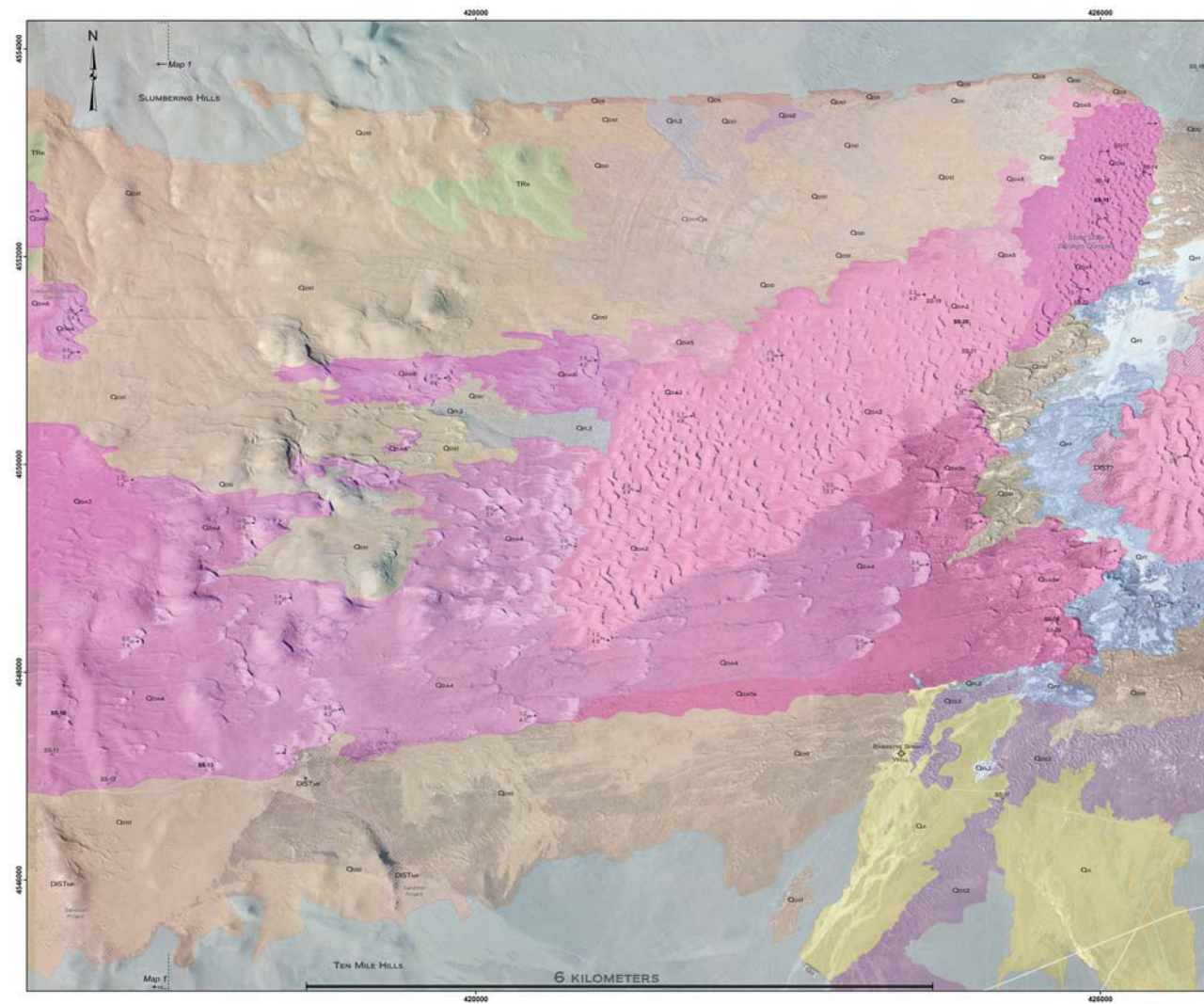


**Figure 4.17:** Western section of Map 2 (Plate 3.2) showing the eastern flank of the Slumbering Hills to the center of Silver State Valley.

***Center of Silver State Valley to the crest of the Bloody Run Hills***

Sand dune formation recommences just to the east of the playas (Qp1) and paludal deposits (Qfp) at the bottom of Silver State Valley. Near the center of the valley is an extension of the dune field from Qda2 on the lower slopes of the Slumbering Hills. The central field from Qda2 consists of lunate to lobate shaped compound barchan, barchanbolic, and parabolic dunes. Inside of Qda2 barchan and barchanbolic dunes merge into small complexes with barchanoidal and transverse ridges. Ridges and compound dunes are advancing 0.3 to 5.6 myr<sup>-1</sup> on an azimuth of 83-106°. The tallest dunes observed were found on the east and west sides of unit Qda2 where ridges extended to a maximum height of 28 meters. Stabilized linear and parabolic dunes from unit Qds1 contact the northern and southern margins of Qda2. At the northern edge of Qda2 is a thin stabilized field boundary from unit Qds. The eastern perimeter of Qda2 integrates with Qda2b and overlaps onto slower moving dunes and degraded surfaces belonging to units Qda4, Qda5b and Qdd (Figure 4.18).

Along the southeast contact of Qda2 slower moving dunes from unit Qda4 are comprised of lobate to elongate shaped compound and individual barchanbolic-parabolic dunes. Qda4 is advancing 0.3 to 3.5 myr<sup>-1</sup> on an azimuth of 95-105°. On the northeast contact of Qda2 and southeast contact of Qda4 are very slow moving dunes from Qda5b. Unit Qda5b is comprised of lobate to elongate shaped compound and individual barchanbolic-parabolic dunes mixed with sheeting sand. Unit Qda5b is advancing 0 to 1.6 myr<sup>-1</sup> on an azimuth of 72-102°. Portions of Qda4 and Qda5b are stabilized by vegetation and degraded by wildfires, ponding water, ATVs, livestock, and bioperturbation. The

presence of sheeting sand within Qda5b suggests the stabilized sections of the unit may have recently been reactivated from the loss of vegetation or due to anthropogenic disturbances. It is also possible that local airflow instabilities have generated supercritical winds which are scouring sand from the upwind unit Qda2.

The north-central eastern edge of Qda2 integrates with unit Qda2b in the center of the valley. Unit Qda2b is composed of hemicyclic to lobate shaped compound barchanobolic-parabolic dunes that are advancing 0.2 to 3.3 myr<sup>-1</sup> on an azimuth of 90-115°. The eastern leading edge of Qda2b merges with the west side of the Silver State Eastern Complex (SSEC) from unit Qda1.

In the east-central part of Silver State Valley are extensive fields of degraded dunes (Qdd) which bisect the active sand dunes from units Qda2, Qda2b, Qda4, Qda5b, and SSEC (Qda1). The degraded dunes are produced from runoff and ponding water in the northern and southern sections of the valley. In the north localized runoff from SSEC spills or seeps eastward and degrades unit Qda5b. Along the south side of the valley a large alluvial fan (Qa) drains off the Krum Hills and intersects the complex. The distal lobes of the fan have extensive floodplains (Qfl2) that extend northwest into the sand dunes. Sheetwash and overland flow from Qfl2 cross-cuts, overlays, and erodes vast parcels of active and stable dunes.

Uphill to the east of the large degraded section is SSEC from unit Qda1. SSEC is comprised of lunate to hemicyclic shaped barchanoidal ridges, transverse ridges, asymmetric star and lunate to lobate shaped compound barchan-barchanobolic dunes. The

unit begins forming on the lower western slopes the Bloody Run Hills and advances uphill at 0.3 to 4.4 myr<sup>-1</sup> on an azimuth of 73-90°. Almost the entire perimeter of SSEC is surrounded by sheeting sand, barchanbolic and parabolic dunes from unit Qda5b. The dunes from Qda5b are advancing 0 to 3 myr<sup>-1</sup> on an azimuth of 80-90°. The presence of reactivated dunes from Qda5b around a majority of SSEC suggests the complex may have been larger during an earlier period of eolian activity. Further evidence supporting this interpretation is the presence of two stabilized field boundaries from unit Qds. The field boundaries from Qds form two parabolic-like tails out of the west side of Qda5b along the southwest and northwest corners of SSEC.

Along the eastern edge of SSEC the dunes intercept steeper slopes and transition into two thin fields of crescentic climbing dunes (Qda7). The crescentic climbing dunes (Qda7) ascend the steeper slopes of the Bloody Run Hills at 0.1 to 5.3 myr<sup>-1</sup> on an azimuth of 64-130°. As the climbing dunes (Figure 4.18) traverse the western flank of the Bloody Run Hills they begin to merge, stack, and form transverse ridges at higher elevations near the leading edge of the unit. Runoff from the southwestern slopes of the Bloody Run Hills degrades, stabilizes, and separates the dune fields. Along the northeast corner of the northern field from Qda7 are three crescentic complexes (Qda1) forming along the crest of the hills. The complexes (Qda1) are composed of transverse ridges, sand ramps, barchanbolic and lee (echo) dunes. Average rates of advancement could not be determined from historical imagery. However the orientation of sand dunes indicates the complexes are crossing the crest of the Bloody Run Hills at an azimuth of 60-90°. Figure 4.16 shows the elevational distribution of units Qda1 (SSEC), Qda2-2b, Qdd, and Qda7.

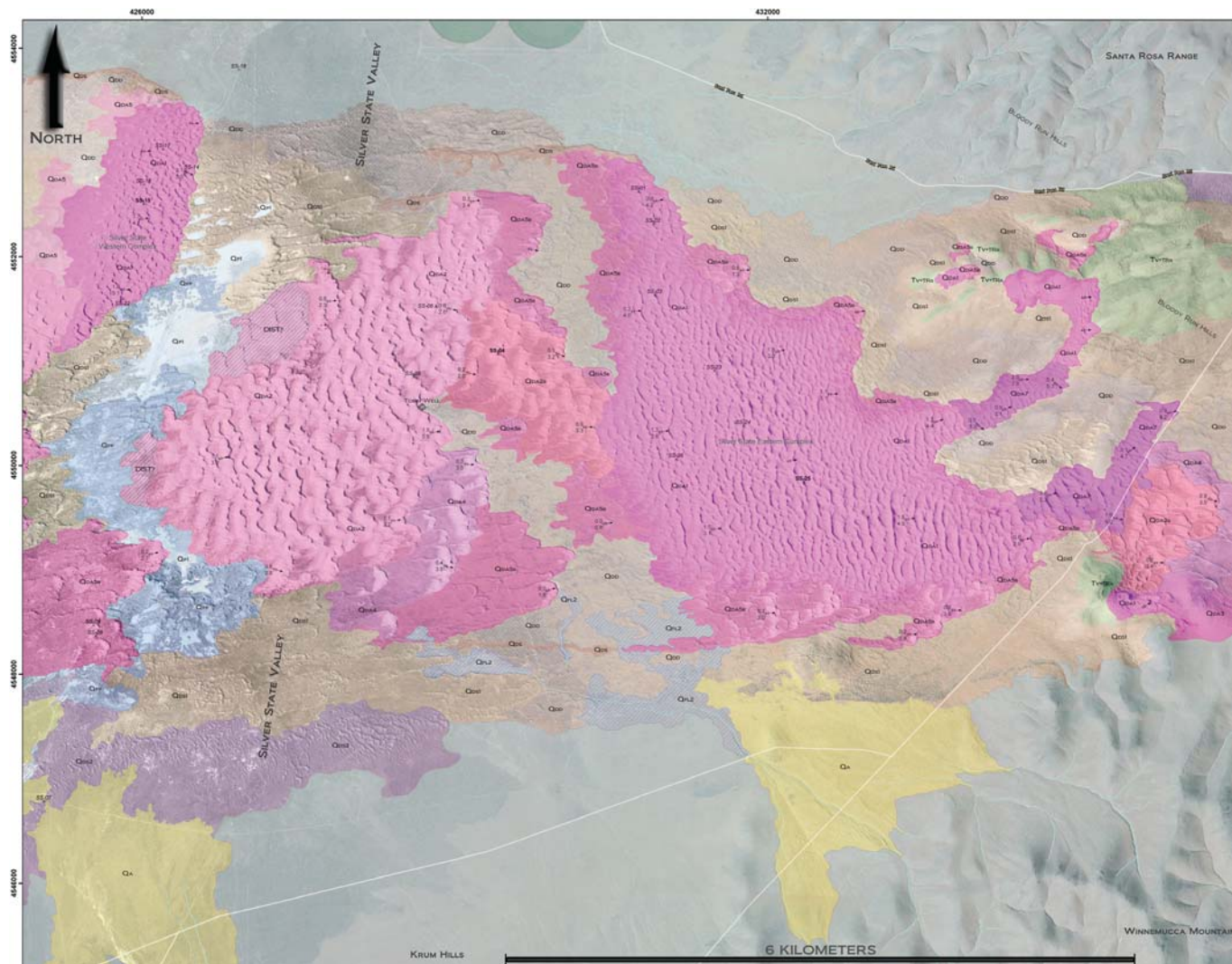


**Figure 4.18:** Central section of Map 2 (Plate 3.2) showing the center of Silver State Valley to the Bloody Run Hills.

#### **4.4.3 Crest of the Bloody Run Hills to Paradise Valley (Map 2)**

The crest of the Bloody Run Hills varies in altitude from 1495 to 1664 meters above MSL. Stabilized wind-blown deposits occupy a majority of the crest although on the far northern and southern perimeters of the hills are semi-active and active sections of sand dunes.

In the north on the southwest side of the intersection of Sand Pass Road and Pipeline Line Road is an isolated field of semi-active transverse dunes belonging to unit Qds2. Since the year 1994 the field has increased in activity and expanded northeast to the south side of Sand Pass Road. Along the southern perimeter of the Bloody Run Hills crescentic climbing dunes (Qda7) from Silver State Valley extend to the crest and cross Pipeline Line Road. On the east side of the road Qda7 merges with Qda2b and overlaps onto slower moving dunes from Qda4. At the merger of units Qda7 and Qda2b are lunate to lobate shaped compound barchan-barchanbolic dunes. The compound dunes from Qda2b descend the Bloody Run Hills at the rate 0.2 to 3.5  $\text{myr}^{-1}$  on the azimuth 88-108° and overlap onto slower moving dunes from unit Qda4.

The slower moving sand dunes from unit Qda4 are comprised of lunate to elongate shaped compound and individual barchanbolic-parabolic dunes that are advancing 0 to 2.1  $\text{myr}^{-1}$  on an azimuth of 57-106°. Unit Qda4 expands into an extensive dune field and descends the entire eastern flank of the Bloody Run Hills to the ATV Park on the west side of Highway 95. On the west side of the ATV Park to the highway crossing Qda4 increases in activity to  $\leq 5.8 \text{ myr}^{-1}$  on an azimuth of 35-90°.

Along the southern perimeter of Qda4 on the southeast flanks of the Bloody Run Hills is a second field of lunate to elongate shaped compound and individual barchanbolic-parabolic dunes from unit Qda3. The dunes from Qda3 are similar to Qda4 however they are smaller, slower moving, and partially stabilized by vegetation. Unit Qda3 begins forming below a small crescentic complex (Qda1) and descends the entire flank of the Bloody Run Hills to the intersection of Highway 95 at the rate 0 to 2.6 myr<sup>-1</sup> on an azimuth of 72-90°.

To the north of Qda4 on the mid-slopes of the Bloody Run Hills are a set of north-south trending bedrock ridges. The ridges are composed of Tertiary volcanic flows and metasedimentary bedrock from the Jungo terrane (indicated as Tv + TRr on Map 2 and Figure 4.20). At the beginning of the ridges in the south Qda4 merges with Qda9. Unit Qda9 consists of climbing, ramping, cliff-top, barchanbolic and lee (echo) dunes that are advancing 0 to 2.3 myr<sup>-1</sup> on an azimuth of 87-90°.

At the end of the ridges on the northeast portion of the Bloody Run Hills are units Qda8, and a second smaller field from Qda4 (Figure 4.20). Unit Qda8 descends the steepest slopes of the Bloody Run Hills and forms descending barchanbolic dunes that stack upon one another and advance 0 to 1.4 myr<sup>-1</sup> on an azimuth of 43-86°. The descending dunes are isolated from the other active units by stabilized dunes from Qds1. In the far north the second smaller field from Qd4 forms parallel to unit Qda8. The dunes from Qda4 are advancing 0 to 4.3 myr<sup>-1</sup> on an azimuth of 76-88°. Unit Qda4 descends to the bottom of the Bloody Run Hills into Paradise Valley and merges with compound parabolic dunes belonging to unit Qda3.

The compound parabolic dunes (Qda3) have elongate shape and advance 0 to 4.6 myr<sup>-1</sup> on an azimuth of 76-82°. Unit Qda3 continues advancing eastward and crosses Highway 95 in the northern section of the map area. The eastern leading edge of Qda3 becomes integrated with barchanbolic-parabolic dunes (Qda2b) to the south of the Feed Lot in east-central Paradise Valley (Figure 4.20).

Figure 4.19 illustrates the elevational distribution of units Qda4, Qds1, and the location of the crossing on Highway 95 using the profile line from Figure 1.2. The rate of sand dune advancement for each unit discussed in this section and following subsection is summarized on Table 8 (Section 4.7).

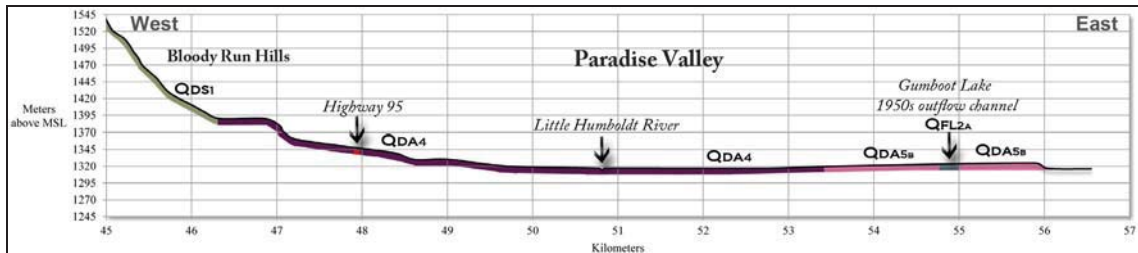


**Figure 4.19:** Topographic profile of the eastern flank of the Bloody Run Hills to the center of Paradise Valley. Unit thickness is not to scale.

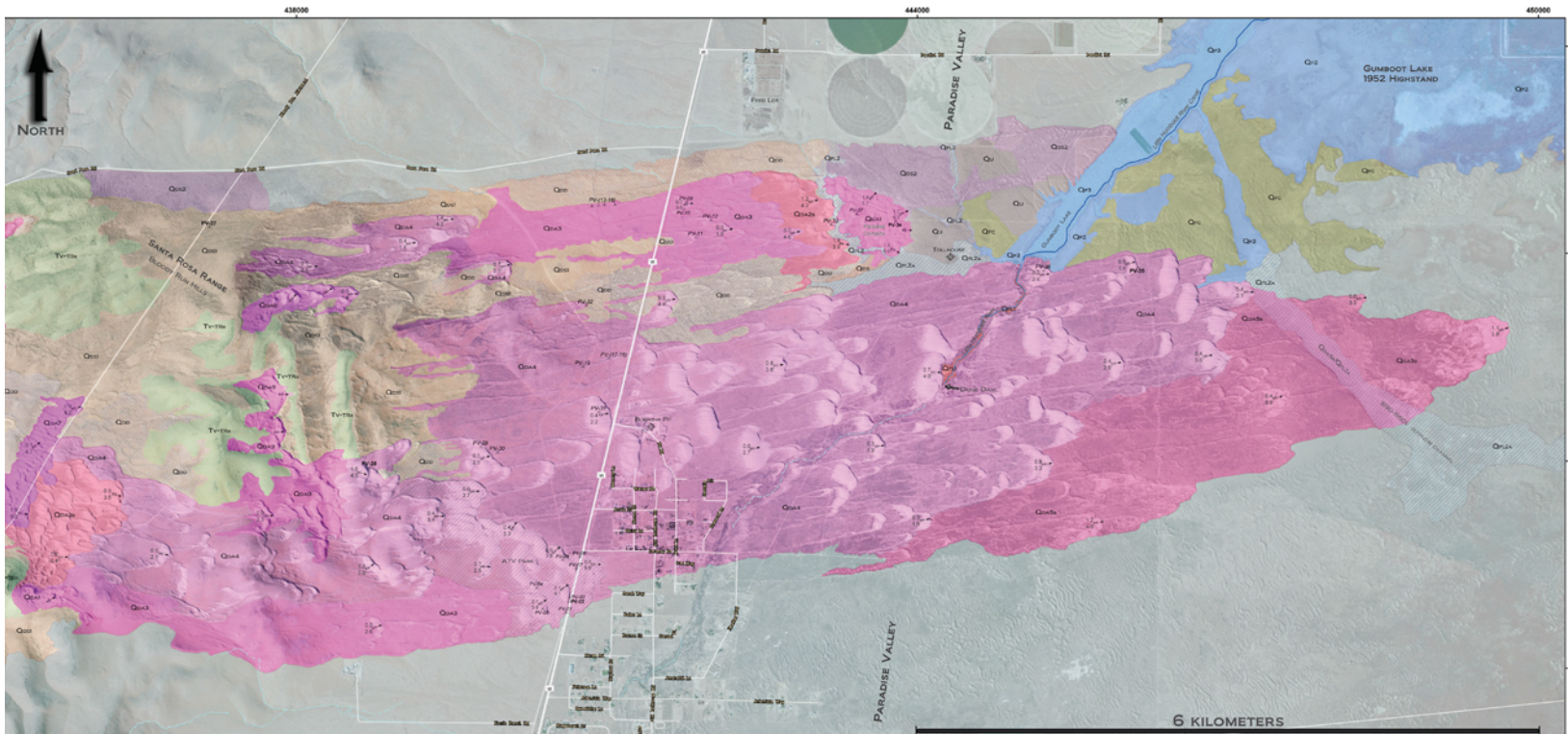


**Figure 4.20:** Eastern section of Map 2 (Plate 3.2) showing the crest of the Bloody Run Hills to the center of Paradise Valley.

### ***Highway 95 to the center of Paradise Valley***

Highway 95 bisects WDC on the west side of Paradise Valley. Sand drifts east across the highway and begins forming dunes in the northern and southern sections of the map area. The advancing dunes approach Gumboot Lake in the north and to the south the advancing dunes pass through a small residential community and engulf the channel of the Little Humboldt River (shown on Map 2 and Figure 4.20).

East of the highway crossing in the northern part of the valley unit Qda3 (discussed previously in Section 4.4.3) integrates with Qda2b to the south of the Feed Lot. Unit Qda2b is composed of lunate to lobate shaped compound and individual barchanbolic-parabolic dunes that are advancing  $1.2$  to  $4.2 \text{ myr}^{-1}$  on an azimuth  $77\text{-}100^\circ$ . Near the leeward side of Qda2b dunes merge and form short discontinuous ridges. Sand dune advancement along the eastern edge of Qda2b is impeded by runoff draining southwest out of the Feed Lot. The runoff forms an ephemeral fluvial channel and floodplain (Qfl2) that extends through Qda2b towards the Tollhouse site (Map 2 and Figure 4.20) in the center of the valley.

On the east side of Qfl2 is the Paradise Complex (PC) from unit Qda1. PC is a small crescentic dune field consisting of hemicyclic barchanoidal ridges and lunate to lobate shaped compound barchan-barchanbolic dunes. The ridges and dunes from PC are advancing  $1$  to  $6 \text{ myr}^{-1}$  on an azimuth of  $45\text{-}102^\circ$ . Along the southern perimeter of PC the fluvial channel from Qfl2 has degraded the complex and formed a stabilized dune field boundary (Qds). Near the southeast corner of PC the channel from Qfl2 has breached the dunes and drains southeast directly towards the Tollhouse site. The eastern leading edge

of PC advances onto stabilized transverse dunes (Qds1), undifferentiated dunes and fluvial fill-cut deposits (Qu) before terminating to the west of Gumboot Lake.

In the southern portion of the map area the extensive barchanbolic-parabolic dune fields from unit Qda4 (discussed previously in Section 4.4.3) continue on the east side of Highway 95. Near the highway crossing at the ATV Park the sand dunes begin to increase in size and merge into compound barchanbolic-parabolic dunes with lobate to elongate shape. The compound barchanbolic-parabolic dunes are advancing 0 to 4.4  $\text{myr}^{-1}$  on an azimuth of 74-90°. As Qda4 approaches the center of the valley the sand dunes descend to an altitude of 1313-1316 meters above MSL at the channel of the Little Humboldt River.

In the center of Qda4 the channel of the Little Humboldt River becomes completely engulfed by two large barchanbolic dunes. The dunes infill the river channel and form a natural earthen dam (Map 2 and Figure 4.20) that cut-offs the floodplain (Qfl1). Approximately every 5 years (Cohen 1964) Gumboot Lake fills to 1315.5 meters above MSL (indicated as Qp3 on Map 2). During these events overflow from Gumboot Lake enters the Little Humboldt River and ponds against the dune dam. Previous studies have estimated that every 15 years (Harrill & Moore 1970; Prudic & Herman 1996) Gumboot Lake fills to 1316.7 meters above MSL (Qp2) and discharge out of the lake into the Little Humboldt River is capable of breaching the dunes. When the dune dam is breached the upper reaches of the Little Humboldt River extend through unit Qda4 and connect with the main stem of the Humboldt River to the southwest. The last documented occurrence for a flood of this scale was in the year 1986 (Nevada Division of Water Planning 2000).

Since 1986 the sand dunes from Qda4 have been able to continue infilling the river channel and advance eastward. On the east side of the Little Humboldt River unit Qda4 continues advancing east–northeast and slowly rises in elevation. In the center of Paradise Valley unit Qda4 merges with Qda5b. Unit Qda5b is comprised of hemicyclic to elongate shaped barchanbolic-parabolic dunes that mix with sheeting sand. The dunes are advancing 0.4 to 5.9 myr<sup>-1</sup> on an azimuth of 73-82°.

In the 1950s a series of floods on Gumboot Lake caused water to spill over its southwestern shorelines into unit Qda5b. The overflow drained down an abandoned channel of the Little Humboldt River on the southeast corner of Gumboot Lake. Flood waters ponded and formed an outflow channel (Qfl2a; shown on Map 2 and Figure 4.20) which extended 7-12 kilometers in the direction of Golconda before running dry (Harrill & Moore 1970). The series of floods also formed a small floodplain that dissected the northern perimeter of Qda4 near the Tollhouse site.

During the years 1890, 1910, and 1943 (U.S. Soil Conservation Service 1962, U.S. Army 1975, Nevada Division of Water Planning 2000) Gumboot Lake flooded over its entire shoreline in Paradise Valley. Overflow from Gumboot Lake completely submerged Qda5b and portions of Qda4 in the center of the valley. Many sections of the dunes were completely degraded or washed away towards the main stem of the Humboldt River. Dredging of the Little Humboldt River channel and the upstream installation of Chimney Reservoir (previously discussed in Section 3.6) have mitigated and prevented floods of this magnitude from reoccurring on Gumboot Lake. The approximate spatial coverage and southern extent of the floods is shown on Figure 1.2.

The sand dunes in the center of Paradise Valley have not been submerged for at least 70 years. During this time unit Qda5b has reactivated and advanced eastward. The sand dunes have crossed and partially infilled the 1950s outflow channel (indicated as Qda5b/Qfl2a on Map 2 and Figure 4.20) however the abandoned drainage is still easily seen on aerial imagery. Sand dune advancement continues eastward and ends in the central part of Paradise Valley. Figure 4.19 illustrates the elevational distribution of units Qda4, Qda5b, Qfl2a, Highway 95, and the channel of the Little Humboldt River.

#### **4.5 Direction and rate of sand dune advancement in Desert Valley**

The direction and average rate of sand dune advancement in Desert Valley to the Slumbering Hills was measured at 93 locations on Map 1 (Plate 3.1). Results from the measurements are presented on Table 6.

**Table 6:** Direction and rate of sand dune advancement in Desert Valley to the Slumbering Hills

Unit	Azimuth	minimum rate ( $\text{myr}^{-1}$ )	maximum rate ( $\text{myr}^{-1}$ )	Location
Isolated Qda1 (crescentic complexes)	75-90°	0 - 2.3	2.7 - 6.1	Desert Valley-west
Isolated Qda1 (crescentic complexes)	70-102°	0 - 1.1	1 - 4.1	Desert Valley-east
Qda4 (barchanbolic-parabolic)	60-88°	0 - 0.1	0.1 - 2.5	Desert Valley-east
Qda2 (ridges-barchan-barchanbolic-parabolic)	65-105°	0.4 - 2.9	2.4 - 5.8	DV to Slumbering Hills
Qda1 (Desert Valley North Complex)	83-102°	1.9	3.9	NE of Mormon Dan Butte
Qda1 (Slumbering Hills Complex)	65-105°	0.5 - 2.6	2.2 - 3.8	Slumbering Hills-west
Qda1 (Crescent Sombrero Complex)	60-110°	0.7 - 2.5	3.3 - 6.9	Slumbering Hills-west
Qda3 (barchanbolic-parabolic)	70-85°	0-1.4	0.8 - 3.3	Slumbering Hills-west
Qda7-8 (climbing & descending)	60-82°	0 - 1.3	3.2 - 5.4	Slumbering Hills-crest
Qda4 (barchanbolic-parabolic)	72-88°	0.6-1.2	1.4-3.2	Slumbering Hills-crest

Figure 4.21 plots the orientations on a rose diagram using 4° intervals. The orientation of sand dunes in Desert Valley and the Slumbering Hills trend from 60-110° with an average direction of 79.3°. Two primary modes can be deciphered from Figure 4.21 that have percent frequencies greater than 5 percent; 77-92° (48.35%) and 65-76° (38.73%).

The bimodal distribution on the rose diagram implies a majority of the winds responsible for the entrainment of sand prevail out of the west-southwest from the average direction of 259.3°.

These observations are consistent with calculations by Jewell & Nicoll (2011) and the WeatherSpark model (Figure 2.1). Jewell & Nicoll (2011) determined between the years 1950-2000 at the Winnemucca WSO airport the resultant drift direction of sand was approximately 78-79° (Figure 2.2). The WeatherSpark model from the years 1948-2013 estimated the strongest annual winds in Winnemucca prevail 28% of the time from the west to southwest during the warm season months of April to the middle of July. During these months the model also shows the average daily maximum wind speed is near 7 ms<sup>-1</sup>. It can be concluded from the similar findings that wind regimes in Desert Valley and the Slumbering Hills are similar to Winnemucca. If this is true it suggests the sand dunes reach peak advancement rates between the months of April to July.

The historical average rate of sand dune advancement in Desert Valley to the Slumbering Hills for the crescentic complexes (Qda1) and largest dune fields (Qda2) is compared between the years 1980-2012 on Figure 4.22. The periods of measurement on the plot are 1980-1994, 1994-2000, 2000-2006, and 2006-2012. Unit Qda1 from the isolated crescentic complexes was not surveyed on the 1980 USGS topographic maps and could not be included in the measurements for the period of 1980-1994.

Figure 4.22 indicates the rate of sand dune advancement has temporally fluctuated and varied by location on Map 1 (Plate 3.1). During the years 1994-2000 the rate of

advancement for the dune fields of Qda2 increased by  $2.2 \text{ myr}^{-1}$  but in the Slumbering Hills-Crescent Sombrero Complexes (Qda1) the rate decreased at least  $1.5 \text{ myr}^{-1}$ . Another significant observation is during the period of 2000-2006 the situation reversed and the advancement rate of Qda2 decreased  $2.5 \text{ myr}^{-1}$  and the Slumbering Hills-Crescent Sombrero Complexes (Qda1) significantly increased  $3.1 \text{ myr}^{-1}$ . Since 2006 the average rate of advancement in both units has been declining  $0.5$  to  $1.3 \text{ myr}^{-1}$ . A third important observation is the advancement rate of isolated crescentic complexes (Qda1) on the basin floor in Desert Valley has not fluctuated. Since the year 2000 the rate of advancement has gradually increased by  $0.7 \text{ myr}^{-1}$ .

The cause of spatiotemporal variance in the rate of sand dune advancement from units Qda1 and Qda2 is uncertain. Landscape feedback mechanisms that control eolian activity may have experienced interference from the Jungo Complex wildfire of 1999 and precipitation from the 1997-98 El Niño season. It is plausible that new or existing sand sources at higher elevations in the Slumbering Hills & Crescent Sombrero Complexes were unlocked by the Jungo Complex wildfire and thus increased the sediment supply and activity of dunes following the event. In contrast the fields of Qda2 may have been affected by changes in weather patterns associated with severe precipitation from the 1997-98 El Niño season. Alluvial sheetwash, overland flow, and ponding water which drain into the unit may have limited sediment availability and accommodation space that was necessary for dune formation. A secondary vegetative response following the floods could have increased plant growth at lower elevations and stabilized portions of Qda2. The combined effects would have resulted with a lower rate of sand dune advancement.

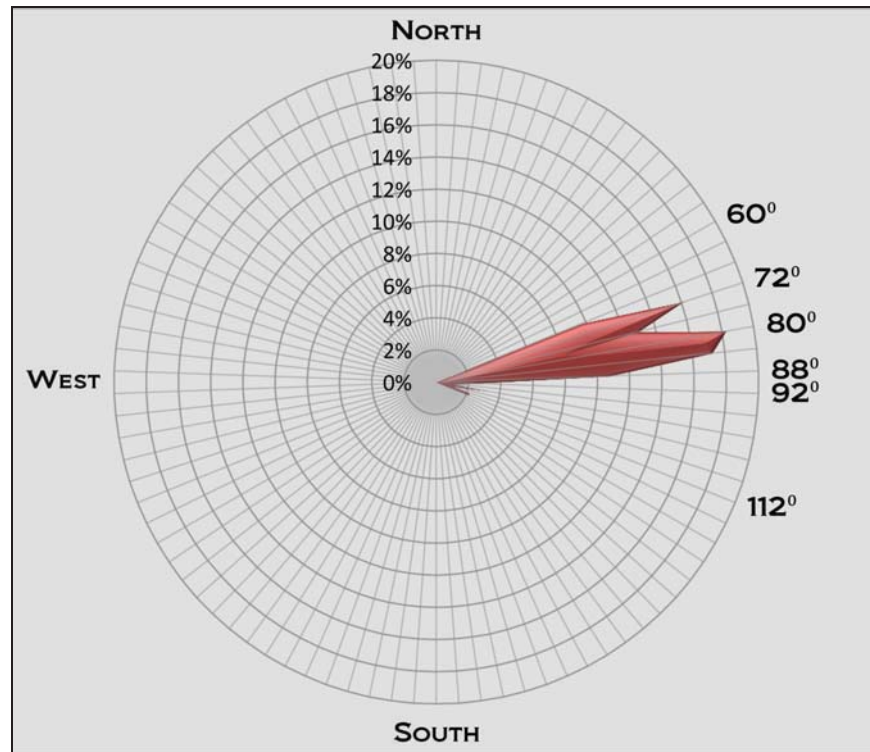


**Figure 4.21:** Rose diagram showing direction of sand dune advancement in Desert Valley to the Slumbering Hills.

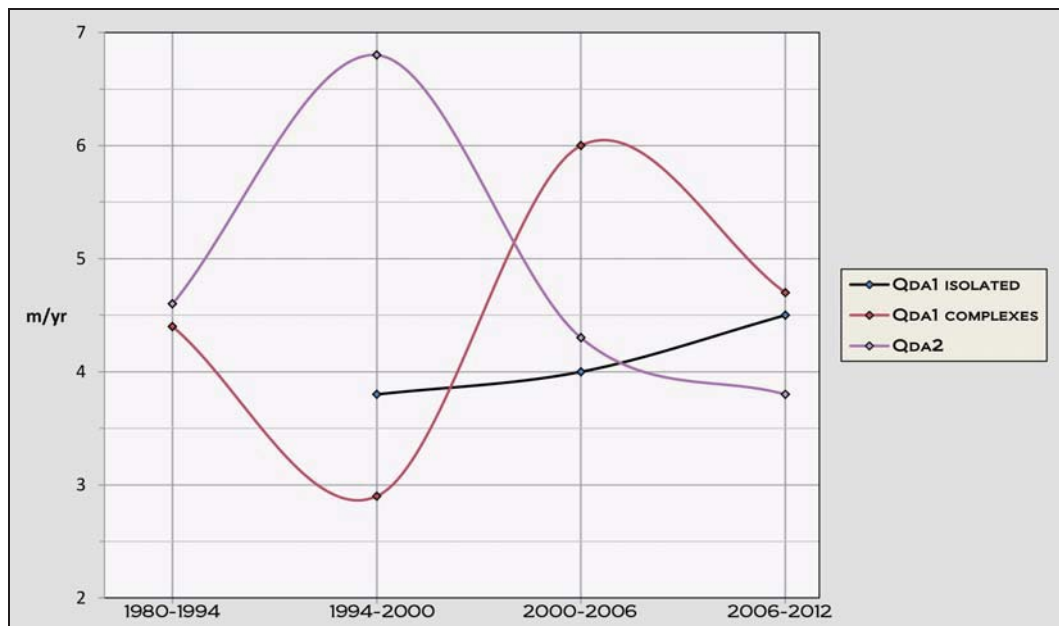


**Figure 4.22:** Rate of sand dune advancement in Desert Valley to the Slumbering Hills.

#### 4.6 Direction and rate of sand dune advancement in Silver State Valley

The direction and average rate of sand dune advancement in Silver State Valley was measured on Map 2 (Plate 3.2) from 75 locations between the eastern flanks of the Slumbering Hills to the crest of Bloody Run Hills. Results from the measurements are presented on Table 7.

**Table 7:** Direction and rate of sand dune advancement in Silver State Valley

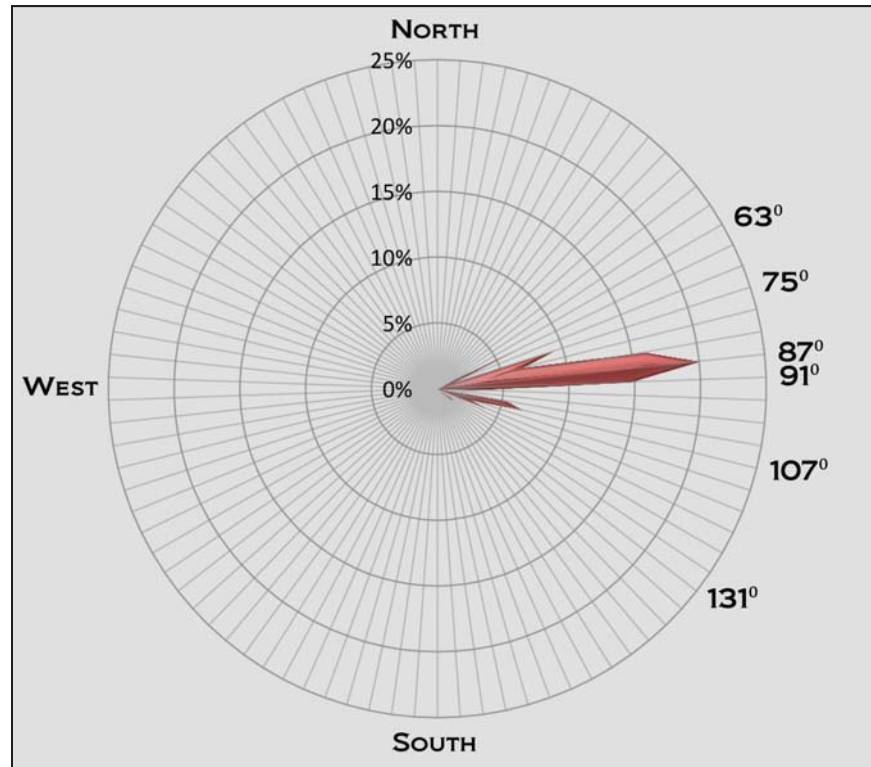
Unit	Azimuth	minimum rate ( $\text{myr}^{-1}$ )	maximum rate ( $\text{myr}^{-1}$ )	Location
Qda4 (barchanbolic-parabolic)	60-102°	0 - 1.2	1.4 - 4.2	Slumbering Hills-east
Qda8 (descending)	84-88°	0.7 - 2.8	4.2 - 4.3	Slumbering Hills-east
Qda2 (barchan-barchanbolic-parabolic)	81-115°	0 - 2.7	3.1 - 5.5	Silver State Valley-west
Qda1 (Silver State Western Complex)	88-115°	1.0 - 2.1	4.1 - 5.5	Silver State Valley-west
Qda5b (barchanbolic-parabolic)	73-76°	0.2	2.4 - 2.7	Silver State Valley-west
Qda2 (ridges-barchan-barchanbolic-parabolic)	83-106°	0.3 - 1.5	2.3 - 5.6	Silver State Valley-center
Qda4 (barchanbolic-parabolic)	95-105°	0.3 - 0.4	3.5	Silver State Valley-center
Qda5b (barchanbolic-parabolic)	72-102°	0	1.6	Silver State Valley-center
Qda2b (ridges-barchan-barchanbolic)	90-115°	0.2 - 0.9	2.0 - 3.3	Silver State Valley-center
Qda1 (Silver State Eastern Complex)	73-90°	0.3 - 1.6	2.9 - 4.4	Silver State Valley-east
Qda5b (barchanbolic-parabolic)	80-90°	0 - 0.6	0.8 - 3.0	Silver State Valley-east
Qda7 (climbing)	64-130°	0.1 - 3.0	3.1 - 5.3	Silver State Valley-east

Figure 4.23 plots the orientations on a rose diagram using  $4^{\circ}$  intervals. The orientation of sand dunes in Silver State Valley trend from  $60-130^{\circ}$  with an average direction of  $87^{\circ}$ . Four modes can be deciphered from Figure 4.23 that have percent frequencies greater than 5 percent;  $80-91^{\circ}$  (50.86%),  $68-79^{\circ}$  (17.33%),  $104-111^{\circ}$  (14.67%), and  $60-67^{\circ}$  (8%). The distribution on the rose diagram implies a majority of the winds responsible for the entrainment of sand prevail out of the northwest to southwest from the average direction of  $267^{\circ}$ .

These observations are not consistent with calculations by Jewell & Nicoll (2011). In Winnemucca during the years 1950-2000 Jewell & Nicoll (2011) determined the resultant drift direction of sand was approximately  $78-79^{\circ}$  (Figure 2.2). The orientation of dunes in

Silver State Valley reveals that sand is drifting at least 8-9° further to the east. A simple explanation for the discrepancy is the topography of Blue Mountain, Ten Mile Hills, Krum Hills, and Winnemucca Mountain in the southern section of Silver State Valley blocks a portion of the regional winds which prevail from the southwest. This setting may enhance the effect of northwesterly winds and move the sand dunes in a more easterly-southeasterly direction. The WeatherSpark model (Figure 2.1) potentially confirms this assumption. It estimates the strongest annual winds occur in the warm season months when the daily maximum wind speed is slightly above 7 ms<sup>-1</sup>. The model also shows during these months 9-12% of the winds prevail from the northwest.

The historical average rate of sand dune advancement in Silver State Valley from the crescentic complexes (Qda1), large dune fields (Qda2), and areas of reactivated barchanbolic-parabolic dunes (Qda5b) are compared during the years 1980-2012 on Figure 4.24. The periods of measurement on the plot are 1980-1994, 1994-2006, and 2006-2012. Results demonstrate that since 1980 the rate of sand dune advancement in Silver State Valley has declined an average of 0.1 to 1.5 myr<sup>-1</sup>. Unit Qda2 from the western side of the valley is the only area which demonstrated an increase (0.2 myr<sup>-1</sup>) however this was only between the years 1994-2006. Figure 4.24 is consistent with drift potential calculations from Jewell & Nicoll (2011) on Figure 2.3. The variation in drift potential of sand is illustrated by Jewell & Nicoll (2011) to relatively decrease in Winnemucca during the years 1954-2000. Measurements on Figure 4.24 illustrate this general pattern has also occurred in Silver State Valley.



**Figure 4.23:** Rose diagram showing direction of sand dune advancement in Silver State Valley.

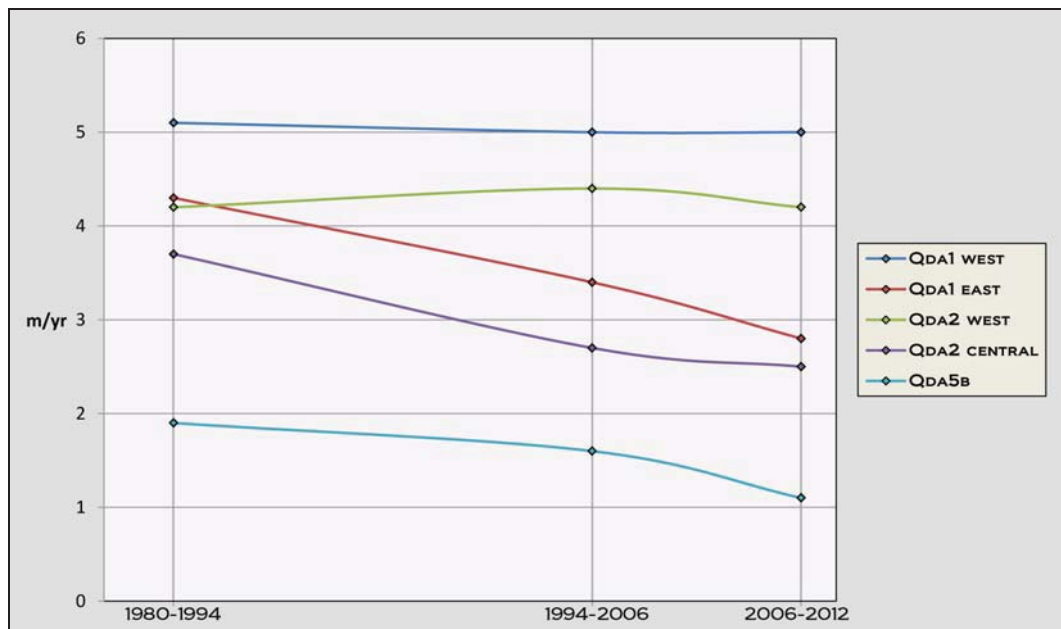


**Figure 4.24:** Rate of sand dune advancement in Silver State Valley.

#### 4.7 Direction and rate of sand dune advancement in Paradise Valley

The direction and average rate of sand dune advancement in Paradise Valley was measured on Map 2 (Plate 3.2) from 52 locations between the crest of the Bloody Run Hills to the center of Paradise Valley. Results from the measurements are presented on Table 8.

**Table 8:** Direction and rate of sand dune advancement in Paradise Valley

Unit	Azimuth	minimum rate (myr <sup>-1</sup> )	maximum rate (myr <sup>-1</sup> )	Location
Qda2b (barchan-barchanbolic)	89-108°	0.2 - 0.9	3.4 - 3.5	Bloody Run Hills-crest
Qda9 (climbing, ramps, cliff-top, lee)	87-90°	0	2.3	Bloody Run Hills-crest
Qda8 (descending)	43-86°	0	1.4	Bloody Run Hills
Qda4 (barchanbolic-parabolic)	57-106	0 - 1.6	0.6 - 4.3	Paradise Valley-west
Qda3 (barchanbolic-parabolic)	72-90°	0	2.6	Paradise Valley-west
Qda4 (barchanbolic-parabolic)	76-88°	0.4 - 1.4	1.6 - 4.3	Paradise Valley-north
Qda3 (parabolic)	76-82°	0	1.6 - 4.6	Paradise Valley-north
Qda2b (barchan-barchanbolic)	77-100°	1.2 - 1.4	3.9 - 4.2	Paradise Valley-north
Qda1 (Paradise Complex)	45-120°	1.0 - 1.8	5.3 - 6.0	Paradise Valley-north
Qda4 (ridges-barchanbolic-parabolic)	35-90°	0 - 2.1	2.5 - 5.8	Paradise Valley-ATV park
Qda4 (barchanbolic-parabolic)	74-90°	0 - 0.9	1.4 - 4.4	Paradise Valley
Qda5b (barchanbolic-parabolic)	73-82°	0.4 - 1.2	3.5 - 5.9	Paradise Valley

Figure 4.25 plots the orientations on a rose diagram using 4° intervals. The orientation of sand dunes in Paradise Valley trend from 35-120° with an average direction of 80.3°. Four modes can be deciphered from Figure 4.25 that have percent frequencies greater than 5 percent; 77-87° (42.32%), 89-92° (15.38%), 73-76° (11.55%), and 60° (5.78%). The distribution on the rose diagram implies a majority of the winds responsible for the entrainment of sand prevail out of the northwest to southwest from the average direction of 260.3°.

These observations are consistent with calculations of resultant drift direction by Jewell & Nicoll (2011). Northeasterly to southeasterly dune orientations in Paradise Valley are also consistent with the WeatherSpark model on Figure 2.1. The model shows the

strongest annual winds in Winnemucca occur during the warm season months when winds prevail 37-40% of the time from the northwest to southwest. It can be inferred from these findings that sand dunes in Paradise Valley reach peak advancement rates between the months of April to July.

On Figure 4.26 the historical average rate of sand dune advancement in Paradise Valley from the Paradise Complex (Qda1), barchanbolic-parabolic dunes (Qda4), the ATV Park (Qda4), and areas of reactivated barchanbolic-parabolic dunes (Qda5b) are compared during the years 1980-2012. The periods of measurement on the plot are 1980-1994, 1994-2006, and 2006-2012. Long-term advancement rates from each field on Figure 4.26 varied although three general patterns can be observed.

Unit Qda4 and the ATV Park along the eastern flanks of the Bloody Run Hills both decreased at least  $1 \text{ myr}^{-1}$  in activity between the years 1994-2006. During the same period the advancement rate of the Paradise Complex (Qda1) and reactivated dunes (Qda5b) in the center of the valley slightly increased by  $0.25 \text{ myr}^{-1}$ .

During the years 2006-2012 the Paradise Complex continued to gradually increase in activity ( $0.25 \text{ myr}^{-1}$ ) and the rate of advancement at the ATV Park stopped declining and increased by at least  $0.5 \text{ myr}^{-1}$ . In the same period of time unit Qda4 continued to decline ( $0.1 \text{ myr}^{-1}$ ) but the advancement rate of Qda5b stopped increasing and gradually declined at the same rate as Qda4.

The third observation from Figure 4.26 revealed that long-term advancement rates from the years 1980-2012 differed by location in the valley. Along the eastern flank of the

Bloody Run Hills (units Qda4 and the ATV Park) the long-term rate of dune advancement decreased 0.5 to 1.2 myr<sup>-1</sup>. In the center of the valley the Paradise Complex (Qda1) and reactivated dunes (Qda5b) slightly increased in activity 0.2 to 0.5 myr<sup>-1</sup>.

The apparent causal effects for the long-term spatiotemporal variance of eolian activity in Paradise Valley are unclear. Several explanations may include; reductions in livestock grazing, responsible or decreased ATV use, and increased vegetative growth on the slopes of the Bloody Run Hills. In the center of Paradise Valley dune activity may have increased due to the mitigation of floods on Gumboot Lake or valley bottom disturbances that are attributable to wildfires, agriculture, and construction projects.

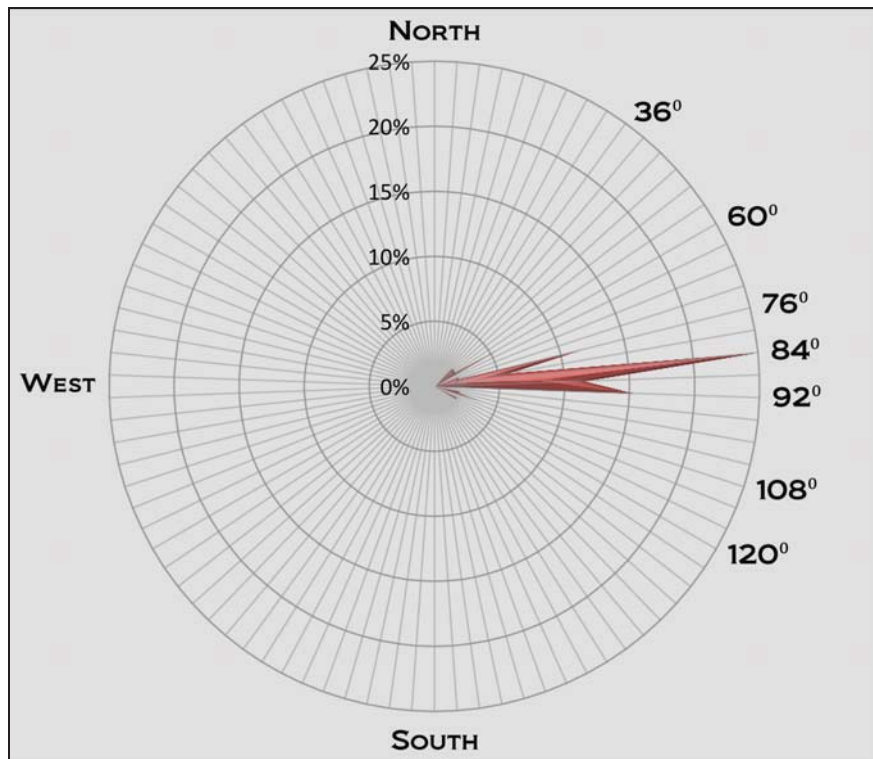


**Figure 4.25:** Rose diagram showing direction of sand dune advancement in Paradise Valley.

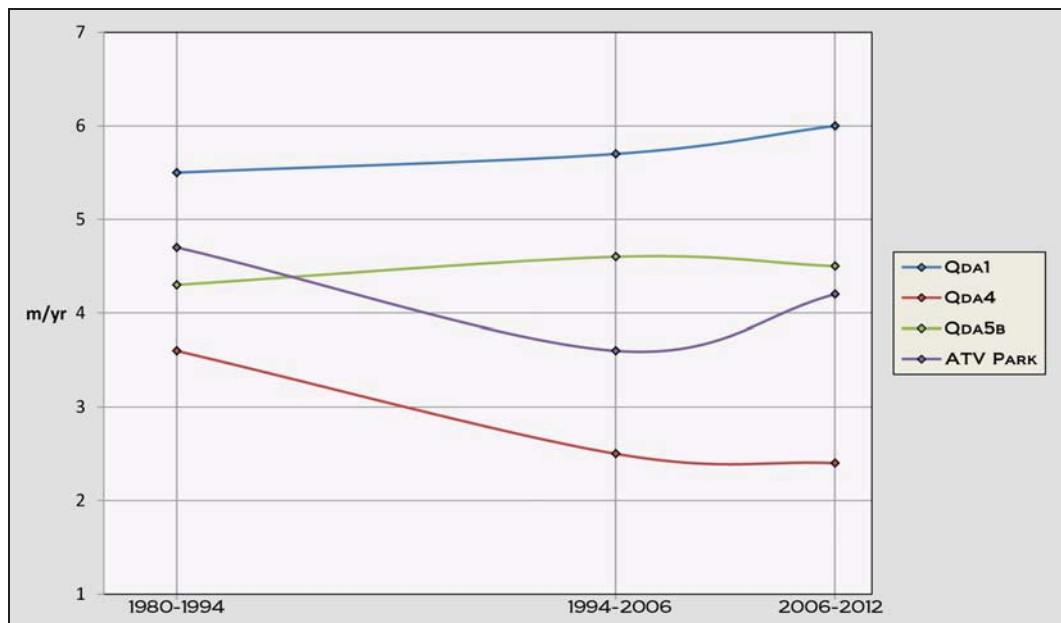


**Figure 4.26:** Rate of sand dune advancement in Paradise Valley.

## CHAPTER 5: PETROLOGY

### 5.1 Introduction

The petrology of sediments from the Winnemucca Dune Complex will be described in this chapter. Sections 5.2-5.3 outline the specific procedure and techniques that were used to collect, pretreat, and determine the grain size parameters of bulk samples retrieved from the field. The following subsections will summarize the distribution of particle size from various landform features. Section 5.4 identifies the various colors of dune sand and explains how the color of sand changes between upwind and downwind locations. In section 5.5 the mineralogy of sand is discussed in regard to the compositional components of Quartz, Feldspar, and minor minerals. Section 5.6 involves a physical classification of dune sand after Folk (1974) using total Quartz-Feldspar-Rock fragments. The potential provenance of sand is examined in Section 5.7 using components of Quartz-Alkali feldspar-Plagioclase and a ternary diagram with overlay after Streckeisen (1976, 1978). A discussion of the relevant petrographic observations (Section 5.8) from this assessment and a comparison of the results to studies by others (Section 5.9) are included at the end of the chapter.

### 5.2 Sampling and pretreatments

Petrographic observations are compiled from the visual inspection and laboratory testing of 110 sand samples. The collection sites are shown on Maps #4-7D (Appendix C). Sampling procedures and laboratory pretreatments are explained in steps 1-10 below.

- 1) Bulk sand samples (~5000 grams each) were collected in WDC from each of the major dune fields. Site descriptions and test results are logged in Appendix B.

- 2) Field samples were collected from the ground surface at the crest or brink of individual dunes and ridge formations away from vegetation or any noticeable disturbances. Dune form was visually determined in the field and confirmed in the lab with satellite imagery.
- 3) UTM coordinates for each sample location were recorded using a handheld Garmin GPS and the WGS 1984 UTM horizontal datum. All samples were logged and placed into air-tight bags prior to being transported offsite.
- 4) Bulk samples were split down to approximately 2500 grams, tagged, and separated for washing.
- 5) Sand grain particles from 6 sample sites were partially cemented by halite and prior to wash required a warm bath of deionized (D.I.) water at ~66<sup>0</sup>C for 10-15 seconds to dissolve the binding minerals.
- 6) Using two 4.73L stainless steel bowls and a US#500 stainless steel sieve (8 inch) each sample was individually mixed with D.I. water, agitated with a stainless steel whisk and stirring rod, then gently drained through the sieve to remove vegetative litter, fecal pellets, insect carcasses, charcoal, and other organic components.
- 7) During each wash, the sieve was placed inside one of the bowls to capture any material passing through the #500 screen. All material recovered from the catch bowl was carefully returned back to the washed sample. 1-2 drops of generic dishwashing detergent was used when needed to help float organics, and flocculate clay clumps and coatings.
- 8) Washed samples were dried in a stainless steel oven at 110<sup>0</sup>C for 18-24 hours.
- 9) After allowing samples to cool to room temperature for at least one hour they

were screened 3 to 5 times through a US#18 stainless steel sieve to remove all +1 millimeter material. One half of each cooled and screened sample was transferred into a plastic bag and stored for archival purposes.

- 10) The remaining half of the sieved bulk material was individually split down into 250 gram samples using a Humboldt 1:11 splitter. Split samples were transferred, sealed, and stored in plastic 40 dram containers.

### **5.3 Determination of grain size parameters**

Laser Granulometer analysis of field samples was performed to measure the distribution of particle size and calculate grain size parameters to determine the textural classification of dune sand. The exact method used in this section is listed below in steps 11-15.

- 11) One 40 dram sample container from each site was used for particle size analysis. Particle size testing was performed on a MASTERSIZER 2000 with a Hydro 2000G wet dispersion unit at the Geophysics facility at the California State University, Bakersfield (CSUB), Department of Geology. All work performed at CSUB was under the supervision and guidance of Dr. Robert M. Negrini.
- 12) The Standard Operating Procedure (SOP) for 1 test run on the MASTERSIZER provided an averaged result for 3 sampler measurements.
- 13) Sampler settings for the MASTERSIZER were set at the following configuration; pump speed = 2000rpm, stirrer speed = 850rpm, and ultrasonic pre-measurement at 60s with a 30% tip displacement. The SOP also consisted of washing the basin in the wet dispersion unit (Hydro 2000G) two times between test runs.
- 14) Due to the absence of significant clay content, flocculent was determined not to

be needed for testing unimodal sands which constituted over 98% of all material sampled.

- 15) User bin sizes from the MASTERSIZER measurements were entered in GRADISTAT v.8 (Blott & Pye 2001) along with the particle size gradations for each sample to compute grain size parameters in accordance with the original Folk & Ward (1957) equations. The physical description and textural classification for each sample was recorded from each GRADISTAT plot.

### ***Mean grain size and Sorting***

The particle size of dune sediments volumetrically distributed from 0.24 microns ( $\mu\text{m}$ ) up to 2 millimeters ( $12\phi$  to  $-1\phi$ ). Dune samples analyzed were all unimodal and had a composition of 90-100% sand,  $\leq 9\%$  silt, and  $\leq 0.2\%$  clay. The mean grain size of dune sand placed between 132.3 to 336.1 $\mu\text{m}$  ( $2.92\phi$ ,  $1.57\phi$ ). Active dunes do not contain clay and typically were 97-100% sand with silt contents that rarely exceeded 2.8%. Stable dunes were observed to have clay  $\leq 0.2\%$  and silt contents extend up to 9.1% total volume. The presence of fines (silt + clay) can possibly be attributed to the accumulation of dust, effects of bioperturbation, chemical, and mechanical weathering of sand grains.

The sorting parameters of active and stable dune sand were similar although the accumulation of fines in stable dunes skewed the distribution of particle size (shown on Figure 5.1). Sand from active dunes varied from moderately well sorted to moderately sorted ( $0.501\phi$  to  $0.743\phi$ ). Sorting of stable dune sand was more variable and ranged between moderately well sorted to poorly sorted ( $0.515\phi$  to  $1.308\phi$ ).

Variation in mean grain size from active and semi-active dunes on the stoss-ward side of the complex to the leeward portion is displayed on Figure 5.2. The samples analyzed deviate in mean grain size from 212.7 to 336.1 $\mu\text{m}$  (2.23 $\phi$ , 1.57 $\phi$ ) in Desert Valley and 154.6 to 326.1 $\mu\text{m}$  (2.69 $\phi$ , 1.62 $\phi$ ) in Silver State Valley before sand travels eastward over the Bloody Run Hills into Paradise Valley. The fluctuation and small decrease of  $\sim 10\mu\text{m}$  in maximum mean grain size over a relatively long distance ( $\sim 36$  km) proposes that an additional sediment supply source must exist somewhere between Desert Valley and eastern Silver State Valley. Below the Bloody Run Hills in Paradise Valley the mean grain size of dune sand begins to decrease from 267.5 to 158.2 $\mu\text{m}$  (1.90 $\phi$ , 2.66 $\phi$ ) as it approaches the leeward side of the complex. The outward decrease in mean grain size across Paradise Valley advocates that additional sediment supply sources are probably absent on the ridge and eastern slopes of the Bloody Run Hills.

Another indication of multiple supply sources was exposed in the discrepancy of grain size among the active dunes and sand sheet in Desert Valley. In all of the areas explored the sand sheet was exclusively fine sand and lacked granular material or medium sized grains. However the dunes located downwind from the sheet contained significant quantities of medium sand. These findings assert it is highly unlikely the upwind sheet delivered the entire sediment load to the dunes in the eastern half of the valley.

Other evaluated landforms include lunettes, dune islands, beaches, and lakebeds. These deposits incorporated mostly bimodal (Figure 5.1) sediments with compositions of 50-97% sand, 3-44% silt, and  $\geq 6.5\%$  clay. The lunettes and beaches held very fine to medium sand and fine silty fine sand with a mean grain size of 122.5 to 260.3 $\mu\text{m}$  (3.03 $\phi$ ,

$1.942\phi$ ). Dune islands were comprised of very fine sand, very fine silty fine sand, and coarse silty fine sand with mean grain sizes between  $75.33$  to  $144.6\mu\text{m}$  ( $3.714\phi$ ,  $2.79\phi$ ). Lakebeds consisted of silt, coarse silty fine sand, and fine sand that had mean grain sizes of  $49.38$  to  $168.5\mu\text{m}$  ( $4.34\phi$ ,  $2.569\phi$ ). The sorting from each of the above deposits was highly variable and ranged from moderately well sorted to very poorly sorted ( $0.538\phi$  to  $2.464\phi$ ).

A bivariate analysis of grain size parameters for 95 dune samples is shown on Figure 5.3. The plots do not show a strong correspondence between mean grain size and sorting although a consequential relationship can be graphically inferred. It is reasonably affirmed on Figure 5.3 that sediments from active dunes trend towards moderately well sorted medium sand. It is also indisputable on the figure that sediments from stable to semi-active dunes trend towards moderately sorted fine sand.

### ***Skew and Kurtosis***

The bivariate analysis of skew and kurtosis shown on Figure 5.3 was fairly inconclusive. Skew (- $0.05\phi$  to  $0.125\phi$ ) and kurtosis ( $0.9\phi$  to  $1.15\phi$ ) for a majority of the samples is tightly clustered and numerically constricted. Sand from active and stable dunes had symmetrical skew and was mesokurtic. The distribution of particle size in barchanoidal and transverse ridges from Desert Valley and Silver State Valley exhibited perfect to near perfect symmetry (shown on Figure 5.1). A small percentage of sand sampled from stable dunes displayed a transition towards fine skewness but still maintained a mesokurtic gradation. This characteristic can most likely be accounted to the accumulate fines and weathering of sand that is associated with the stabilization of active dunes as they

transform into static landforms. Sediments from lunettes, dune islands, and lakebed deposits in Desert Valley and Silver State Valley were partially cemented by halite and clay minerals resulting with a bimodal and skewed distribution of particle size. Sand mixed with silt and clay from these deposits had fine to very fine skew and graphically the kurtosis classified from leptokurtic to very leptokurtic.

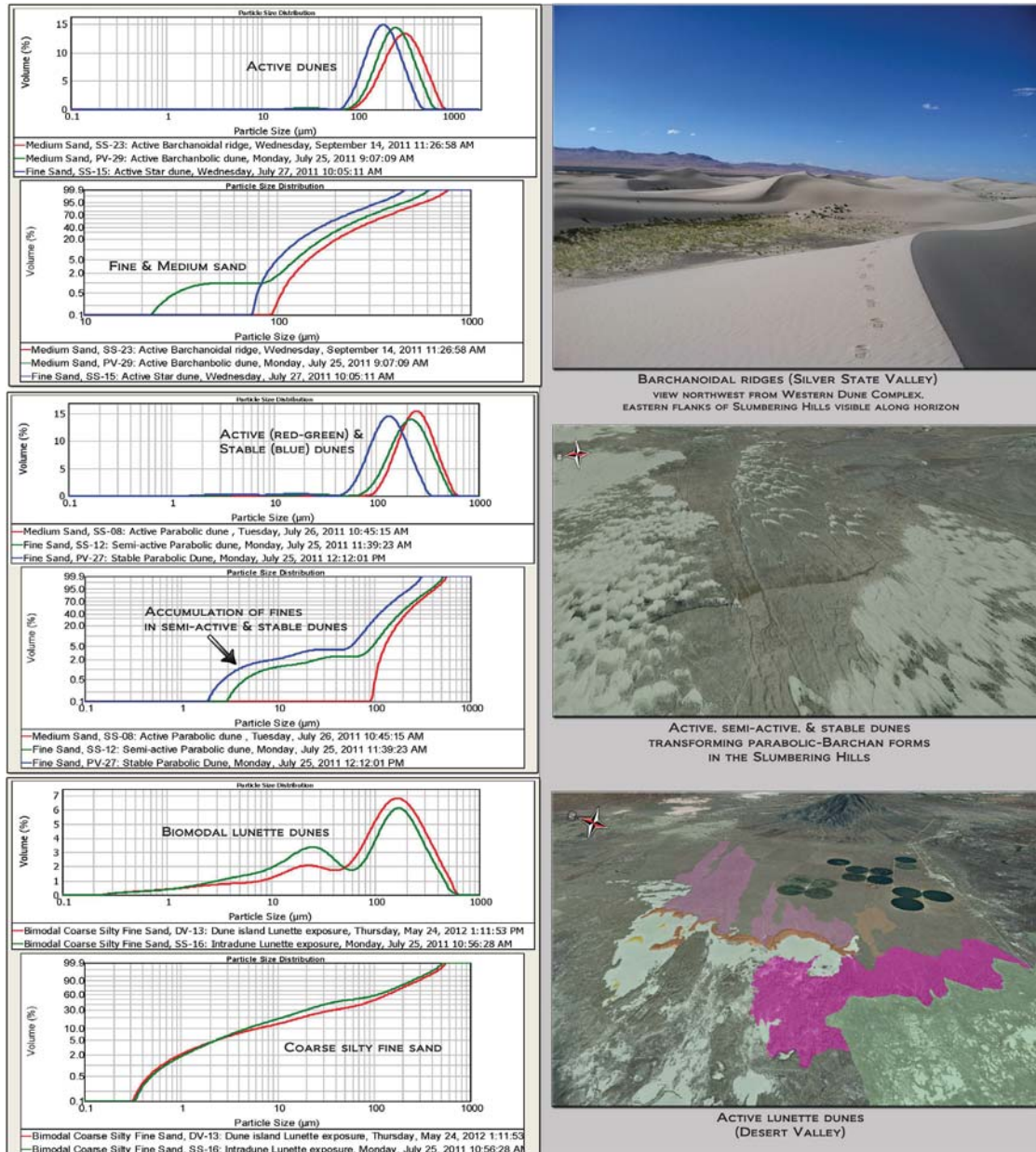


**Figure 5.1:** Particle size distribution of active and stable sand dunes in the Winnemucca Dune Complex. Plots are in accumulative percent volume determined from MASTERSIZER Laser Granulometer analysis.

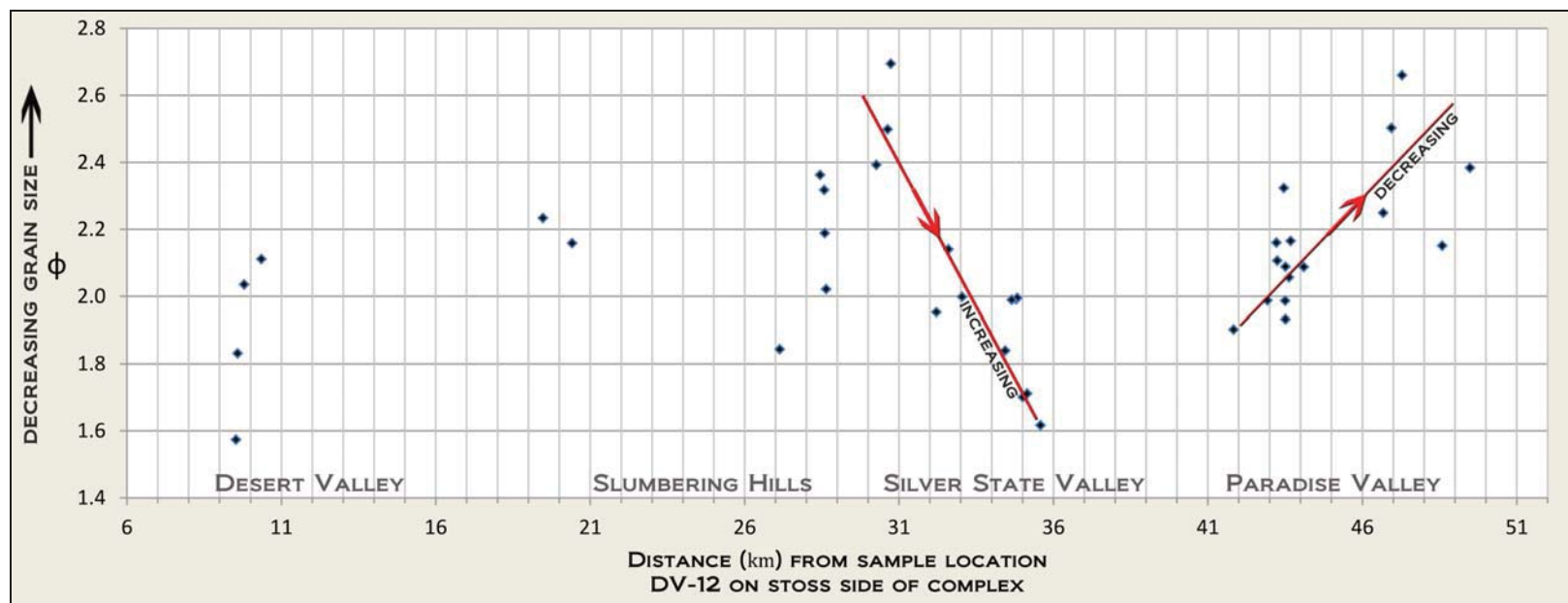
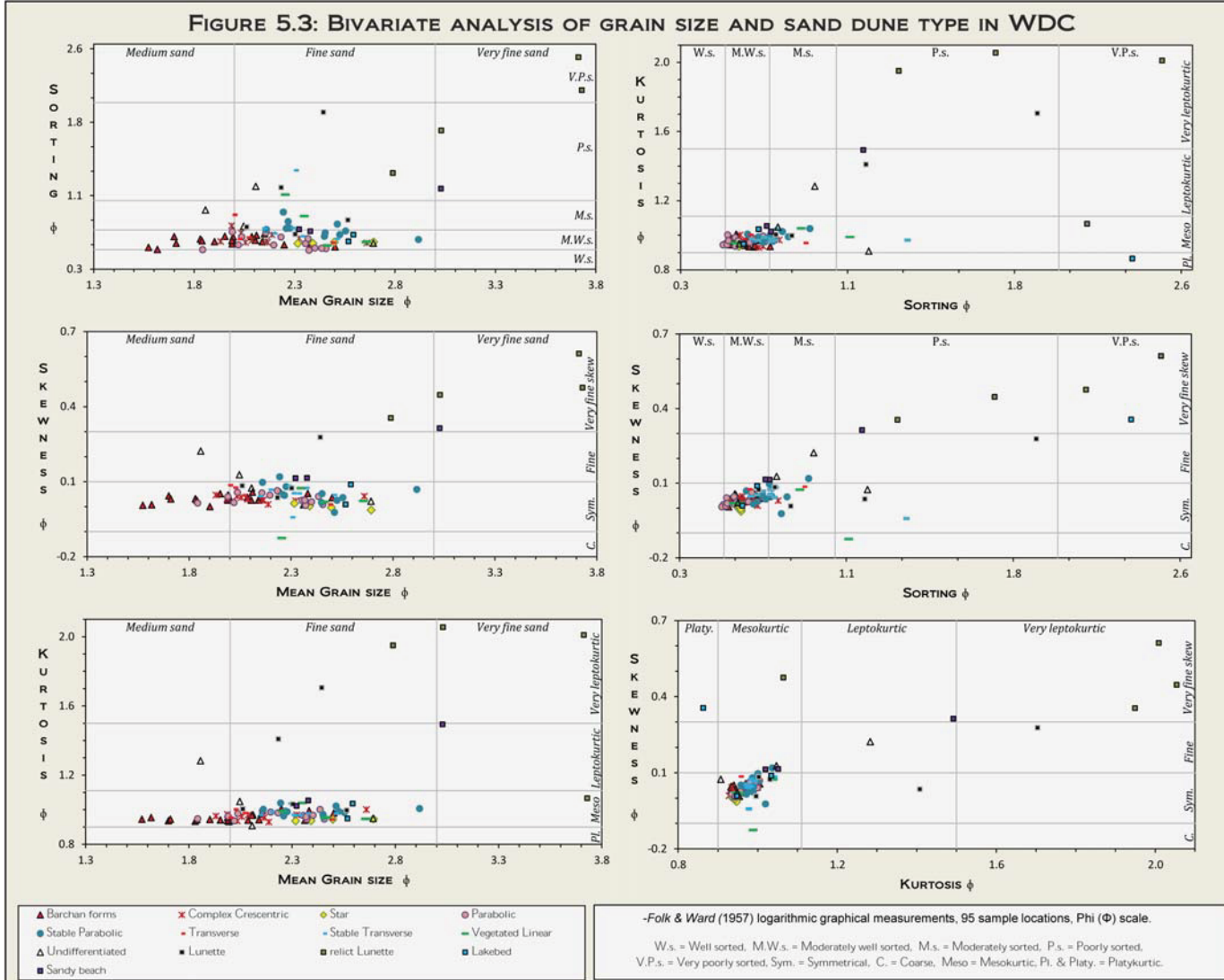
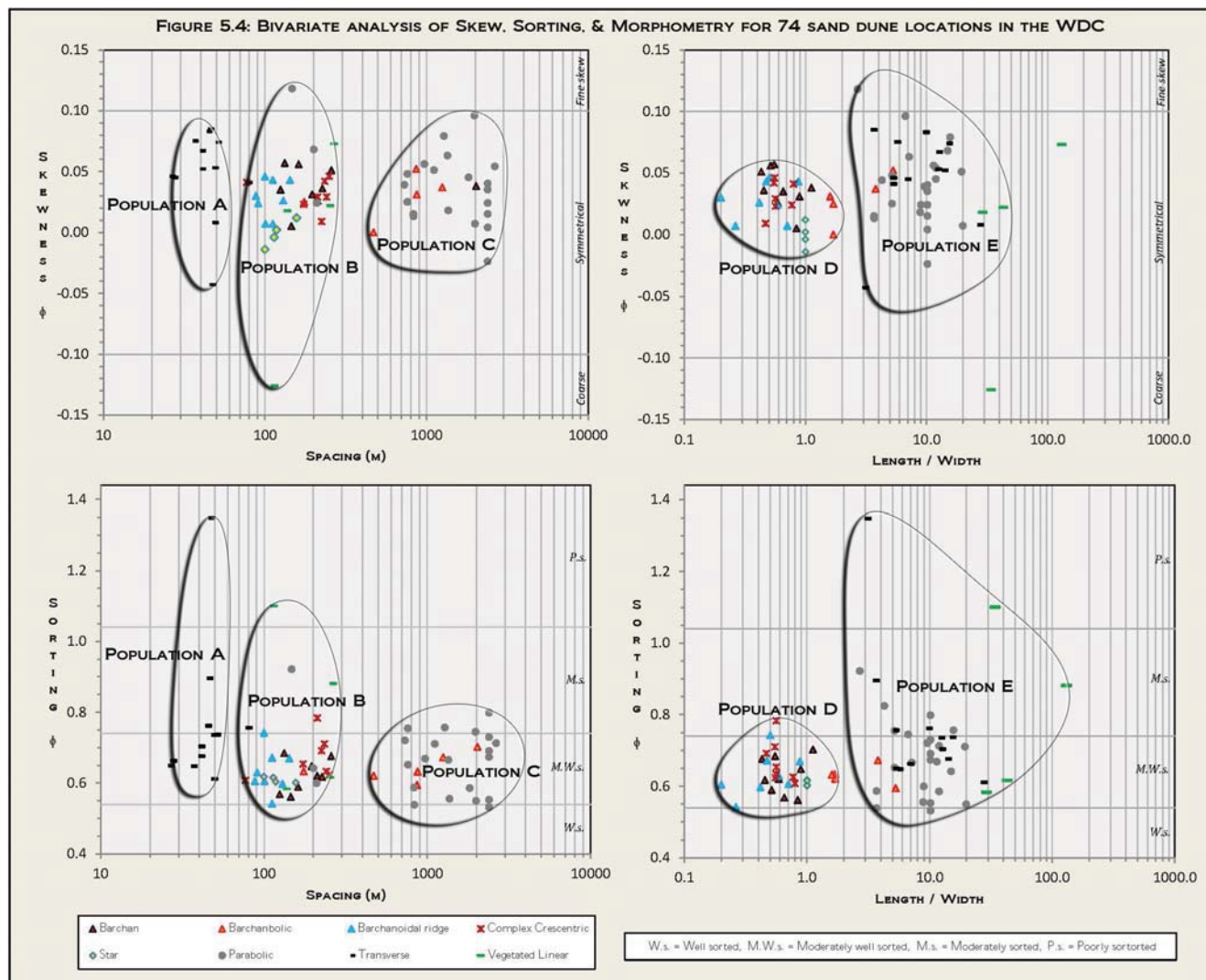


Figure 5.2: Change in mean grain size of dune sand from west side to east side of WDC.

**FIGURE 5.3: BIVARIATE ANALYSIS OF GRAIN SIZE AND SAND DUNE TYPE IN WDC**





### ***Grain size and dune morphometry***

Figure 5.4 shows a bivariate analysis of grain size and the dimensional shape of sand dunes. The following parameters were compared at 74 different locations within the complex; sorting, skew, length to width ratio, and dune spacing. A comparison of geomorphometry and distribution of particle size shows a total of 5 potential populations that can be grouped together by dune form. Observations from dune spacing plots reveal 3 possible groups (Population A to C) and graphs of length to width ratios indicate an additional 2 groups (Population D & E). Each population is summarized on Table 9. The transverse dune category used in this section was applied to measurements from stabilized to semi-active transverse dunes that were present along the periphery of WDC.

**Table 9:** Grain size and morphometry of various dune forms

	Spacing (m)	L/W	Sort. ( $\phi$ )	Skew ( $\phi$ )	Dune forms
Population A	26 - 50	n/a	0.55→1.35	-0.05→0.9	Semi-active/Stable Transverse
Population B	77 - 268	n/a	0.0→1.0	-0.13→0.12	All forms except Transverse
Population C	471 - 2650	n/a	0.45→0.9	-0.07→0.09	Most Barchanbolic-Parabolic
Population D	n/a	0.2→1.7	0.5→0.75	-0.02→0.06	Barchan-Star-Ridges & most Barchanbolic
Population E	n/a	2.7→43	0.5→13	-0.14→0.12	Transverse-Linear-Parabolic & some Barchanbolic

Stable to semi-active transverse dunes from Population A & E were the most distinct group. They closely spaced between 26 to 50 meters apart and had a large range of sorting that varied from moderately well to poorly sorted. The distribution of particle size and the shape of barchanoidal ridges, barchanbolic and parabolic dunes from Populations B, C, D, & E are also distinct. Ridges had low length to width ratios (0.2 to 1.7) and in Population B showed moderate spacing (77 to 268 meters). In contrast, barchanbolic and parabolic dunes from Population C & E had an extended range of sorting and skew, large length to width ratios (2.7 to 43), and broadly spaced from 471 to 2650 meters apart.

#### 5.4 Sand color

Sand color was qualitatively determined using color chips from the revised Munsell Soil Color Book (2009) and a three color description scheme. A total of 30 representative sand samples were chosen from collection sites at 16 active and 14 stable dunes. Due to complexities in mineralogy and grain size it was not possible to blend samples into one homogenous color. The 3 color scheme employed describes the rock fragments of sand (lithics) using 2 color notations and the matrix (medium and fine particles) using a 1 color notation. Table 10 summarizes the results and computes the average color.

Results conclusively show that there is little change in color across a majority of the landscape. Active dune sands consistently had a yellow-red Hue (10YR), high lightness value (7+), and neutral to low Chroma (1-3). Variance in sand color was only readily observed between active and stable sand dunes. Munsell color chips classified sand from active dunes as having White to Light Gray lithics and a Pale Brown to Very Pale Brown matrix. Lithic material from stable dunes was slightly varnished and showed Light Gray to Very Dark Grey & Light Yellowish Brown color with a matrix of Very Pale to Pale Brown color. Weathered sand from stable dunes in Paradise Valley had similar lithic color however the matrix exhibited a Yellow Hue and stronger Chroma with a resultant color of Light Yellowish Brown.

It can be surmised from the above observations that as sand travels eastward through the complex and becomes trapped in stable dunes; the lithic color varnishes from Whitish Light Gray to Gray & Dark Gray and the matrix color of sand weathers from Very Pale Brown to Pale Brown & Light Yellowish Brown. The average color listed below for

active and stable sand dunes was determined by averaging Munsell values for lithic and matrix material.

-Active dunes: Very Pale Brown (10YR 8.1/1.7)

-Lithics: White (White 9.5/1) & Light Gray (10YR 7/1.4)

-Stable dunes: Pale Brown (10YR 5.8/2.6) & Light Yellowish Brown (2.5YR 6/3)

-Lithics: Gray (10YR 4.8/1.3) & Light Yellowish Brown (10YR 6/4)

**Table 10:** Summary of sand color in the Winnemucca Dune Complex

Active Dunes	Type	Hue	Value	Chroma	Color
sample# PV-3 PV-8 PV-31 PV-34	rock lithics (prim.)	Wht	9.5	1	White
	rock lithics (sec.)	10YR	7	1	Light Gray
	fines (matrix)	10YR	8	2	Very Pale Brown
sample# PV-12 PV-35	rock lithics (prim.)	Wht	9.5	1	White
	rock lithics (sec.)	10YR	7	2	Light Gray
	fines (matrix)	10YR	7	3	Pale Brown
sample# SS-2 SS-14 SS-21	rock lithics (prim.)	Wht	9.5	1	White
	rock lithics (sec.)	10YR	7	1	Light Gray
	fines (matrix)	10YR	8	3	Very Pale Brown
sample# SS-3 SS-6 SS-15 SS-25	rock lithics (prim.)	Wht	9.5	1	White
	rock lithics (sec.)	10YR	7	1	Light Gray
	fines (matrix)	10YR	8	2	Very Pale Brown
sample# DV-25 DV-26 DV-27	rock lithics (prim.)	Wht	9.5	1	White
	rock lithics (sec.)	10YR	7	2	Light Gray
	fines (matrix)	10YR	7	3	Very Pale Brown
		Active avg.	10YR	8.1	1.7
					Very Pale Brown

Stable Dunes	Type	Hue	Value	Chroma	Color
sample# PV-17 PV-30 SS-7 SS-8	rock lithics (prim.)	10YR	6	4	Light Yellowish Brown
	rock lithics (sec.)	10YR	4	1	Dark Gray
	fines (matrix)	10YR	6	4	Very Pale Brown
sample# SS-7 SS-10 SS-12 SS-18	rock lithics (prim.)	10YR	7	2	Light Gray
	rock lithics (sec.)	10YR	4	1	Dark Gray
	fines (matrix)	10YR	8	4	Pale Brown
sample# DV-8 DV-11 DV-29	rock lithics (prim.)	10YR	7	2	Light Gray
	rock lithics (sec.)	10YR	3	1	Dark Gray
	fines (matrix)	10YR	7	4	Very Pale Brown
		Stable avg.	10YR	5.8	2.6
					Pale Brown

sample# PV-10 PV-14 PV-27	rock lithics (prim.)	2.5YR	3	1	Very Dark Gray
	rock lithics (sec.)	10YR	4	1	Dark Gray
prim. = primary sec. = secondary	fines (matrix)	2.5YR	6	3	Light Yellowish Brown

LITHICS abundance	Active avg.	White	9.5	1	White
	Active avg.	10YR	7	1.4	Light Gray
	Stable avg.	10YR	4.8	1.3	Gray
	Stable isolated	10YR	6	4	Light Yellowish Brown

### 5.5 Compositional analysis of dune sand

Loose sand from each sample was briefly inspected under a reflected-light stereomicroscope at low magnification (20X-100X). Representative samples from 20 collection sites were chosen for further evaluation in the laboratory using X-ray Diffractometry (XRD) and prepared standard thin sections. A summary of the results is outlined on Table 11.

28 sand samples from 14 collection sites were submitted to Arizona Quality Thin Sections. Each sample was vacuum impregnated in blue epoxy, cut, polished to a thickness of 30 microns, etched with Hydrofluoric acid and stained using multiple techniques. Staining procedures after (Houghton 1980) used K-rhodizonate, Na-cobaltinitrite, and Ba-chloride to dye Potassium feldspar and Plagioclase crystals. Staining with Alizarin red-S after Dickson (1965) was used to identify carbonates.

The percent relative abundance of total Quartz (monocrystalline + polycrystalline), Feldspar, and lithic rock fragments (QFL) were calculated using a relative abundance scale (Shvetsov 1955) and mineral grain counts from stained thin sections. Relative proportions of QFL for each sample were calculated from 10 wide field views per slide (20-40X magnification). The results were then plotted on a Ternary diagram using TriPlot v4.1.2 and a QFL overlay after Folk (1974) to physically classify sand (Figure 5.5).

20 sand samples from 20 collection sites were submitted to Attard Minerals for fine powder XRD. Results were graphically plotted and tabulated in relative weight percent for each mineral identified. Proportional relative weight percent of total Quartz, Alkali

feldspar, and Plagioclase (QAP) were determined from each test. The percent relative abundance of QAP was then counted on stained thin sections. Values for QAP from both methods were plotted on a Ternary diagram (Figure 5.6) with a plutonic-volcanic equivalent rock type overlay after Streckeisen (1976, 1978).

### ***Quartz***

The relative weight percent of Quartz in dune sand ranges between 20-68% and is comprised of monocrystalline, polycrystalline, cryptocrystalline, and volcaniclastic forms of silica.

Monocrystalline Quartz is medium to coarse grain in size and composed of fractured translucent hexagons and pyramids. Polycrystalline forms are more plentiful and primarily are composed of coarse to medium sized grains of angular, subangular to subrounded crystals of massive and drusy Quartz with milky, smokey, and rose color.

Cryptocrystalline varieties of Quartz include; Chalcedony, Opal, Agate, and Chert. Mineral grains range in size from fine to coarse and have varying degrees of angularity that include; angular, subangular, subrounded, and very rounded. Coarse angular fragments of waxy Chalcedony are plentiful and most likely derived from amygdules that have weathered out of the underlying vesicular basalt flows in Desert Valley, Blue Mountain, Krum Hills, Ten Mile Hills, and the Slumbering Hills.

Volcaniclastic components of sand include vitreous glass (translucent shards & Obsidian), fragmented lava rock, pumice, and spherules. Translucent shards are coarse to medium size and composed of blocky plates, elongate spherical bubbles, cuspathe bubble

walls, and bubble wall junctions. Flaky coarse grains of Obsidian are prevalent and have a clear to black and mahogany color. Pumice clasts are porous, white to light grey colored, subangular and subrounded to very rounded with fine to medium grain size. Spherules are translucent, very fine in size, and occasionally contain a perfect spherical bubble inclusion. In a majority of the samples inspected the spherules and pumice grains were partially to completely infiltrated by silt.

### ***Feldspars***

The total Feldspar content of sand graded from 32 to 80 relative weight percent. Fine to coarse grained Feldspar with euhedral and anhedral crystalline texture are pervasive. Feldspars laths in blue to red colored rock fragments of Rhyolite and Basalt lava rock are also common and frequently were found in sand from the western portion of the complex. These specific lithics bear a strong resemblance to the color and texture of Rhyolite and Rhyodacite that locally outcrops in the neighboring Jungo-Slumbering Hills area.

Albite was the most abundant Feldspar in dune sand and measured at 15 to 58 relative weight percent. Thin sections and XRD analysis did not reveal the presence of any other minerals from the Plagioclase series. Plagioclase from sand samples collected in Pumpernickel Valley, Humboldt Valley, Quinn River Valley, and the Black Rock Desert were also exclusive to Albite.

The Alkali feldspar content of sand assorted from 0 to 51 relative weight percent and included the following members listed from most to least abundant; Orthoclase, Sanidine, Potassium feldspar, and Microcline. In at least half of the samples analyzed Orthoclase was coincident with Barium.

### ***Other minerals***

Metamorphic rock fragments of Phyllite, Slaty Shale, Quartzite, biogenic shells, and sedimentary pellets of silt-clay were identified in dune sand. Lithics of pale brown to dark blue colored Phyllite-Slaty Shale have elongate to compact shape and are angular, subangular to subrounded. Micro-stereoscopic inspection of Phyllite-Slaty Shale in thin section revealed Diopside & Ferroan Diopside crystals actively being replaced by Orthoclase and Potassium feldspar.

The XRD analysis semi-quantitatively estimated the Diopside & Ferroan Diopside mineral content was 0 to 16 relative weight percent. Coarse to fine sheets of Muscovite-Sericite were identified and estimated up to 7% relative abundance. In the very active sections of Desert Valley and Silver State Valley coarse sized sheets of Muscovite-Sericite commonly accumulate and become trapped in airflow eddies located at brinks, crests, lee faces, and dune boundaries. Typically in these areas Muscovite-Sericite grains concentrate and develop small patches (Image #21) that have a distinctive silver color and shimmered reflectance. Investigation of thin sections displayed very fine grains of Calcite, Ferroan Calcite and fragmented coarse grains of Aragonite that occur up to 5% relative abundance in dune sand. Intact and fragmented Mollusk shells from *Vortifex solidus* and *Hydrobiidae* (image shown on Map #4C; Appendix C) are sporadically present in Sehoo shorelines and fill-cut deposits of Gumboot Lake. Other minerals identified in trace amounts on thin sections and loose samples were Kaolinite, Gypsum, Halite, Iron oxide coatings of Goethite or Siderite, Magnetite, and unidentified magnetic minerals that are conceivably very fine grains of Titanium dioxide.

**Table 11:** Summary of X-ray Diffractometry and inspection of thin sections

Sample	XRD				QAP diagram			relative weight %			QFL diagram				QFL diagram		
	Quartz	Alkali feldspar	Plagioclase	other	Thin sections	avg. of 2 slides	Lithic type	percent relative abundance	Lmetamorphic	Lsed.	Lcarbonate	Lbiogenic	% rel. abun.	2 slides (Afk fs+frag)	Feldspar	Lithics	
					Quartz	Alkali feldspar	Plagioclase		Lvolcanic								
RP-01	low 40	Orthoclase 20	Alb. calcian low 40	/ 0													
PnV-02		Ortho. w/ Ba <sup>+</sup> 48	Alb. calcian low 11	?													
BRD-01		Ortho. w/ Ba <sup>+</sup> 25	Albite high 22	?													
QRV-03		/ 20	Albite high 42 0	/ Alb. ordered 38													
DV-10		Microcline interm. 23	Alb. calcian low 38	?													
PV-02	low 59	Ortho. sodian, syn 15	Albite low 26	/ 0	Thin sections	avg. of 2 slides	Lithic type	percent relative abundance	Lmetamorphic	Lsed.	Lcarbonate	Lbiogenic	QFL diagram % rel. abun.	2 slides (Afk fs+frag)	Feldspar	Lithics	
DV-20		Orthoclase 40	Alb. calcian low 13	?	Quartz	7	glass>pumice> spheres 22-28%	Musc-Seri.+ Phyllite 18-20%	Silt+Halite 3-4%	Gyp.+Cal.+ Arg. 0-2%	N/A	25	23	52			
DV-11	low 23	Potassium fs. 37	Alb. calcian low 40	?		45	Phyllite 30-32%	Chalcedony+ Silt+ Halite	Gyp.+Cal.+ shell frags	> 1.0%	30	25	45				
DV-14	low 41	Ortho. w/ Ba <sup>+</sup> 23	Alb. calcian low 35	?		30	Phyll.+Quartzite+ glass 20%	Phyll. Chalcedony 20-22%	Silt+Clay+ Halite 12-13%	Cal.+Arg. 4-5%	N/A	10	15	75			
SS-13		Potassium fs. 20	Albite low 51	?		35	glass>spheres>> pumice 80-85%	Musc-Seri.+Chalc.+ Opal+Chert 12%	Silt	N/A	Bones	12	22	60			
SS-10	low 48	/ 0	Albite high 25 Albite low 27	?		43	Opal+Chert 3-4%	Chalc+Seri. 15%	Silt	Gyp.+Cal. ferr. 3%	shell frags	4	2	3	100		
DV-26		/ 26	Albite low 0	Diopside 58		40	glass>pumice> sphere 18-20%	Diopside+Musc-Seri.+ Chalc+Opal+Chert 30-40%	N/A	Calcite ferroan+ Gypsum 0-2%	shell frags	15	10	30	50		
PV-28		Orthoclase 68	Albite low 12	?		16	pumice>> glass 20-22%	Phyll.+Chert+Agate Musc-Seri. 27-33%	N/A	N/A	N/A	25	30	20	55		
SS-20	low 20	Sanidine 30 Ortho. w/ Ba <sup>+</sup> 10	Albite high 40	?		33	glass>spheres> pumice 80-92%	Chalcedony+Opal Musc-Seri. 0-8%	N/A	N/A	shell frags	4	6	4	92		
SS-04	low 31	Sanidine 27	Albite high 42	?		38	glass>spheres> pumice 62%	Chalcedoney+Opal+ Musc-Seri. 5-8%	N/A	Gyp.+Cal. Arg. 1-3%	N/A	18	16	14	68		
SS-15	Low 30	Sanidine 39	Alb. calcian low 21	?		23	glass>pumice> spheres 55-60%	Chalcedoney+Opal+ Musc-Seri. 20-22%	N/A	Gyp.+Cal. ferr. 1-2%	N/A	18	14	10	84		
SS-25	Low 42	/ 0	Alb high 31 Alb low 26	?		45	glass>pumice> spheres 35-36%	Chalcedoney+Opal+ Musc-Seri. 40%	N/A	Gyp.+Cal. ferr.+ Arg. 0-2%	N/A	10	15	10	76		
PV-34		Orthoclase 65	Albite high 19	?		15	pumice>> glass 20-26%	Phyll.+Chert+Agate Musc-Seri. 26%	Silt	Gyp.+Cal.+ 2-3%	N/A	32	30	20	48		
PV-35	Low 46	Ortho. w/ Ba <sup>+</sup> 21	Alb. calcian low 32	?		25	pumice>> glass 22-24%	Phyll.+Chert+Agate Musc-Seri. 20-24%	Silt	Gyp.+Cal. 2%	N/A	24	31	24	52		
PV-27	Low 44	/ 0	Albite high 45	Diopside ferroan 11		48	glass = pumice 30%	Diopside+Phyll. Chert+Agate 28-30%	Silt+Clay 4-5%	Calcite ferroan 2%	N/A	19	14	17	64		

MUSC-SERI. = MUSCOVITE-SERICITE

PHYLL. = PHYLLITE &amp; SLATY SHALE

GYP. = GYPSUM

CAL. = CALCITE

CAL. FERR. = CALCITE FERROAN

ARG. = ARGONITE



**Image 21:** Coarse platy grains of Muscovite-Sericite in dune sand.

## 5.6 QFL ternary analysis and classification of sand

Relative proportions of total Quartz (monocrystalline + polycrystalline), Feldspar, and lithic rock fragments for 28 samples are plotted on a QFL ternary diagram (Figure 5.5) with a physical classification overlay after Folk (1974). All of the samples classified as either Litharenite or Feldspathic litharenite sand. The total amount of rock fragments in WDC sand was estimated to place within 45 to 100% relative abundance. Volcanic rock fragments comprised a majority of the lithics in WDC sand. Metamorphic rock fragments were second most abundant and lithic material from sedimentary deposits was fairly rare.

Samples from the Slumbering Hills and Silver State Valley classified as Litharenite sand. The lithic content of sand on the eastern crest of the Slumbering Hills variegated between 85 to 100% relative abundance and was almost completely composed of volcaniclastic material. Most of the sand sampled in Desert Valley and Paradise Valley had average lithic contents between 45 to 88% relative abundance and classified as a Feldspathic litharenite sand. The lower lithic content of dune sediments in Desert Valley suggests that sand in the Slumbering Hills could not be completely provided by advancing dunes in Desert Valley. The decrease in lithic content between the Slumbering Hills and Paradise Valley also indicates that as sand travels eastward over the Bloody Run Hills it weathers and physically matures from a Litharenite to a Feldspathic litharenite sand.

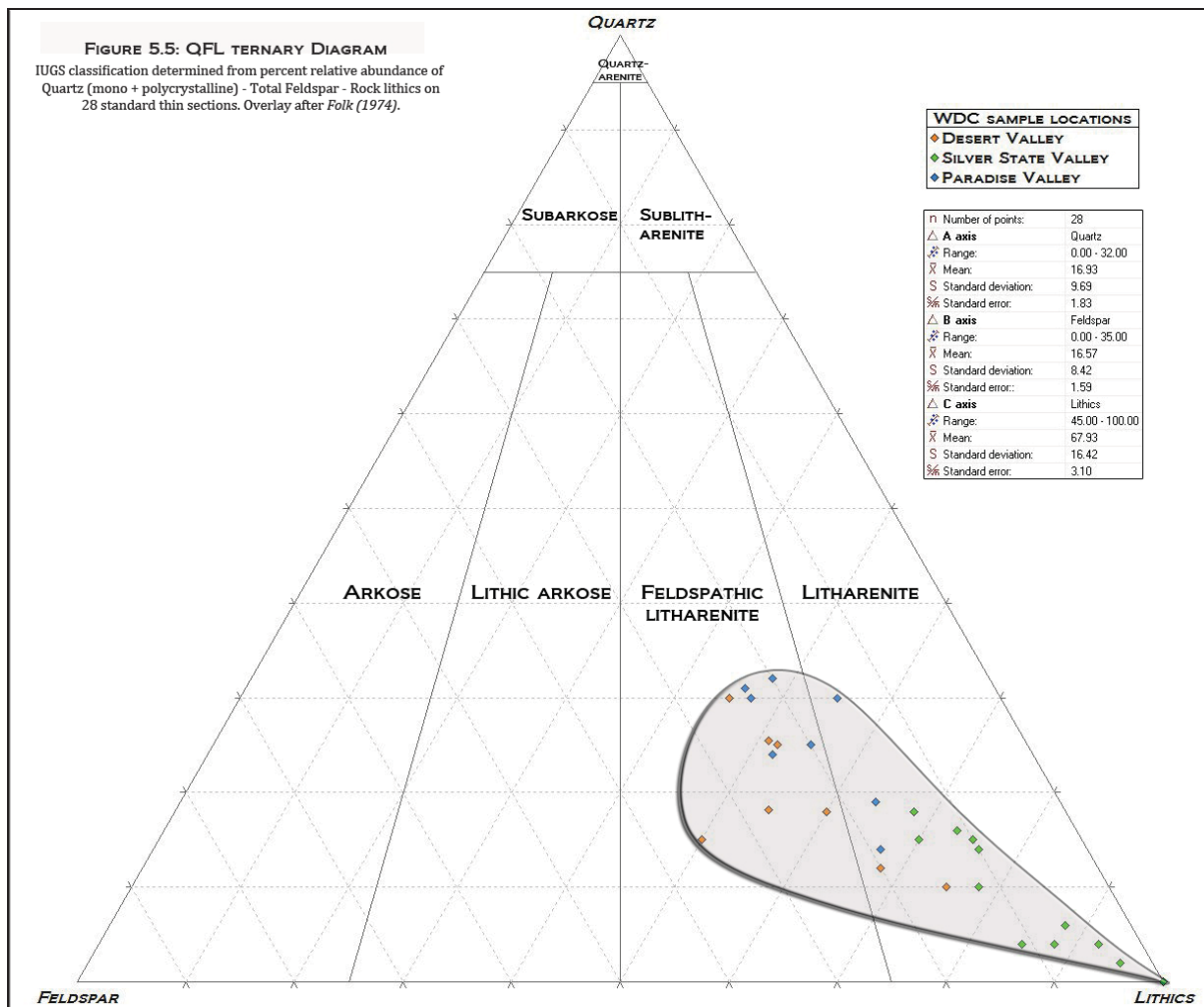


**Figure 5.5:** Quartz (monocrystalline + polycrystalline)-total Feldspar-Rock lithics (QFL) ternary diagram determined from 28 thin sections sampled in the Winnemucca Dune Complex. Physical classification of sand determined using International Union of Geological Sciences (IUGS) overlay after Folk (1974).

## 5.7 QAP ternary analysis and provenance of sand

Relative proportions of total Quartz, Alkali feldspar, and Plagioclase (QAP) from 34 samples are plotted on a ternary diagram (Figure 5.6) with a plutonic-volcanic equivalent rock type overlay after Streckeisen (1976, 1978). The samples analyzed unequivocally fit into three populations (groups I→III) that primarily can be distinguished by the composition of lithic material and relative weight percent of Quartz and Plagioclase.

Group I plots in the Quartz-rich granitoid region on the Streckeisen overlay. All of the samples from this group were collected near the leeward boundary of the complex in Paradise Valley. QAP components are comprised of 20 to 68% total Quartz, 0 to 51% Alkali feldspar, and 15 to 80% Albite from the Plagioclase series. Thin sections and loose sand samples did not contain plutonic rock fragments so it is very unlikely that sand from Group I was derived from a Quartz-rich granitoid. Samples from Group I are interpreted to be weathered and sorted sands from Groups II & III.

Group II placed into the Rhyolite-Rhyodacite region of the ternary diagram. A majority of the samples were collected from the crest and eastern flanks of the Slumbering Hills in Silver State Valley. Volcaniclastic material was plentiful in samples from Group II and amassed in value from 26 to 92% relative abundance. Total Quartz was 20 to 33% and Alkali feldspars (27 to 51%) of mostly Sanidine slightly exceeded the relative weight and abundance of Albite (21 to 43%). The provenance of sand in Group II is inferred to have felsic parent material from lava rock, pyroclastic rock, and volcanic tuff. The sufficiency of Sanidine, vitreous glass, pumice, and spherules from sand samples in Group II further confirms this assumption.

Group III was the largest group on the QAP ternary diagram. Samples from Group III plotted between the Monzogranite/Rhyodacite, Granodiorite/Dacite, and Tonalite region. Plutonic rock fragments were not observed in samples from this group so it is highly unlikely they are solely derived from Monzogranite, Granodiorite, or Tonalite bedrock. Metamorphic rock fragments of phyllite and slaty shale are common with minerals of Diopside, Ferroan Diopside, Muscovite-Sericite, and Ferroan Calcite. Total Quartz varied from 26 to 48% and Albite (32 to 58%) from the Plagioclase series well exceeded the content of Alkali feldspars (0 to 23%) which were primarily composed of Orthoclase and Potassium feldspar. The lithic composition and mineralogy of samples from Group III implies a majority of the sand was degraded from a metamorphic substratum. However the lithic content of Group III does contain marginal amounts of volcaniclastic material. Whether plutonic rocks have also contributed to the composition of Group III is unresolved.

The placement of Groups II & III on the QAP ternary diagram is very strong evidence that sand in WDC was delivered from various locations and does not solely originate from the stoss-side of the complex in the central portion of Desert Valley. Obvious potential bedrock sources for Groups II & III may consist of basement rocks from the metasedimentary Jungo terrane and Grus from decomposed outcrops of Granodiorite in the Jungo Hills, Slumbering Hills, and Santa Rosa Range. Other probable supply sources include the underlying Basaltic Trachy-Andesite flows and Rhyolite-Dacite tuffs from the Comforter Basin Formation in the Slumbering Hills, Ten Mile Hills, and Krum Hills.

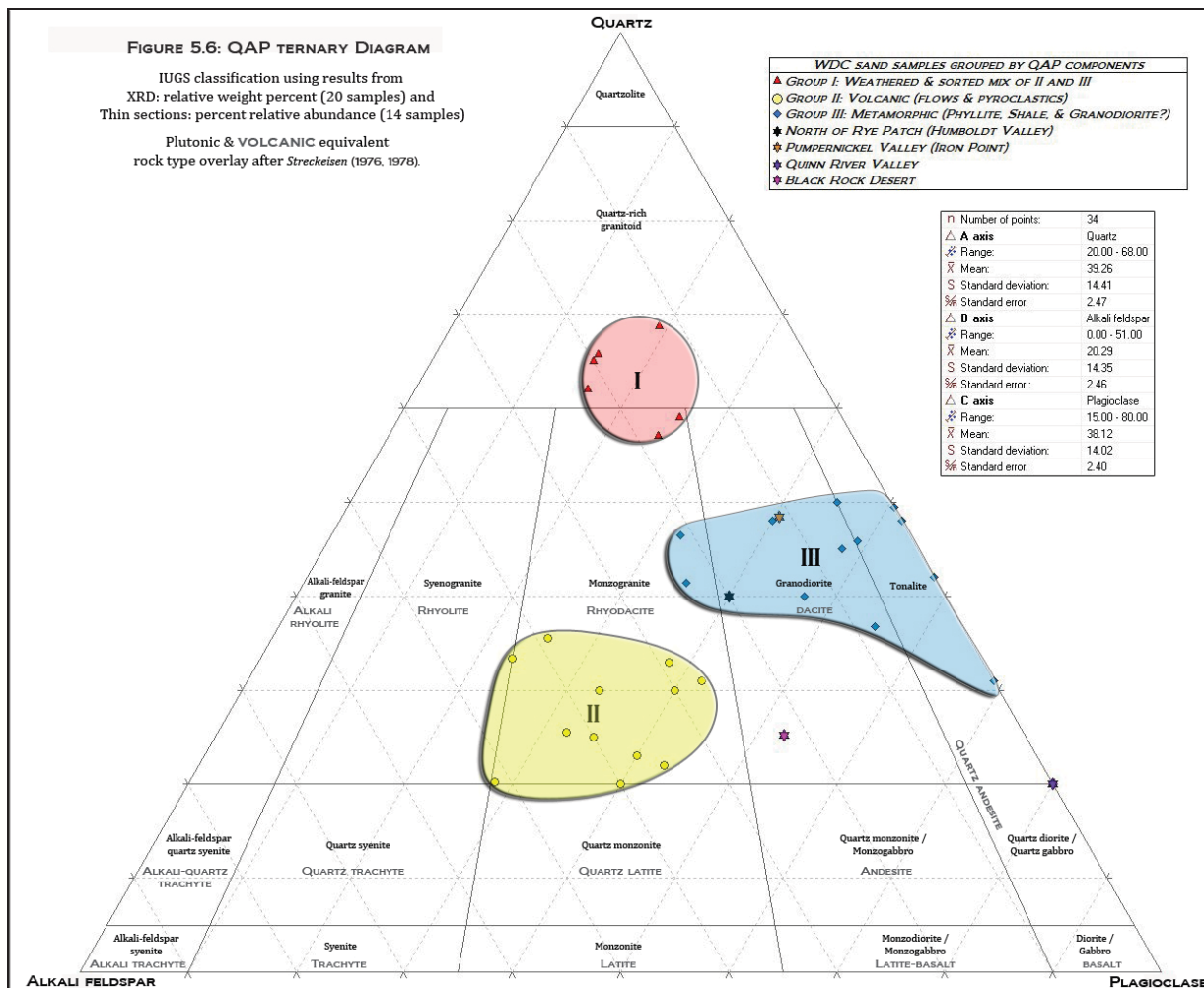


**Figure 5.6:** Total Quartz-Alkali feldspar-Plagioclase (QAP) ternary diagram determined from 20 X-ray Diffractometry tests and 14 thin sections sampled from the Winnemucca Dune Complex and adjacent dune fields. International Union of Geological Sciences (IUGS) plutonic and volcanic equivalent rock type overlay after Streckeisen (1976, 1978).

## 5.8 Relevant petrographic observations

Sediments from active dunes were mesokurtic, symmetrical, and trended towards moderately well sorted medium sand. Sediments from stable dunes were mesokurtic and trended towards moderately sorted fine sand but varied in skew from symmetrical to fine. Observations from Figures 5.1 & 5.3 show the accumulation of fines in stable dunes will skew the distribution of particle size, decrease sorting, and reduce the mean grain size of sand.

Qualitative color measurements and the QFL ternary diagram revealed that sand traveling down the sediment transport corridor will evidently weather from a White to Light Grey & Very Pale Brown Litharenite into a Very Dark Grey to Light Yellowish Brown & Pale Brown Feldspathic litharenite sand. Petrographic observations on Figures 5.5 & 5.6 also indicate that during the processes of dune stabilization and mineralogical maturation of sand the relative weight percent of total Quartz will increase ( $20 \rightarrow 68\%$ ) and the percent relative abundance of lithic material will decrease ( $100 \rightarrow 45\%$ ).

Sand from WDC is clearly demonstrated on the QAP ternary diagram (Figure 5.6) and in thin section to be derived from multiple local sources which involve metamorphic, plutonic, and volcanic bedrock. Observations from Figure 5.2 affirm the possible existence of different sediment supplies somewhere between Desert Valley and Silver State Valley. Variability of mean grain size between the basins would not occur if all of the sand transporting over the Slumbering Hills had originated downwind at the beginning of the complex in Desert Valley. The abundance of lithics (Figure 5.5) in dune sand from the Slumbering Hills exceeds the lithic content of sand from Desert Valley.

This observation verifies that dune sand in the Slumbering Hills is not completely sourced from Desert Valley and must have been supplied from a different location.

## 5.9 Discussion

This section will compare the results from Chapter 5 to previous studies regarding the color, size, mineralogical maturity, provenance, transportation, and weathering history of dune sand.

The matrix color of WDC sand had an average Munsell value of 10YR 7/2. This value is very close to the reported pale color of 10YR 6/2 that has been observed in sand from a majority of North American dune fields (Blount & Lancaster 1990; Lancaster 1993).

Globally the mean grain size of desert dune sand ranges from 160-330 $\mu\text{m}$  (2.65 $\phi$ , 1.60 $\phi$ ) (Lancaster 1995). The McKee (1979) collection from dune fields in the United States documents a mean grain size range of 120-484 $\mu\text{m}$  (3.056 $\phi$ , 1.047 $\phi$ ) and a worldwide average (191 sites) mean grain size of 281 $\mu\text{m}$  (1.83 $\phi$ ) (Ahlbrandt 1979). The range and average value from Lancaster & Ahlbrandt is similar to this study. Results from the Laser Granulometer showed the mean grain size of active dune sand in WDC was 154.6-336.1 $\mu\text{m}$  (2.694 $\phi$ , 1.573 $\phi$ ) with a mean value of 231.1 $\mu\text{m}$  (2.317 $\phi$ ).

Descriptive terminology applied by Blatt et al (1972) and Muhs et al (1995) utilizes the ratio of Quartz and Feldspar to classify the mineralogical maturity of dune sand. The premise of the scheme is that Quartz enrichment of dune sand will develop because Feldspar is highly susceptible to chemical weathering in contrast to Quartz which has a very low dissolution rate (Siever 1988). If sufficient time, water, and geochemistry are

present Feldspars should break down into silt and eventually be removed (Greeley & Iversen 1985) from sand by wind or water. Low ratio values of Qtz/Fs  $< 1.5$  designate sand as immature, ratios of  $1.5 < \text{Qtz/Fs} < 4.9$  term sand as intermediate, and large ratio values of  $\text{Qtz/Fs} > 4.9$  correspond with mature sand (Muhs 2004). Applying this system to the relative weight of Quartz (20 to 68%) and Feldspar (32 to 80%) in WDC yields ratios of 0.25 to 2.1. These values easily classify the maturity of dune sediments as predominantly immature and fractionally intermediate.

The distribution of Groups II & III on the QAP ternary diagram exposes a variance in the content of Alkali feldspar and Plagioclase. Contrasting Feldspar components in dune sand can indicate a difference in chemical weathering history and be an indicator for the mixing of sediments from varying sources (Zimbelman & Williams 2002). It would be improbable that sediments transported from the same source with similar mineralogy and weathering histories would produce disparate compositions of Feldspar. Albite was found universally throughout the complex but in varying amounts. Groups II & III had the same amount of Quartz but differed by quantity of Albite. Group II had relative weights of Albite that only slightly exceeded Alkali feldspar. Group III had contents of Albite that easily exceeded Alkali feldspar. This distinction supports one or more of the following conclusions; Groups II & III have slightly different chemical weathering histories and most likely they are sourced from separate locations.

Pettijohn et al (1972) evaluated the composition of sandstones and the provenance of terrigenous, carbonate, and pyroclastic sands. They pointed out that the mineralogical composition of volcaniclastic detritus can be directly inherited from its parent material

even if it is derived from an older volcanic terrain that has marginally weathered (Pettijohn et al 1972). Volcanic lithics of Sanidine in Silver State Valley show little alteration or replacement textures and possibly reflect the mineralogy of Rhyolite-Dacite tuffs from the Comforter Basin Formation or Rhyolite-Rhyodacite flows from the McDermitt-Santa Rosa volcanic field. If this is true then there must have not been substantial weathering of bedrock in the regions that supplied sand to WDC.

Chemical weathering from meteoric water and organic-acid generating vegetation can happen within dune fields during periods of stagnated activity and lead to the enrichment of Quartz (Muhs 2004). The tendency for the reduction of Feldspars and the enrichment of Quartz in sand during fluvial transport to a site of eolian activity is well documented (Nesbitt et al 1997; Potter et al 2001). Poor enrichment of Quartz suggests it is unlikely the complex has experienced long periods of inactivity or has chemically weathered from meteoric water and organic-acids. The geochemical consequence of sand being submerged in Lake Lahontan prior to the formation of dunes also does not appear to have enriched Quartz. Considering the abundance of sand sized Feldspar the effects of Lake Lahontan on the mineralogical maturity of sand must have been negligible.

Removal of Feldspars when chemical weathering is absent can be produced by abrasion and ballistic impacts from silt and sand during long periods of eolian activity (Greeley & Iversen 1985; Dutta et al 1993; Nesbitt & Young 1996; Arbogast & Muhs 2000). The prominent angular to subangular grains and relative abundance of Feldspar indicates WDC sand has not travelled over very long distances and that dune activity is geologically young. As sand transports from the stoss-side to leeward side of WDC the

relative weight and abundance of Quartz transforms from 20-68% with little signs of chemical weathering. The change in mineralogical maturity without significant evidence of chemical alteration implies the mechanical force of ballistic impact and abrasion from silt and sand are the most influential factors which control the size and quantity of Feldspar in WDC sediments.

## CHAPTER 6: DISCUSSION

### 6.1 Spatial extent of sand and major dune forms

Active and stabilized wind-blown deposits extend over 500 km<sup>2</sup> and blanket 472.2 km<sup>2</sup> of terrain in Desert Valley, Silver State Valley, and Paradise Valley. The active dunes are universally dominated by unique configurations of intermediate shaped barchan and parabolic dunes. For the purpose of this study these features were termed as barchanbolic. WDC is primarily covered by 6 crescentic complexes, 1 large sand sheet, and discontinuous sets of compound barchanbolic-parabolic dune fields. The crescentic complexes are composed of closely spaced barchanoidal and transverse ridges with occasional star dunes. Between the complexes are repetitive sequences of compound and individual barchanbolic-parabolic dunes that laterally radiate towards the bounding perimeter of WDC. Sand sheets, ramps, climbing, descending, cliff-top, and lee dunes are also present along mountain crests and hillsides. Sand sheets (56.3 km<sup>2</sup>) and active dunes (162 km<sup>2</sup>) extend across 218.3 km<sup>2</sup> which constitutes 46.2% of the wind-blown deposits in WDC.

The remaining wind-blown deposits are comprised of stabilized, semi-active, and degraded sand dunes. Overlapping plant communities consisting of invasive weeds, grasslands, desert shrub, sagebrush steppe, and psammophytes cover these features in varying density. Stabilized and semi-active dunes consist of parabolic, transverse, linear, and braided linear dunes that longitudinally border the active dunes and latitudinally encompass the western boundary of WDC. They also discontinuously interlace with the

active dune fields. En masse the stabilized and semi-active dunes shroud a total of 204.1 km<sup>2</sup> that accounts for 43.2% of eolian landforms on Maps 1-2.

Degraded sand dunes have parabolic or undifferentiated forms and normally are found adjacent to stable dunes on hills and valley floors. The morphology and location of these features denote they are modulated by a combination of forces which involve; growth of vegetation, flooding of drainage channels, ponding water, wildfires, livestock, and anthropogenic disturbances. Many of the degraded deposits are situated on southwesterly facing slopes below the peaks in each range of the complex. Runoff from snowmelt and rainfall is the probable cause that is responsible for the formation of degraded surfaces on hillsides and mountain ranges. Degraded sand dunes are distributed on 49.7 km<sup>2</sup> and cover up to 10.5% of WDC.

The spatial coverage of stabilized and degraded wind-blown deposits is underestimated in this report. Stabilized sand dunes extend well beyond the area which was mapped. Most of the Slumbering Hills to the north of Map 1 is covered by stabilized linear and parabolic dunes. Additional large fields of stabilized transverse dunes are located in the south-southeastern corner of Paradise Valley on Map 2. The transverse dunes stretch all the way to Golconda and the Weso Terrace on the south side of the Humboldt River. Attempting to map all of the neighboring stabilized and degraded dunes in Humboldt and Pershing Counties was not an objective of this research.

It is important to note the spatial extent of stabilized and degraded sand dunes (53.7% of Maps 1-2) reveals WDC has fluctuated in size. The presence of reactivated dune fields and broad distribution of stabilized deposits suggests WDC has experienced multiple

generations of dune activity since its inception. In terms of geologic time the cessation or triggering of dune activity has most likely been influenced by oscillations in long-term climate patterns such as temperature, precipitation, wildfire return intervals, and the direction of storm-tracks. The historical variance of dune activity in response to modern infrastructure is undetermined.

Anthropogenic disturbances from mining, livestock, agriculture, all-terrain vehicles, and the spread of invasive plants have had a significant impact on the environmental setting of WDC. Dune activity has responded differently to each of these variables. Mining, livestock, and recreational activities remove vegetation and increase sediment availability that contributes to the activity of dunes. However the installation of water supply wells and irrigation of farm fields has halted the advancement of dunes. Invasive plants shorten wildfire return intervals but also spread quickly and stabilize large areas of wind-blown sand. The net effect of these variables on the activity of dunes is difficult to evaluate with existing research and aerial imagery.

## **6.2 Activity and shape of sand dunes**

The direction of sand dune advancement in the Winnemucca Dune Complex was measured on Maps 1-2 (Plates 3.1 & 3.2) from 212 locations in Desert Valley, Silver State Valley, and Paradise Valley. Results from the measurements were plotted on a rose diagram using  $3^{\circ}$  intervals (Figure 6.1). The orientation of sand dunes trended from  $35^{\circ}$ - $130^{\circ}$  with an average direction of  $82.6^{\circ}$ . Three modes can be deciphered from Figure 6.1 that have percent frequencies greater than 2 percent;  $69\text{-}92^{\circ}$  (73.6%),  $99\text{-}110^{\circ}$  (10.85%), and  $60\text{-}65^{\circ}$  (5.66%). The trimodal distribution on the rose diagram implies a majority of

the winds responsible for the entrainment of sand prevail out of the northwest to southwest from the average direction of  $262.6^{\circ}$ .

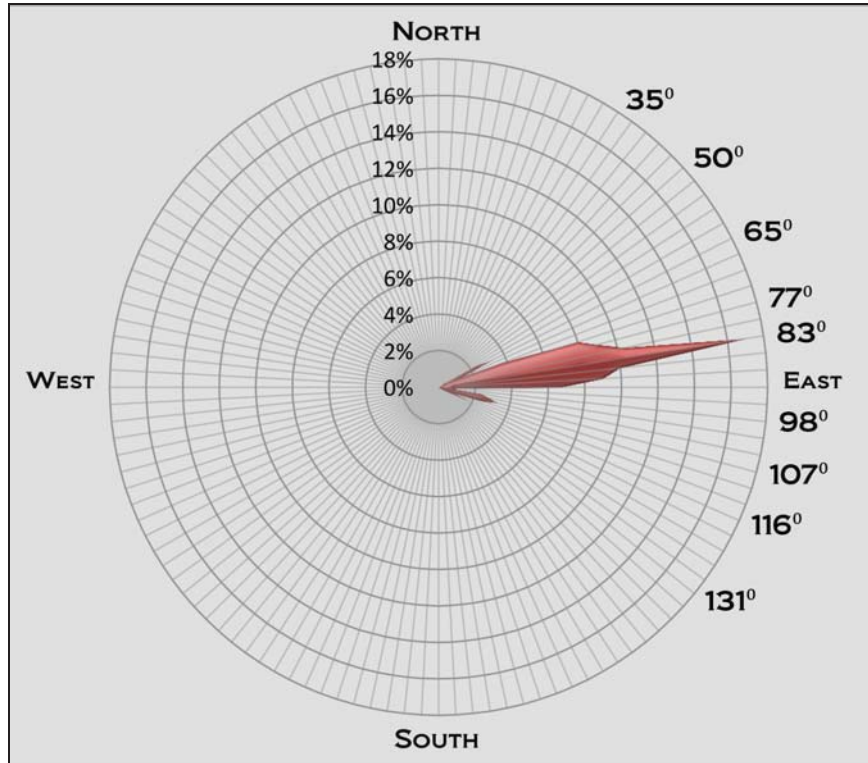


**Figure 6.1:** Rose diagram showing direction of sand dune advancement for the entire Winnemucca Dune Complex.

The observations on Figure 6.1 are consistent with calculations by Jewell & Nicoll (2011) and the WeatherSpark model (Figure 2.1). Jewell & Nicoll (2011) determined between the years 1950-2000 at the Winnemucca WSO airport the resultant drift direction of sand was approximately  $78-79^{\circ}$  (Figure 2.2). The WeatherSpark model from the years 1948-2013 estimated the strongest annual winds in Winnemucca prevail 37-40% of the time from the northwest to southwest during the warm season months of April to the middle of July. During these months the model also shows the average daily maximum wind speed is near  $7 \text{ ms}^{-1}$ . It can be concluded from the similar findings that WDC's wind regime is

similar to Winnemucca and annually the sand dunes reach peak advancement rates between the months of April to July.

Rates of sand dune advancement from the years 1980-2012 was compared on Figures 4.22, 4.24, and 4.26. The comparison revealed that rates of sand dune advancement have spatiotemporally fluctuated within the complex. These observations are not necessarily consistent with drift potential calculations performed by Jewell & Nicoll (2011). Figure 2.3 from Jewell & Nicoll (2011) shows the drift potential of sand at the Winnemucca WSO airport has steadily decreased during the years 1954-2000. The only parts of WDC which exhibited a similar pattern were the dune fields in Silver State Valley (Figure 4.24). Between the years 1994-2012 sand advancement rates in Silver State Valley have dropped 0.1 to 1.5  $\text{myr}^{-1}$ . In several portions of Desert Valley and Paradise Valley long-term sand dune advancement rates have increased. Measurements on Map 1 found that since the year 2000 rates of advancement for the crescentic complexes in Desert Valley have increased by 0.7 to 1.8  $\text{myr}^{-1}$  (Figure 4.22). On Map 2 since the year 1994 rates of advancement for the crescentic complexes and reactivated barchanbolic-parabolic dunes has increased by 0.2 to 0.5  $\text{myr}^{-1}$  in Paradise Valley (Figure 4.26).

Maximum sand dune advancement rates varied within each valley of the complex although a broad relationship between dune type and advancement rate was recorded in the measurements. The crescentic complexes were very active and had maximum advancement rates of 3.3 to 6.9  $\text{myr}^{-1}$ . Barchanbolic-parabolic dunes were slower and had maximum rates between 1.6 to 5.9  $\text{myr}^{-1}$ . Transforming linear-parabolic dunes were

partially stabilized and semi-active. In areas where advancement could be detected the linear-parabolic dunes expanded or stretched up to  $1 \text{ myr}^{-1}$ .

Figure 6.2 compares the morphometric measurements of length to width, spacing, and activity of dunes from 74 sites. The Pye (1993) classification scheme is employed on the lower portion of Figure 6.2 with dune type to describe the shape of various dunes which grouped together on the diagram. Four general conclusions can be drawn from Figure 6.2.

- 1) Lunate to hemicyclic shaped barchanoidal ridges, barchan, and crescentic dunes advance at the highest rates and are spaced close together.
- 2) Lobate to elongate shaped barchanbolic and parabolic dunes have slower rates of advancement and space far apart.
- 3) Initial spacing between dunes begins to increase as stabilized to semi-active linear dunes transform to active parabolic dunes.
- 4) As the rate of sand dune advancement continues to increase and reach maximum values the spacing between dunes decreases as barchanbolic-parabolic dunes merge and coalesce into barchans, ridges and complex crescentic forms.

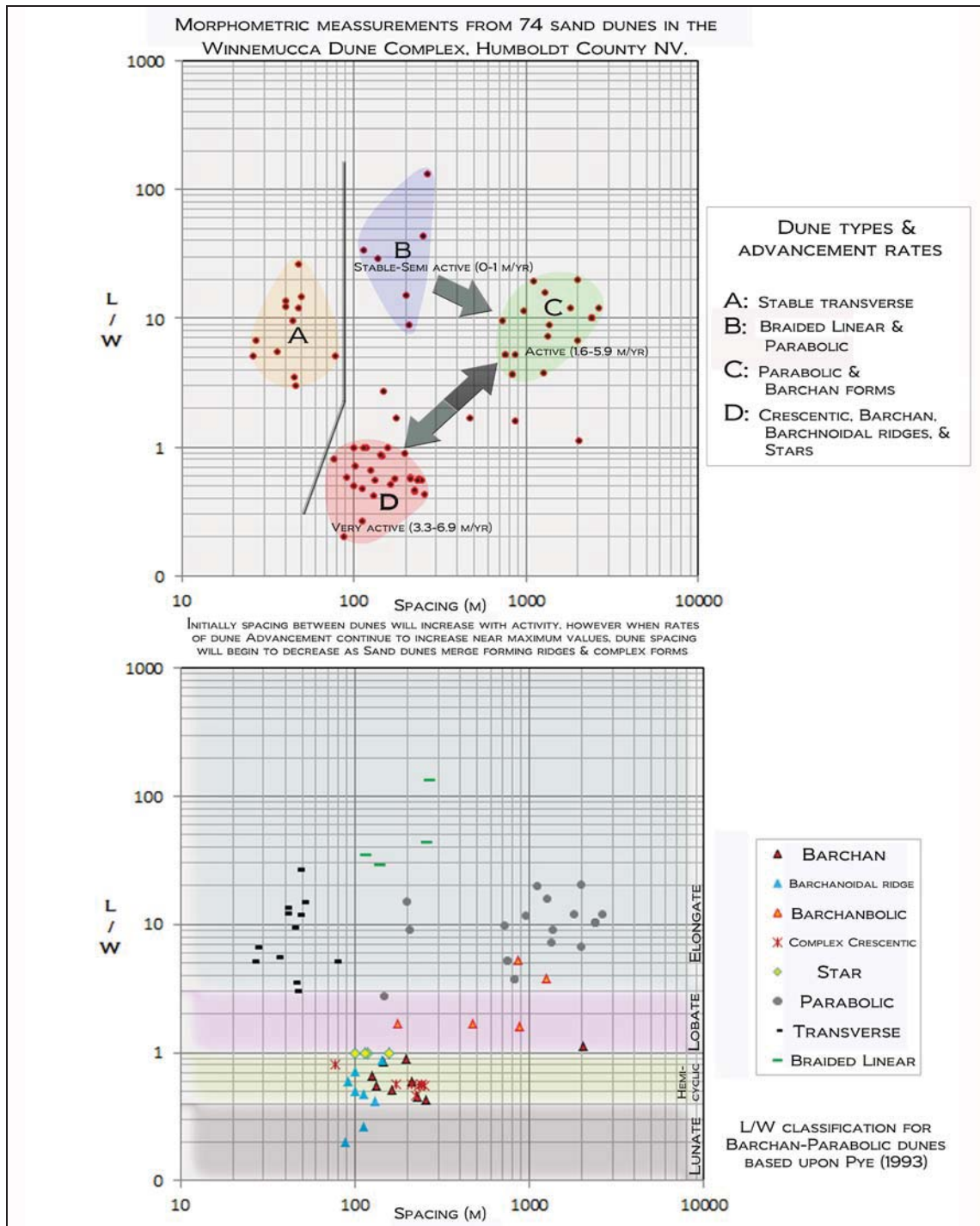


Figure 6.2: Length to width ratios, spacing, activity, and shape of sand dunes in WDC.

### 6.3 Textural, physical, and mineralogical characteristics of dune sand

The textural characteristics of 110 samples were quantitatively determined using a Laser Granulometer and the software program GRADISTAT. Sediments from active dunes were observed on Figure 5.3 to be mesokurtic, symmetrical, and trend towards moderately well sorted medium sand. Stable dune sediments were observed on Figure 5.3 to be mesokurtic and trend towards moderately sorted fine sand but varied in skew from symmetrical to fine.

Identifying the physical color and classification of dune sand was achieved using Munsell soil color chips, micro-stereoscopic inspection of loose sand, stained thin sections, and a Quartz (polycrystalline + monocrystalline)-Feldspar-Lithic (QFL) ternary diagram with overlay after Folk (1974). Qualitative color measurements and the QFL ternary diagram on Figure 5.5 revealed that sand traveling down the sediment transport corridor will physically weather from a White to Grey & Very Pale Brown Litharenite into a Very Dark Grey to Light Yellowish Brown & Pale Brown Feldspathic litharenite sand. Volcanic detritus comprises a majority of the lithics, metamorphic rock fragments are second most abundant, and particles from sedimentary deposits are fairly rare.

In addition to stained thin sections the application of X-ray Diffractometry (XRD) was used to assess the mineralogical characteristics of samples retrieved from the field. The relative weight percent of Quartz ranged between 20 to 68%. Feldspar content of sand graded from 32 to 80 relative weight percent. Albite was the prevalent Feldspar in dune sand and measured at 15 to 58 relative weight percent. Thin sections and XRD analysis did not reveal the presence of any other minerals from the Plagioclase series. The Alkali

feldspar content of sand assorted from 0 to 51 relative weight percent and included the following members listed in order of decreasing occurrence; Orthoclase, Sanidine, Potassium feldspar, and Microcline. Petrographic observations divulge that during the processes of dune stabilization and mineralogical maturation the relative weight percent of total Quartz will increase ( $20 \rightarrow 68\%$ ) and the percent relative abundance of lithic material will decrease ( $100 \rightarrow 45\%$ ).

A comparison of the petrographic observations to previous research validates sand in WDC has the same basic color and distribution of particle size as most desert dunes. The mineralogical maturity of sand when interpreted by the ratio of Quartz to Feldspar grades the maturation as low to fractionally intermediate. Groups II & III from the QAP ternary diagram on Figure 5.6 confirm there are distinct mineralogical differences within the sand and mixing of sediments from various supply sources have contributed to its composition. Similar to findings from the Mojave Desert (Zimbelman & Williams 2002) the abundance of Feldspar and lack of Quartz of enrichment may imply the mineralogical maturity of WDC dune sand is directly inherited from the parent material. The lack of Quartz enrichment also indicates dune activity in WDC is geologically young and most likely has not endured extended periods of inactivity. Prevalent angular to sub-angular grains within WDC sediments suggest dune sand has not been transported over extremely long distances.

#### 6.4 Provenance of sand

The provenance of sand in WDC is unknown. Very little effort has been put forth to investigate its origin although extravagant theories regarding the Humboldt River and Lake Lahontan have gained wide recognition. Previous research on the Pleistocene lacustrals of Lake Lahontan (Davis 1990; Benson, Kashgarian & Rubin 1995) has claimed the Humboldt River flowed into Lake Lahontan through southern Desert Valley via the narrow spill point at Pronto Pass (Image #22). Davis (1982, 1983, 1987<sup>1</sup>) speculated the Humboldt River formed a delta in Desert Valley to the northwest of Pronto Pass. Davis believed the delta sediments subsequently became the source of sand that was responsible for the formation of dunes in WDC. Other studies (Eissmann 1990; Adams, Wesnousky & Bills 1999) have insisted this occurred but all have failed to provide supporting evidence from the field.

Figure 6.3 displays a theoretical model of lake flow at Pronto Pass between 1257-1310 meters above MSL. It is evident on Figure 6.3 that water could not flow into Desert Valley but rather it would spill out of the valley to the southeast in the direction of the Humboldt River. At least 7-9 vertical meters of isostatic deformation in the area bounded by Pronto Pass and Gaskell would have been required to reverse the direction of flow. Unfortunately isostatic reconstructions of Lake Lahontan by Adams, Wesnousky & Bills (1999) discovered only 1 meter of rebound was possible in the vicinity of Pronto Pass. Furthermore, current structural models of Blue Mountain (Faulds & Melosh 2008) display Gaskell as down-dropping relative to Pronto Pass in the Humboldt Sink. The structural model of Blue Mountain further complicates the existence of an inlet from the

Humboldt River because Desert Valley would have been at a higher elevation during the Pleistocene.

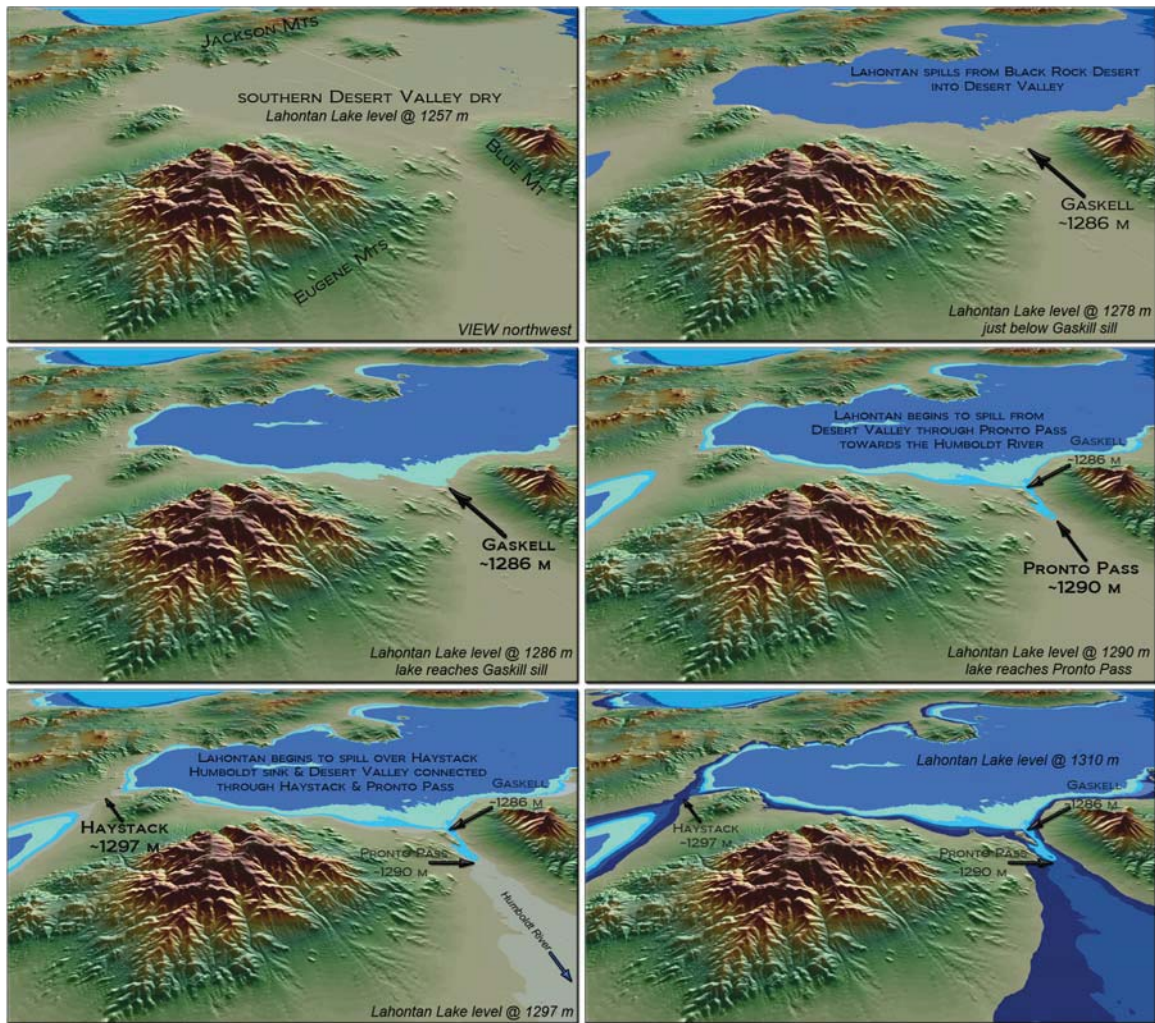
Contrary to Davis's theory and work by others, the dissection of Lake Lahontan shorelines, lakebeds, weathering of bedrock, and erosion of loose volcaniclastic deposits are the most probable sources responsible for the provenance of sand. Results from Chapter 5 easily verify this hypothesis. The fluctuation in grain size, lithic rock fragments, and variance of mineralogy are compelling lines of evidence that sand in WDC is provided locally by different parent materials of varying composition and are not solely sourced from Desert Valley.

Figure 5.2 clearly shows the mean grain size of sand does not begin to decrease until after the dunes traverse the ridge of the Bloody Run Hills and descend into Paradise Valley. The figure actually depicts a slight increase in grain size from the bottom of Desert of Valley to the eastern flanks of the Slumbering Hills. If sand was completely sourced from Desert Valley it would not be possible for it to increase in size as it is transported eastward through the complex. The discrepancy in sediment size from the fine grained sand sheet and the downwind dunes with medium grain sand are additional indications that different sediment supplies must exist. The quantity of lithics in dune sand is greatest along the crest of the Slumbering Hills. In this location rock fragments composed of volcaniclastic and metamorphic detritus reached 100% relative abundance whereas in Desert Valley lithic contents did not exceed 75%. This finding is well illustrated on Figure 5.5 and highlights the crest of the Slumbering Hills as a potential location that delivers part of the sediment load to WDC.

WDC dune sand is undoubtedly emphasized on the Quartz-Alkali feldspar-Plagioclase ternary diagram (Figure 5.6) to be derived from multiple local sources. Variance in the composition of Feldspars is prominent on the diagram. The contrasting mineralogy and placement of Groups II & III is a further indication that sand from each group was transported from separate locations. Group II is distinctly felsic and composed of Sanidine, vitreous glass, spherules, and pumice grains. Mineralogy from the group is markedly volcanic and displays as Rhyodacite on the Streckeisen (1978) overlay. The Rhyolite-Rhyodacite flows and tephra deposits from the McDermitt-Santa Rosa volcanic field located in the Jungo Hills, Slumbering Hills, Jackson Mountains, Kings River Valley, and Quinn River Valley may be parent material for the group. Additional potential sources for Group II are Rhyolite-Dacitic tuffs and Basaltic Trachy-Andesite flows from the Comforter Basin Formation.

Group III was more mafic and in several samples did not contain any Alkali feldspar. Crystalline Quartz, Potassium feldspar, Orthoclase coincident with Barium, Diopside, and Muscovite-Sericite mixed with metamorphic lithics of Phyllite, Slaty Shale, Quartzite, Opal, and Chalcedony assert plutonic and metamorphic parent material. The Streckeisen (1976) overlay interprets the plutonic provenance of Group III as Tonalite, Granodiorite, or Monzogranite. Obvious sources for the plutonic grouping would be the outcrops of Granodiorite and Tonalite in the Jungo Hills, Slumbering Hills and Santa Rosa Range. The copious metamorphic rock fragments and visual similarities to neighboring bedrock pinpoint the Jungo terrane with contributions of Opal and

Chalcedony from amygdules in the underlying andesite-basalt flows from the Comforter Basin Formation in the Slumbering Hills and Ten Mile Hills area.



**Figure 6.3:** Theoretical model of middle-late Pleistocene to early Holocene Lake Lahontan shorelines in southern Desert Valley. Figure generated using ArcGlobe and USGS 24k 5 meter resolution Digital Elevation Models. View in all figures is to the northwest.



**Image #22:** Train travelling east over Pronto Pass on the Transcontinental railroad.

## 6.6 Suggestions for further research

There are numerous techniques that may be used to further investigate the petrology and petrography of WDC sand. Additional bulk samples can be collected and evaluated to understand the mineralogy, provenance, and weathering of sand within the sediment transport corridor. Semi-quantitative analysis with X-ray Diffractometry and inspection of stained standard thin sections will assist with identifying the mineralogy of dune sand. A complete quantitative assessment of major oxides and trace elements using X-ray Fluorescence and Whole Rock analysis can help locate sediment supply sources and evaluate weathering processes.

The approximate age of the dunes and shorelines from Lake Lahontan in Desert Valley, Silver State Valley, and Paradise Valley is uncertain. There are plenty of gastropods, archeological lithic scatters, and charcoal in the complex that may provide excellent dating material for radiocarbon tests. Optical Stimulated Luminescence on older stabilized sand dunes, underlying lacustrine deposits and dune islands can effectively estimate the age of landforms. The utilization of Varnish Microlamination (VML) dating on dune sand and Lake Lahontan beach gravels may also be useful. In concert with other dating techniques VML will aid the development of a timescale and framework for the formation of WDC.

Over the last few thousand years Gumboot Lake has inevitably flooded several hundred times and permitted the Little Humboldt River to extend through the sand dunes in Paradise Valley to the confluence of the Humboldt River. The sediment transport capacity of the Humboldt River and sedimentary inputs from the Gumboot delivery mechanism has never been researched. It would be useful to evaluate the effects of fluvially entrained dune sand on the downstream morphology and stability of the Humboldt River. Large magnitude floods on Gumboot Lake may be linked to the giant meander scars at the inlets and outlets of Humboldt Lake. More detailed field studies could easily help unravel the potential relationship.

A wealth of meteorological data has been collected from numerous stations in the region. The application of a Multi-channel Singular Spectrum Analysis of wind records, temperature, precipitation, grain size parameters, mineralogy, dune morphometry, and

rates of sand dune advancement might uncover new insights into possible correlations between climate, eolian activity, and mineralogical maturation of dune sand.

This thesis slightly opens the door for impending studies of WDC. The report was intentionally designed to make the observations and conclusions applicable to sand dune localities in the Great Basin and other semi-arid deserts on Earth. Hopefully these suggestions for further research will be helpful and encourage future exploration of the Winnemucca Dune Complex.

## CITED REFERENCES

- Adams, K.D., Wesnousky, S.G., 1998. Shoreline processes and the age of the Lake Lahontan highstand in the Jessup embayment, Nevada: Geological Society of America Bulletin, v. 110, no. 10, p. 1318-1332.
- Adams, K.D., Wesnousky, S.G., Bills, B.G., 1999. Isostatic rebound, active faulting, and potential geomorphic effects in the Lahontan basin, Nevada and California: Geological Society of America Bulletin, v. 111, no. 12, p. 1739-1756.
- Adams, K.D., Goebel, T., Graf, K., Smith, G.M., Camp, A.J., Briggs, R.W., Rhode, D., 2008. Late Pleistocene and Early Holocene Lake-Level Fluctuations in the Lahontan Basin, Nevada: Implications for the Distribution of Archaeological Sites: Geoarchaeology, v. 23, no. 5, p. 608-643.
- Ahlbrandt, T.S., 1979. Textural Parameters of Eolian Deposits: *in* McKee, E.D., ed., A Study of Global Sand Seas: United States Geological Survey Professional Paper 1052, Ch. B, p. 21-58.
- Anderson, R.M., Jr., 2013. Stratigraphy of the Sandman low sulfidation Au deposits, Winnemucca, Nevada [M.S. Thesis]: University of Nevada, Reno, 175 p.
- Arbogast, A.F., Muhs, D.R., 2000. Geochemical and mineralogical evidence from eolian sediments for northwesterly mid-Holocene paleowinds, central Kansas, USA: Quaternary International, v. 67, p. 107-118.
- Arizona Quality Thin Sections, 9835 East Celeste Drive, Tucson, Arizona 85730.
- Attard Minerals, 5081 Field Street, San Diego, California 92110.
- Benson, L., Kashgarian, M., Rubin, M., 1995. Carbonate deposition, Pyramid Lake subbasin, Nevada: 2, Lake levels and polar jet stream positions reconstructed from radiocarbon ages and elevations of carbonates (tufa) deposited in the Lake Lahontan Basin: Paleogeography, Paleoclimatology, Paleoecology, v. 117, p. 1-30.
- Blatt, H., Middleton, G., Murray, R., 1972. Origin of sedimentary rocks: Englewood Cliffs, New Jersey, Prentice-Hall, 634 p.
- Blott, S.J., Pye, K., 2001. GRADISTAT: a grain size distribution and statistic package for the analysis of unconsolidated sediments: Earth Surface Processes and Landforms, v. 26, p. 1237-1248.
- Blount, G., Lancaster, N., 1990. Development of the Gran Desierto Sand Sea: Geology, v. 18, no. 8, p. 724-728.
- Breed, C.S., Grow, T., 1979. Morphology and Distribution of Dunes in Sand Seas Observed by Remote Sensing: *in* McKee, E.D., ed., A Study of Global Sand Seas: U.S. Geological Survey Professional Paper 1052, Ch. J, p. 258.

- Bureau of Land Management, United States Department of the Interior, Geospatial data:  
[http://www.blm.gov/nv/st/en/prog/more\\_programs/  
geographic\\_sciences/gis/geospatial\\_data.html](http://www.blm.gov/nv/st/en/prog/more_programs/geographic_sciences/gis/geospatial_data.html).
- Bureau of Land Management, Wildland Fire Management Information: 2012. Annual dataset archive, [http:// www.nifc.blm.gov/fire\\_reporting/annual\\_dataset\\_archive/](http://www.nifc.blm.gov/fire_reporting/annual_dataset_archive/)  
Annual /Dataset/Archive.html.
- Bureau of Land Management, Winnemucca District Office, December 2007. Blue Mountain Geothermal Development Project, Humboldt County, Pershing County, Nevada: Environmental Assessment, EA#:NV-020-08-01, p. 22-41.
- Bureau of Land Management, Winnemucca District Office, May 2010. Sandman Exploration Project, Humboldt County, Nevada: Environmental Assessment, EA#:NWK010-2010-0005, p. 3-1.
- Bureau of Land Management, Winnemucca District Office, May 2013<sup>1</sup>. Winnemucca District Drought Response Plan, Environmental Assessment, DOI-BLM-NV-WOOO-2013-0001-EA, 176 p.
- Bureau of Land Management, Winnemucca District Office, August 2013. Proposed Resource Management Plan and Final Environmental Impact Statement for managing public lands administered by the Winnemucca District in northern Nevada: Ch. 3.2.5-3.2.12, p. 36-90.
- Burke, D.B., Silberling, N.J., 1973. The Auld Lang Syne Group, of Late Triassic and Jurassic (?) age, North-Central Nevada: United States Geological Survey Bulletin 1394-E, p. E1-E14.
- Cohen, P., 1964. Preliminary Results of Hydrogeologic Investigations in the Valley of the Humboldt River near Winnemucca, Nevada: U.S. Geological Survey Water-Supply Paper 1754, p. 36-48.
- Colgan, J.P., Dumitru, T.A., Miller, E.L., 2004. Diachroneity of Basin and Range extension and Yellowstone hotspot volcanism in northwestern Nevada: Geology, v. 32, no. 2, p. 121-124.
- Colgan, J.P., Dumitru, T.A., Reiners, P.W., Wooden, J.L., Miller, E.L., 2006. Cenozoic Tectonic Evolution of the Great Basin Province in Northwestern Nevada: American Journal of Science, v. 306, p. 616-654.
- Compton, R.R., 1960. Contact metamorphism in the Santa Rosa Range, Nevada: Geological Society of America Bulletin, v. 71, no. 9, p. 1383-1416.
- Conrad, J.E., McKee, E.H., Rytuba, J.J., Nash, J.T., Utterback, W.C., 1993. Geochronology of the Sleeper deposit, Humboldt County, Nevada: Epithermal gold-silver mineralization following emplacement of a silicic flow-dome complex: Economic Geology, v. 88, p. 317-327.
- Davis, J.O., 1982. Geological Studies at Rye Patch Reservoir Phase IV, *in* Rusco, M.K., Davis, J.O., eds., Humboldt project, Rye Patch archeology, Phase IV final field report: Nevada State Museum Archeological Services Reports.

- Davis, J.O., 1983. The Late Cenozoic Arch at Rye Patch, Pershing County, Nevada: Stratigraphy, Structure, and Tectonic Geomorphology: Desert Research Institute unpublished report, University of Nevada, Reno, Special Collections, no. 98-36, box 1, series1, subseries 159, 30 p.
- Davis, J.O., 1987. Tephrochronology of middle Pleistocene lake sediments in Kobeh Valley, Nevada: Implications for neotectonics and drainage history of the central Great Basin: Geological Society of America Abstracts with Programs 19, no. 6, p. 370.
- Davis, J.O., 1987<sup>1</sup>. Geology at Rye Patch, *in* Rusco, M.K., Davis, J.O., eds., Studies in Archaeology, Geology, and Paleontology at Rye Patch Reservoir, Pershing County, Nevada: Nevada State Museum Anthropological Papers, no. 20, p. 21-22.
- Davis, J.O., 1990. Giant Meanders on Humboldt River near Rye Patch Nevada Due to Catastrophic Flooding: Geological Society of America Abstracts with Programs, v. 22, no.7, p. A309.
- Dickson, J.A.D., 1965. A Modified Staining Technique for Carbonates in Thin Section: Nature, v. 205, no. 4971, p. 587.
- Dufurrena, C.K., Rigby, J.G., 1988. Reconnaissance Geologic Maps of the Slumbering Hills and surrounding areas, Humboldt County, Nevada 1:1,000,000 scale: Nevada Bureau of Mines and Geology Open File report 88-6, 13 p.
- Dutta, P.K., Zhou, Z., dos Santos, P.R., 1993. A theoretical study of mineralogical maturation of eolian sand: Geological Society of America Special Paper 284, p. 203-209.
- Eissmann, L.J., 1990. Eolian Sand Transport in Western Nevada: Applications of LANDSAT TM Imagery [M.S. Thesis]: University of Nevada, Reno, 107 p.
- Elison, M.W., Speed, R.C., 1989. Structural development during flysch basin collapse: the Fencemaker allochthon, East Range, Nevada: Journal of Structural Geology, v. 11, no. 5, p. 523-538.
- Epps, T.M., Britten, H.B., Rust, R.W., 1998. Historical biogeography of *Eusattus muricatus* (Coleoptera: Tenebrionidae) within the Great Basin, western North America: Journal of Biogeography, v. 25, p. 957-968.
- Fairbank, B.D., Ross, H.P., 1999. Geology and Temperature Gradient Surveys Blue Mountain Geothermal Discovery, Humboldt County, Nevada: GRC Transactions, v. 23, p. 513-517.
- Faulds, J.E., Melosh, G., 2008. A Preliminary Structural Model for the Blue Mountain Geothermal Field, Humboldt County, Nevada: GRC Transactions, v. 32, p. 273-278.
- Federal Register, v.72, no. 84, Wednesday, May 2, 2007, p. 24256.
- Folk, R.L., Ward, W.C., 1957. Brazos River bar: a study in the significance of grain size parameters: Journal of Sedimentary Petrology, v. 27, p. 3-26.

- Folk, R.L., 1974. The Petrology of Sedimentary Rocks: Hemphill Publishing Co., Austin, Texas, p. 182.
- Fryberger, S.G., Dean, G., 1979. Dune forms and wind regime: United States Geological Survey Professional Paper 1052-F, p.137-169.
- Giroux, G., Kornze, L., Martin, L.G., September 22, 2008. Technical Report on the Sleeper Gold Property, Slumbering Hills, Awakening Mining District, Humboldt County, Nevada, USA: prepared for: X-CAL Resources Ltd., Vancouver, British Columbia, Canada, 301 p.
- Greeley, R., Iversen, J.D., 1985. Wind as a geological process on Earth, Mars, Venus and Titan: Cambridge University Press, Cambridge. 333 p.
- Gustin, M.M., Lanier, G., Ashton, J., November 2007. Updated Technical Report, Sandman Gold Project, Humboldt County, Nevada USA: prepared for: Fronteer Development Group Inc., submitted by Mine Development Associates, Reno, Nevada, 209 p.
- Hardy, A.R., Andrews, F.G., 1987. Studies in the Coleoptera of western sand dunes. 3. Remarks upon *Serica* (Scarabaeidae) from some Nevada sand dunes with descriptions of two new taxa: The Coleopterists Bulletin, v. 41, no. 2, p. 173-179.
- Harrill, J.R., Moore, D.O, 1970. Effects of Groundwater Development on the Water Regime of Paradise Valley, Humboldt County, Nevada, 1948-1969: Water Resources Bulletin, Nevada Department of Conservation and Natural Resources, no. 39, 123 p.
- Henry, C.D., John, D.A., 2013. Magmatism, ash-flow tuffs, and calderas of the ignimbrite flareup in the western Nevada volcanic field, Great Basin, USA: Geosphere, v. 9, no. 4, p. 951-1008.
- Houghton, H.F., 1980. Refined techniques for staining plagioclase and alkali feldspars in thin section: Journal of Sedimentary Petrology, v. 50, p. 629-631.
- Jewell, P.W., Nicoll, K., 2011. Wind regimes and aeolian transport in the Great Basin, USA: Geomorphology, v.129, p. 1-13.
- John, D.A., Wallace, A.R., Ponce, D.A., Fleck, R.B., Conrad, J.E., 2000. New Perspectives on the Geology and Origin of the Northern Nevada Rift: Geology and Ore Deposits 2000: The Great Basin and Beyond Proceedings, v.1, p. 127-154.
- Keller, E.A., 1985. Environmental Geology, Fourth Edition: Charles E. Merrill Publishing Company, Ch. 3, Fig. 3.34, p. 50.
- Lauha, E.A., Postlethwaite, C., Reid, R.F., Vance, R.B., Blackmone, J.E., Gopon, P.N., 2010. Geology of the Sandman epithermal gold prospects, Humboldt County, Nevada: Great Basin Evolution and Metallogeny: Geological Society of Nevada Symposium, v. 1, p. 813-824.
- Lancaster, N., 1993. Development of the Kelso Dunes, Mojave Desert, California: National Geographic Research and Exploration, v. 9, no. 4, p. 444-459.

- Lancaster, N., 1995. *Geomorphology of Desert Dunes*: Routledge, London, 290 p.
- Leoltz, O.J., Phoenix, D.A., Robinson, T.W., 1949. Groundwater in Paradise Valley, Humboldt County, Nevada: Water Resource Bulletin, State of Nevada Office of the State Engineer, no. 10, p. 52.
- Liu, T., Broecker, W.S., 2013. Millennial-scale varnish microlamination dating of late Pleistocene geomorphic features in the drylands of western USA: *Geomorphology*, v. 187, p. 38-60.
- Lupe, R., Silberling, N.J., 1985. Genetic relationship between Lower Mesozoic continental strata of the Colorado Plateau and marine strata of the western Great Basin: Significance for accretionary history of Cordilleran lithotectonic terranes: *in* Howell, D.G., ed., *Tectonostratigraphic Terranes of the Circum-Pacific Region: Earth Science Series 1*: Houston, Texas, Circum-Pacific Council for Energy and Mineral Resources, p. 263-271.
- Martin, R., 2012. The Climate of Winnemucca, Nevada: NOAA Technical Memorandum NWS WR-288, National Weather Service, Weather Forecast Office, Elko, Nevada, 202 p.
- McKee, E.D., 1979. A Study of Global Sand Seas: U.S. Geological Survey Professional Paper 1052, Ch. B, p. 44.
- Morrison, R.B., 1991. Quaternary stratigraphic, hydrologic, and climatic history of the Great Basin, with emphasis on Lakes Lahontan, Bonneville, and Tecopa, *in* The Geology of North America, v. K-2, Quaternary Nonglacial Geology: Conterminous U.S.: Geological Society of America, Ch.10, Fig. 8., p. 283-320.
- Muhs, D.R., Bush, C.A., Cowherd, S.D., Mahan, S., 1995. Geomorphic and geochemical evidence for the source of sand in the Algodones dunes, Colorado Desert, southeastern California: *in* Tchakerian, V.P., ed., *Desert aeolian processes*: New York, Chapman and Hall, p. 37-74.
- Muhs, D.R., 2004. Mineralogical maturity in dunefields of North America, Africa and Australia: *Geomorphology*, v. 59, p. 247-269.
- Munsell Soil Color Book, 2009. Munsell Color x-rite, Grand Rapids, Michigan.
- Nash, J.T., Utterback, W.C., Trudel, W.S., 1995. Geology and geochemistry of Tertiary volcanic host rocks, Sleeper gold-silver deposit, Humboldt County, Nevada: United States Geological Survey Bulletin 2090, 63 p.
- Nesbitt, H.W., Young, G.M., 1996. Petrogenesis of sediments in the absence of chemical weathering: effects of abrasion and sorting on bulk composition and mineralogy: *Sedimentology*, v. 43, p. 341-358.
- Nesbitt, H.W., Fedo, C.M., Young, G.M., 1997. Quartz and feldspar stability, steady and non-steady-state weathering, and petrogenesis of siliciclastic sands and muds: *Journal of Geology*, v. 105, p.173-191.

- Nevada Division of Water Planning, July 25, 2000. Humboldt River Chronology- Part I to III: Nevada Water Basin Information and Chronology Series, Nevada Division of Water Resources, 406 p.
- Oldow, J.S., 1984. Evolution of a late Mesozoic back-arc fold and thrust belt, northwestern Great Basin, USA: *Tectonophysics*, v. 102, p. 245-274.
- Pettijohn, F.J., Potter, P.E., Siever, R., 1972. *Sand and Sandstone*. Springer-Verlag, New York, 618 p.
- Ponce, D.A., Glen, J.M., Watt, J.T., Casteel, J., 2010. Geophysical Setting of the Blue Mountain Geothermal Area, North-Central Nevada and its Relationship to a Crustal-Scale Fracture Associated with the Inception of the Yellowstone Hotspot: *GRC Transactions*, v. 34, Fig. 1, p. 881-885.
- Potter, P.E., Huh, Y., Edmond, J.M., 2001. Deep-freeze petrology Lena River sand, Siberia: *Geology*, v. 29, no. 11, p. 999-1002.
- Prudic, D.E., Herman, M.E., 1996. Ground-water flow and simulated effects of development in Paradise Valley, a basin tributary to the Humboldt River in Humboldt County, Nevada: United States Geological Survey Professional Paper 1409-F, 90 p.
- Pye, K., 1993. Late Quaternary development of coastal parabolic megadune complexes in northeastern Australia: Special Publication of the International Association of Sedimentologists, v.16, p. 23-24.
- Pye, K., Tsoar, H., 2009. *Aeolian Sand and Sand Dunes*: Springer-Verlag Berlin Heidelberg, Fig. 6.18a-c, p. 202.
- Reheis, M., 1999. Highest Pluvial-Lake Shorelines and Pleistocene Climate of the Western Great Basin: *Quaternary Research*, v. 52, no. 196, p. 196-205.
- Resource Concepts Inc., 2005. Nevada Community Wildfire Risk; Hazard Assessment Project: Bureau of Land Management Nevada State Office, Nevada Division of Forestry, and the Nevada Association of Counties, <http://www.rci.nv.com>.
- Rogers, J.W., 1999. Jurassic-Cretaceous deformation in the Santa Rosa Range, Nevada: implications for the development of the northern Luning-Fencemaker fold-and-thrust belt [M.S. Thesis]: University of Georgia, Athens.
- Russell, I.C., 1885. Geological History of Lake Lahontan, a Quaternary Lake of Northwestern Nevada: United States Geological Survey Monographs vol. XI, Washington Government Printing Office, p. 153-156.
- Shvetsov, M.S., September 1955. Concerning some additional aids in studying sedimentary formations: *Journal of Sedimentary Petrology*, v. 25, no.2, p. 229-234.
- Siever, R., 1988. *Sand*: New York, W.H. Freeman and Co., 237 p.

- Silberling, N.J., Jones, D.L., Blake, M.C., Jr., Howell, D.G., 1987. Lithotectonic terrane map of the western conterminous United States: United States Geological Survey Miscellaneous Field Studies Map MF-1874-C, scale 1:2,500,000.
- Smith, R.S.U., 1982. Sand Dunes in North American deserts, *in* Beder, G.L., ed., Reference Handbook on the Deserts of North America: Greenwood Press, London, p. 481-524.
- Streckeisen, A.L., 1976. Classification of the common igneous rocks by means of their chemical composition: a provisional attempt: Neues Jahrbur Für Mineralogie, Monatshefte, H.1, p. 1-15.
- Streckeisen, A.L., 1978. IUGS Subcommission on the Systematics of Igneous rocks. Classification and Nomenclature of Volcanic Rocks, Lamprophyres, Carbonatites and Melitite rocks. Recommendations and Suggestions: Neues Jahrbuch Für Mineralogie, Abhandlungen, v. 141, p. 1-14.
- Thompson, R.S., Benson, L.V., Hattori, E.M., 1986. A revised chronology for the last Pleistocene lake cycle in the central Lahontan basin: Quaternary Research, v. 25, p. 1-9.
- Trexler, D.T., Melhorn, W.N., July 1986. Singing and booming sand dunes of California and Nevada: California Geology, San Francisco, CA: California Division of Mines and Geology, v. 39, no. 7, p. 147-152.
- TriPlot v.4.1.2, 2009, Todd Thompson software, Indiana University, <http://www.mypage.iu.edu/~tthomps/programs/html/tnttripplot.htm>.
- U.S. Army, September 1975. Humboldt River and Tributaries, Nevada: Hydrology, United States Army Corps of Engineers, Sacramento District, California, CH2M Hill, Inc., revised June 1976.
- U.S. Soil Conservation Service, March 1962. Humboldt River Basin, Nevada, Water and Related Land Resources, Report Number One, Little Humboldt Sub-Basin: Nevada Department of Conservation and Natural Resources and the United States Department of Agriculture, 131 p.
- Vector Magic Inc., San Francisco, California, WeatherSpark beta, <http://www.weatherspark.com>.
- Western Regional Climate Center: Desert Research Institute, <http://www.wrcc.dri.edu>.
- Willden, R., 1964. Geology and mineral deposits of Humboldt County, Nevada: Nevada Bureau of Mines and Geology Bulletin 59, 154 p.
- Wyld, S.J., 2000. Triassic evolution of the arc and backarc of northwest Nevada, and evidence for extensional tectonism: *in* Soreghan, M.J., and Gehrels, G.E., eds., Paleozoic and Triassic Paleogeography and Tectonics of Western Nevada and Northern California: Boulder, Colorado, Geological Society of America Special Paper 347.

- Wyld, S.J., Rogers, J.W., Wright, J.E., 2001. Structural evolution within the Luning-Fencemaker fold-thrust belt, Nevada: progression from back-arc basin closure to intra-arc shortening: *Journal of Structural Geology*, v. 23, p. 1971-1995.
- Wyld, S.J., 2002. Structural evolution of a Mesozoic backarc fold-and-thrust belt in the U.S. Cordillera: New evidence from northern Nevada: *Geological Society of America Bulletin*, v. 114, no. 11, p. 1452-1468.
- Zimbelman, J.R., Williams, S.H., 2002. Geochemical indicators of separate sources for eolian sands in the eastern Mojave Desert, California, and western Arizona: *Geological Society of America Bulletin*, v. 114, no. 4, p. 490-496.

**APPENDIX A: Direction and rate of sand dune advancement**

APPENDIX A: SHEET 1				94-2012		94-2006		2000-12		2000-06		2006-12		Notes
#	Azim.	Unit	Section	min (m) m/yr	max (m) m/yr									
1	78	Qda1	CSC	n/a	n/a	n/a	n/a	10.7	78	8.2	37	2.5	41	CSC = Crescent Sombrero Complex (18yr) max rate of advancement: 3.2 - 5.4 m/yr azimuth range: 60-110
2	75	Qda1	CSC	n/a	n/a	n/a	n/a	8	47	4	28.2	4	18.8	
3	72	Qda1	CSC	n/a	n/a	n/a	n/a	24	83	17	53	7	30	
4	110	Qda1	CSC	n/a	n/a	n/a	n/a	30	42	16	26	14	16	
5	84	Qda1	CSC	n/a	n/a	n/a	n/a	2.5	3.5	2.7	4.3	2.3	2.7	
6	110	Qda1	CSC	n/a	n/a	n/a	n/a	27	40	n/a	n/a	n/a	n/a	
								2.3	3.3					unable to measure dune @ site #5 with available 2006 imagery
								2	3.6					unable to measure dune @ site #6 with available 2006 imagery
										4.6m/yr	6m/yr			
7	88	Qda1	CSC											no advancement measurements @ site #7 no advancement measurements @ site #8
8	68	Qda1	CSC											
9	80	Qda1	CSC	19	61	14	35.1	n/a	n/a	n/a	n/a	5	25.9	
				1.1	3.4	1.1	3					0.8	4.3	
10	72	Qda7	CSC	0	57	0	20	n/a	n/a	n/a	n/a	0	37	
				0	3.2	0	3.3					0	6.2	
11	82	Qda7	CSC	8	76	3.7	42	n/a	n/a	n/a	n/a	4.3	34	
				0.4	4.2	0.6	3.5					0.7	5.7	
12	70	Qda7	CSC	24	98	11.2	51	n/a	n/a	n/a	n/a	12.8	47	
				1.3	5.4	0.9	4.3					2.1	7.8	
13	60	Qda8	CSC	9	98	6.2	45	n/a	n/a	n/a	n/a	2.8	53	
				0.5	5.4	0.5	3.8					0.5	8.8	
14	72	Qda1	SHC	15	58	10	41	n/a	n/a	n/a	n/a	5	17	SHC = Slumbering Hills Complex (18yr) max rate of advancement: 2.2 - 3.8 m/yr azimuth range: 65-105
				0.8	3.2	0.8	3.4					0.8	2.8	
15	75	Qda1	SHC	28.2	68.4	n/a								
				1.6	3.8									
16	88	Qda1	SHC	48	68	n/a								
				2.6	3.8									
17	105	Qda1	SHC											
18	95	Qda1	SHC	15	38	n/a								
				0.8	2.2									
19	65	Qda1	SHC	42.3	65.3	29	45	n/a	n/a	n/a	n/a	13.3	20	
				2.4	3.6	2.4	3.8					2.2	3.3	
20	100	Qda1	SHC	29.3	55	20.3	39	n/a	n/a	n/a	n/a	9	14	
				1.6	3	1.7	3.3					1.5	2.3	
21	80	Qda1	SHC	34	66.3	25.4	43.8	n/a	n/a	n/a	n/a	8.6	22.5	
				1.9	3.7	2.1	3.7					1.4	3.8	
22	105	Qda1	SHC	41.2	59	31	41	n/a	n/a	n/a	n/a	11.2	18	
				2.3	3.3	2.5	3.4					1.9	3	
23	100	Qda1	SHC	9	58	n/a								
				0.5	3.2									
				18yr.	3.7m/yr		3.6m/yr				4.7 m/yr			

APPENDIX A: SHEET 2

APPENDIX A: SHEET 3

#	Azim.	Unit	Section	94-2012		Notes
				min (m) m/yr	max (m) m/yr	
74	82	Qda3	East	0.8	1.2	
75	82	Qda3	East	0	0.8	
76	85	Qda3	East	1.2	1.7	
77	80	Qda3	East	0.7	2.1	
78	82	Qda3	West	0.5	1.2	
79	74	Qda3	West	1.2	2.6	
80	85	Qda3	West	1.4	3.3	
81	80	Qda3	West	0	0.9	
82	70	Qda3	West			
83	80	Qda3	West	0.3	1	
84	82	Qda3	West	0.3	1.5	
85	72	Qda3	West	0	1.1	
			18yr.	1.6 m/yr		no advancement measurements @ site #45

**APPENDIX A:**  
**SHEET 4**

#	Azim.	Unit	Section	1980 to 2012		1980 to 1999		1999-12		1999-06		2006-12		Notes			
				min (m) m/yr	max (m) m/yr	min (m) m/yr	max (m) m/yr	min (m) m/yr	max (m) m/yr	min (m) m/yr	max (m) m/yr	min (m) m/yr	max (m) m/yr				
58	70	Qda2	SW	26.2 <b>0.8</b>	76 <b>2.4</b>	26.2 <b>1.4</b>	46 <b>2.4</b>	0 <b>0</b>	30 <b>2.3</b>	0 <b>0</b>	12 <b>1.7</b>	0 <b>0</b>	18 <b>3</b>				
59	70	Qda2	SW	46.2 <b>1.4</b>	97.3 <b>3</b>	20.5 <b>1.1</b>	38 <b>2</b>	15.7 <b>1.2</b>	59.3 <b>4.6</b>	14.7 <b>2.5</b>	40.1 <b>5.7</b>	11 <b>1.8</b>	19.2 <b>3.2</b>				
60	85	Qda2	SW	47.5 <b>1.5</b>	169 <b>5.3</b>	36 <b>1.9</b>	112 <b>5.9</b>	9.5 <b>0.7</b>	57 <b>4.4</b>	9.5 <b>1.4</b>	33 <b>4.7</b>	0 <b>0</b>	24 <b>4</b>				
61	65	Qda2	SW	13 <b>0.4</b>	161.7 <b>5.1</b>	13 <b>0.7</b>	82.4 <b>4.3</b>	0 <b>0</b>	79.3 <b>6.1</b>	0 <b>0</b>	60 <b>8.6</b>	0 <b>0</b>	19.3 <b>3.2</b>				
				32yr	4.3 m/yr			4.2 m/yr			3.8 m/yr						
				1980 to 2012		1980 to 1994		1994 to 1999		1994 to 2012		1999 to 2012					
#	Azim	Unit	Sub unit	min (m) m/yr	max (m) m/yr	min (m) m/yr	max (m) m/yr	min (m) m/yr	max (m) m/yr	min (m) m/yr	max (m) m/yr	min (m) m/yr	max (m) m/yr	Notes			
62	82	Qda2	SW	84.5 <b>2.6</b>	184.1 <b>5.8</b>	34 <b>2.4</b>	64.5 <b>4.6</b>	24 <b>4.8</b>	54.5 <b>10.9</b>	50.5 <b>2.8</b>	119 <b>6.6</b>	26.5 <b>2</b>	65.1 <b>5</b>	16.5 <b>4.4</b>	30.6 <b>1.7</b>	10 <b>5.8</b>	
63	70	Qda2	SW	n/a	n/a	n/a	n/a	5 <b>1</b>	24.4 <b>4.9</b>	17.2 <b>1</b>	69.4 <b>3.9</b>	12.2 <b>0.9</b>	45 <b>3.5</b>	6.1 <b>0.9</b>	20 <b>2.9</b>	6.1 <b>1</b>	25 <b>4.2</b>
64	75	Qda2	SW	n/a	n/a	n/a	n/a	18 <b>3.6</b>	39 <b>7.8</b>	48.1 <b>2.7</b>	104.3 <b>5.8</b>	30.1 <b>2.3</b>	65.3 <b>5</b>	17 <b>2.4</b>	33 <b>4.7</b>	13.1 <b>2.2</b>	32.3 <b>5.4</b>
65	80	Qda2	SW	n/a	n/a	n/a	n/a	n/a <b>1.9</b>	n/a <b>4.8</b>	33.3 <b>2.7</b>	86 <b>5.8</b>	n/a <b>5</b>	n/a <b>2.4</b>	n/a <b>4.7</b>	n/a <b>2.2</b>	6.3 <b>5.4</b>	
66	83	Qda2	N	n/a	n/a	n/a	n/a	n/a	n/a	22.1 <b>1.7</b>	53.4 <b>4.1</b>	13.4 <b>1.9</b>	27 <b>3.9</b>	8.7 <b>1.5</b>	26.4 <b>4.4</b>		
67	78	Qda2	N	63.5 <b>2</b>	113 <b>3.5</b>	42 <b>3</b>	47 <b>3.4</b>	11 <b>2.2</b>	26 <b>5.2</b>	21.5 <b>1.2</b>	66 <b>3.7</b>	10.5 <b>0.8</b>	40 <b>3.1</b>	6 <b>0.9</b>	14.3 <b>2</b>	4.5 <b>0.8</b>	15.7 <b>2.6</b>
68	70	Qda2	N	n/a	n/a	n/a	n/a	15 <b>3</b>	27 <b>5.4</b>	28.9 <b>1.6</b>	80 <b>4.4</b>	13.9 <b>1.1</b>	53 <b>4.1</b>	7.8 <b>1.1</b>	34 <b>4.9</b>	6.1 <b>1</b>	19 <b>3.2</b>
69	78	Qda2	N	92.4 <b>2.9</b>	165.4 <b>5.2</b>	50 <b>3.6</b>	82.4 <b>5.9</b>	13 <b>2.6</b>	33 <b>6.6</b>	42.4 <b>2.4</b>	83 <b>4.6</b>	19.4 <b>1.5</b>	50 <b>3.8</b>	14 <b>2</b>	25 <b>3.6</b>	15.4 <b>2.6</b>	25
70	75	Qda2	N	n/a	n/a	n/a	n/a	n/a	n/a	50.4 <b>2.8</b>	73.8 <b>4.1</b>	n/a	n/a	n/a	n/a	9.5 <b>1.6</b>	25.8 <b>4.3</b>
71	82	Qda2	N	n/a	n/a	n/a	n/a	n/a	n/a	7.2 <b>0.4</b>	54 <b>3</b>	n/a	n/a	n/a	n/a	0 <b>0</b>	12.3 <b>2.1</b>
72	76	Qda2	N	n/a	n/a	n/a	n/a	n/a	n/a	54 <b>3</b>	84.6 <b>4.7</b>	n/a	n/a	n/a	n/a	6.4 <b>1.1</b>	14.6 <b>2.4</b>
73	100	Qda2	N	n/a	n/a	n/a	n/a	n/a	n/a	25.5 <b>1.4</b>	80 <b>4.4</b>	n/a	n/a	n/a	n/a	5.5 <b>0.9</b>	20 <b>3.3</b>
				32yr	4.3 m/yr			4.6 m/yr		6.8 m/yr	18yr.	4.5 m/yr	4.2 m/yr	4.3 m/yr	3.8 m/yr		

Qda2 SW (southwest)  
(32yr) max rate of advancement: 2.4 - 5.8 m/yr  
azimuth range: 65 - 85

averages include # 62-77

Qda2 SW (southwest)  
(32yr) max rate of advancement: 2.4 - 5.8 m/yr  
azimuth range: 65 - 85

Qda2 N (north)  
(32yr) max rate of advancement: 3.5 - 5.2 m/yr  
azimuth range: 70 - 105

averages include # 58-61

**APPENDIX A:**  
**SHEET 5**

#	Azim	Unit	Section	1980 to 2012		1980 to 1994		1994 to 2006		2006-12		94-2012	
				min (m)	max (m)	min (m)	max (m)	min (m)	max (m)	min (m)	max (m)	min (m)	max (m)
				m/yr	m/yr	m/yr	m/yr	m/yr	m/yr	m/yr	m/yr	m/yr	m/yr
86	88	Qda4	East	n/a	n/a	n/a	n/a	n/a	n/a	n/a	n/a	10.8	25.2
87	75	Qda4	East	n/a	n/a	n/a	n/a	n/a	n/a	n/a	n/a	0.6	1.4
88	72	Qda4	East	n/a	n/a	n/a	n/a	n/a	n/a	n/a	n/a	21.6	54
89	65	Qda4	Iso.	n/a	n/a	n/a	n/a	n/a	n/a	n/a	n/a	1.2	3
90	65	Qda4	Iso.	n/a	n/a	n/a	n/a	n/a	n/a	n/a	n/a	n/a	n/a
91	60	Qda4	Iso.	n/a	n/a	n/a	n/a	n/a	n/a	n/a	n/a	n/a	n/a
92	65	Qda4	Iso.	n/a	n/a	n/a	n/a	n/a	n/a	n/a	n/a	n/a	n/a
93	80	Qda4	Iso.	n/a	n/a	n/a	n/a	n/a	n/a	n/a	n/a	n/a	n/a
94	88	Qda4	SS-W	n/a	n/a	n/a	n/a	n/a	n/a	n/a	n/a	n/a	n/a
95	80	Qda4	SS-W	0	135	0	51	0	66	0	18	0	84
				0	4.2	0	3.6	0	5.5	0	3	0	4.7
96	82	Qda4	SS-W	12	50	12	25	0	14	0	11	0	25
				0.4	1.6	0.9	1.8	0	1.2	0	1.8	0	1.4
97	84	Qda4	SS-W	n/a	n/a	n/a	n/a	0	22	0	23	0	45
								0	1.8	0	3.8	0	2.5
98	67	Qda4	SS-W	n/a	n/a	n/a	n/a	0	43	0	13.2	0	56.2
								0	3.6	0	2.2	0	3.1
99	105	Qda4	SS-W	n/a	n/a	n/a	n/a	0	35	0	19.6	0	54.6
								0	2.9	0	3.3	0	3
100	84	Qda4	SS-W	38.4	129.8	24.4	69	14	35	0	25.8	14	60.8
				1.2	4.1	1.7	4.9	1.2	2.9	0	4.3	0.8	3.4
101	83	Qda4	SS-W	28	96.2	13	38	15	45	0	13.2	15	58.2
				0.9	3	0.9	2.7	1.3	3.8	0	2.2	0.8	3.2
102	78	Qda4	SS-W	18	87	9	36	9	37	0	14	9	51
				0.6	2.7	0.6	2.6	0.8	3.1	0	2.3	0.5	2.8
				32yr.	3.1 m/yr		3.1 m/yr		3.1 m/yr		2.9 m/yr	18yr.	2.9 m/yr
103	85	Qda8	CSC	18	113	18	42	0	35	0	36	0	71
				0.6	3.5	1.3	3	0	2.9	0	6	0	3.9
104	84	Qda8	SS-W	21.2	134	10	69	11.2	40	0	25	11.2	65
				0.7	4.2	0.7	4.9	0.9	3.3	0	4.2	0.6	3.6
105	88	Qda8	SS-W	88.6	139	60.4	77	22.5	37	5.7	25	22.5	62
				2.8	4.3	4.3	5.5	1.9	3.1	1	4.2	1.3	3.4
				32yr.	4 m/yr		4.5 m/yr		3.1 m/yr		4.8 m/yr	18yr.	3.6 m/yr
106	107	Qda2	SS-W	n/a	n/a	n/a	n/a	23	44.2	11.5	35	34.5	79.2
								1.9	3.7	1.9	5.8	1.9	4.4
107	109	Qda2	SS-W	31.3	145.8	20	68.4	11.3	46	0	31.4	11.3	77.4
				1	4.6	1.4	4.9	0.9	3.8	0	5.2	0.6	4.3
108	115	Qda2	SS-W	16	98	8.8	54	7.2	32	0	12	7.2	44
				0.5	3.1	0.6	3.9	0.6	2.7	0	2	0.4	2.4
109	108	Qda2	SS-W	0	104.3	0	42	0	43.5	0	18.8	0	62.3
				0	3.3	0	3	0	3.6	0	3.1	0	3.5
110	81	Qda2	SS-W	n/a	n/a	n/a	n/a	49	62.4	0	24	49	86.4
								4.1	5.2	0	4	2.7	4.8
111	87	Qda2	SS-W	n/a	n/a	n/a	n/a	34	74	5.5	25.2	39.5	99.2
								2.8	6.2	0.9	4.2	2.2	5.5
112	102	Qda2	SS-W	54.1	160.6	27.6	68.6	26.5	60	0	32	26.5	92
				1.7	5	2	4.9	2.2	5	0	5.3	1.5	5.1
113	84	Qda2	SS-W	n/a	n/a	n/a	n/a	33	58	9	23.5	42	81.5
								2.8	4.8	1.5	3.9	2.3	4.5
				32yr.	4 m/yr		4.2 m/yr		4.4 m/yr		4.2 m/yr	18yr.	4.3 m/yr
114	92	Qda1	SS-W	32.8	162.2	14	65.2	13.8	64	5	33	18.8	97
				1	5.1	1	4.7	1.2	5.3	0.8	5.5	1	5.4
115	89	Qda1	SS-W	n/a	n/a	n/a	n/a	18	48	12	26	30	74
								1.5	4	2	4.3	1.7	4.1
116	115	Qda1	SS-W	66.5	176	37	76	21.5	68	8	32	29.5	100
				2.1	5.5	2.6	5.4	1.8	5.7	1.3	5.3	1.6	5.6
117	88	Qda1	SS-W	n/a	n/a	n/a	n/a	n/a	n/a	n/a	n/a	n/a	n/a
118	90	Qda1	SS-W	n/a	n/a	n/a	n/a	n/a	n/a	n/a	n/a	n/a	n/a
				32yr.	5.3 m/yr		5.1 m/yr		5 m/yr		5 m/yr	18yr.	5 m/yr
119	76	Qda5b	SS-W	7.5	84.8	7.5	42	0	26.8	0	14	0	42.8
				0.2	2.7	0.5	3	0	2.2	0	2.3	0	2.4
120	73	Qda5b	SS-W	6	77	6	57.5	0	17.5	0	2	0	19.5
				0.2	2.4	0.4	4.1	0	1.5	0	0.3	0	1.1
				32yr.	2.6 m/yr		3.6 m/yr		1.9 m/yr		1.3 m/yr	18yr.	1.8 m/yr
121	106	Qda2	SS-C	24	88	20	45	4	30	0	13	4	43
				0.8	2.8	1.4	3.2	0.3	2.5	0	2.2	0.2	2.4
122	85	Qda2	SS-C	36	102.8	27	58	9	31	0	13.8	9	44.8
				1.1	3.2	1.9	4.1	0.8	2.6	0	2.3	0.5	2.5
123	88	Qda2	SS-C	34	95.4	18	54	16	30	0	11.4	16	41.4
				1.1	3	1.3	3.9	1.3	2.5	0	1.9	0.9	2.3
124	83	Qda2	SS-C	46.4	178.2	30	100	16.4	53	0	25.2	16.4	78.2
				1.5	5.6	2.1	7.1	1.4	4.4	0	4.2	0.9	4.3
125	102	Qda2	SS-C	20.6	84.5	11	42	9.6	28.5	0	14	9.6	42.5
				0.6	2.6	0.8	3	0.8	2.4	0	2.3	0.5	2.4
126	85	Qda2	SS-C	18.7	74.4	18.7	32	0	29	0	13.4	0	42.4
				0.6	2.3	1.3	2.3	0	2.4	0	2.2	0	2.4
127	83	Qda2	SS-C	11	76.8	11	36.2	0	27	0	13.6	0	40.6
				0.3	2.4	0.8	2.6	0	2.3	0	2.3	0	2.3
				32yr.	3.1 m/yr		3.7 m/yr		2.7 m/yr		2.5 m/yr	18yr.	2.7 m/yr
128	95	Qda4	SS-C	9.8	111.5	9.8	53	0	40	0	18.5	0	58.5
				0.3	3.5	0.7	3.8	0	3.3	0	3.1	0	3.3
129	105	Qda4	SS-C	13.7	110.8	13.7	41.8	0	41	0	28	0	69
				0.4	3.5	1	3	0	3.4	0	4.7	0	3.8
				32yr.	3.5 m/yr		3.4 m/yr		3.4 m/yr		3.9 m/yr	18yr.	3.6 m/yr
130	104	Qda2b	SS-C	5.7	65	5.7	34	0	21	0	10	0	31
				0.2	2	0.4	2.4	0	1.8	0	1.7	0	1.7
131	90	Qda2b	SS-C	n/a	n/a	n/a	n/a	16	40	0	18.5	16	58.5
								1.3	3.3	0	3.1	0.9	3.3
132	115	Qda2b	SS-C	14.5	103	9.5	48	5	39	0	16	5	55
				0.5	3.2	0.7	3.4	0.4	3.3	0	2.7	0.3	3.1
				32yr.	2.6 m/yr		2.9 m/yr		2.8 m/yr		2.5 m/yr	18yr.	2.7 m/yr

**APPENDIX A:**  
**SHEET 6**

#	Azim.	Unit	Section	1980 to 2012 min (m)	max (m)	1980 to 1994 min (m)	max (m)	1994 to 2006 min (m)	max (m)	2006-12 min (m)	max (m)	94-2012 min (m)	max (m)	
133	102	Qda5b	SS	n/a	n/a	n/a	n/a	n/a	n/a	n/a	n/a	n/a	n/a	
134	72	Qda5b	SS	0	52	0	24	0	19	0	9	0	28	
135	83	Qda5b	SS	0	1.6	0	1.7	0	1.6	0	1.5	0	1.6	
136	88	Qda5b	SS	0	25	0	18	0	7	0	0	0	7	
137	80	Qda5b	SS	0	0.8	0	1.3	0	0.6	0	0	0	0.4	
138	86	Qda5b	SS	0.6	1.3	1.3	2.1	0	0.8	0	0.8	0	0.8	
139	90	Qda5b	SS	18.4	42.9	18.4	29.4	0	9	0	4.5	0	13.5	
				1.3	1.3	2.1	0	0.8	0	0.8	0	0	0.8	
				32yr.	1.6 m/yr		1.9 m/yr		1.6 m/yr		1.1 m/yr		18yr.	1.5 m/yr
140	84	Qda1	SS-E	48.4	98.8	32	50	16.4	35	0	13.8	16.4	48.8	
				1.5	3.1	2.3	3.6	1.4	2.9	0	2.3	0.9	2.7	
141	81	Qda1	SS-E	41.6	121	27	56	14.6	44	0	21	14.6	65	
				1.3	3.8	1.9	4	1.2	3.7	0	3.5	0.8	3.6	
142	86	Qda1	SS-E	9	129	9	78	0	36	0	15	0	51	
				0.3	4	0.6	5.6	0	3	0	2.5	0	2.8	
143	79	Qda1	SS-E	30	135.5	15	70.5	15	44	0	21	15	59	
				0.9	4.2	1.1	5	1.3	3.7	0	3.5	0.8	3.3	
144	81	Qda1	SS-E	n/a	n/a	n/a	n/a	n/a	n/a	n/a	n/a	n/a	n/a	
145	75	Qda1	SS-E	51	94.5	32	48	19	36.5	0	10	19	46.5	
				1.6	3	2.3	3.4	1.6	3	0	1.7	1.1	2.6	
146	81	Qda1	SS-E	50.4	129.2	28	67.2	22.4	44	0	18	22.4	62	
				1.6	4	2	4.8	1.9	3.7	0	3	1.2	3.4	
147	76	Qda1	SS-E	n/a	n/a	n/a	n/a	10	36	0	16	10	52	
								0.8	3	0	2.7	0.6	2.9	
148	73	Qda1	SS-E	n/a	n/a	n/a	n/a	15.5	57	8	23	23.5	80	
								1.3	4.8	1.3	3.8	1.3	4.4	
149	87	Qda1	SS-E	34	98.2	24	52	10	29.8	0	16.4	10	46.2	
				1.1	3.1	1.7	3.7	0.8	2.5	0	2.7	0.6	2.6	
150	90	Qda1	SS-E	25.7	116	19	60	6.7	43	0	13	6.7	56	
				0.8	3.6	1.4	4.3	0.6	3.6	0	2.2	0.4	3.1	
151	87	Qda1	SS-E	n/a	n/a	n/a	n/a	n/a	n/a	n/a	n/a	n/a	n/a	
152	85	Qda1	SS-E	n/a	n/a	n/a	n/a	n/a	n/a	n/a	n/a	n/a	n/a	
				32yr.	3.6 m/yr		4.3 m/yr		3.4 m/yr		2.8 m/yr		18yr.	3.1 m/yr
153	130	Qda7	SS	n/a	n/a	n/a	n/a	5.2	31.5	4	27.8	9.2	59.3	
								0.4	2.6	0.7	4.6	0.5	3.3	
154	70	Qda7	SS	n/a	n/a	n/a	n/a	16.6	38	0	18.6	16.6	56.6	
								1.4	3.2	0	3.1	0.9	3.1	
155	85	Qda7	SS	n/a	n/a	n/a	n/a	36	53.8	0	16.5	36	70.3	
								3	4.5	0	2.8	2	3.9	
156	125	Qda7	SS	n/a	n/a	n/a	n/a	4.5	63.3	1.8	31.4	6.3	94.7	
								0.4	5.3	0.3	5.2	0.4	5.3	
157	73	Qda7	SS	95.4	171	70	107	25.4	44.5	0	19.5	44.5	64	
				3	5.3	5	7.6	2.1	3.7	0	3.3	2.5	3.6	
158	101	Qda7	SS	62	159.8	62	104.8	0	36.8	0	18.2	0	55	
				1.9	5	4.4	7.5	0	3.1	0	3	0	3.1	
159	64	Qda7	SS	n/a	n/a	n/a	n/a	2.5	52.5	0	31.7	2.5	84.2	
								0.2	4.4	0	5.3	0.1	4.7	
160	76	Qda7	SS	28.2	134.5	13	88.5	7.2	21	8	25	15.2	46	
				0.9	4.2	0.9	6.3	0.6	1.8	1.3	4.2	0.8	2.6	
				32yr.	4.8 m/yr		7.1 m/yr		3.6 m/yr		3.9 m/yr		18yr.	3.7 m/yr
161	108	Qda2b	BRH	27.5	113.5	15.5	54.5	12	40.5	0	18.5	12	59	
				0.9	3.5	1.1	3.9	1	3.4	0	3.1	0.7	3.3	
162	89	Qda2b	BRH	5	109	5	49	0	40	0	20	0	60	
				0.2	3.4	0.4	3.5	0	3.3	0	3.3	0	3.3	
				32yr.	3.5 m/yr		3.7 m/yr		3.4 m/yr		3.2 m/yr		18yr.	3.3 m/yr
163	60	Qda1	BRH	n/a	n/a	n/a	n/a	n/a	n/a	n/a	n/a	n/a	n/a	
164	72	Qda3	BRH	n/a	n/a	n/a	n/a	0	40	0	7.5	0	47.5	
								0	3.3	0	1.3	0	2.6	
165	102	Qda4	PV-W	14.8	66.9	14.8	36	0	21.5	0	9.4	0	30.6	
				0.5	2.1	1.1	2.6	0	1.8	0	1.6	0	1.7	
166	106	Qda4	PV-W	n/a	n/a	n/a	n/a	18.7	54.5	9.8	22.8	28.5	77.3	
								1.6	4.5	1.6	3.8	1.6	4.3	
167	90	Qda4	PV-W	n/a	n/a	n/a	n/a	7.5	40.6	0	20	7.5	60.6	
								0.6	3.4	0	3.3	0.4	3.4	
168	57	Qda4	PV-W	n/a	n/a	n/a	n/a	0	11	0	0	0	11	
								0	0.9	0	0	0	0.6	
				32yr.	2.1 m/yr		2.6 m/yr		2.7 m/yr		2.2 m/yr		18yr.	2.5 m/yr
169	87	Qda9	BRH	n/a	n/a	n/a	n/a	0	32.2	0	9	0	41.2	
								0	2.7	0	1.5	0	2.3	
170	88	Qda9	BRH	n/a	n/a	n/a	n/a	n/a	n/a	n/a	n/a	n/a	n/a	
171	90	Qda4	BRH	n/a	n/a	n/a	n/a	n/a	n/a	n/a	n/a	n/a	n/a	
172	90	Qda4	ATV	n/a	n/a	n/a	n/a	5	25.2	7.8	20.5	12.8	45.7	
								0.4	2.1	1.3	3.4	0.7	2.5	
173	60	Qda4	ATV	n/a	n/a	n/a	n/a	24.8	40	12.7	24.2	37.5	64.2	
								2.1	3.3	2.1	4	2.1	3.6	
174	54	Qda4	ATV	n/a	n/a	n/a	n/a	26.3	47	11	27.3	37.3	74.3	
								0	4.1	0	3.2	0	3.8	
175	90	Qda4	ATV	0	185.1	0	89.3	0	57.8	0	38	0	95.8	
				0	5.8	0	6.4	0	4.8	0	6.3	0	5.3	
176	50	Qda4	ATV	n/a	n/a	n/a	n/a	0	49.2	0	19.4	0	60.6	
								0	4.1	0	3.2	0	3.8	
177	35	Qda4	ATV	12.3	105.7	12.3	40.4	0	42	0	23.3	0	65.3	
				0.4	3.3	0.9	2.9	0	3.5	0	3.9	0	3.6	
178	87	Qda4	ATV	n/a	n/a	n/a	n/a	0	41.5	0	25.2	0	66.7	
								0	3.5	0	4.2	0	3.7	
				32yr.	4.6 m/yr		4.7 m/yr		3.6 m/yr		4.2 m/yr		18yr.	3.8 m/yr

**APPENDIX A:**  
**SHEET 7**

#	Azim.	Unit	Section	1980 to 2012		1980 to 1994		1994 to 2006		2006-12		94-2012	
				min (m)	max (m)	m/yr	m/yr	min (m)	max (m)	m/yr	m/yr	min (m)	max (m)
179	86	Qda8	BRH	n/a	n/a	n/a	n/a	0	20.6	0	5	0	25.6
								0	1.7	0	0.8	0	1.4
180	43	Qda8	BRH	n/a	n/a	n/a	n/a	n/a	n/a	n/a	n/a	n/a	n/a
181	68	Qda8	BRH	n/a	n/a	n/a	n/a	n/a	n/a	n/a	n/a	n/a	n/a
182	81	Qda4	PV	n/a	n/a	n/a	n/a	6.6	21.6	0	7.2	6.6	28.8
								0.6	1.8	0	1.2	0.4	1.6
183	83	Qda4	PV	43.8	138.1	38.8	100	5	25.3	0	12.8	5	38.1
				1.4	4.3	2.8	7.1	0.4	2.1	0	2.1	0.3	2.1
184	88	Qda4	PV	15	80.1	10	46.3	5	21.8	0	12	5	33.8
				0.5	2.5	0.7	3.3	0.4	1.8	0	2	0.3	1.9
185	76	Qda4	PV	22.9	80.1	17.4	47.3	5.5	21.4	0	11.4	5.5	32.8
				0.7	2.5	1.2	3.4	0.5	1.8	0	1.9	0.3	1.8
186	74	Qda4	PV	15.5	79.8	15.5	47.8	0	25	0	7	0	32
				0.5	2.5	1.1	3.4	0	2.1	0	1.2	0	1.8
187	78	Qda4	PV	n/a	n/a	n/a	n/a	6.4	28	0	12	6.4	40
								0.5	2.3	0	2	0.4	2.2
188	81	Qda4	PV	17.2	141.7	11.5	88.2	5.7	38	0	15.5	5.7	53.5
				0.5	4.4	0.8	6.3	0.5	3.2	0	2.6	0.3	3
189	83	Qda4	PV	24.8	116.4	17.4	47.7	7.4	51.3	0	17.4	7.4	68.7
				0.8	3.6	1.2	3.4	0.6	4.3	0	2.9	0.4	3.8
190	75	Qda4	PV	n/a	n/a	n/a	n/a	0	32.2	0	16	0	48.2
								0	2.7	0	2.7	0	2.7
191	84	Qda4	PV	11	60.3	11	33.3	0	20.6	0	6.4	0	27
				0.3	1.9	0.8	2.4	0	1.7	0	1.1	0	1.5
192	90	Qda4	PV	21.5	129.2	21.5	70	0	36.2	0	23	0	59.2
				0.7	4	5	0	3	0	3.8	0	3.3	
193	83	Qda4	PV	6.4	82.9	6.4	52	0	15.3	0	15.6	0	30.9
				0.2	2.6	0.5	3.7	0	1.3	0	2.6	0	1.7
194	82	Qda4	PV	9	60	3.5	26	5.5	24.5	0	9.5	5.5	34
				0.3	1.9	0.3	1.9	0.5	2	0	1.6	0.3	1.9
195	84	Qda4	PV	27.2	107.1	18.2	41.3	9	48.8	0	17	9	65.8
				0.9	3.3	1.3	3	0.8	4.1	0	2.8	0.5	3.7
196	82	Qda4	PV	11.6	84.5	7.4	41	4.2	29.7	0	13.8	4.2	43.5
				0.4	2.6	0.5	2.9	0.4	2.5	0	2.3	0.2	2.4
197	76	Qda4	PV	17.3	44.5	12.7	22	4.6	15	0	7.5	4.6	22.5
				0.5	1.4	0.9	1.6	0.4	1.3	0	1.3	0.3	1.3
198	90	Qda4	PV	13.1	98.1	4.4	40	8.7	37.9	0	20.2	8.7	58.1
				0.4	3.1	0.3	2.9	0.7	3.2	0	3.4	0.5	3.2
199	81	Qda4	PV	14	120.8	14	46.7	0	38.6	0	35.5	0	74.1
				0.4	3.8	1	3.3	0	3.2	0	5.9	0	4.1
				32yr.	3 m/yr		3.6 m/yr	2.5 m/yr	2.4 m/yr	18yr.	2.4 m/yr		

200	73	Qda5b	PV	34	121.2	7.5	36	19	60	7.5	25.2	26.5	85.2
				1.1	3.8	0.5	2.6	1.6	5	1.3	4.2	1.5	4.7
201	81	Qda5b	PV	17.9	113.4	7	46	5.6	50	5.3	17.4	10.9	67.4
				0.6	3.5	0.5	3.3	0.5	4.2	0.9	2.9	0.6	3.7
202	75	Qda5b	PV	11.2	187.3	5.2	72.5	6	78	0	36.8	6	114.8
				0.4	5.9	0.4	5.2	0.5	6.5	0	6.1	0.3	6.4
203	82	Qda5b	PV	38	143.9	31	82	7	32.5	0	29.4	7	61.9
				1.2	4.5	2.2	5.9	0.6	2.7	0	4.9	0.4	3.4
				32yr.	4.4 m/yr		4.3 m/yr	4.6 m/yr	4.5 m/yr	18yr.	4.6 m/yr		

204	45	Qda1	PV-FI	57.5	182	41.5	85	16	66	0	31	16	97
				1.8	5.7	3	6.1	1.3	5.5	0	5.2	0.9	5.4
205	115	Qda1	PV-FI	32.8	169.5	0	60	32.8	76.5	0	33	32.8	109.5
				1	5.3	0	4.3	2.7	6.4	0	5.5	1.8	6.1
206	120	Qda1	PV-FI	42.7	191.2	0	84	29.7	64	13	43.2	42.7	107.2
				1.3	6	0	6	2.5	5.3	2.2	7.2	2.4	6
207	90	Qda1	PV-FI	n/a	n/a	n/a	n/a	n/a	n/a	n/a	n/a	n/a	no measurement #207
				32yr.	5.7 m/yr		5.5 m/yr	5.7 m/yr	6 m/yr	18yr.	5.8 m/yr		

208	100	Qda2b	PV-FI	n/a	n/a	n/a	n/a	18.3	45	6	26	24.3	71
								1.5	3.8	1	4.3	1.4	3.9
209	77	Qda2b	PV-FI	n/a	n/a	n/a	n/a	16.2	54.5	4.5	21.3	20.7	75.8
								1.4	4.5	0.8	3.6	1.2	4.2
								4.2 m/yr	4 m/yr	18yr.	4.1 m/yr		

210	76	Qda3	PV-FI	n/a	n/a	n/a	n/a	0	53.3	0	30	0	83.3
								0	4.4	0	5	0	4.6
211	79	Qda3	PV-FI	n/a	n/a	n/a	n/a	0	13	0	16.6	0	29.6
								0	1.1	0	2.8	0	1.6
212	82	Qda3	PV-FI	n/a	n/a	n/a	n/a	0	41.5	0	23	0	64.5
								0	3.5	0	3.8	0	3.6
								3 m/yr	3.9 m/yr	18yr.	3.3 m/yr		

**APPENDIX B: Sample logs**

APPENDIX B Sheet 1 SUMMARY WDC sample log																	
Proj. - sample - site	Sample Date	Waypt. Figure #	Coordinates	Lahontan sub-basin WDC study site	Sample location Location description	Classification Folk & Ward	Mean ( $\mu$ ) ( $\phi$ )	Sort. ( $\mu$ ) ( $\phi$ )	Skew. ( $\mu$ ) ( $\phi$ )	Kurt. ( $\mu$ ) ( $\phi$ )	Grain Size Parameters	% Silt: %Clay % Silt + Clay	= max. Height (m)	Length (m)	Width (m)	L/W Class. Spacing $\lambda$ (m)	
WDC-001-PV-01	3/4/11	117	11 N 0440600 Map 7A	4548547	Paradise Valley, ATV Park	center of brink on active Complex Crescentic dune	Fine sand unimodal	199.8 2.323	1.529 0.613	-0.023 0.023	0.970 0.970	Symmetrical, Mesokurtic Moderately Well Sorted	1.2 : 0.0 1.2	4.6 Brink	197 350	0.563 Hemicyclic	174
WDC-002-PV-02	3/4/11	118	11 N 0440627 Map 7A	4548652	Paradise Valley, ATV Park	center of brink on active Complex Crescentic dune	Medium sand unimodal	252.3 1.987	1.674 0.743	-0.029 0.029	0.972 0.972	Symmetrical, Mesokurtic Moderately Sorted	1.6 : 0.0 1.6	7.6 Brink	197 350	0.563 Hemicyclic	212
WDC-003-PV-03	3/4/11	119	11 N 0440633 Map 7A	4548689	Paradise Valley, ATV Park	center of brink on active Complex Crescentic dune	Fine sand unimodal	235.3 2.088	1.509 0.593	-0.029 0.029	0.969 0.969	Symmetrical, Mesokurtic Moderately Well Sorted	1.3 : 0.0 1.3	9.4 Brink	197 350	0.563 Hemicyclic	241
WDC-004-PV-04	3/4/11	120	11 N 0440319 Map 7A	4548785	Paradise Valley, ATV Park	center of crest SW arm active Complex Crescentic dune	Fine sand unimodal	223.7 2.160	1.501 0.585	-0.024 0.024	0.964 0.964	Symmetrical, Mesokurtic Moderately Well Sorted	1.2 : 0.0 1.2	5.5 Crest	112 145	0.772 Hemicyclic	disturbed
WDC-005-PV-05	3/4/11	121	11 N 0440378 Map 7A	4548579	Paradise Valley, ATV Park	center of crest on active Barchanobolic dune	Fine sand unimodal	232.3 2.106	1.509 0.593	-0.025 0.025	0.967 0.967	Symmetrical, Mesokurtic Moderately Well Sorted	1.1 : 0.0 1.1	6.7 Crest	718 339	2.1 Lobate	175
WDC-006-PV-06	3/4/11	122	11 N 0440735 Map 7A	4549084	Paradise Valley, ATV Park	center of brink NE arm active Complex Crescentic dune	Fine sand unimodal	222.9 2.165	1.485 0.570	-0.026 0.026	0.953 0.953	Symmetrical, Mesokurtic Moderately Well Sorted	0.7 : 0.0 0.7	5.4 Brink	disturbed disturbed	disturbed	disturbed
WDC-007-PV-07	3/4/11	123	11 N 0440700 Map 7A	4548970	Paradise Valley, ATV Park	center of brink NE arm active Complex Crescentic dune	Fine sand unimodal	240.4 2.056	1.487 0.573	-0.036 0.036	0.959 0.959	Symmetrical, Mesokurtic Moderately Well Sorted	1.4 : 0.0 1.4	7.2 Brink	disturbed disturbed	disturbed	disturbed
WDC-008-PV-08	3/4/11	124	11 N 0440571 Map 7A	4549053	Paradise Valley, ATV Park	center of crest NE arm active Complex Crescentic dune	Medium sand unimodal	262.0 1.932	1.498 0.583	-0.046 0.046	0.963 0.963	Symmetrical, Mesokurtic Moderately Well Sorted	1.5 : 0.0 1.5	8.8 Crest	144 260	0.554 Hemicyclic	252
Paradise Valley Complex Crescentic dunes pv-01→08						Fine sand with sparse ATV Park avg.	Mean ( $\phi$ )	Sort. ( $\phi$ )	Skew. ( $\phi$ )	Kurt. ( $\phi$ )	Symmetrical, Mesokurtic Moderately Well Sorted sparse Moderate Sorting	1.25 : 0.00 1.25	range 4.6 - 9.4	151 268	0.592 Hemicyclic	211	
WDC-088-PV-33	8/24/11	236	11 N 0443165 Map 7D	4552285	Paradise Valley, South of Feed lot	center of brink on active Compound Barchan dune	Fine sand unimodal	210.3 2.249	1.463 0.549	-0.056 0.056	1.005 1.005	Symmetrical, Mesokurtic Moderately Well Sorted	2.9 : 0.0 2.9	3.7 Brink	49 95	0.516 Hemicyclic	162
WDC-089-PV-34	8/24/11	237	11 N 0443787 Map 7D	4552314	Paradise Valley, South of Feed lot	center of brink on active Complex Crescentic dune	Fine sand unimodal	158.2 2.660	1.482 0.567	-0.041 0.041	1.000 1.000	Symmetrical, Mesokurtic Moderately Well Sorted	2.8 : 0.0 2.8	10.7 Brink	68 85	0.800 Hemicyclic	77
WDC-090-PV-35	8/24/11	238	11 N 0446127 Map 7D	4551873	Paradise Valley, South of Feed lot	center of brink on active Barchanobolic dune	Fine sand unimodal	191.8 2.383	1.469 0.554	-0.052 0.052	0.994 0.994	Symmetrical, Mesokurtic Moderately Well Sorted	2.7 : 0.0 2.7	12.2 - 15.2 Brink	966 184	5.3 Elongate	865
WDC-091-PV-36	8/24/11	239	11 N 0445216 Map 7D	4551840	Paradise Valley, South of Feed lot	center of brink on active Compound Barchan-B bolic dune	Fine Sand unimodal	225.2 2.151	1.583 0.662	-0.038 0.038	0.978 0.978	Symmetrical, Mesokurtic Moderately Well Sorted	2.2 : 0.0 2.2	7.6 - 9.1 Brink	230 205	1.122 Lobate	2030
WDC-092-PV-37	8/24/11	241	11 N 0443411 Map 7D	4552388	Paradise Valley, South of Feed lot	center of brink on active Barchan dune	Fine sand unimodal	176.5 2.502	1.442 0.528	-0.035 0.035	0.980 0.980	Symmetrical, Mesokurtic Moderately Well Sorted	1.9 : 0.0 1.9	6.1 - 7.6 Brink	70 107	0.654 Hemicyclic	125
WDC-036-SS-01	5/30/11	166	11 N 0430760 Map 6	4552633	Silver State Valley, Eastern Complex	center of brink on active Barchanoidal ridge	Medium sand unimodal	251.6 1.991	1.627 0.702	-0.046 0.046	0.934 0.934	Symmetrical, Mesokurtic Moderately Sorted	0.0 : 0.0 0.0	6.1 - 12.2 Brink	96 191	0.503 Hemicyclic	100
WDC-037-SS-02	5/30/11	167	11 N 0430900 Map 6	4552323	Silver State Valley, Eastern Complex	center of brink on active Barchanoidal ridge	Medium sand unimodal	250.9 1.995	1.546 0.629	-0.043 0.043	0.932 0.932	Symmetrical, Mesokurtic Moderately Well Sorted	0.0 : 0.0 0.0	6.1 - 14 Brink	84 96	0.875 Hemicyclic	143
WDC-038-SS-03	5/30/11	168	11 N 0430916 Map 6	4551643	Silver State Valley, Eastern Complex	center of brink on active Barchanoidal ridge	Medium sand unimodal	251.9 1.989	1.471 0.557	-0.026 0.026	0.939 0.939	Symmetrical, Mesokurtic Moderately Well Sorted	0.0 : 0.0 0.0	18.3 Brink	75 180	0.417 Hemicyclic	130
WDC-093-SS-23	8/25/11	242	11 N 0431486 Map 6	4550917	Silver State Valley, Eastern Complex	center of brink on active Barchanoidal ridge	Medium sand unimodal	307.7 1.701	1.549 0.631	-0.043 0.043	0.936 0.936	Symmetrical, Mesokurtic Moderately Well Sorted	0.0 : 0.0 0.0	16.7 Brink	90 190	0.474 Hemicyclic	112
WDC-094-SS-24	8/25/11	243	11 N 0431764 Map 6	4550391	Silver State Valley, Eastern Complex	center of brink on active Barchanoidal ridge	Medium sand unimodal	305.5 1.711	1.478 0.564	-0.030 0.030	0.944 0.944	Symmetrical, Mesokurtic Moderately Well Sorted	0.0 : 0.0 0.0	13.7 - 15.2 Brink	82 410	0.200 Lunate	88
WDC-095-SS-25	8/25/11	245	11 N 0432342 Map 6	4549849	Silver State Valley, Eastern Complex	center of brink on active Barchanoidal ridge	Medium sand unimodal	326.1 1.617	1.415 0.501	-0.007 0.007	0.954 0.954	Symmetrical, Mesokurtic Moderately Well Sorted	0.0 : 0.0 0.0	24.4 Brink	62 235	0.264 Lunate	112
WDC-096-SS-26	8/25/11	246	11 N 0431119 Map 6	4550070	Silver State Valley, Eastern Complex	center of brink on active Barchanoidal ridge	Medium sand unimodal	279.5 1.839	1.504 0.589	-0.024 0.024	0.942 0.942	Symmetrical, Mesokurtic Moderately Well Sorted	0.0 : 0.0 0.0	18.3 Brink	66 112	0.589 Hemicyclic	91
Silver State Valley Barchanoidal ridges SS-01→03, SS-23→26						Medium sand	Mean ( $\phi$ )	Sort. ( $\phi$ )	Skew. ( $\phi$ )	Kurt. ( $\phi$ )	Symmetrical, Mesokurtic Moderately Well Sorted sparse Moderate Sorting	0.0 : 0.0 0.0	range 6.1 - 24.4	79 202	0.475 Hemicyclic	111	
WDC-039-SS-04	5/30/11	169	11 N 0429409 Map 6	4551074	Silver State Valley, Central dune field	center of brink on active Compound Barchan dune	Medium sand unimodal	250.3 1.998	1.492 0.577	-0.036 0.036	0.945 0.945	Symmetrical, Mesokurtic Moderately Well Sorted	0.0 : 0.0 0.0	24.4 Brink	132 291	0.454 Hemicyclic	227
WDC-040-SS-05	5/30/11	170	11 N 0428602 Map 6	4550856	Silver State Valley, Central dune field	center of brink on active Barchan dune	Medium sand unimodal	258.3 1.953	1.554 0.636	-0.051 0.051	0.940 0.940	Symmetrical, Mesokurtic Moderately Well Sorted	0.0 : 0.0 0.0	9.1 - 15.2 Brink	112 260	0.431 Hemicyclic	258
WDC-041-SS-06	5/30/11	171	11 N 0428814 Map 6	4551534	Silver State Valley, Central dune field	center of brink on active Barchan dune	Fine sand unimodal	226.8 2.140	1.495 0.580	-0.026 0.026	0.941 0.941	Symmetrical, Mesokurtic Moderately Well Sorted	0.0 : 0.0 0.0	9.1 - 15.2 Brink	100 170	0.588 Hemicyclic	212
Silver State Valley Barchan dunes SS-04→06						Medium sand with some Fine sand	Mean ( $\phi$ )	Sort. ( $\phi$ )	Skew. ( $\phi$ )	Kurt. ( $\phi$ )	Symmetrical, Mesokurtic Moderately Well Sorted	0.0 : 0.0 0.0	range 9.1 - 24.4	115 240	0.491 Hemicyclic	232	

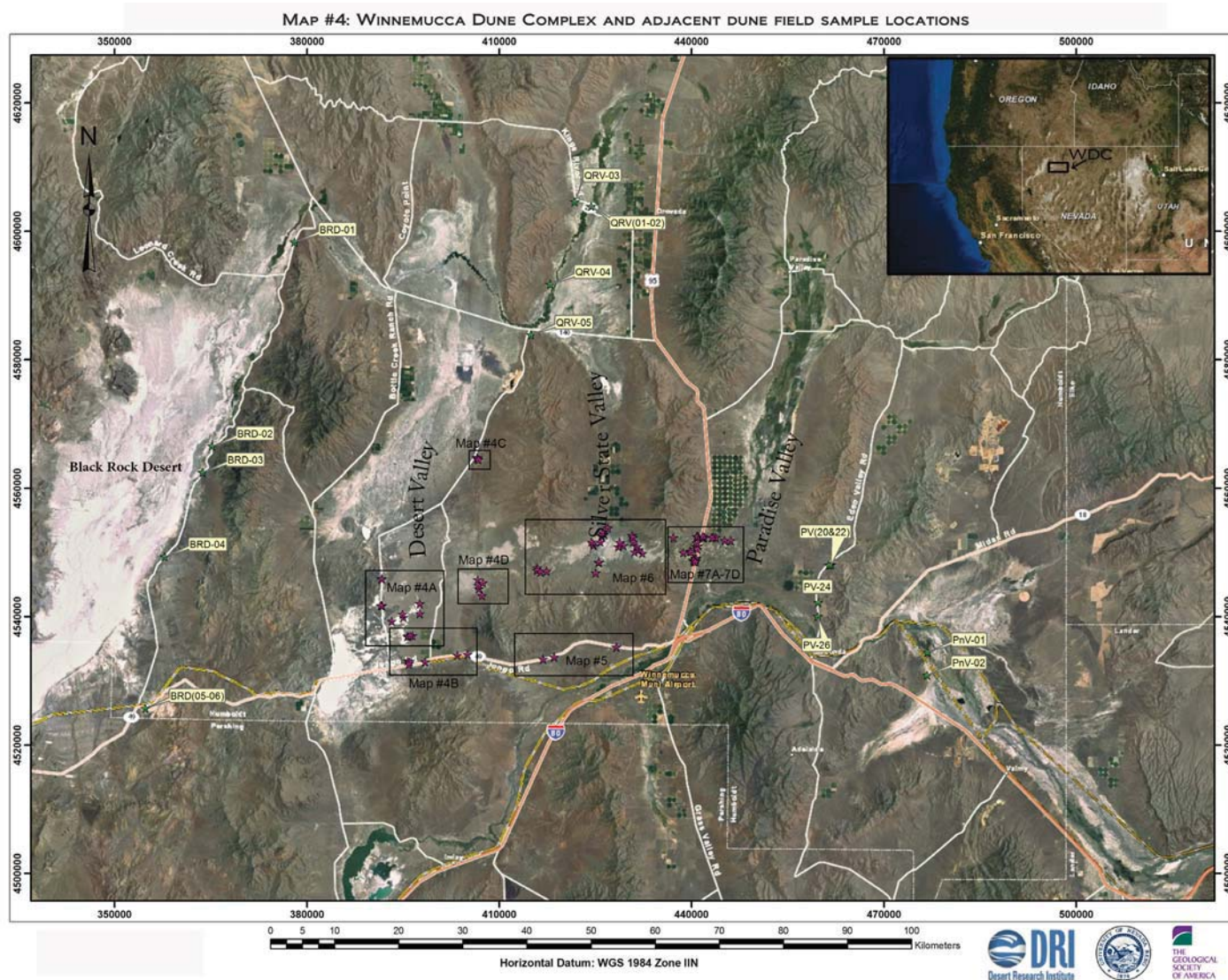
APPENDIX B Sheet 2			SUMMARY		WDC sample log												
Proj. - sample - site	Sample Date	Waypt. Figure #	Coordinates WGS 1984 11 N	Lahontan sub-basin WDC study site	Sample location Location description	Classification Folk & Ward	Mean ( $\mu$ ) ( $\phi$ )	Sort. ( $\mu$ ) ( $\phi$ )	Skew. ( $\mu$ ) ( $\phi$ )	Kurt. ( $\mu$ ) ( $\phi$ )	Grain Size Parameters	% Silt: %Clay	= max. % Silt + Clay	Length (m) Height (m)	Width (m)	L/W Class.	Spacing $\lambda$ (m)
WDC-078-SS-19	8/11/11	224 Map 6	11 N 0424401 4551616	Silver State Valley, Western dune field	center of brink on active Barchanoidal ridge	Fine sand unimodal	194.5 2.362	1.479 0.565	-0.007 0.007	0.938 0.938	Symmetrical, Mesokurtic Moderately Well Sorted	0.0 : 0.0 0.0	10.7 - 12.2 Brink	75 106	0.708 Hemicyclic	101	
WDC-079-SS-20	8/11/11	225 Map 6	11 N 0424664 4551345	Silver State Valley, Western dune field	center of brink on active Complex Crescentric dune	Fine sand unimodal	219.5 2.188	1.570 0.651	-0.009 0.009	0.928 0.928	Symmetrical, Mesokurtic Moderately Well Sorted	0.0 : 0.0 0.0	7.6 - 9.1 Brink	48 103	0.466 Hemicyclic	225	
				Silver State Valley	Complex Crescentric ridges	Fine sand	<i>Mean (<math>\phi</math>)</i>	<i>Sort. (<math>\phi</math>)</i>	<i>Skew. (<math>\phi</math>)</i>	<i>Kurt. (<math>\phi</math>)</i>	Symmetrical, Mesokurtic Moderately Well Sorted	0.0 : 0.0 0.0	range 7.6 - 12.2	62 105	0.587 Hemicyclic	163	
WDC-102-DV-25	9/9/11	255 Map 4D	11 N 0407476 4545223	Desert Valley, NE of Power Plant	center of brink on active Barchan dune	Fine Sand unimodal	231.4 2.111	1.563 0.644	-0.057 0.057	0.970 0.970	Symmetrical, Mesokurtic Moderately Well Sorted	1.7 : 0.0 1.7	7.6 - 10.7 Brink	70 127	0.551 Hemicyclic	133	
WDC-103-DV-26	9/9/11	256 Map 4D	11 N 0406675 4545765	Desert Valley, NE of Power Plant	center of brink on active Complex Crescentric dune	Fine Sand unimodal	244.0 2.035	1.592 0.670	-0.042 0.042	0.935 0.935	Symmetrical, Mesokurtic Moderately Well Sorted	0.0 : 0.0 0.0	15.2 - 16.8 Brink	115 210	0.548 Hemicyclic	235	
				Desert Valley	Complex Crescentric ridges	Fine sand	<i>Mean (<math>\phi</math>)</i>	<i>Sort. (<math>\phi</math>)</i>	<i>Skew. (<math>\phi</math>)</i>	<i>Kurt. (<math>\phi</math>)</i>	Symmetrical, Mesokurtic Moderately Well Sorted	0.85 : 0.00 0.85	range 7.6 - 16.8	93 169	0.550 Hemicyclic	184	
WDC-104-DV-27	9/9/11	257 Map 4D	11 N 0406784 4544834	Desert Valley, NE of Power Plant	center of brink on active Compound Barchan dune	Medium sand unimodal	281.0 1.831	1.523 0.607	-0.031 0.031	0.933 0.933	Symmetrical, Mesokurtic Moderately Well Sorted	0.0 : 0.0 0.0	4.6 - 6.1 Brink	98 110	0.891 Hemicyclic	196	
WDC-105-DV-28	9/9/11	258 Map 4D	11 N 0406863 4544359	Desert Valley, NE of Power Plant	center of brink on active Compound Barchan dune	Medium sand unimodal	336.1 1.573	1.435 0.521	-0.005 0.005	0.944 0.944	Symmetrical, Mesokurtic Moderately Well Sorted	0.0 : 0.0 0.0	13.7 - 15.2 Brink	80 95	0.842 Hemicyclic	146	
				Desert Valley	Compound Barchan dunes	Medium sand	<i>Mean (<math>\phi</math>)</i>	<i>Sort. (<math>\phi</math>)</i>	<i>Skew. (<math>\phi</math>)</i>	<i>Kurt. (<math>\phi</math>)</i>	Symmetrical, Mesokurtic Moderately Well Sorted	0.0 : 0.0 0.0	range 4.6 - 15.2	89 103	0.867 Hemicyclic	171	
WDC-067-SS-14	7/7/11	207 Map 6	11 N 0426407 4552818	Silver State Valley, Western Complex	Peak active Star dune	Fine Sand unimodal	154.6 2.694	1.492 0.577	0.014 -0.014	0.947 0.947	Symmetrical, Mesokurtic Moderately Well Sorted	0.4 : 0.0 0.4	7.6 - 9.1 Peak	d = 44	n/a	100	
WDC-068-SS-15	7/7/11	208 Map 6	11 N 0426014 4552513	Silver State Valley, Western Complex	Peak active Star dune	Fine Sand unimodal	190.5 2.392	1.477 0.563	-0.002 0.002	0.936 0.936	Symmetrical, Mesokurtic Moderately Well Sorted	0.0 : 0.0 0.0	13.7 - 15.2 Peak	d = 85	n/a	118	
WDC-070-SS-17	7/7/11	210 Map 6	11 N 0426202 4553041	Silver State Valley, Western Complex	Peak active Star dune	Fine Sand unimodal	177.0 2.498	1.490 0.575	0.004 -0.004	0.943 0.943	Symmetrical, Mesokurtic Moderately Well Sorted	0.0 : 0.0 0.0	6.1 - 7.6 Peak	d = 40	n/a	114	
WDC-080-SS-21	8/11/11	226 Map 6	11 N 0424741 4551060	Silver State Valley, Western dune field	Peak active Star dune	Fine sand unimodal	200.7 2.317	1.476 0.561	-0.012 0.012	0.935 0.935	Symmetrical, Mesokurtic Moderately Well Sorted	0.0 : 0.0 0.0	10.7 - 12.2 Peak	d = 100	n/a	157	
				Silver State Valley	Star dunes	Fine sand	<i>Mean (<math>\phi</math>)</i>	<i>Sort. (<math>\phi</math>)</i>	<i>Skew. (<math>\phi</math>)</i>	<i>Kurt. (<math>\phi</math>)</i>	Symmetrical, Mesokurtic Moderately Well Sorted	0.1 : 0.0 0.1	range 6.1 - 15.2	diameter 67	n/a	122	
WDC-061-SS-09	6/27/11	201 Map 6	11 N 0425532 4548480	Silver State Valley, NE Barretts Spring	crest of tail on active Simple Parabolic dune	Medium sand unimodal	278.8 1.843	1.413 0.498	-0.013 0.013	0.947 0.947	Symmetrical, Mesokurtic Well Sorted	0.0 : 0.0 0.0	4.6 - 7.6 Crest	754 206	3.7 Elongate	834	
WDC-060-SS-08	6/27/11	200 Map 6	11 N 0425553 4548376	Silver State Valley, NE Barretts Spring	crest of nose on active Simple Parabolic dune	Fine Sand unimodal	246.4 2.021	1.460 0.546	-0.015 0.015	0.935 0.935	Symmetrical, Mesokurtic Moderately Well Sorted	0.0 : 0.0 0.0	7.6 - 9.2 Crest	754 206	3.7 Elongate	831	
				Silver State Valley	Simple Parabolic dunes	Medium sand and Fine sand	<i>Mean (<math>\phi</math>)</i>	<i>Sort. (<math>\phi</math>)</i>	<i>Skew. (<math>\phi</math>)</i>	<i>Kurt. (<math>\phi</math>)</i>	Symmetrical, Mesokurtic Moderately Well Sorted to Well Sorted	0.0 : 0.0 0.0	range 4.6 - 9.2	754 206	3.7 Elongate	833	
WDC-065-SS-13	7/6/11	205 Map 6	11 N 0417406 4547077	Silver State Valley, East slope Slumbering Hills	crest of nose on active Compound Parabolic dune	Fine Sand unimodal	224.0 2.158	1.593 0.672	-0.054 0.054	0.993 0.993	Symmetrical, Mesokurtic Moderately Well Sorted	2.8 : 0.0 2.8	1.8 - 3.7 Crest	3210 268	12 Elongate	2650	
WDC-073-PV-28	7/8/11	214 Map 7B	11 N 0438705 4549945	Paradise Valley, North ATV-Sand Pass rd.	center of brink on active Barchanoblic dune	Medium sand unimodal	267.5 1.902	1.495 0.580	0.000 0.000	0.943 0.943	Symmetrical, Mesokurtic Moderately Well Sorted	0.0 : 0.0 0.0	13.7 - 16.8 Brink	455 261	1.7 Lobate	471	
WDC-074-PV-29	7/8/11	216 Map 7B	11 N 0439780 4550147	Paradise Valley, North ATV-Sand Pass rd.	center of brink on active Barchanoblic dune	Medium sand unimodal	252.2 1.988	1.507 0.592	-0.031 0.031	0.955 0.955	Symmetrical, Mesokurtic Moderately Well Sorted	0.9 : 0.0 0.9	10.7 - 13.7 Brink	940 478	1.97 Lobate	872	
WDC-076-PV-31	7/8/11	218 Map 7B	11 N 0440921 4550480	Paradise Valley, North ATV-Sand Pass rd.	crest of nose on active Barchanoblic dune	Fine Sand unimodal	235.4 2.087	1.550 0.632	-0.037 0.037	0.939 0.939	Symmetrical, Mesokurtic Moderately Well Sorted	0.6 : 0.0 0.6	7.6 - 10.7 Crest	1546 403	3.8 Elongate	1255	
				Paradise Valley	Barchanoblic dunes	Medium sand with some Fine sand	<i>Mean (<math>\phi</math>)</i>	<i>Sort. (<math>\phi</math>)</i>	<i>Skew. (<math>\phi</math>)</i>	<i>Kurt. (<math>\phi</math>)</i>	Symmetrical, Mesokurtic Moderately Well Sorted	0.5 : 0.0 0.5	range 7.6 - 16.8	980 417	2.4 Lobate	866	

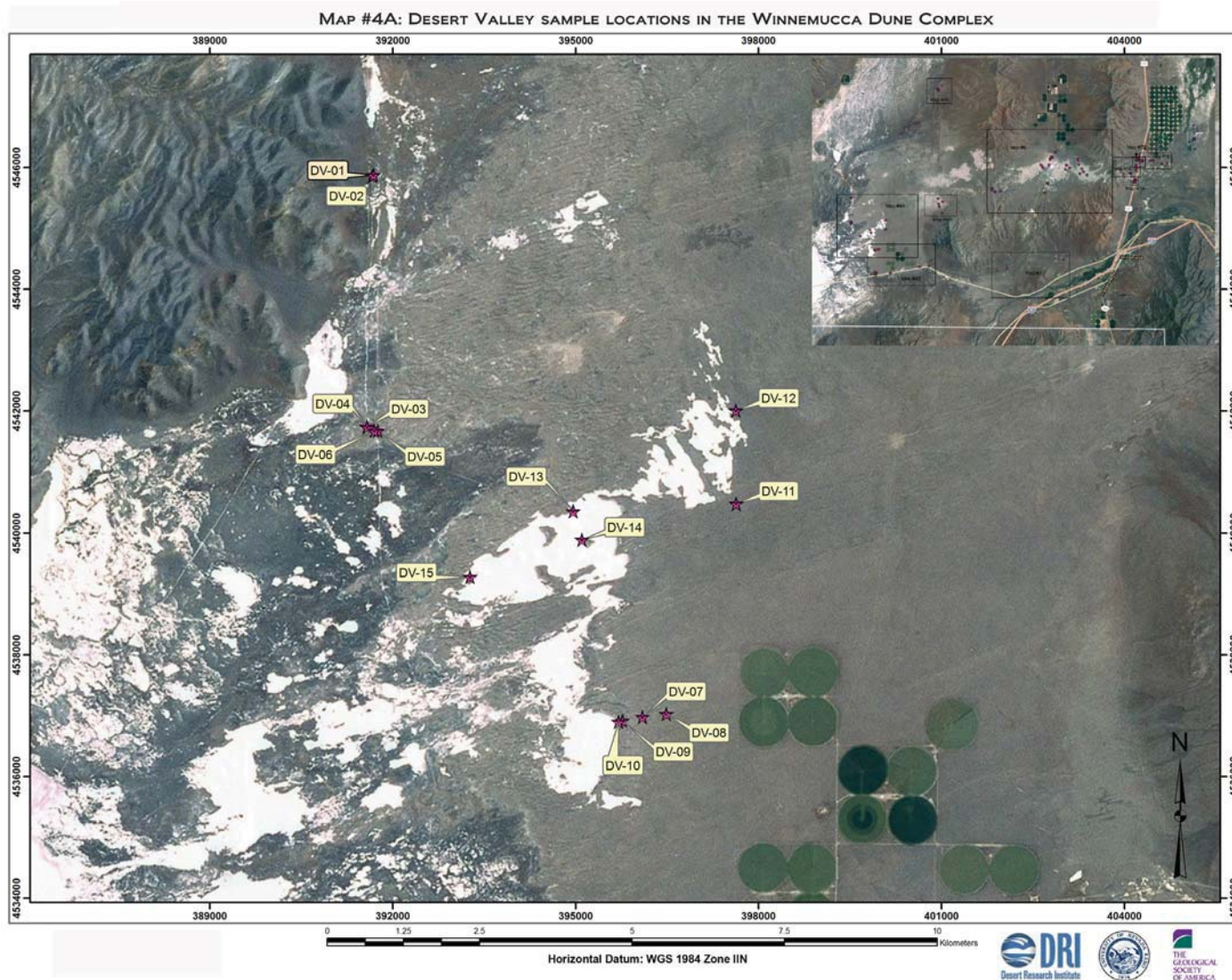


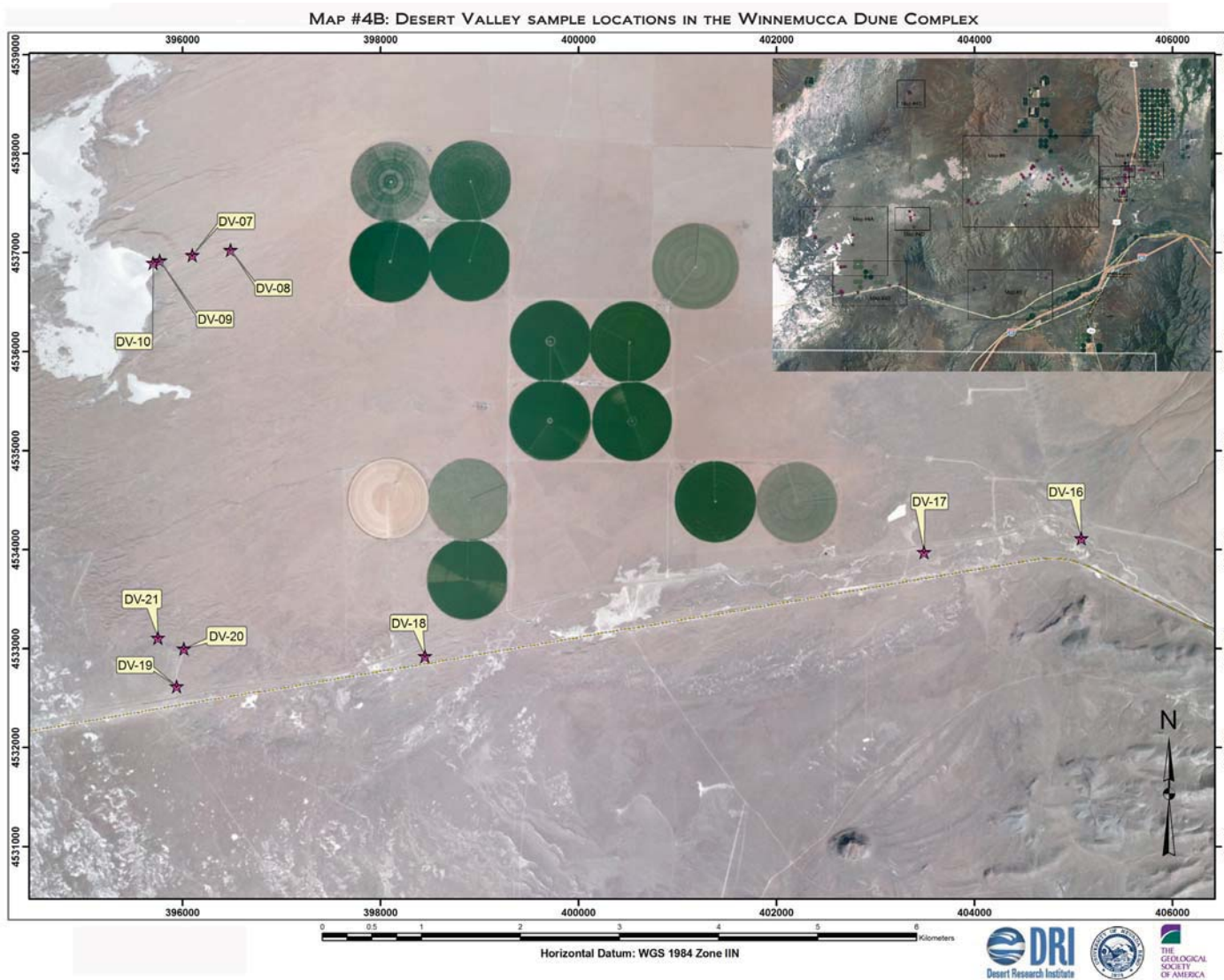
APPENDIX B Sheet 4 SUMMARY WDC sample log															
Proj. - sample - site	Sample Date	Waypt. Figure #	Coordinates WGS 1984 11 N	Lahontan sub-basin WDC study site	Sample location Location description	Classification Folk & Ward	Mean ( $\mu$ ) ( $\phi$ )	Sort. ( $\mu$ ) ( $\phi$ )	Skew. ( $\mu$ ) ( $\phi$ )	Kurt. ( $\mu$ ) ( $\phi$ )	Grain Size Parameters	% Silt: %Clay % Silt + Clay	= max. range Height (m)	Length (m) Width (m)	L/W Class. Spacing λ (m)
WDC-062-SS-10	7/6/11	202 Map 6	11 N 0415990 4547577	Silver State Valley, East slope Slumbering Hills	crest of tail on semi-active Compound Parabolic dune	Fine Sand unimodal	243.6 2.058	1.546 0.628	-0.056 0.056	0.976 0.976	Symmetrical, Mesokurtic Moderately Well Sorted	2.0 : 0.0 2.0	2.4 175	2007 Elongate	11.5 972
WDC-064-SS-12	7/6/11	204 Map 6	11 N 0416466 4546940	Silver State Valley, East slope Slumbering Hills	crest of nose on semi-active Compound Parabolic dune	Fine Sand unimodal	212.7 2.233	1.542 0.625	-0.061 0.063	0.981 0.981	Symmetrical, Mesokurtic Moderately Well Sorted	2.3 : 0.0 2.3	5.4 190	1372 Elongate	7.2 1350
				Silver State Valley 55-10, SS-12	semi-active Compound Parabolic dunes East slope Slumbering Hills avg.	Fine Sand	Mean ( $\phi$ ) 2.136	Sort. ( $\phi$ ) 0.672	Skew. ( $\phi$ ) 0.060	Kurt. ( $\phi$ ) 0.979	Symmetrical, Mesokurtic Moderately Well Sorted	2.1 : 0.0 2.1	range 2.4 - 5.4	1690 183	9.4 Elongate
WDC-075-PV-30	7/8/11	217 Map 7B	11 N 0439942 4550094	Paradise Valley, North ATV-Sand Pass rd.	crest of tail on semi-active Parabolic dune	Medium sand unimodal	251.6 1.991	1.602 0.680	-0.039 0.039	0.961 0.961	Symmetrical, Mesokurtic Moderately Well Sorted	1.7 : 0.0 1.7	3.2 Crest	745 78	9.6 Elongate
WDC-063-SS-11	7/6/11	203 Map 4	11 N 0415920 4547219	Silver State Valley, 55-DV pass	crest of tail on stable Parabolic dune	Fine Sand unimodal	206.3 2.277	1.643 0.716	-0.079 0.079	0.987 0.987	Symmetrical, Mesokurtic Moderately Sorted	2.7 : 0.0 2.7	1.8 Crest	1332 85	15.7 Elongate
WDC-072-PV-27	7/7/11	213 Map 7B	11 N 0431758 4552260	Paradise Valley, South-East below Sand Pass	crest of tail on stable Parabolic dune	Fine Sand unimodal	132.3 2.918	1.517 0.601	-0.068 0.068	1.005 1.005	Symmetrical, Mesokurtic Moderately Well Sorted	4.9 : 0.1 5.0	1.2 Crest	1575 105	15.0 Elongate
WDC-022-PV-22	4/23/11	137 Map 5	11 N 0461756 4548112	Paradise Valley, West of Osgood Mts	crest of nose on stable Parabolic dune	Fine sand unimodal	211.0 2.245	1.841 0.881	-0.118 0.118	1.037 1.037	Fine Skewed, Mesokurtic Moderately Sorted	4.7 : 0.0 4.7	3.0 - 4.3 Crest	451 168	2.7 Labate
WDC-066-RP-03	7/6/11	206 Map 4	11 N 0428326 4535224	North Humboldt sink, Southwest of Racetrack	crest of tail on Vegetated Braided Linear dune	Fine Sand unimodal	209.7 2.254	2.084 1.060	0.126 -0.126	0.989 0.989	Coarse Skewed, Mesokurtic Poorly Sorted	3.7 : 0.0 3.7	3.7 Crest	1610 47	34.3 Braided Linear
WDC-106-DV-29	9/9/11	259 Map 4D	11 N 0407355 4543286	Desert Valley, NE of Power Plant	crest of tail on Vegetated Linear dune	Fine Sand unimodal	196.2 2.349	1.792 0.841	-0.073 0.073	1.039 1.039	Symmetrical, Mesokurtic Moderately Sorted	4.5 : 0.0 4.5	2.4 - 3.7 Crest	6300 48	131 Linear
WDC-029-QRV-03	5/11/11	155 Map 3	11 N 0421792 4604621	Quinn River Valley, W-side Riverside rd.	center of crest on semi-active Transverse dune	Medium sand unimodal	250.8 1.995	1.808 0.855	-0.085 0.085	0.954 0.954	Symmetrical, Mesokurtic Moderately Sorted	2.0 : 0.0 2.0	3.7 - 4.9 Crest	134 38	3.5 Transverse
WDC-030-QRV-04	5/11/11	156 Map 3	11 N 0417977 4591760	Quinn River Valley, W-side Riverside rd.	center of crest on semi-active Transverse dune	Fine sand unimodal	246.5 2.020	1.524 0.607	-0.075 0.075	1.001 1.000	Symmetrical, Mesokurtic Moderately Well Sorted	3.1 : 0.0 3.1	2.4 - 3.7 Crest	204 37	5.5 Transverse
WDC-032-BRD-01	5/12/11	160 Map 3	11 N 0378094 4598331	Black Rock Desert, W-side of Jackson Range	center of crest on semi-active Transverse dune	Fine sand unimodal	239.2 2.064	1.539 0.622	-0.045 0.045	0.980 0.980	Symmetrical, Mesokurtic Moderately Well Sorted	2.2 : 0.0 2.2	2.4 - 4.3 Crest	151 22	6.7 Transverse
WDC-044-RP-01	6/16/11	176 Map 5	11 N 0418575 4533718	North Humboldt sink, South of Ten Mile Hills	blow-out on crest of stable Transverse dune	Fine Sand unimodal	205.3 2.284	1.648 0.721	-0.083 0.083	1.035 1.035	Symmetrical, Mesokurtic Moderately Sorted	3.9 : 0.1 4.0	3.0 Crest	360 38	9.5 Transverse
WDC-045-RP-02	6/16/11	177 Map 5	11 N 0416841 4533373	North Humboldt sink, South of Ten Mile Hills	blow-out on crest of stable Transverse dune	Fine Sand unimodal	218.5 2.194	1.583 0.663	-0.067 0.067	0.988 0.988	Symmetrical, Mesokurtic Moderately Well Sorted	2.5 : 0.0 0.0	4.0 Crest	366 30	12.2 Transverse
WDC-031-QRV-05	5/11/11	159 Map 3	11 N 0414982 4538378	QR crossing QRV to DV SW above Gallagher Flat	center of crest on stable Transverse dune	Fine sand unimodal	176.1 2.506	1.525 0.609	-0.046 0.046	0.977 0.977	Symmetrical, Mesokurtic Moderately Well Sorted	2.4 : 0.0 2.4	3.0 - 4.3 Crest	128 25	5.1 Transverse
WDC-084-DV-18	8/12/11	231 Map 4B	11 N 0398452 4532922	Desert Valley, South of Delong Farms	center of crest on stable Transverse dune	Fine sand unimodal	202.1 2.307	1.619 0.695	-0.053 0.053	0.966 0.966	Symmetrical, Mesokurtic Moderately Well Sorted	2.1 : 0.0 2.1	4.6 - 7.6 Crest	406 34	12.0 Transverse
WDC-099-DV-22	9/8/11	251 Map 4C	11 N 0406791 4564414	Desert Valley, Gabica Butte	center of crest on stable Transverse dune	Fine sand unimodal	193.4 2.370	1.620 0.696	-0.074 0.074	0.978 0.978	Symmetrical, Mesokurtic Moderately Well Sorted	2.8 : 0.0 2.8	2.4 - 3.7 Crest	356 24	14.8 Transverse
WDC-101-DV-24	9/8/11	254 Map 4C	11 N 0406561 4564743	Desert Valley, Gabica Butte	center of crest on stable Transverse dune	Fine sand unimodal	198.5 2.333	1.554 0.636	-0.052 0.052	0.969 0.969	Symmetrical, Mesokurtic Moderately Well Sorted	1.9 : 0.0 1.9	1.8 - 2.4 Crest	353 26	13.6 Transverse
WDC-035-BRD-04	5/12/11	164 Map 3	11 N 0357832 4549324	Black Rock Desert, W-side of Jackson Range	center of crest on stable Transverse dune	Fine sand unimodal	226.6 2.142	1.642 0.716	-0.041 0.041	0.969 0.969	Symmetrical, Mesokurtic Moderately Well Sorted	2.0 : 0.0 2.0	2.4 - 4.3 Crest	173 34	5.1 Transverse
WDC-034-BRD-03	5/12/11	162 Map 3	11 N 0363743 4562470	Black Rock Desert, W-side of Jackson Range	center of crest on stable Transverse dune	Fine sand unimodal	203.1 2.300	2.476 1.308	0.043 -0.043	0.971 0.971	Symmetrical, Mesokurtic Poorly Sorted	8.9 : 0.2 9.1	3.0 - 5.5 Crest	107 36	3.0 Transverse
WDC-082-DV-16	8/12/11	229 Map 4B	11 N 0405081 4534114	Desert Valley, South of Delong Farms	center of crest on stable Beach barrier?	Fine Sand unimodal	229.9 2.121	1.633 0.708	-0.085 0.085	0.988 0.988	Symmetrical, Mesokurtic Moderately Sorted	2.6 : 0.0 2.6	2.4 Crest	n/a n/a	n/a ?
WDC-024-PV-24	4/23/11	138 Map 3	11 N 0459805 4542185	Paradise Valley, SW of Osgood Mts	center of crest on stable Undifferentiated dune	Fine sand unimodal	242.1 2.047	1.667 0.737	-0.127 0.127	1.047 1.047	Fine Skewed, Mesokurtic Moderately Sorted	3.3 : 0.0 3.3	1.2 - 1.8 Crest	n/a n/a	n/a Undiff.
WDC-026-PV-26	4/23/11	140 Map 3	11 N 0459711 4540019	Paradise Valley, SW of Osgood Mts	center of crest on stable Undifferentiated dune	Medium sand unimodal	276.1 1.857	1.870 0.903	-0.222 0.222	1.283 1.283	Fine Skewed, Leptokurtic Moderately Sorted	5.1 : 0.0 5.1	1.8 - 2.4 Crest	n/a n/a	n/a Undiff.
WDC-071-SS-18	7/7/11	212 Map 6	11 N 0426928 4553801	Silver State Valley, N of Western Complex	center of crest on stable Undifferentiated dune	Fine Sand unimodal	154.6 2.693	1.478 0.563	-0.021 0.021	0.949 0.949	Symmetrical, Mesokurtic Moderately Well Sorted	1.3 : 0.0 1.3	2.7 Crest	n/a n/a	n/a Undiff.
WDC-086-BRD-05	8/12/11	233 Map 3	11 N 0354803 4525735	Black Rock Desert, Northwest of Hycroft Mine	center of crest on Undifferentiated dune	Fine Sand unimodal	232.1 2.107	2.212 1.145	-0.074 0.074	0.907 0.907	Symmetrical, Mesokurtic Poorly Sorted	5.4 : 0.4 5.8	2.1 Crest	n/a n/a	n/a Undiff.
WDC-107-PnV-01	1/19/12	260 Map 3	11 N 0476811 4534451	Pumpernickel Valley, SE of Iron Point	center of crest on semi-active Undifferentiated dune	Fine Sand unimodal	155.6 2.684	1.896 0.923	0.073 -0.073	1.112 1.112	Symmetrical, Leptokurtic Moderately Sorted	6.3 : 0.3 6.6	2.5 Crest	n/a n/a	n/a Undiff.
WDC-108-PnV-02	1/19/12	261 Map 3	11 N 0476791 4530892	Pumpernickel Valley, SE of Iron Point	center of crest on semi-active Undifferentiated dune	Fine Sand unimodal	137.2 2.866	1.677 0.746	0.009 -0.009	0.992 0.992	Symmetrical, Mesokurtic Moderately Sorted	6.3 : 0.0 6.3	4.1 Crest	n/a n/a	n/a Undiff.

APPENDIX B Sheet 5			SUMMARY		WDC sample log												
Proj. - sample - site	Sample Date	Waypt. Figure #	Coordinates WGS 1984 11 N	Lahontan sub-basin WDC study site	Sample location Location description	Classification Folk & Ward	Mean ( $\mu$ ) ( $\phi$ )	Sort. ( $\mu$ ) ( $\phi$ )	Skew. ( $\mu$ ) ( $\phi$ )	Kurt. ( $\mu$ ) ( $\phi$ )	Grain Size Parameters	% Silt: %Clay % Silt + Clay	= max. Height (m)	Length (m) Width (m)	L/W Class.	Spacing $\lambda$ (m)	
WDC-042-DV-01	6/12/11	173 Map 4A	11 N 0391685 4545873	Desert Valley, East of Jungo Hills	crest of semi-active Lunette dune, blue sand	Fine Silty Fine Sand unimodal	183.8 2.444	3.741 1.903	-0.277 0.277	1.704 1.704	Fine Skewed, Very Leptokurtic Poorly Sorted	12.7 : 2.7 15.4	1-2 Crest	n/a n/a	n/a Lunette	n/a	
WDC-043-DV-02	6/12/11	174 Map 4A	11 N 0391669 4545853	Desert Valley, East of Jungo Hills	crest of active Lunette dune, blue sand	Fine Sand unimodal	212.5 2.234	2.193 1.133	-0.035 0.035	1.048 1.048	Symmetrical, Mesokurtic Poorly Sorted	5.8 : 0.7 6.5	1-2 Crest	n/a n/a	n/a Lunette	n/a	
				Desert Valley DV-01→DV-02	semi-active Lunette dune East of Jungo Hills avg.	Fine Silty Fine Sand	Mean ( $\phi$ ) 2.339	Sort. ( $\phi$ ) 1.518	Skew. ( $\phi$ ) 0.156	Kurt. ( $\phi$ ) 1.376		9.3 : 1.7 11.0	range 1-2	n/a n/a	n/a Lunette	n/a	
WDC-052-DV-09	6/26/11	192 Map 4A, 4B	11 N 0395773 4536919	Desert Valley Playa Complex, West of DeLong Farms	Stoss side, beach wash, active Lunette dune	Fine Sand unimodal	168.9 2.566	1.741 0.800	-0.007 0.007	0.996 0.996	Symmetrical, Mesokurtic Moderately Sorted	4.0 : 0.0 4.0	3.2 - 4.8 Crest	n/a n/a	n/a Lunette	n/a	
WDC-033-BRD-02	5/12/11	161 Map 3	11 N 0365233 4566558	Black Rock Desert, W-side of Jackson Range	center of crest on Lunette dune	Fine sand unimodal	202.5 2.304	1.576 0.656	-0.073 0.073	1.031 1.031	Symmetrical, Mesokurtic Moderately Well Sorted	3.6 : 0.1 3.7	3.0 - 5.5 Crest	n/a n/a	n/a Lunette	n/a	
WDC-083-DV-17	8/12/11	230 Map 4B	11 N 0403492 4533974	Desert Valley, South of DeLong Farms	center of crest on Lunette dune	Fine sand unimodal	239.4 2.062	1.657 0.729	-0.083 0.083	1.003 1.003	Symmetrical, Mesokurtic Moderately Sorted	2.9 : 0.0 2.9	2.4 - 4.3 Crest	n/a n/a	n/a Lunette	n/a	
WDC-046-DV-03 <i>TUFA</i>	6/17/11	179 Map 4A	11 N 0391583 4541742	Desert Valley tufa site, Southeast of Jungo Hills	base of exposure Dune or Lake bed deposit	Fine Sand unimodal	165.6 2.594	1.570 0.650	-0.088 0.088	1.034 1.034	Symmetrical, Mesokurtic Moderately Well Sorted	4.0 : 0.1 4.1	n/a n/a	n/a Palustrine	n/a Palustrine	n/a	
WDC-049-DV-06	6/17/11	182 Map 4A	11 N 0391703 4541671	Desert Valley tufa site, Southeast of Jungo Hills	Blow-out Lakebed	Fine Sand unimodal	168.5 2.569	1.498 0.583	-0.008 0.008	0.948 0.948	Symmetrical, Mesokurtic Moderately Well Sorted	0.6 : 0.0 0.6	n/a n/a	n/a Palustrine	n/a Palustrine	n/a	
WDC-081-S5-22	8/11/11	227 Map 6	11 N 0425815 4551603	Silver State Valley, Western Complex	outcrop Lakebed	Fine Sand unimodal	155.8 2.682	1.764 0.819	0.011 -0.011	1.025 1.025	Symmetrical, Mesokurtic Moderately Sorted	5.5 : 0.0 5.5	n/a n/a	n/a Palustrine	n/a Palustrine	n/a	
WDC-053-DV-10	6/26/11	193 Map 4A, 4B	11 N 0395705 4536895	Desert Valley Playa Complex, West of DeLong Farms	1' above playa Dune island-active Lunette exposure	V.F. Silty Fine Sand unimodal	76.23 3.714	5.517 2.464	-0.611 0.611	2.009	Very Fine Skewed, Very Leptokurtic Very Poorly Sorted	16.4 : 6.5 22.9	n/a n/a	n/a Palustrine	n/a Palustrine	n/a	
WDC-056-DV-13	6/27/11	196 Map 4A	11 N 0394962 4540355	Desert Valley Playa Complex, West of DeLong Farms	1.5' above playa Dune island	Coarse Silty Fine Sand bimodal	75.33 3.731	4.368 2.127	-0.475 0.475	1.065 1.065	Very Fine Skewed, Mesokurtic Very Poorly Sorted	30.2 : 3.9 34.1	n/a n/a	n/a Palustrine	n/a Palustrine	n/a	
WDC-057-DV-14	6/27/11	197 Map 4A	11 N 0395104 4539888	Desert Valley Playa Complex, West of DeLong Farms	4' above playa Dune island	Coarse Silty Fine Sand unimodal	144.6 2.790	2.429 1.280	-0.354 0.354	1.949 1.949	Very Fine Skewed, Very Leptokurtic Poorly Sorted	12.4 : 1.3 13.7	n/a n/a	n/a Palustrine	n/a Palustrine	n/a	
WDC-058-DV-15	6/27/11	198 Map 4A	11 N 0393270 4539278	Desert Valley Playa Complex, West of DeLong Farms	0.5' above playa Dune island	Very Fine Sand unimodal	122.2 3.032	3.285 1.716	-0.446 0.446	2.054 2.054	Very Fine Skewed, Very Leptokurtic Poorly Sorted	14.9 : 3.6 18.5	n/a n/a	n/a Palustrine	n/a Palustrine	n/a	
WDC-055-DV-12	6/27/11	195 Map 4A	11 N 0397632 4542003	Desert Valley Playa Complex, West of DeLong Farms	Back beach, foreberm area active Lunette	Medium sand unimodal	260.3 1.942	2.179 1.124	-0.299 0.299	1.418 1.418	Fine Skewed, Leptokurtic Poorly Sorted	6.0 : 1.2 7.2	n/a n/a	n/a Palustrine	n/a Palustrine	n/a	
WDC-069-S5-16	7/7/11	209 Map 4B	11 N 0426018 4552703	Silver State Valley, Western dune field	Intradune area Lakebed	Coarse Silty Fine Sand bimodal	49.38 4.340	5.029 2.330	-0.355 0.355	0.863 0.863	Very Fine Skewed, Platykurtic Very Poorly Sorted	43.6 : 5.0 48.6	n/a n/a	n/a Palustrine	n/a Palustrine	n/a	
WDC-085-DV-19	8/12/11	232 Map 4B	11 N 0395942 4532619	Desert Valley, South of DeLong Farms	outcrop Sandy beach deposit	Very Fine Sand unimodal	122.5 3.030	2.174 1.121	-0.313 0.313	1.492 1.492	Very Fine Skewed, Leptokurtic Poorly Sorted	15.0 : 1.0 16.0	n/a n/a	n/a Palustrine	n/a Palustrine	n/a	
WDC-097-DV-20	8/26/11	248 Map 4B	11 N 0396016 4532999	Desert Valley, Southwest of DeLong Farms	outcrop Sandy beach deposit	Fine Sand unimodal	199.8 2.323	1.632 0.706	-0.113 0.113	1.020 1.020	Fine Skewed, Mesokurtic Moderately Sorted	3.4 : 0.0 3.4	n/a n/a	n/a Palustrine	n/a Palustrine	n/a	
WDC-098-DV-21	8/26/11	250 Map 4B	11 N 0395755 4533108	Desert Valley, Southwest of DeLong Farms	outcrop Sandy beach deposit	Fine Sand unimodal	192.2 2.379	1.610 0.687	-0.114 0.114	1.052 1.052	Fine Skewed, Mesokurtic Moderately Well Sorted	4.3 : 0.0 4.3	n/a n/a	n/a Palustrine	n/a Palustrine	n/a	
				Desert Valley DV-19→DV-21	Sandy beach deposit Southwest of DeLong Farms avg.	Fine Sand	Mean ( $\phi$ ) 2.577	Sort. ( $\phi$ ) 0.838	Skew. ( $\phi$ ) 0.180	Kurt. ( $\phi$ ) 1.188	V.F.-Fine Skewed, Lepto-Mesokurtic Poorly to Moderately Well Sorted	7.6 : 0.4 8.0	range n/a	n/a n/a	n/a Palustrine	n/a	
WDC-087-BRD-06	8/12/11	234 Map 3	11 N 0354798 4525788	Black Rock Desert, Northwest of Hycroft Mine	ephemeral riverbank Sandy lake terrace	V.C. Silty Fine Sand unimodal	161.0 2.635	2.875 1.524	-0.401 0.401	1.553 1.553	Very Fine Skewed, Very Leptokurtic Poorly Sorted	16.2 : 0.6 16.8	n/a n/a	n/a Fluvial	n/a n/a	n/a	
WDC-100-DV-23 <i>SNAILS</i>	9/8/11	252 Map 4C	11 N 0406696 4564569	Desert Valley, Gabica Butte	surface to 6" Sehoo shoreline	Fine Sand unimodal	173.5 2.527	1.694 0.760	-0.070 0.070	0.999 0.999	Symmetrical, Mesokurtic Moderately Sorted	4.1 : 0.2 4.3	n/a n/a	n/a n/a	n/a Palustrine	n/a n/a	

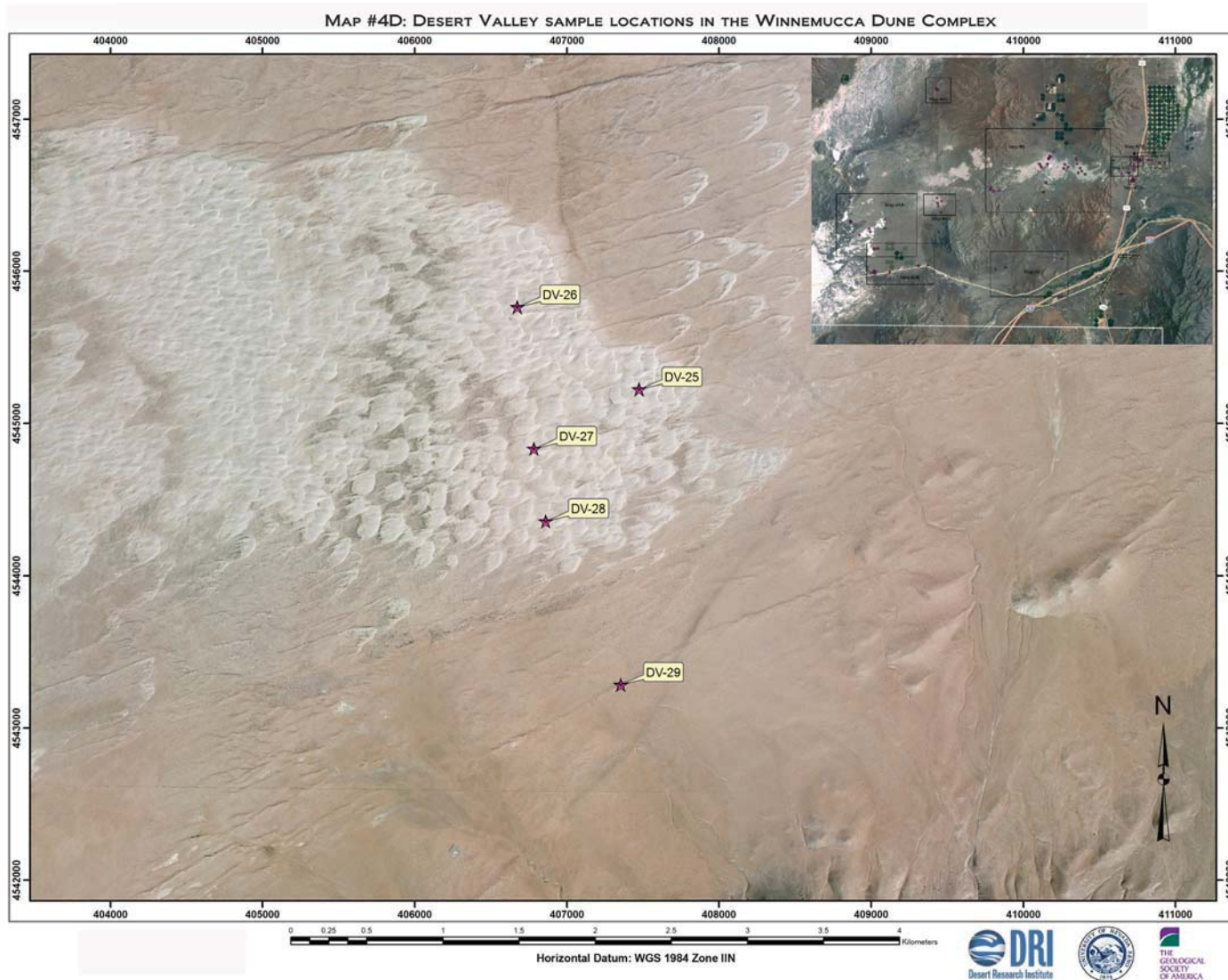
**APPENDIX C: Sample location maps**

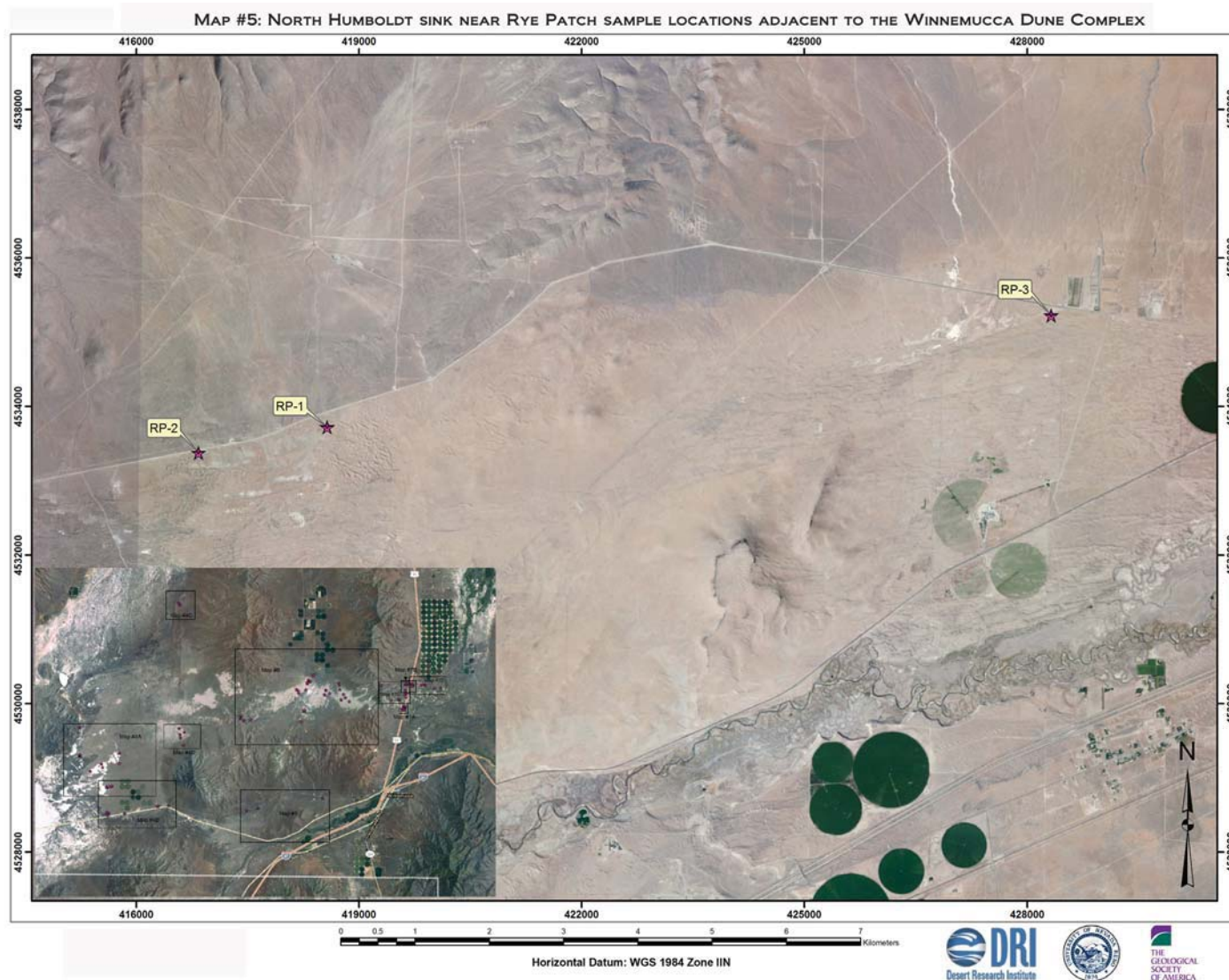


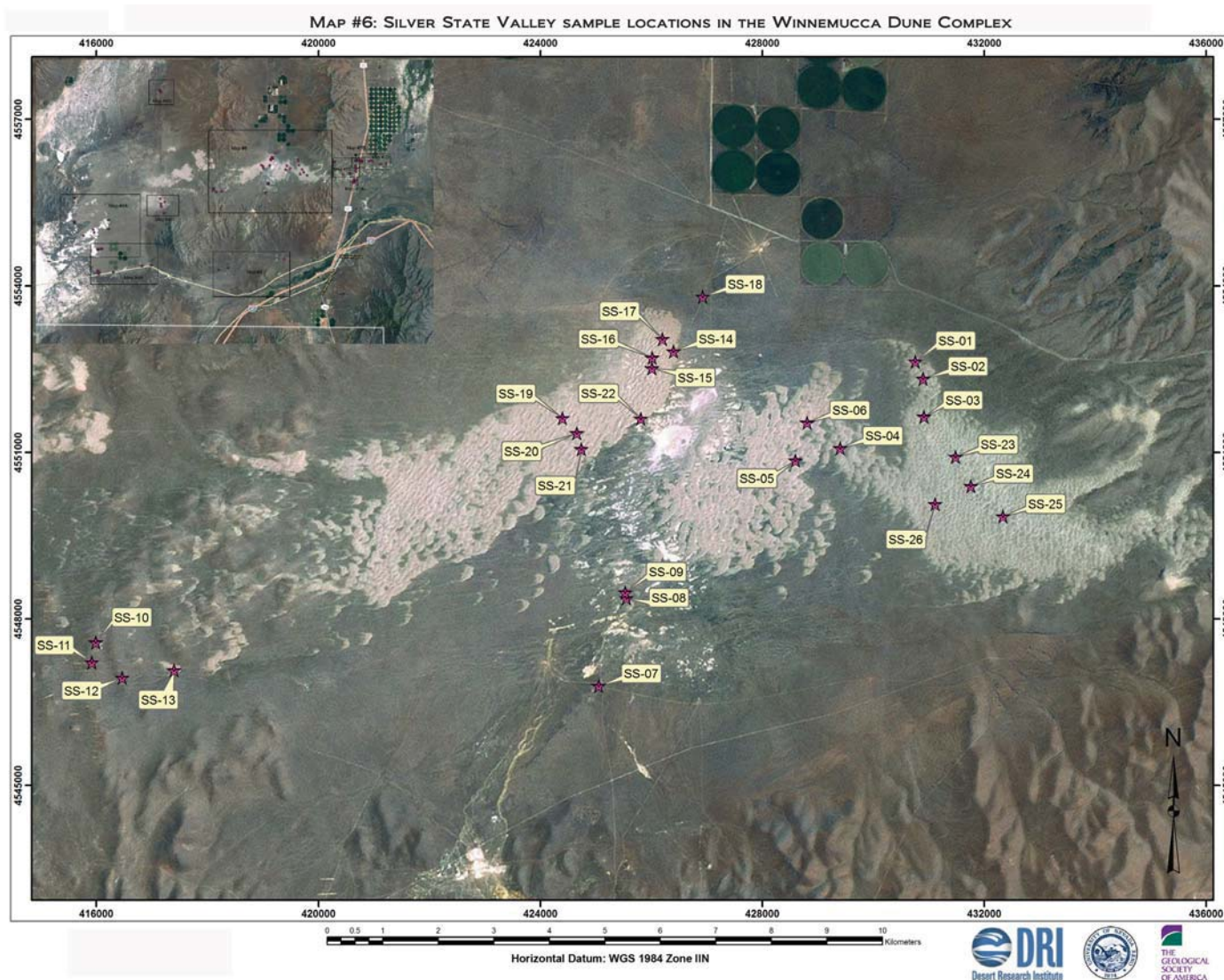


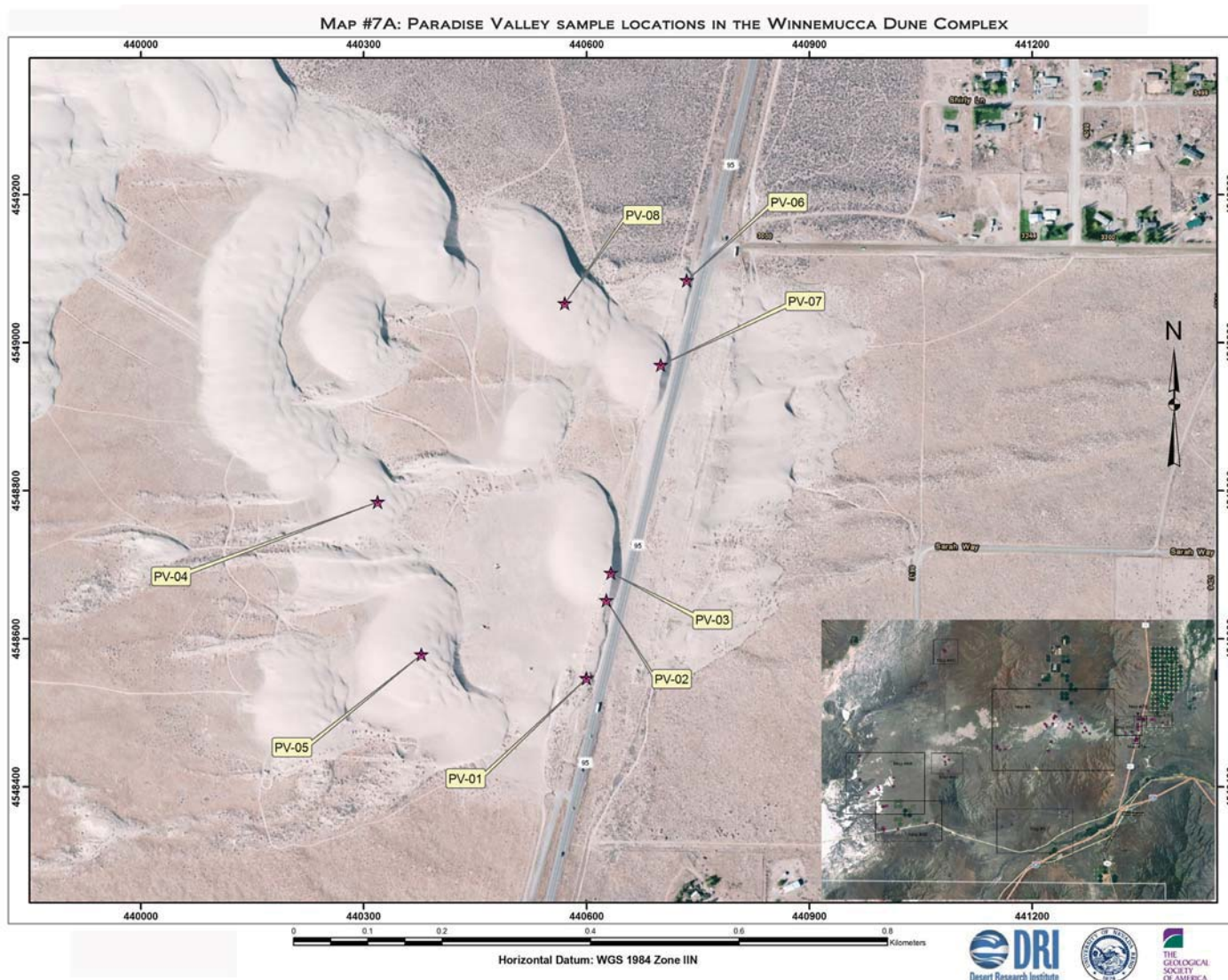


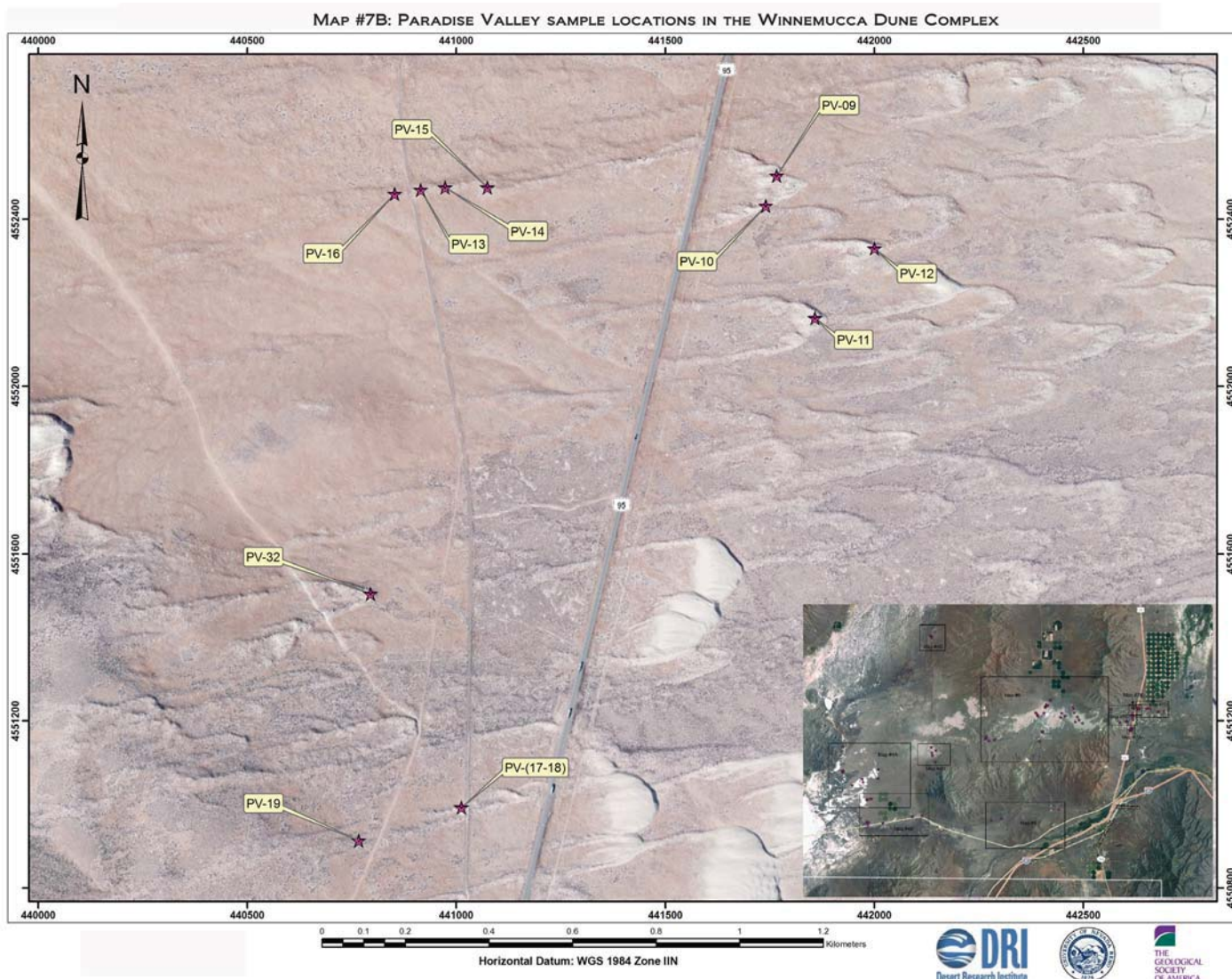


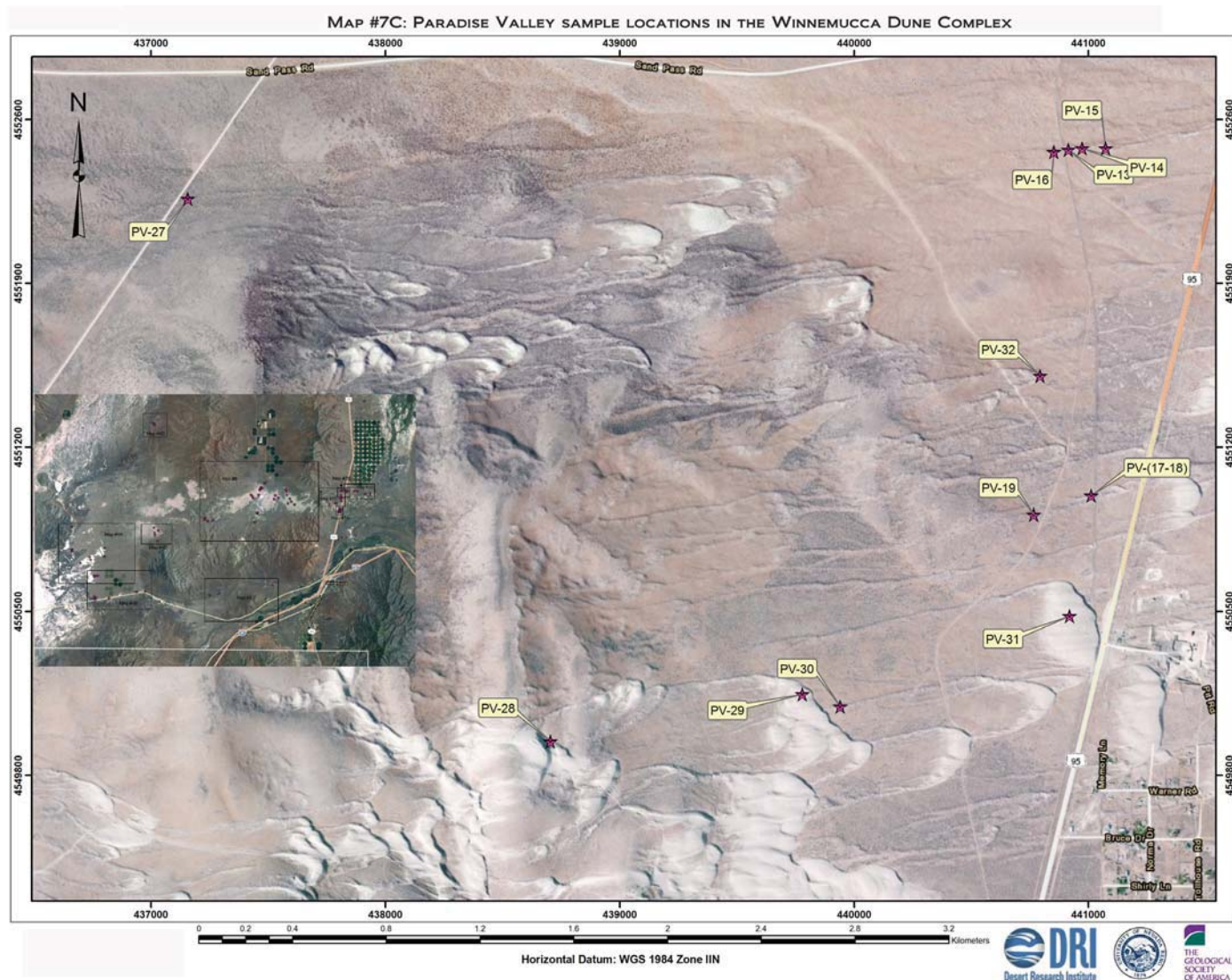












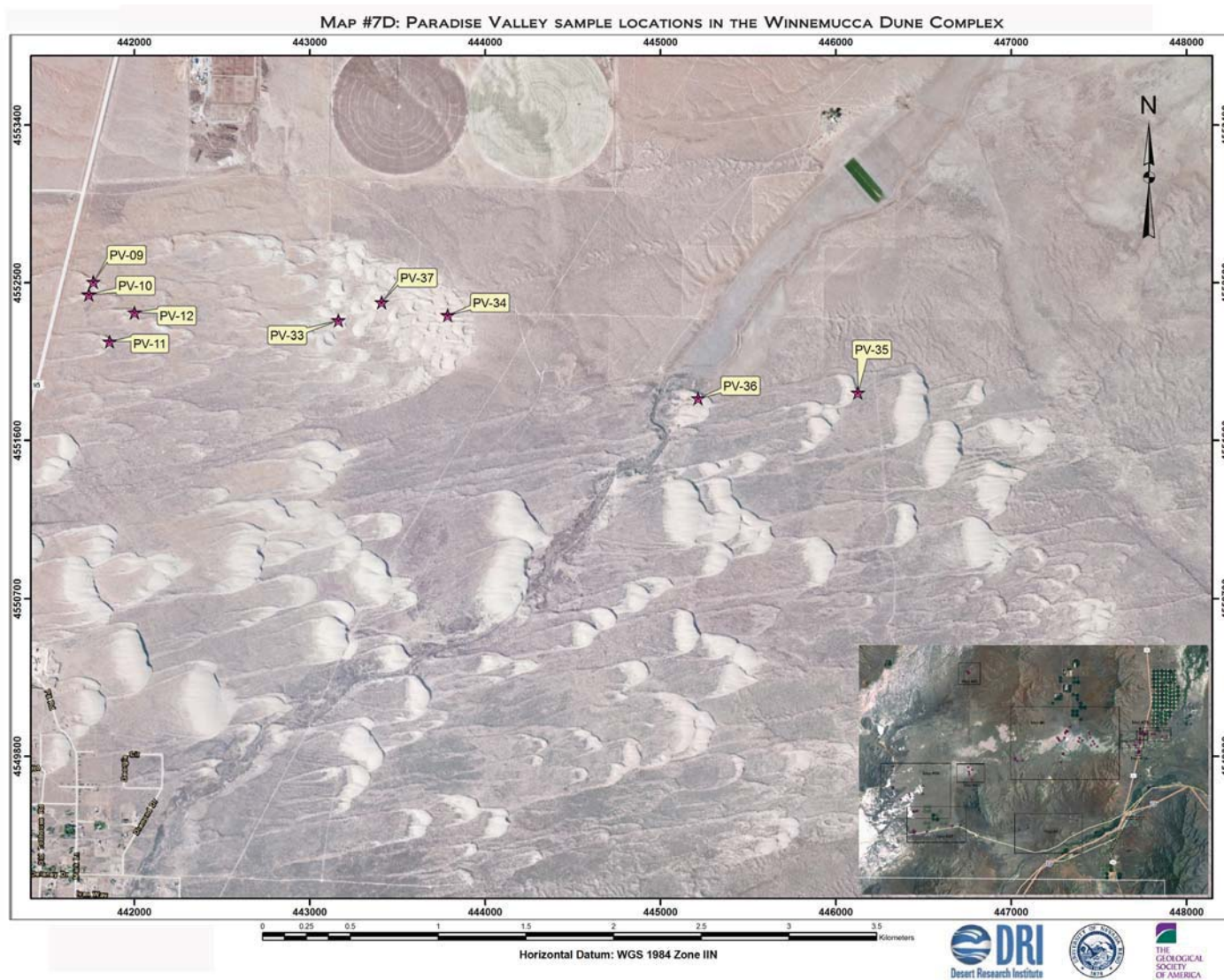
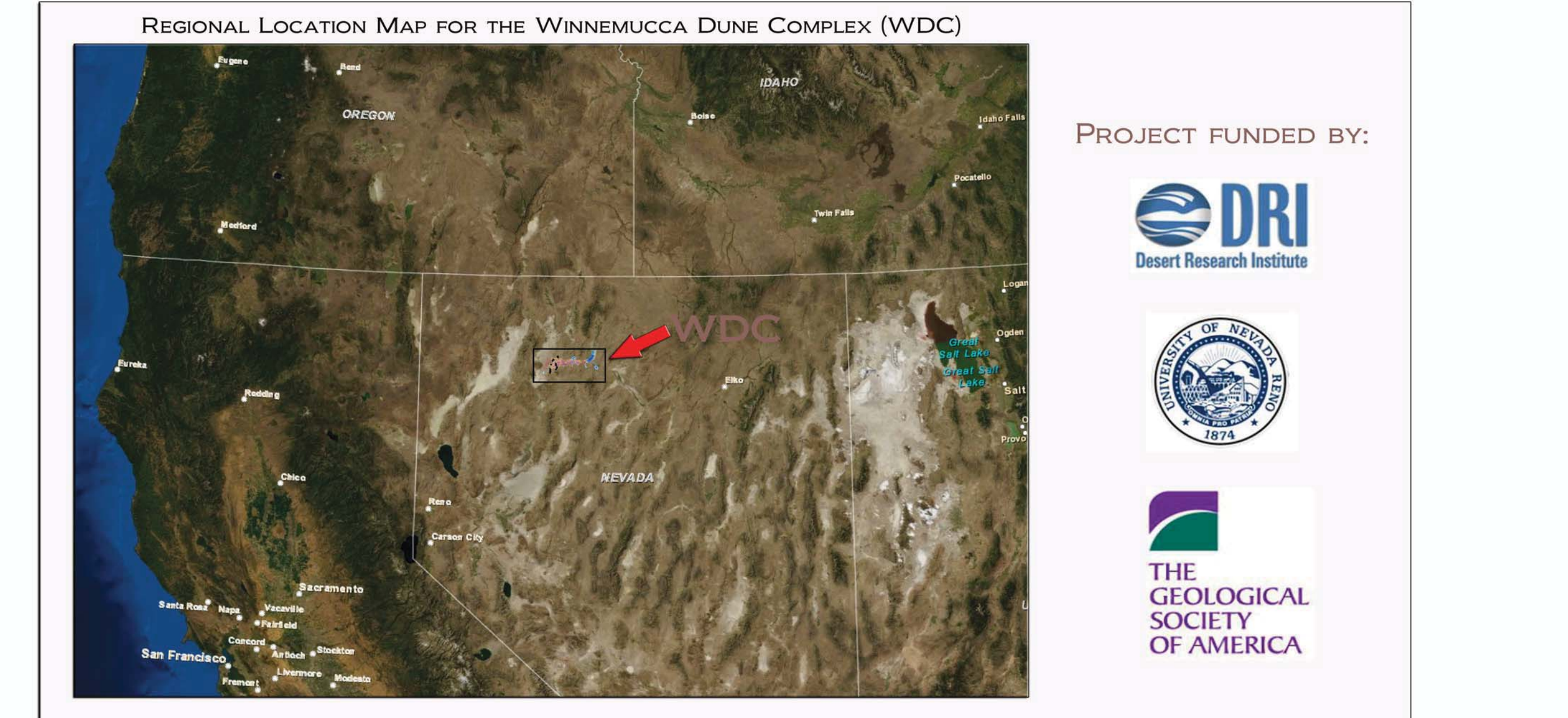
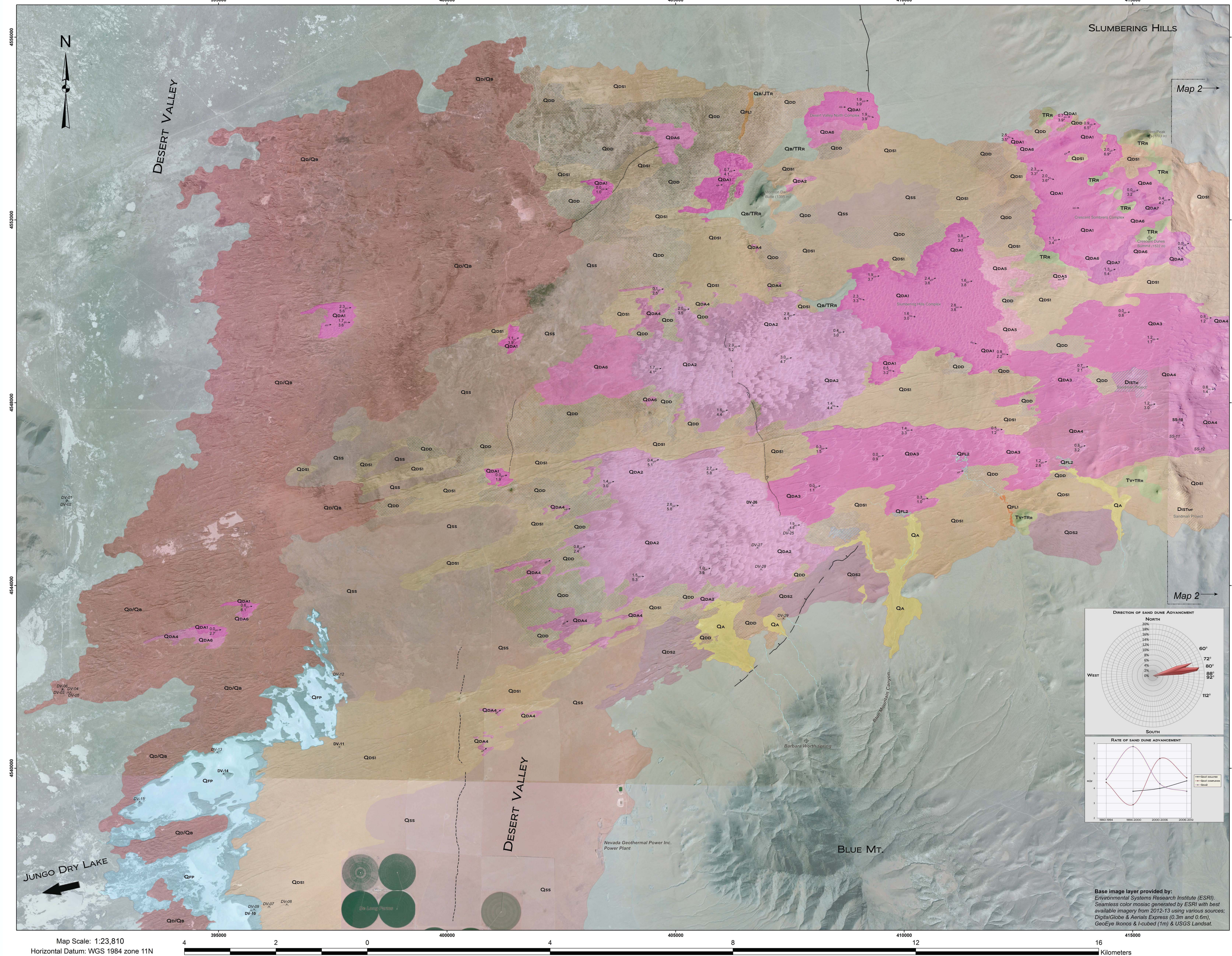


PLATE 3.1

# MAP 1: SURFICAL LANDFORMS IN THE DESERT VALLEY AND SLUMBERING HILLS PORTION OF THE WINNEMUCCA DUNE COMPLEX, HUMBOLDT COUNTY, NEVADA U.S.A.

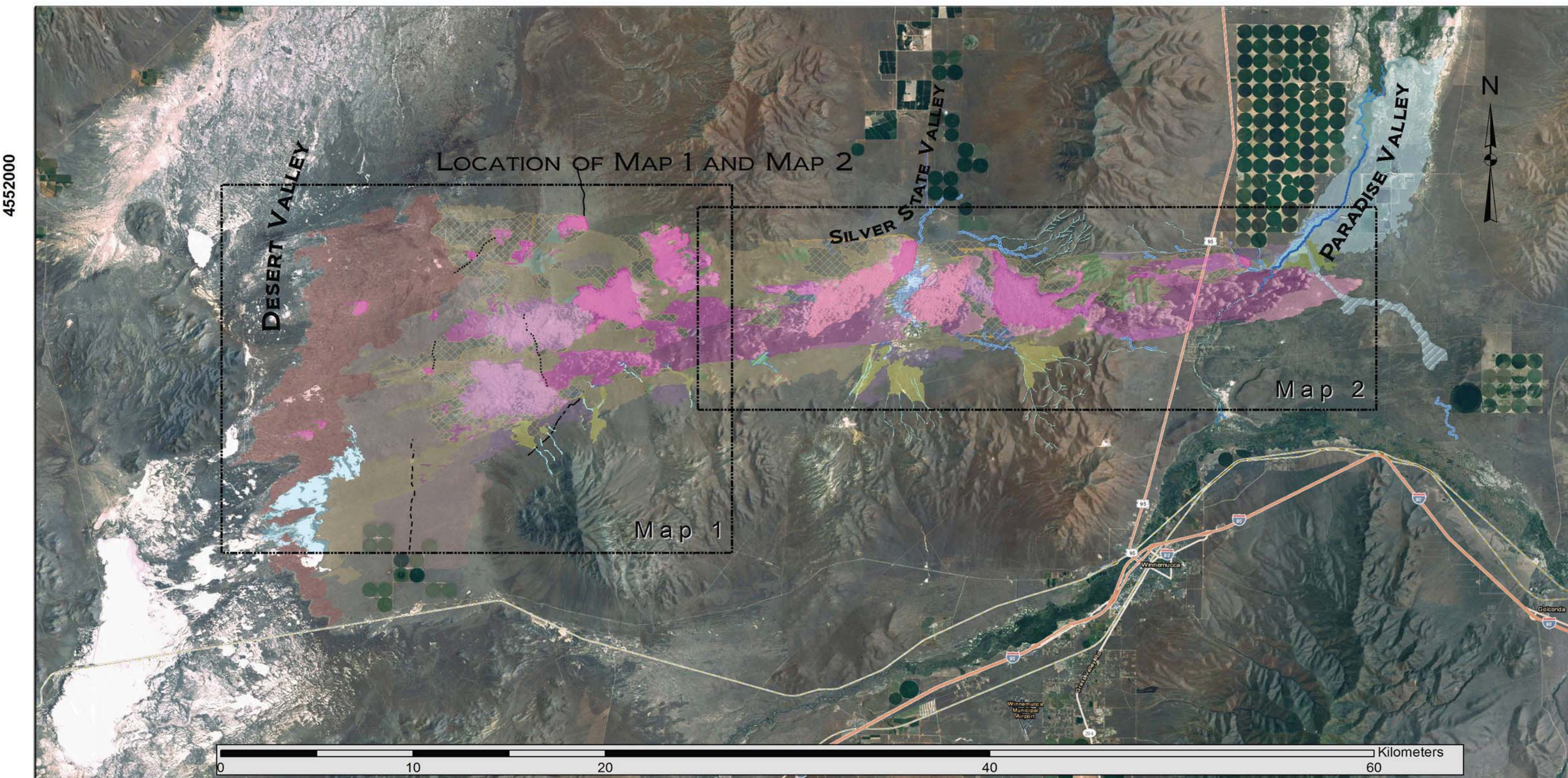
NATHANIEL ELIAS PEPE, 2014: "THE GEOMORPHOLOGY, EOLIAN ACTIVITY, AND PETROLOGY OF THE WINNEMUCCA DUNE COMPLEX", DESERT RESEARCH INSTITUTE, DIVISION OF EARTH & ECOSYSTEM SCIENCES, RENO NEVADA



## PROJECT FUNDED BY:

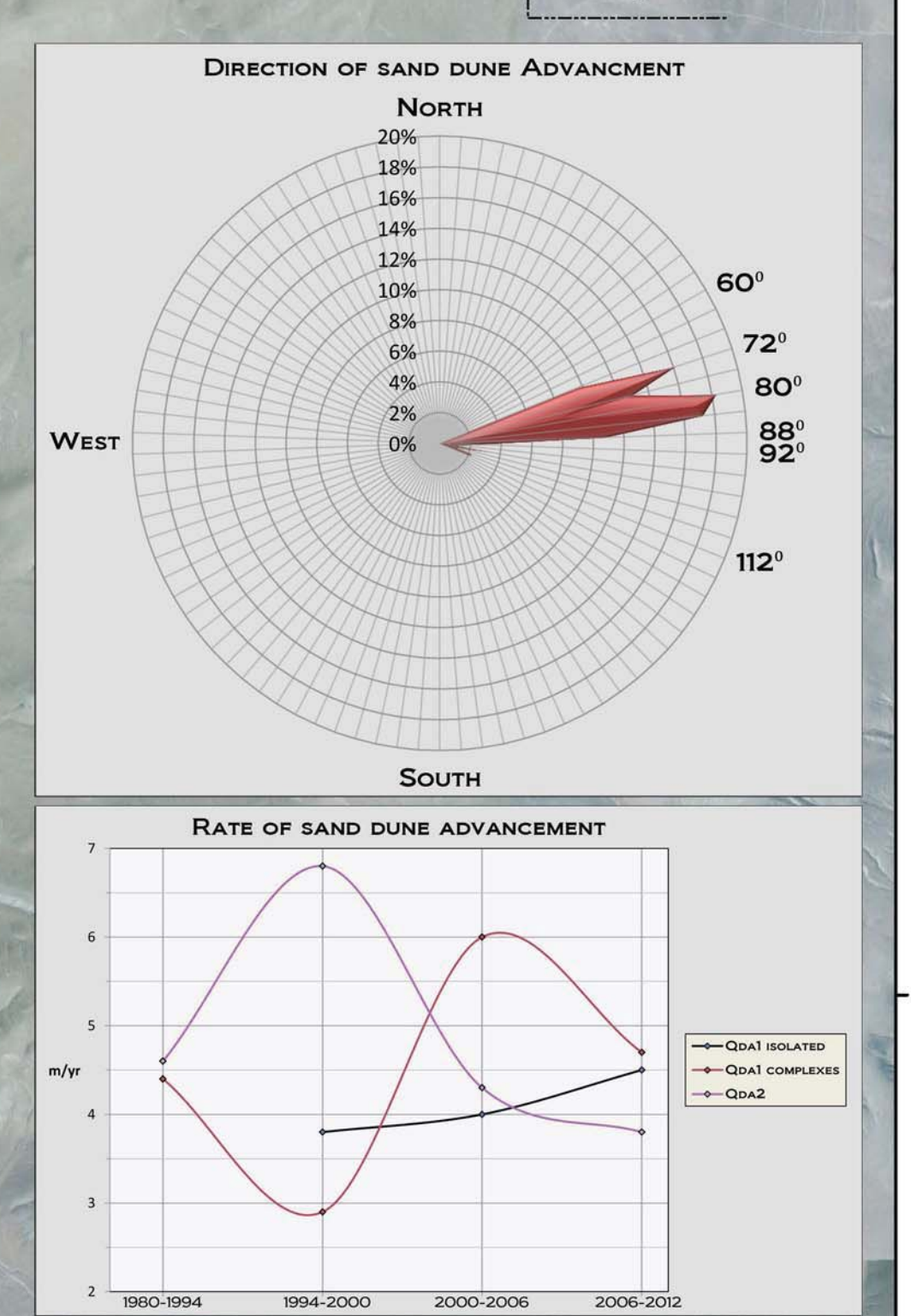


THE  
GEOLOGICAL  
SOCIETY  
OF AMERICA



## MAP DESCRIPTION:

 Relevant geographic loc



**Base image layer products**  
Environmental System  
Seamless color mosaics  
available imagery from  
DigitalGlobe & Aerial  
GeoEye Ikonos & I-cube

**DV-00** Sand sample number and location  
**DV-00** (Italic) Particle size granulometer analysis  
**(Bold)** Particle size & X-ray diffractometry analysis, including stereoscopic evaluation of stained standard thin sections

**min (m/yr)** **max (m/yr)**

dune form on 2012 base imagery

Direction of sand transport with minimum and maximum rates of dune advancement shown in meters per year. Measured using base imagery, 1999-2000 NAIP (12yr. avg) asterick \*  
 1994 NAIP (18yr. avg) no indicator  
 1980 USGS (32yr. avg) quote '

Normal fault with ball indicating down thrown side  
 Inferred fault location along deformed lakebed and beach deposits. ? section mapped by (Faulds, 2008).  
 Soft sediment deformation lineament. Underlays active and stable sand dunes. Lineament forms parallel to piedmont of Slumbering Hills and regional trend of the Central & Western Northern Nevada Rift (Ponce, 2010).

**YOUNGEST** ↑ QSS, & QDA1 TO QDA8 NOT IN CHRONOLOGICAL ORDER.....| **OLDEST** ↓

**QFL2** Recent floodplain and playettes prone to sheetwash and ponding water from run-off and snowmelt

**Qss** Sand Sheet and undifferentiated sand dunes occupying low laying areas in Desert Valley and the western slopes of the Slumbering Hills. Composed of light grey-pale brown, moderately to poorly sorted, medium to fine sand. Sand sheet begins along the eastern contact of Qd/Qb & Qss, and the terminal playas of unit Qfp. Qss overlays sections of Qb/TRr to the east of Mormon Dan Butte in the Slumbering Hills.

**QDA4** Individual & compound barchanobolic and parabolic dunes with lobate and elongate shapes. Dune heights range ~2-10 meters. Portions of Qda4 are stabilized by vegetation & degraded from wildfires, mining disturbances, precipitation, & bioperturbation. Max. rate of advancement varies ~1.4 to 3.2 m/yr in the direction of 60-88°.

**QDA8** Descending crescentic sand dunes in the Crescent Sombrero Complex. Dunes descend the eastern slope of the Slumbering Hills below Crescent Dunes Summit & begin stacking near the eastern boundary of the dune field. Max. rate of dune advancement is ~5.4 m/yr in the direction of 60°.

**QFP** Late Holocene - recent ephemeral delta-palustrine deposits from Jungo Dry Lake overflow. Intermittent braided drainages incise unit Qd/Qb forming a prograding delta that spills NE of DeLong Farms & forms a complex network of playas, dune islands & lunettes.

**QA** Middle Holocene - recent alluvial fans forming below Blue Mountain Canyon, Barbara Worth Spring & several un-named channels. Depositional lobes from unit Qa degrade, cross-cut, &/or overlay portions of Qda & Qds.

**TRR** Late Triassic - Early Jurassic metasedimentary bedrock belonging to the Jungo Terrane. TRr is composed of phyllite slaty shale, quartzite, and undifferentiated sand-silt-mudstone. Bedrock outcrops are subdued & mantled by sand. (Willden 1964)

**DISTM** Sandman Project mining disturbance

**DISTMF** Sandman Project mining & burnscar disturbance

**Unmapped areas outside project site**

**(QDA) WHITE TO LIGHT GREY & VERY PALE BROWN, MODERATELY WELL SORTED, FINE TO MEDIUM FELDSPATHIC LITHARENITE TO LITHARENITE SAND**

**QDA1** Wind rippled crescentic sand dune complex composed of barchanoidal & transverse ridges, star dunes, & lunate to lobate shaped barchan, barchanobolic-parabolic dunes. Dune heights range ~2-22. meters. Unit Qda1 is comprised of the; Crescent Sombrero, Slumbering Hills, North Desert Valley Complexes & 7 small isolated dune fields. Max. rate of advancement is ~1.9 to 6.9 m/yr in the direction of 60-110°.

**QDA2** Compound barchan, barchanobolic, & parabolic dunes with hemicyclic to lobate shape. In the medial portions of Qda2 dunes merge into small complexes & form transverse-barchanoidal ridges. Unit Qda2 is comprised of 2 parallel dune fields. Dune heights range ~2-18 meters. The max. rate of advancement varies ~2.4 to 5.8 m/yr in the direction of 65-105°.

**QDA3** Compound barchanobolic-parabolic dunes with lobate to elongate shape. Near the eastern leading edge of each field dunes merge & stack into crescentic ridges. Dune heights range ~2-10 meters. Portions of Qda3 are stabilized by vegetation & degraded from wildfires, mining disturbances, precipitation & bioperturbation. Max. rate of advancement varies ~0.8 to 3.3 m/yr in the direction of 70-85°.

**QDA4** Individual & compound barchanobolic and parabolic dunes with lobate and elongate shapes. Dune heights range ~2-10 meters. Portions of Qda4 are stabilized by vegetation & degraded from wildfires, mining disturbances, precipitation, & bioperturbation. Max. rate of advancement varies ~1.4 to 3.2 m/yr in the direction of 60-88°.

**QDA5** Parabolic & undifferentiated sand dunes with sand sheet. Unit occurs in areas of re-activated dune activity. Dunes & sheet form along lee-side of the Slumbering Hills Complex below Sobreiro Peak and Crescent Dunes Summit. Unit Qda5 overlays a section of Qdd and Qds1.

**QDA6** Sand sheet & isolated parabolic sand dunes. Qda6 forms along the stoss side of Qda2 and the SW corners of Qda1 in Desert Valley. Qda6 also forms along the lee side and SW corners of unit Qda1 in the Crescent Sombrero Complex on the western slopes of the Slumbering Hills.

**QDA7** Climbing crescentic sand dunes and transverse ridges within the Crescent Sombrero Complex. Dunes ascend the SW slopes below Sombrero Peak and the Crescent Dunes Summit. Max. rate of advancement varies ~3.2 to 5.4 m/yr in the direction of 70-82°.

**(QDD & QDS) GREY TO LIGHT YELLOWISH BROWN & PALE BROWN, MODERATELY TO POORLY SORTED, FINE FELDSPATHIC LITHARENITE SAND**

**QDD** Partially to completely degraded sand dunes. Unit Qdd is concentrated on the SW facing slopes of the Slumbering Hills and low lying areas in the northern portion of Desert Valley. Dunes are primarily degraded by precipitation, flooding, and ponding water.

**QDS1** Vegetated stable sand dunes in older inactive sections of the complex. Mostly parabolic dunes with some linear, transverse and barchan dunes. Qds1 occurs along the perimeter & interior of Qda. On the SE corner of Map1, Qds1 is mantled by fugitive dust.

**QDS2** Vegetated stable sand dunes. Linear dunes transforming to transverse dunes along the southern boundary of WDC. Run-off from unit Qa and the NW slopes of Blue Mt is captured by Qds2 and forms small playettes between the linear dunes in several areas NE of the Blue Mountain Power Plant.

**QFL1** Late Holocene abandoned fluvial channels & floodplain terraces along the lower reaches of Blue Mountain Canyon & north of Mormon Dan Butte below the NW corner of Qb/TRr.

**QD/QB** Quaternary sand dunes (*middle Holocene - recent*) overlaying Quaternary beach & lakebed deposits belonging to the middle member of the Sehoo Alloformation (*late Pleistocene - early Holocene*). Sub-unit Qd is comprised of vegetated & braided linear sand dunes transforming to parabolic and transverse dunes. Run-off from dunes, Jungo Dry Lake, and adjacent hillslopes to the west form numerous playettes throughout the entire unit. Sehoo Alloformation & relative age of deposits inferred using Morrison (1991) ages of Lake Lahontan shorelines between the elevations of

**QB/TRR** Late Pleistocene - early Holocene offshore, nearshore, and foreshore lake deposits from the middle member of Sehoo Alloformation overlaying *late Triassic - early Jurassic* meta-sedimentary bedrock from the Jungo terrane. Subunit Qb nearshore & foreshore beach deposits are composed of pebbly sand, moderately sorted fine to medium sand, & small tufa heads (to 8 cm) with basal stems (length ~ 3 cm, width ~3 cm) of coarse sand. Lithoid and dendritic tufa encrusts parts of Mormon Dan Butte. Qb offshore lakebed deposits are composed of very poorly sorted, very fine to fine silty sand, & partially cemented laminated beds of bimodal & unimodal medium

